Bearing Capacity Evaluation of Various Types of Foundations Subjected to Combined Load in Layered Grounds Considering Nonlinearity of Strength against Confining Pressure

by

Hamidou Hamadoum TAMBOURA

MSc. Civil Engineering

A thesis submitted in partial fulfilment of the requirements for the degree of Doctor of Philosophy

Examination Committee:

Assoc. Prof. Koichi ISOBE

Prof. Yoichi WATABE

Prof. Yoshiaki FUJII

Thesis No.

Division of Field Engineering For Environment

Graduate School of Engineering, Hokkaido University

September 2022

DEDICATION

I dedicate my dissertation work to my hometown, the city of Djibo in the province of Soum, and to my country Burkina Faso. The city of Djibo is where I was born and where I grow up and studied until the end of high school. I have never felt so good elsewhere than in this city. Thinking about my country and the situation it is undergoing since 2016 has given me more strength and motivation to study and forge myself to be a future pillar of its development.

My work is also dedicated to my grandmother Haoua. She was the only human being who loved me more than my mother does. "*Manga am*" she used to call me. From the beginning to the end, she has been my rudder and my main source of motivation. I thank God for letting me know you in my life. From where you are grandma your "Manga am" has succeeded.

I also dedicate this dissertation to my wife and my daughter who have been a constant source of support, encouragement, and motivation during the challenges of graduate school and life. I am truly thankful for having you in my life.

This work is also dedicated to my father and my mother who, despite their live condition have made it possible for me to go to school, who have always loved me unconditionally and whose good examples have taught me to work hard for the things that I aspire to achieve.

This thesis work is also dedicated to my grandfather Nouhoun Ousseni. I have a special feeling of gratitude for him; he is my model of a human being. Thank you, grandfather, for being who you are and for teaching me how to be a better man in all life plans.

ACKNOWLEDGEMENTS

The author gratefully acknowledges the financial assistance, provided through the receipt of the fellowship JST SPRING, Grant Number JPMJSP2119 during his third year of Ph.D. The author is deeply indebted to his supervisors, Associate Professor Koichi ISOBE for their valuable guidance, critical suggestions, and limitless help throughout the period of his Ph.D. Their commitment and assistance are greatly appreciated. The author would also like to thank Professor Satoru Ohtsuka of the department of Civil and Environmental Engineering, Nagaoka University of Technology for his assistance, collaboration and advice. His support was highly appreciated.

Table of Contents

ABSTRACT:

Due to the complexity of the interaction mechanism between soil and foundation, foundation design, is still considered as one of the most difficult tasks in geotechnical engineering. There are many types of foundation, and the bearing capacity of each foundation type is governed both by its structural strength, the supporting soil properties and the forces acting on it. In this thesis, the bearing capacities of three types of foundations are being investigated using: An in-house FEM code, namely, the rigid-plastic finite element method; Physical modeling and 3D elastic-Plastic FEM. (1) the bearing capacity of strip footing on two-layered *c-ϕ* soils, (2) the end bearing capacity of Incompletely End Supported Pile (IESP), (3) the bearing capacity characteristics of spiral pile subjected to combined loads.

In the case of strip footing, the bearing capacity was investigated by considering layer factors. The influences of the following ratios on the bearing capacity factors were investigated: The ratio of the tangent of the angle of friction of the bottom layer to that of the top layer; the ratio of the cohesion of the bottom layer to that of the top layer; the ratio of the unit weight of the bottom layer to that of the top layer, and the ratios of the embedment of the footing and the thickness of the top layer to the footing width. Based on the influences of those ratios, layer factors are determined. Several types of failure mechanics were found and the conditions of occurrence of each failure type are summarized in a chart. A new approach for estimating the bearing capacity of strip footings on two-layered c-ϕ soils is proposed. A comparison with available methods in the literature has confirmed the reliability of the proposed method, showing the application limitation of the past research.

In the case of IESP, the end bearing capacity was investigated considering shear strength nonlinearity of soil against confining pressure, and soil-foundation interaction. The effect of the distance between the pile tip and the bottom hard soil layer (d/B) on the end-bearing capacity of IESP was mainly investigated. The influence of ratio (r) of the end bearing capacity of the pile when it reaches the bottom hard layer to the end bearing capacity of the pile when the bottom layer has no influence was also investigated. As a result, the consideration of the shear strength non-linearity leads to accurate estimation of the end bearing capacity, affects the failure patterns and matches previous analytical, experimental and numerical solutions. It is found that the end bearing capacity inversely decreases with the distance d/B and becomes constant around $d/B = 3$. Based on the results, a formula for estimating the end bearing

capacity of IESP is proposed. And comparisons with methods in existing literature have confirmed the reliability of the proposed equation.

In the case of the spiral pile, a series of push-in, pull-out and horizontal loading tests on spiral piles constructed on soft and viscous ground was conducted, and a method to easily consider the integration effect of surrounding ground by rotational press-fitting is proposed. Subsequently, based on the proposed method, a small-diameter spiral pile is modelled with FEM analysis, various test results were reproduced and parameters to consider the integration effect of the surrounding ground, in numerical analysis, are identified. By the same FEM analysis method, using the identified parameters, the bearing capacity characteristics of the vertical and batter spiral pile for the combined load are obtained. Finally, based on the results, formulas for the bearing capacity envelopes in H-V-M space are proposed and the accuracies of the formulas are verified.

ABBREVIATIONS

The following abbreviations are used in this thesis:

- RPFEM = Rigid Plastic Finite Element Method
- FEM = Finite Element Method
- D.P. = Drucker Prager
- H.O. = High Order
- IESP = Incompletely End Supported Pile
- B.C. = Bearing Capacity
- B.C.R. = Bearing Capacity Ratio
- H-V-M = Horizontal, Vertical and Moments

SYMBOLS

The following symbols are used in this thesis:

- B = footing or pile width
- c = cohesion of uniform ground
- c_1 = cohesion of the top soil layer of a two-layered c-ϕ soil
- c_2 = cohesion of the bottom soil layer of a two-layered c-ϕ soil
- D = embedment of the footing
- d_c, d_q and d_γ = depth factors
- H = thickness of the top layer of a two-layered c-ϕ soil
- i_c, i_q and i_γ = inclination factors for the load inclined at an angle θ to the vertical
- L_c, L_q and L_γ = layer factors, proposed in this study, for cohesion, overburden pressure and self-weight of soils
- N_c, N_q and N_γ = bearing capacity factors for cohesion, overburden pressure, and self-weight of a uniform soil
- q = overburden pressure at the level of the footing base
- $r_c = c_2 / c_1$
- $r_\phi = \tan\phi_2 / \tan\phi_1$
- $r_\gamma = \gamma_2 / \gamma_1$
- S_c, S_q and S_γ = shape factors
- ϕ_1 = angle of friction of soil in the top layer of a two-layered c-ϕ soil
- ϕ_2 = angle of friction of soil in the bottom layer of a two-layered c-ϕ soil
- γ = unit weight of surcharge soil above a footing base, on a two-layered c-ϕ soil or unit weight of a uniform soil
- γ_1 = unit weight of soil in the top layer of a two-layered c-ϕ soil
- γ_2 = unit weight of soil in the bottom layer of a two-layered c-ϕ soil
- ξ_c, ξ_q and ξ_γ = influence factors, of r_c, D_f and r_γ on N_c, N_q, and N_γ respectively
- d/B = the distance between the pile tip and the bottom layer (d) normalized by the pile width (B)
- q_x = the end bearing capacity for any position $d/B = x$ of IESP

- q_H = the end bearing capacity when IESP is on the bottom layer (d/B = 0)
- q_s = the end bearing capacity of IESP when the bottom layer has no influence
- r = q_H / q_s ratio of the end bearing capacity of IESP
- ξ_x = the degradation factor of the end bearing capacity when the IESP moves away from the bottom layer
- H = horizontal load applied to the spiral pile
- V = Vertical load applied to the spiral pile
- M = Moment load applied to the spiral pile
- h = loading height of the spiral pile
- ξ, η and ζ = correction coefficients for the bearing capacity of small diameter spiral pile for the apparent increase in the pile diameter, the increase in the strength of the ground immediately below the pile tip, and the increase in the flexural rigidity of the pile, respectively.

PREFACE

The research work, presented in this thesis was conducted at the University of Hokkaido in the laboratory of Analytical Geomechanics of the Division of Field Engineering For Environment of Graduate School of Engineering during the period October 2017 to September 2022. This work was performed under the supervision of Associate Professor Koichi ISOBE with the assistance of Professor Satoru Ohtsuka of the Nagaoka University of Technology. This thesis is presented in the form of a thesis by publications, based on the publications listed below.

1. International conferences

(1) Hamidou, H. and Isobe, K.: Bearing Capacity of an Incompletely End-Supported Pile Based on Rigid Plastic Finite Element Method (RPFEM), Sustainability Issues for the Deep Foundations (Proceedings of the 2nd GeoMEast International Congress and Exhibition on Sustainable Civil Infrastructures, Egypt 2018 - The Official International Congress of the Soil-Structure Interaction Group in Egypt (SSIGE)), Cairo, Egypt, pp. 85-103, 2018.

2. Domestic conferences

(1) Hamidou Hamadoum Tamboura, Koichi Isobe, Takashi Hoshina: Bearing Capacity of Strip Footings in Two Layered Cohesive Friction Soils using Rigid Plastic Finite Element Method, Proceedings of 55th Japan National Conference on Geotechnical Engineering, 21-8-3-08, 2020.
(2) Hamidou Hamadoum, Koichi Isobe, Takashi Hoshina: End Bearing Capacity of a single pile in layered ground using Rigid Plastic Finite Element Method with the non-linear strength property, Proceedings of 54th Japan National Conference on Geotechnical Engineering, pp. 1297-1298, 2019.
(3) Hamidou Hamadoum, Koichi Isobe, Takashi Hoshina: Evaluation of the End Bearing Capacity of a single pile in layered ground using Rigid Plastic Finite Element Method with the non-linear strength property, Proceedings of Technical Reports of Japanese Geotechnical Society Hokkaido Branch, No.59, pp. 31-36, 2019.
(4) Hamidou Hamadoum, Koichi Isobe: Bearing capacity of an incompletely end-supported pile based on RPFEM, Proceedings of 53rd Japan National Conference on Geotechnical Engineering, pp. 1397-1398, 2018.
(5) Hamidou Hamadoum, Koichi Isobe: Evaluation of bearing capacity of incompletely end-supported piles based on Rigid Plastic Finite Element Analysis, Proceedings of Technical Reports of Japanese Geotechnical Society Hokkaido Branch, No. 58, pp. 345-352, 2018.

3. International journals

(1) Tamboura, H. H., Isobe, K. and Ohtsuka, S.: End bearing capacity of a single incompletely end-supported pile based on the rigid plastic finite element method with non-linear strength property against confining stress, Soils and Foundations Volume 62, Issue 4, 2022, 101182 (https://doi.org/10.1016/j.sandf.2022.101182)

(2) Tamboura, H. H., Yamauchi, R. and Isobe, K.: Bearing capacity evaluation of small-diameter spiral piles in soft ground subjected to combined loads, Soils and Foundations Volume 62, Issue 5, October 2022, 101204 (https://doi.org/10.1016/j.sandf.2022.101204)

(3) Tamboura, H. H. and Isobe, K.: Estimation of the Bearing Capacity Factors of Two-Layered c-φ soils based on the Rigid Plastic Finite Element Method, Soils and Foundations, (*Ongoing work under internal review*)

CHAPTER 1- GENERAL INTRODUCTION

1.1 Introduction

Foundation design is more complex when it comes to foundation on layered ground. In nature, the soil is generally non-homogeneous with mixtures of sand, silt, and clay in different proportions. In practice, foundations are sometimes located on a soil layer of finite thickness overlying a thick stratum of another soil. The underlying stratum may be either bedrock or another soil possessing different strength properties. The bearing stratum of the two-layers deposits can be either softer or stiffer than the underlying stratum. A case of bearing stratum stiffer than the underlying stratum is mostly obtained in practices when placing dense sand over loose sand or soft clay to increase the bearing capacity of the foundations. On the other hand, a case of bearing stratum softer than the underlying stratum may be obtained when the foundations do not reach a targeted stiff layer because of miss implementation or because of complex geological soil layers, where the layers are not horizontal. Another complication in foundation engineering is when foundations are subjected to combined loadings. In that case, the foundation is subjected to horizontal and vertical loadings at the same time. The vertical load can be either a compressive load or a pull-out load.

A Series of researchers contributed their findings towards estimating the bearing capacity of strip footings on natural or artificial stratified soil media. Four (04) general cases of footing on a layered soil may be found; 1) Footing on layered sand and clay soils (sand overlying clay or clay overlying sand), 2) footing on layered clays, 3) footing on layered sands, and 4) footing on layered c-ϕ soils. Many researchers focused on the three first cases and relatively the studies concerning the bearing capacity of strip on two-layered c-ϕ soils have received less attention. The ultimate bearing capacity of strip on two-layered c-ϕ soil was studied by Purushothamaraj et al. (1974), Satyanarayana and Garg (1980), Florkiewicz (1989), Azam and Wang (1991), and Bowles (1996). However, most of these studies are empirical and use the average strength of the two-layered c-ϕ soil (average ϕ and average c) which is not strictly valid and leads to misestimation of the bearing capacity. In this thesis, by attributing each soil layer its shear strength, the Rigid Plastic FEM analysis was used to estimate the bearing capacity of two-layered c-ϕ soils. The estimation of layer factors Lc, Lq and $L\gamma$ was focused on. Just like the shape factors, inclination factors and depth factors to take into account foundation shape, load inclination, and foundation depth respectively, this study aims to propose layer factors Lc, Lq and Lγ to take into account the effect of the bottom layer of two-layered c-ϕ soil on the bearing capacity of the top layer. Therefore,

this thesis aims to propose a new formula for the bearing capacity of strip footing on two-layered c-ϕ soils.

In 2014 the Japanese Nikkei newspaper has published an investigation of the cause of the tilting of a building in Yokohama (**Photo 1-1** and **Fig. 1-1**) (https://www.nikkei.com). It is an 11-storey reinforced concrete building. A height difference of about 5.5 cm in the southeast direction was found on the rooftop of the building. The building has a mixed foundation with piles and footing foundations. It was found after investigation that, a total of nine piles did not reach the supporting layer due to the complexity of the layered ground of the foundation. A cross-section image showing the position of the foundations and the profile of the supporting ground is shown in **Fig. 1-1.** The blue piles have reached the supporting ground, those piles are referred to as End Supported Piles (ESP) in this thesis. The red piles have not reached the supporting hard ground and ended up in the softer top layer, those piles are referred to as Incompletely End Supported Piles (IESP) in this thesis. The skin friction resistance of IESP might be the same as that of ESP, however, the end bearing capacity of IESP will be reduced by the presence of the softer soil at the pile toe. The amount of reduction of the end bearing capacity of IESP depends on the distance to the stiffer bottom layer. A Statistical Calculation Statement revealed that, for the IESPs, there were some parts where the maximum stress occurring in the ground was 9.99 times the allowable stress degree. Hence, the main concern of IESP is the influence of the distance to the bottom layer on the end bearing capacity of IESP. IESP can threaten the integrity of the structure it supports; it can cause the failure of the structure which can lead to fatalities and economic losses. Therefore, it is necessary to assess the end-bearing capacity of IESP appropriately to evaluate the stability and safety of the structure supported. Some researchers have used numerical analysis to investigate the end-bearing capacity of IESP. Teramoto et al. (2015) have conducted a FEM analysis to investigate the mechanical behaviours of Incompletely End-Supported Piles. They also found that the gap between the pile tip and bottom layer influences the bearing capacity but did not propose a formula. Hyodo et al. (2020) studied the end bearing capacity of IESP in sand using a three-dimensional elastoplastic FEM analysis. They proposed a ratio of the degradation of the end bearing capacity of IESP when the pile tip moves away from the bottom layer. However, their proposed formula applied to sand only. There is no concrete solution for the end bearing capacity of piles in layered grounds that considers the effect of the distance to a bottom stiffer layer for all different types of soils. In this thesis the influence of the bottom layer on the end bearing capacity of IESP is investigated, that is, the decrease (degradation)

of the end bearing capacity of IESP when the distance from the pile tip to the bottom layer increases; by using two-dimensional Rigid Plastic FEM, considering non-linear shear strength property against the confining pressure and soil-pile interaction. The effect of the ratio (*r*) of the end bearing capacity of the pile when it reaches the bottom hard layer (ESP) to that of the pile when the bottom layer has no influence becomes an important factor. In addition, a formula of the end bearing capacity of IESP for all types of soils (cohesive soils, cohesionless soils and intermediate soils) is proposed based on the results, while considering the influence of the end bearing capacity ratio *r*.

Photo 1-1: Leaning building due to IESP in Yokohama

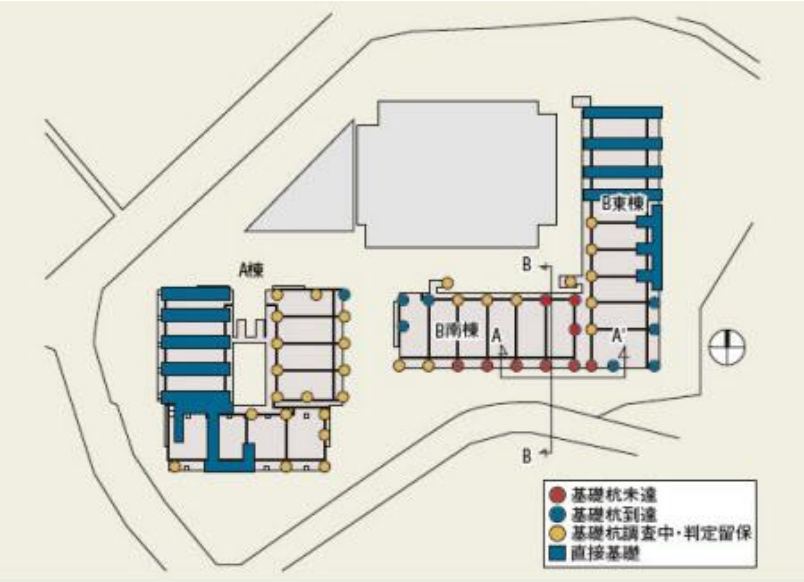

a) The layout of the foundation

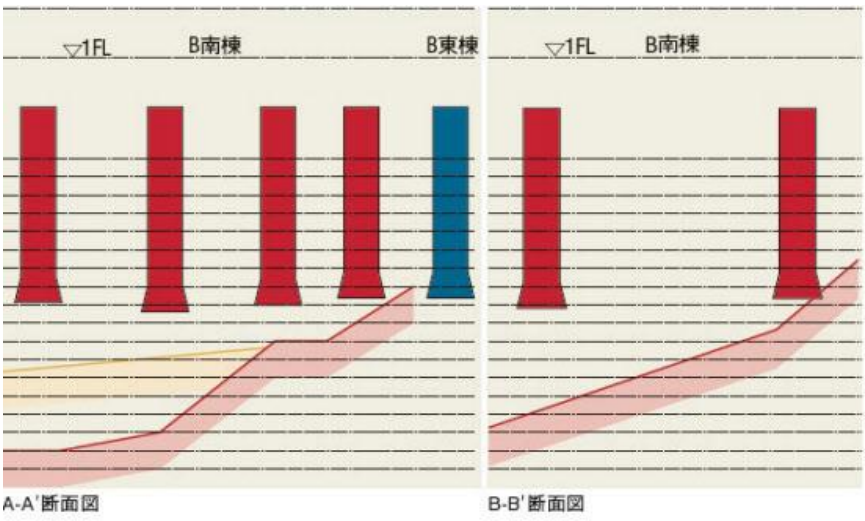

b) Cross-section A-A" and B-B'

Fig. 1-1: layout and cross-section of the foundation of the building

The construction of photovoltaic power generation facilities has been increasing with the increasing demand for renewable energy. The development of new foundation types using small-diameter vertical, and batter spiral piles has progressed for the foundation of photovoltaic power generation facilities in Japan (Araki 2013; Hirata et al. 2005; Sato et al. 2015) (**Photo 1-2** and **Photo 1-3** The spiral pile is also expected to be used as an anchor by taking advantage of its excellent pull-out

resistance. Generally, compressive, horizontal, uplift and moment loads act on these spiral piles simultaneously due to the actions of wind, earthquake, landslide, etc. The spiral pile is an advantageous pile type because it has a large resistance to vertical loads (push-in and pull-out loads). On the other hand, its disadvantage is its low flexural rigidity, its horizontal resistance is smaller than that of the steel pipe pile of the same diameter. When the conventional design method in Japan, which uses 1% of the pile diameter (lower limit: 15 mm) as the allowable displacement, is applied to the small-diameter piles, there is a possibility of resulting in overdesign. This is because the elastic ground reaction force method, which is generally used in the pile foundation design, overestimates the horizontal displacement of the small-diameter piles. In addition, the large resistance to the vertical load of spiral piles is due to the effect of its integration with the surrounding ground generated during the rotational press-fitting. However, in many cases, the design takes the safe side without considering this integration effect from the rotational press-fitting. Therefore, it is required to properly evaluate the bearing capacity characteristics of small-diameter spiral piles and give more rational designs. In the conventional design, allowable values are set for vertical load direction and horizontal load direction, and individual evaluations are performed separately. However, in reality, combined horizontal and vertical loads act on the structure. In this thesis, we have conducted a series of push-in, pull-out and horizontal loading tests on spiral piles constructed on soft and viscous ground and we have proposed a method to simply consider the integration effect between the rotationally press-fit spiral pile and the surrounding ground. Next, based on the proposed method, we have modelled a small-diameter spiral pile in FEM analyses, reproduced the physical test results, and identified some additional parameters necessary for the numerical analysis. By the same analysis method, using the identified parameters, the bearing capacity characteristics of vertical and batter spiral pile under the combined load were obtained. Finally, based on the results, formulas for the bearing capacity envelopes in H-V-M space are proposed for both vertical and batter spiral piles.

Photo 1-2: Spiral piles used for the foundation of photovoltaic power generation facilities

Photo 1.3: photovoltaic power generation facilities founded with spiral piles

1.2 Research Objectives

The main objective of this thesis was to improve and extend the field of application of current design methods for bearing capacity of some exceptional foundation cases in layered, that include: the bearing capacity of strip footing foundation on two-layered *c*-ϕ soils, the end bearing capacity of IESP considering the strength non-linearity against the confining pressure and the bearing capacity characteristics of vertical and batter small diameter spiral piles under the combined loads. The objective is reached by providing simple bearing capacity formulas, derived from the interpretation of advanced numerical solutions.

The main objective of this project can be divided into three objectives. The first main objective is to propose a new and more accurate formula for the bearing capacity of strip footing on two-layered *c*-ϕ soils using layer factors L_c, L_q and L_γ. Just like the shape factors, inclination factors and depth factors to consider foundation shape, load inclination, and foundation depth respectively, this thesis aims to propose layer factors L_c, L_q and L_γ to consider the effect of the bottom layer of two-layered c-ϕ soil on the bearing capacity of the top layer. The second main objective is to propose a formula to estimate the end bearing capacity of IESP after clarifying the effect of the strength non-linearity against the confining pressure and clarifying the relationship between and the end bearing capacity of IESP and the distance d/B between the IESP pile tip and the bottom layer. The last main objective is to investigate the bearing capacity characteristics of vertical and batter spiral piles under the combined loads and propose new equations of bearing capacity envelope in H-V-M space.

1.3 Methodology

Three main objectives are cited in the previous section. The methodology used to achieve the two first objectives is the Rigid Plastic Finite Element method (RPFEM) code, which is an in-house code developed and upgraded by Hoshina et al. (2011) and Du et al. (2016). For the third objective, a combination of physical modeling and a 3D elastoplastic finite element analysis code “DBLEAVES” developed by Ye et al. (2007) is used. In the elastoplastic finite element analyses, a spiral pile with a complicated shape was simplified into a model using the skeleton-beam type hybrid element proposed by Zhang et al. (2000) and verified for usefulness by Danno and Kimura (2009). To reach each objective the following plan was followed.

The first main objective, the bearing capacity of strip footing on two-layered c-ϕ soils: (1) Exhibiting the limits of current methods of estimation bearing capacity and demonstrating why the existing formulas misestimate the bearing capacity and failure modes of strip footing on two-layered *c-ϕ* soils. (2) Validating the simulation method with RPFEM by comparison with existing literature. (3) Examination of the effects of the thickness of the top soil layer and the strength properties of the two soil layers as well as the failure patterns that govern the stability of footings on two-layered *c-ϕ*. (4) Proposing layer factors, L_c, L_q and L_γ to consider the effects of the bottom soil layer on the bearing capacity factors N_c, N_q and N_γ of the top layer, respectively. (5) Proposing a new approach for estimating the bearing capacity of strip footings in two-layered *c-ϕ* soils. (6) Proposing a chart that summarizes the conditions of occurrence of different possible failure patterns. (7) Demonstrating the validity of the proposed formula. (8) Submitting a manuscript of the study to an international journal.

The second main objective, the end bearing capacity of IESP: (1) Exhibiting the limits of currently available methods of estimation of the end bearing capacity of IESP. (2) Validating the simulation method with RPFEM by comparison with existing literature. (3) Analysing the effect of the strength non-linearity against the confining pressure for a pile. (4) Establishing the relationship between the end bearing capacity of IESP and the distance between the IESP tip and the bottom hard soil layer. (5) Investigating the influence of the ratio of the bearing capacity of the bottom layer to that of the top layer and the influence of the confining pressure on the end bearing capacity of IESP. (6) Proposing parameters of a constitutive equation for the non-linear strength property for pile bearing capacity. (7) Proposing a formula for estimating the end bearing capacity of IESP in different types of soils. (8) Demonstrating the validity of the proposed formula. (8) Submitting a manuscript of the results to an international journal.

The last main objective, the bearing capacity characteristics of small-diameter spiral piles under the combined loads: (1) Demonstrating the misestimation of the bearing capacity of small diameter spiral piles under combined load by existing formulas, by using physical modeling experiments. (2) Proposing parameters to correct and adapt the existing formulas to the reality of spiral pile. (3) Propose a numerical model for spiral piles by using the obtained correction parameters (4) Use the numerical model to investigate the new formulas of bearing capacity of vertical] and batter spiral piles under combined load. (5) Validating the results of proposed the numerical model with those from physical modelling. (6) Validating the proposed formula against existing literature. (7) Submit for

publication in a journal.

1.4 Thesis Structure

This thesis consists of **6 chapters** including this introductory chapter. The following **Chapter 2** presents a review of existing methods for estimating the bearing capacity of the exceptional foundation cases in layered cited in **Section 1.2**, followed by a brief presentation of the numerical methods used in the research, and identifies gaps in estimating the bearing capacity of these exceptional foundation cases in layered. **Chapter 3** provides an overview of the published technical papers that form the main structure of the thesis. These papers are presented in **Chapter 4** through to **Chapter 6**. **Chapter 7** summarises the main contributions of this research, and the concluding remarks, together with recommendations for future works on this topic. **Chapter 8** list of references.

CHAPTER 2- LITERATURE REVIEW

2.1 Introduction

A detailed review of the literature on methods for estimating the bearing capacity of the three exceptional foundations on homogeneous and layered soils is presented in this chapter. By omitting this introduction, in the first section of this chapter, Terzaghi's conventional bearing capacity theory is introduced, as well as other solutions proposed by other researchers to estimate the ultimate bearing capacity of shallow foundations on homogeneous soils. A comprehensive discussion on the bearing capacity of strip footing on two-layered c-ϕ soils is presented next in the second section. This was followed by the presentation of existing failure patterns type of footing on two-layered c-ϕ soils. In the third section, a conventional pile end bearing capacity formula based on Terzaghi's theory is introduced, as well as other solutions proposed by other researchers. Existing theories of pile end bearing capacity that apply to IESP are discussed in the fourth section. The conventional formulas for horizontal and vertical bearing capacity for the bearing capacity of spiral piles are presented in section 5. The backgrounds of the numerical methods used in the investigations are presented in section 6. Finally, identified limitations of the existing methods of estimating the bearing capacity of the three exceptional foundations are discussed.

2.2 Bearing Capacity of Strip Footing on Homogeneous Soils

There have been several methods developed for estimating the bearing capacity of strip footings. Terzaghi (1948) introduced the first comprehensive bearing capacity theory, whose principles are still used in geotechnical engineering today. The fundamentals of Terzaghi's theory of strip footings over homogeneous soils, along with some major contributions by other researchers, are briefly presented here. In 1943, Terzaghi developed his method for estimating the bearing capacity by utilizing the limit equilibrium principle. The strip footing resting on a homogenous soil layer requires assuming the general shear failure which is depicted in **Fig. 2-1a**. There are three zones that contribute to foundation failure; a triangular elastic block that is immediately beneath the bottom of the foundation, a Prandtl radial shear fan, and a Rankine passive zone. A bearing capacity equation was derived by Terzaghi based on the equilibrium of the elastic wedge (**see Fig. 2-1b**). For a unit length of strip footing the wedge ABJ is equilibrated in the vertical direction as follows (Eshkevari, S. S., 2018):

$$q_u \times 2b \times (1) = -w + 2c_u \sin\phi + 2p_p \quad \text{.....(2-1)}$$

Where B = 2b and W is the weight of the elastic wedge $\gamma b^2 \tan\phi$. Thus.

$$2bq_u = 2p_p + 2bc_u \tan\phi - \gamma b^2 \tan\phi \quad \text{.....(2-2)}$$

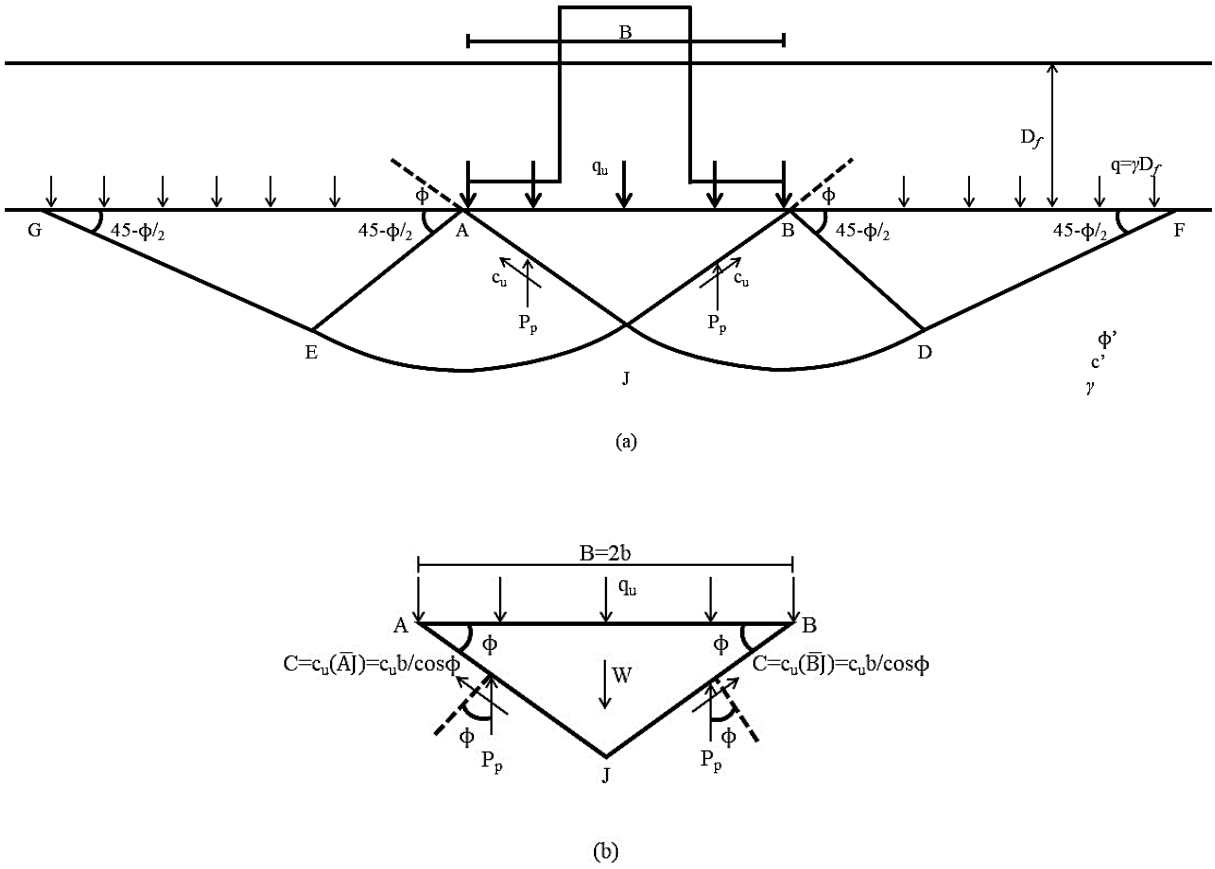

Fig. 2-1: General shear failure of a rough rigid strip footing on homogenous soil (after Terzaghi 1943).

When the passive forces (Pp) acting on the wedge sides of the footing are determined, the bearing capacity of the footing can be calculated. According to the equation, the passive force (Pp) is dependent on the soil unit weight, the soil cohesion, and the soil charge. Using an approximation method, Terzaghi estimated the mobilized passive forces Pp, taking into account separately the contribution of the factors discussed above, which vary with the soil friction angle. The passive soil force Pp can be written as follows according to **Fig. 2-2**:

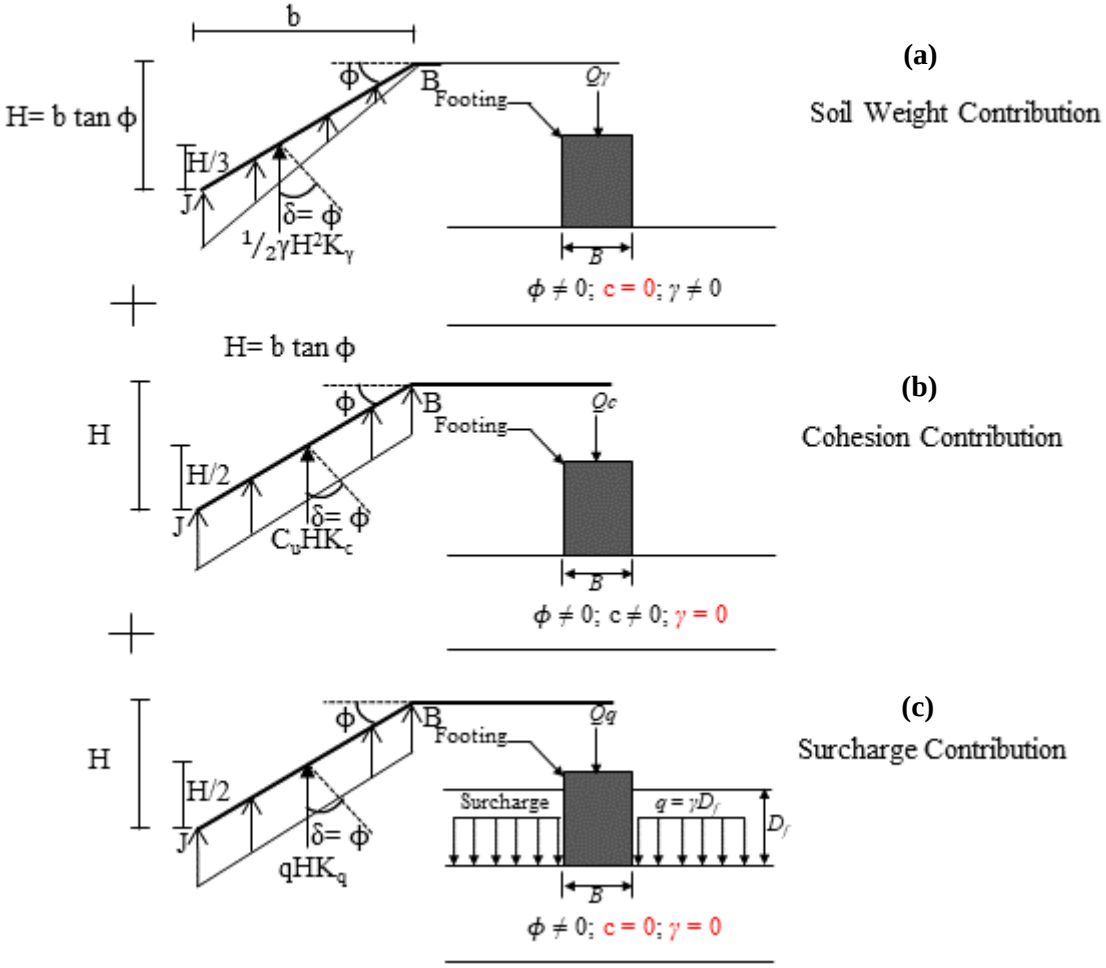

Fig. 2-2: Contributions of different factors to the bearing capacity of shallow foundations (after Terzaghi 1943).

$$P_p = \frac{1}{2}\gamma(b\tan\phi)^2 K_\gamma + c_u(b\tan\phi) K_c + q(b\tan\phi) K_q \quad \text{.....(2-3)}$$

where K_γ, K_c and K_q are coefficients that depend on the internal friction angle of soil. Substituting Equation 2-3 in **Eq. (2-2)** gives:

$$2bq_u = 2b\, c_u [\tan\phi\,(K_c + 1)] + 2b\, q\, [(\tan\phi K_q)] + b^2\gamma\, [\tan\phi\,(K_\gamma \tan\phi - 1)] \quad \text{.....(2-4)}$$

which, when rearranged gives the bearing capacity as:

$q_u = c_u [\tan\phi\ (K_c + 1)] + q [(\tan\phi K_q)] + \gamma \frac{B}{2} [\frac{1}{2} \tan\phi\ (K_\gamma \tan\phi - 1)]$ ……(2-5)

Or, in a simpler way

$q_u = c_u N_c + q N_q + \gamma \frac{B}{2} N_\gamma$ ……(2-5)

In the following three special cases, Terzaghi determined the passive force Pp and provided the following bearing capacity factors:

when $\phi \neq 0$, $\gamma = 0$, $q \neq 0$, $c_u = 0$ (see **Fig. 2-2c**), it is $N_q = \left[\frac{e^{2\left(\frac{3\pi}{4}-\frac{\Phi}{2}\right)\tan\Phi}}{2\cos^2\left(45+\frac{\Phi}{2}\right)}\right]$

when $\phi \neq 0$, $\gamma = 0$, $q = 0$, $c_u \neq 0$ (see **Fig. 2-2b**), it is $N_c = \cos\Phi \left[\frac{e^{2\left(\frac{3\pi}{4}-\frac{\Phi}{2}\right)\tan\Phi}}{2\cos^2\left(45+\frac{\Phi}{2}\right)} - 1\right]$ and

when $\phi \neq 0$, $\gamma \neq 0$, $q = 0$, $c_u = 0$ (see **Fig. 2-2a**), it is $N_\gamma = \left[\frac{1}{2} K_p \tan^2\Phi \left(\tan\Phi - \frac{\tan\Phi}{2}\right)\right]$

Terzaghi's assumed failure mechanism was generally confirmed by tests on model footings (**Fig. 2-1a**). Nevertheless, more research indicates the angle between the sides of the elastic wedge is closer to $45+\phi/2$ than ϕ. Meyerhof (1951) considered the failure mechanism of **Fig. 2-3** in which the angle between the sides of the elastic wedge and horizontal was assumed to be $45+\phi/2$ (Eshkevari, S. S., 2018).

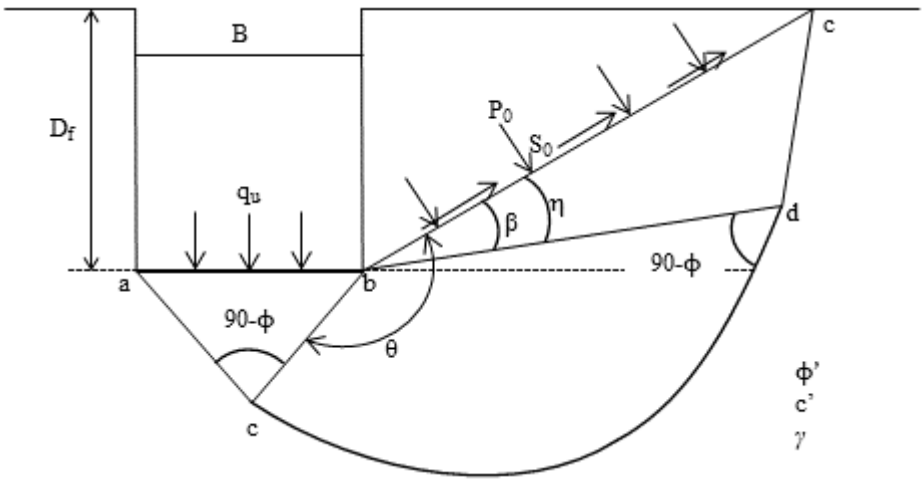

Fig. 2-3: Failure mechanism of a rough footing (after Meyerhof 1951)

Developed for cohesive-frictional soils, Meyerhof's bearing capacity theory applies to deep and shallow foundations. According to this theory, the shear resistance varies between radial and plane shear depending on the depth and roughness of the foundation. Meyerhof's failure mechanism includes an equivalent free surface (line be in **Fig. 2- 3**), over which mobilized shear stress is given by (Eshkevari, S. S., 2018):

$S_0 = m\,(c + P_0 \tan \phi)$ ……(2-7)

in which, m is the degree of mobilization of shear strength. Considering equilibrium of the plane bcd in **Fig. 2-3**, Meyerhof derived the cohesion and surcharge bearing capacity factors as:

$$N_c = \cot \phi \left[\frac{(1+\sin \phi)e^{2\theta \tan \phi}}{1-\sin \phi \sin(2\eta+\phi)} - 1\right] \quad \text{……...(2-8)}$$

$$N_q = \left[\frac{(1+\sin \phi)e^{2\theta \tan \phi}}{1-\sin \phi \sin(2\eta+\phi)}\right] \quad \text{……...(2-9)}$$

These bearing capacity factors are influenced by the angle of inclination of the equivalent free surface (b) and the degree of mobilization of shear strength on this plane (m). For surface strip footings both b and m are zero. In this case, θ = π /2 and h =45- ϕ /2. Thus, *N*q and *N*c are given by:

$$N_q = e^{\pi \tan \phi}\left[\frac{1+\sin \phi}{1-\sin \phi}\right] \quad \text{……...(2-10)}$$

$$N_c = \cot \phi \left(N_q - 1\right) \quad \text{……...(2-11)}$$

Essentially, for surface footings, Meyerhof's solution degenerates to the solution of Reissner (1924) and Prandtl (1920).

*N*γ may be found using a trial-and-error procedure, in which the center of the log-spiral zone is varied so that minimum passive force (Ppγ) is obtained. The passive force is only due to weight and friction i.e. c and P_0 are zero. In this case, Nγ is given by:

$$N_\gamma = \left[\frac{4p_{p\gamma}\sin[45+\phi/2]}{\gamma B^2} - \frac{1}{2}\tan[45+\phi/2]\right] \quad \text{(2-12)}$$

For surface strip footings, b= 0 and m= 0, thus Meyerhof suggested the following expression to approximate Nγ:

$$N_\gamma = \left(N_q - 1\right)\tan(1.4\phi) \quad \text{(2-13)}$$

Other researchers have proposed different formulas to calculate Nγ. Some of the most well-known solutions are presented in **Table 2-1**. All these expressions assume that the friction angle of soil is constant with depth. However, this is not an accurate assumption as the soil friction angle depends on the level of confining stress and varies with depth. Given the sensitivity of Nγ to variation of ϕ, these expressions should be used with caution to calculate the bearing capacity of shallow foundations on granular soils (ϕ soil).

Table 2-1: Bearing capacity factors Nγ by different researchers (Eshkevari, S. S., 2018).

Reference	Method of analysis	Proposed expression for N_γ
Hansen (1970)	Limit Equilibrium	$N_\gamma = 1.5N_c \tan^2 \phi$
Vesic (1973)	Limit Equilibrium	$N_\gamma = 2(N_q + 1)\tan \phi$
Biarez et al. (1961)	Upper Bound Limit Analysis	$N_\gamma = 1.8(N_q - 1)\tan \phi$
Booker (1969)	Slip Line Method	$N_\gamma = 0.1045e^{9.6\,\phi}$
Michalowski (1997)	Upper Bound Limit Analysis	$N_\gamma = e^{(0.66+5.1\tan\phi)}\tan\phi$
Hjiaj et al. (2005)	Finite Element Limit Analysis	$N_\gamma = e^{1/6(\pi+3\pi^2\tan\phi)}\tan\phi^{(2\pi/5)}$
Martin (2005)	Method of characteristics	$N_\gamma = (Nq - 1)\tan(1.32\phi)$

N_q and N_c are given by **Eq. (2-10)** and **Eq. (2-11)**, respectively. ϕ is in radian, Nγ = 0 for ϕ = 0.

Subsequently, the bearing capacity theory went through many modifications to take into account different features such as foundation shape, load inclination, ground slope, non-symmetrical loads, and water table by many researchers. The form of the bearing capacity equation taking account of these parameters can be written as follows:

$$q_{\text{ult}} = cN_cS_cd_ci_c + qN_qS_qd_qi_q + 0.5\gamma BN_\gamma S_\gamma d_\gamma i_\gamma \quad \text{(2-14)}$$

where S_c, S_q and S_γ = shape factors; d_c, d_q and d_γ = depth factors; i_c, i_q and i_γ = inclination factors; c, q, γ, N_c, N_q and N_γ and B are the same as defined above.

2.3 Some Existing Formulas of Bearing Capacity of Strip Footing on Two-Layered C-ϕ Soils

2.3.1 General

The studies concerning the shallow foundations on two-layered c-ϕ soils (**Fig. 2-4**) have received less attention in the literature. An exact analytical solution is not available. The ultimate bearing capacity of footings on such layered soil also depends on the properties of the bottom layer, unless the thickness of the top soil is large enough to contain the entire failure mechanism. Therefore, the conventional bearing capacity theory, discussed in the previous section is not valid for this type of layered soil. Various techniques have been employed by researchers to estimate the ultimate bearing capacity of footings on two-layered c-ϕ soils. However, a robust bearing capacity model that considers the behavior of layered soils for a wide range of material parameters and problem geometries encountered in practice, is yet to be developed. Some of the most influential studies on this topic are reviewed in the following section. Including the studies by Purushothamaraj et al. (1974), Satyanarayana and Garg (1980), Florkiewicz (1989), Azam and Wang (1991), and Bowles (1996).

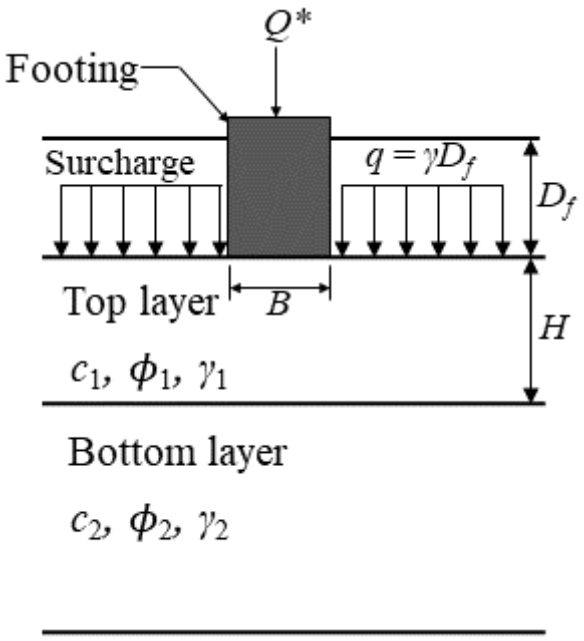

Fig. 2-4. shallow foundations on two-layered c-ϕ soils

2.3.2 Method of Purushothamaraj et al. (1974)

Following the Prandtl-Terzaghi mechanism with changing the wedge angles, Purushothamaraj et al. (1974) have formulated a method applicable for any combination of key properties of a homogeneous two-layered soils system. **Fig. 2-5** illustrates the failure mechanism proposed by Purushothamaraj et al. (1974).

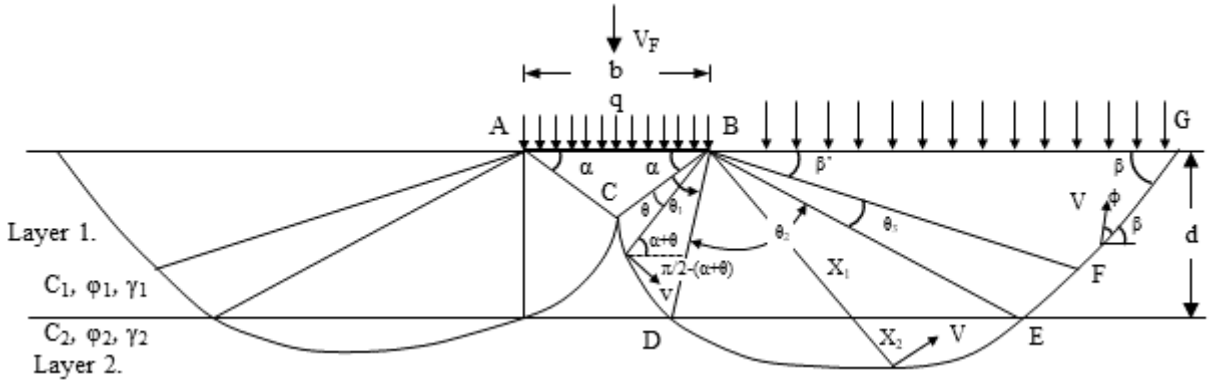

Fig. 2-5. Failure mechanism used by Purushothamaraj *et al.* (1974)

They have studied two cases regarding the location of the central wedge, i.e. on the top layer and extending to the bottom layer, determining both the external and internal work done, including that of the weight of soil, and eventual summation of them. In the case of a central wedge located on the top layer only (d > b/2 tan α, on **Fig. 2-5**), Purushothamaraj et al. (1974) have proposed **Eq.2-15** below for the calculation of the bearing capacity.

$$q_{ult} = c_1 N_c + \gamma_1 D_f q N_q \ + 0.5\gamma_1 b N_\gamma \quad \text{(2-15)}$$

Where *N*c, *Nq*, and *Nγ*, are nondimensional factors that are functions of φ_1/φ_2, c_1/c_2, γ_1/γ_2, α, and β. Expressions for *Nc*, *Nq* and *Nγ* are given by.

$$\text{[i]}\ N_c = \frac{\cot\varphi_1}{[\sin(\alpha-\varphi_1)+\cos\alpha]}\left\{\left[(\sin\varphi_1 - 1) + \frac{(1-c_2/c_1)\sin(\alpha+\theta_1)}{\cot\varphi_1} e^{2\theta_1\tan\varphi_1} I_1 + e^{2\theta_1\tan\varphi_1}\left[1 - \frac{c_2\tan\varphi_1}{c_1\tan\varphi_2} + e^{2\theta_2\tan\varphi_2}\left[\left(\frac{c_2\tan\varphi_1}{c_1\tan\varphi_2} - 1\right) + e^{2\theta_3\tan\varphi_1}[1+\sin\varphi_1]\right]\right]\right]\right\}$$

[ii] $N_q = \frac{e^{2\theta_1 \tan\varphi_1} e^{2\theta_2 \tan\varphi_2} e^{2\theta_3 \tan\varphi_1}}{[\sin(\alpha-\varphi_1)+\cos\alpha]\cos\alpha} \frac{\cos\varphi_1}{\sin\beta} \sin(\beta+\varphi_1)$

[iii] $N_\gamma = -\frac{1}{[\sin(\alpha-\varphi_1)+\cos\alpha]\cos^2\alpha}\Big[\sin\alpha\cos\alpha\sin(\alpha-\varphi_1) + (1-\gamma_2/\gamma_1)\frac{\sin(\alpha+\theta_1)I_2}{2} + \frac{e^{3\theta_1\tan\varphi_1}}{(1+9\tan^2\varphi_1)}\Big\{\Big[\cos(\alpha+\theta_1) + e^{3\theta_2\tan\varphi_1} - e^{3\theta_3\tan\varphi_1}\cos(\alpha+\theta_1+\theta_2+\theta_3)\Big] + \frac{1}{3\tan\varphi_1}\Big[\sin(\alpha+\theta_1) + e^{3\theta_2\tan\varphi_2}e^{3\theta_3\tan\varphi_1}\sin(\alpha+\theta_1+\theta_2+\theta_3)\Big] - \cos\alpha - e^{3\theta_1\tan\varphi_1}e^{3\theta_2\tan\varphi_2}\cos(\alpha+\theta_1+\theta_2) - \frac{1}{3\tan\varphi_1}\Big[\sin\alpha + e^{3\theta_1\tan\varphi_1}e^{3\theta_2\tan\varphi_2}\sin(\alpha+\theta_1+\theta_2)\Big]\Big\} + \frac{3\gamma_2/\gamma_1\tan\varphi_2}{2(1+9\tan^2\varphi_2)}\Big\{e^{3\theta_2\tan\varphi_2}\Big[\cos(\alpha+\theta_1+\theta_2) + \frac{\sin(\alpha+\theta_1+\theta_2)}{3\tan\varphi_2}\Big] - \cos(\alpha+\theta_1) - \frac{\sin(\alpha+\theta_1)}{3\tan\varphi_2}\Big\} - \frac{1}{2}e^{3\theta_1\tan\varphi_1}e^{3\theta_2\tan\varphi_2}e^{3\theta_3\tan\varphi_1}\sin 2\beta\sin(\beta+\varphi_1)\Big]$

Where,

[iv] $I_1 = \int_0^{\theta_2} \frac{e^{\theta\tan\varphi_2}}{\sin(\alpha+\theta_1+\theta)}\,d\theta$ (for $\theta_1 = \theta_2$)

[v] $I_2 = \int_0^{\theta_2} e^{2\theta\tan\varphi_2}\cot(\alpha+\theta_1+\theta)\,d\theta$

2.3.3 Method of Satyanarayana and Garg (1980)

Satyanarayana and Garg (1980) have proposed a simplified bearing-capacity theory for shallow foundations in *c*-ϕ soils. In their method, a limited thickness of the bottom layer H_2 is contributing to the bearing capacity (See **Fig. 2-6**). According to their theory, the ultimate bearing capacity of a two-layered soil is given by:

$$q_{\text{ult}} = c_{\text{av}}N_{\text{c}} + qN_{\text{q}} + 0.5\gamma_1 BN_\gamma \quad \cdots\cdots (2\text{-}16)$$

where

$$c_{\text{av}} = \frac{Hc_1 + H_2{}^* c_2}{H + H_2{}^*}, \quad \phi_{\text{av}} = \tan^{-1}\left(\frac{H\tan\phi_1 + H_2{}^*\tan\phi_2}{H+H_2{}^*}\right), \quad H_2{}^* = (2B-H)\left(\frac{c_1+\tan\phi_1}{c_2+\tan\phi_2}\right)$$

N_{c}, N_{q} and N_γ are bearing capacity factors based on ϕ_{av}.

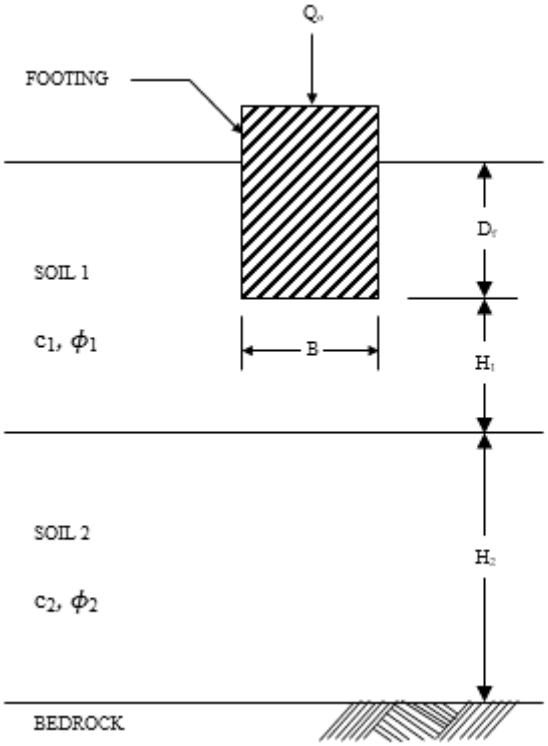

Fig. 2-6 Model used by Satyanarayana and Garg (1980)

2.3.4 Method of Azam and Wang (1991)

Azam and Wang 1991 investigated the bearing capacity of an embedded strip footing supported by two-layer *c*-ϕ soils using an elastoplastic finite-element computer program. Based on the analysis results, they developed a semiempirical equation for determining the ultimate bearing capacity. The equation proposed by Azam and Wang 1991 is:

$$q_0 = q_t + (q_b - q_t)\,[1 - m(H/B)]^2 \quad \text{(2-17)}$$

q_0 = ultimate bearing capacity of strip footing over two-layer soil

q_t = ultimate bearing capacity of the footing supported by an infinitely thick top-layer soil, computed by the traditional bearing capacity equation using factors recommended by Vesic 1973

q_b = ultimate bearing capacity of the footing supported by an infinitely thick bottom-layer soil, computed by the same method as q_t

m = empirical parameter, which is 0.17-0.23 for two layers of clay (use of the lower value is recommended if one clay layer is highly compressible, otherwise use the average value) and 0.30 for a

sand-clay layer combination and

H/*B* = top-layer-thickness-to-footing-width ratio, which is no more than 6 for clay-clay layers and no more than 3.5 for sand-clay layers

2.3.5 Method of Bowles (1996)

Bowles 1996 has also proposed a formula for the calculation of the bearing capacity of two-layered soils considering the location of the central wedge, i.e. on the top layer ($H > B/2 \tan(45+ \phi_1/2)$) and extending to the bottom layer ($H < B/2 \tan(45+ \phi_1/2)$), with $B/2 \tan(45+ \phi_1/2) = d$ the depth of the central wedge. The formula proposed by Bowles 1996 is like the one of Satyanarayana and Garg 1980 and is as follows.

$$q_{\text{ult}} = c_{\text{m}} N_{\text{c}} + q N_{\text{q}} + 0.5 \gamma_1 B N_{\gamma} \quad \cdots\cdots\cdots\cdots\cdots\cdots\cdots\cdots\cdots\cdots\cdots\cdots\cdots\cdots\cdots\cdots\cdots\cdots\cdots\cdots\cdots\cdots\cdots\cdots\cdots\cdots \quad (2\text{-}18)$$

$$d = \frac{B}{2} \tan\left(45 + \frac{\phi_1}{2}\right), \text{ if } d > H \;\; \phi_m = \left(\frac{H\phi_1 + (d-H)\phi_2}{d}\right), \quad c_m = \left(\frac{Hc_1 + (d-H)c_2}{d}\right)$$

N_{c}, N_{q} and N_{γ} are bearing capacity factors based on ϕ_{m}.

2.3.6 Type of Failure

The nature of bearing capacity failure in two-layered soils proposed by several authors is presented in **Fig. 2-7** There are “General shear failure”, “Local shear failure”, “Transitional shear failure” and “Punching shear failure”.

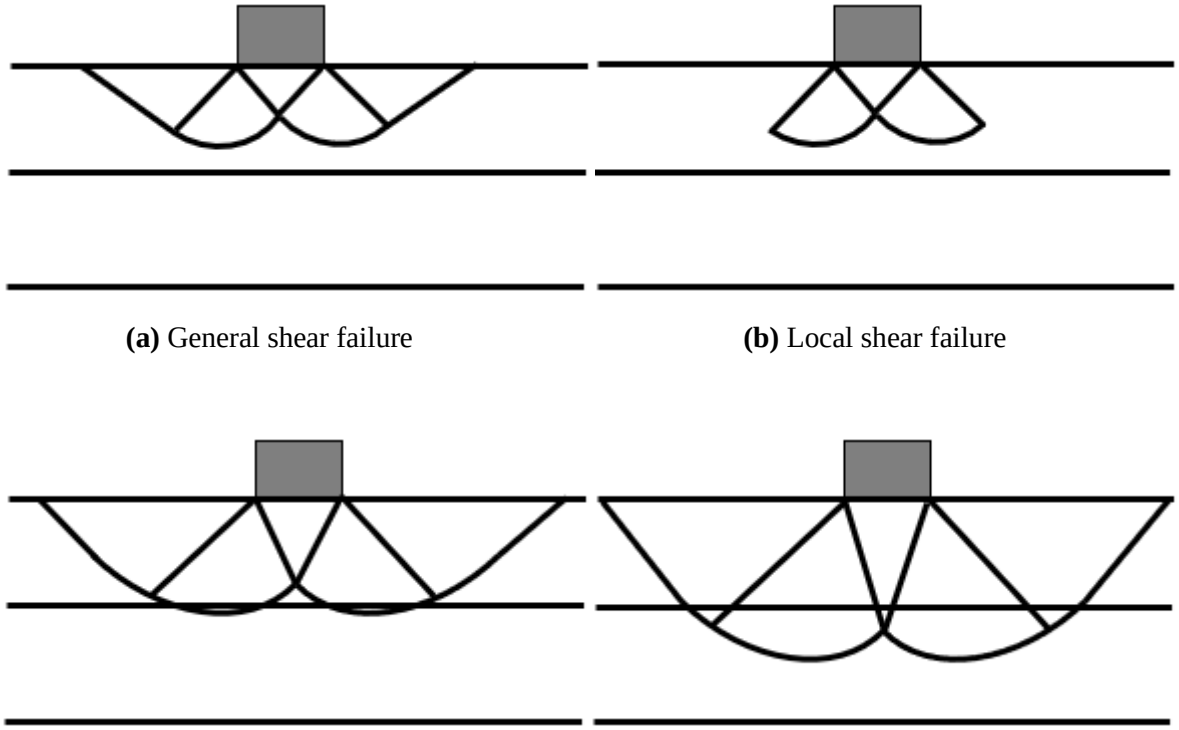

(a) General shear failure **(b)** Local shear failure

(c) Transitional shear failure **(d)** Punching shear failure

Fig. 2-7 Nature of bearing capacity failure in soil drawn after Vesic [46]; (a) General shear failure, (b) Local shear failure; drawn after Salimi et al. [40], (c) Transitional shear failure and (d) Punching shear failure

2.4 Theoretical Formula of Pile End Bearing Capacity

The ultimate end bearing capacity of a pile, q_{pult}, may be expressed by an equation similar to that of a footing proposed by Terzaghi (1943) as follow:

$$q_{\text{pult}} = cN_{\text{c}} + qN_{\text{q}} + 0.5\gamma BN_{\gamma} \quad \text{(2-19)}$$

where B = diameter or width of the pile, q = overburden pressure, c = cohesion of soil, γ= unit weight of soil and N_{c}, N_{q} and N_{γ} are bearing capacity factors for deep foundations which are different from those of shallow foundations.

Because the width B of the pile is relatively small, the third term $0.5\gamma BN_{\gamma}$ becomes insignificant in comparison with the second term qN_{q} and is dropped. Therefore **Eq. (2-19)** reduces to

$$q_{\text{pult}} = cN_{\text{c}} + qN_{\text{q}} \quad \text{(2-20)}$$

Vesic (1967) has revealed that the bearing capacity of a pile remains constant beyond a critical depth, and N_q depends on ϕ and D/B (where D = length of embedment, B = diameter or width of the pile).

Meyerhof (1976) proposed the critical depth ratio (D_c/B) in **Fig. 2-8** for N_c and N_q. N_c and N_q increase with D_b/B and reach a maximum value at D_b/B equal to about 0.5 (D_c/B), where D_b is the actual thickness of the bearing stratum. In a homogeneous soil, D_b is equal to the embedded length of the pile (L); whereas, in layered soil, D_b is less than L.

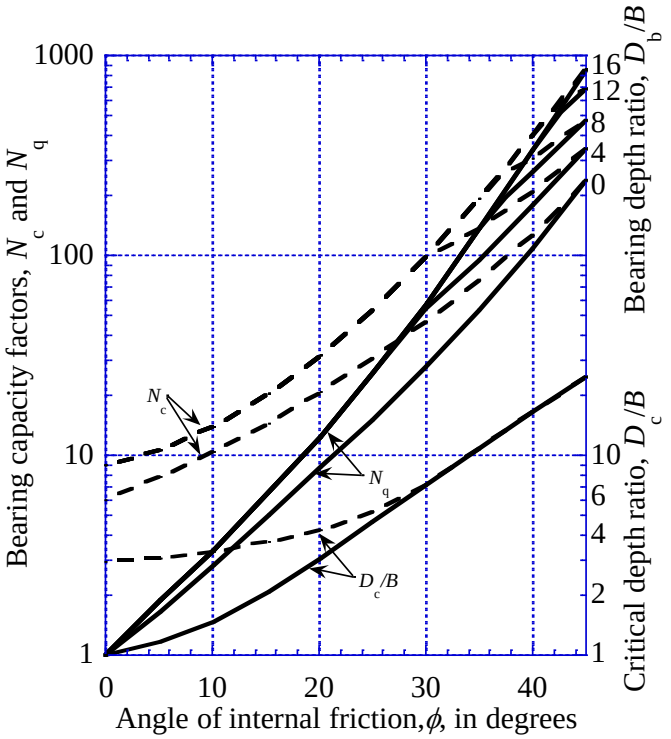

Fig. 2-8 Bearing capacity factors and critical depth ratios for driven piles. (After Meyerhof (1976))

Meyerhof prescribed a limiting value for q_{pult}. The expression for the limiting value, q_{pl} is:

for dense sand: $q_{pl} = 50N_q \tan\phi$ (kN/m^2) ····· (2-21)

for loose sand: $q_{pl} = 25N_q \tan\phi$ (kN/m^2) ····· (2-22)

The equation for tip resistance in sand may now be expressed as

$$q_{pult} = q'_0 N_q \leq q_{pl} \quad \cdots\cdots (2\text{-}23)$$

where q'_0 = effective overburden pressure at the tip of the pile corresponding to D_c/B and N_q = bearing capacity factor **(Fig. 2-8)**. **Eq. (2-23)** is applicable only for driven piles in sand. For bored cast-in-situ

piles, the value of q_{pult} is to be reduced by one-third to one-half.

2.5 Theoretical Formulas Applicable to end Bearing Capacity of IESP

2.5.1 General

Some researchers have to investigate the end bearing capacity of pile in layered ground similar to IESP. Ikeda et al. (2012) have conducted laboratory loading tests of pile in layered sand and found that the end bearing capacity decreases significantly when the pile moves away from the bottom hard layer, which is very similar to the case of IESP. However, they did not propose any formula for the influence of the bottom layer on the end bearing capacity.

Pholkainuwatra1et al. (2022) conducted an experimental study of pile set-up of driven piles in Bangkok clay using seven piles with their pile tips varied between 8-21 meters below ground level. The soil condition is changing with depth from soft clay with 12 meters of thickness passing by 6 meters of medium clay to 4 meters of stiff clay. These soil conditions and the pile's position make the study of Pholkainuwatra1et al. (2022) similar to IESP. However, they did not mention the effect of the layers on the bearing capacity or the formula for it.

Teramoto et al. (2015) have conducted a FEM analysis to investigate the mechanical behaviors of Incompletely End-Supported Piles. They also found that the gap between the pile tip and bottom layer influences the bearing capacity but did not propose a formula. Hyodo et al. (2020) studied the end bearing capacity of IESP in sand using a three-dimensional elastoplastic FEM analysis. They proposed a ratio of the degradation of the end bearing capacity of IESP when the pile tip moves away from the bottom layer. However, their proposed formula applied to sand only.

According to Gunaratne (2006), the end bearing capacity of pile is like the bearing capacity of footing with large embedment. Considering this, the theories cited in **Section 2.3** above for strip footings on two-layered c-ϕ soils [Satyanarayana and Garg (1980), Azam and Wang (1991), Bowles (1996)…], which consider the influence of the distance H between the footing and the bottom layer, can be used to analyze the characteristics of the end bearing capacity of IESP for any type of soil, in that case, the bearing capacity factors in **Fig 2. 8** are used.

2.5.2 Method of Hyodo et al. (2020)

Hyodo et al. (2020) studied the end bearing capacity of IESP in sand using an elastoplastic FEM and proposed **Eq. (2.24)** below to estimate the end bearing capacity.

$$q_{\text{unreached}} = \alpha q_{\text{base}} + (1-\alpha) q_{\text{nobase}} \quad \text{(2-24)}$$

where $q_{\text{unreached}}$ is the pile end resistance of IESP, q_{base} is the pile end resistance of the completely end-supported pile, q_{nobase} is the pile end resistance of the pile with no lower hard layer and α is the degradation factor which represents the incompleteness of the pile end support.

In the study by Hyodo et al. (2020), the bottom layer was very dense sand with relative density D_r = 90% and the top layer was changed from loose sand to medium sand and dense sand with relative densities D_r = 45%, D_r = 60% and D_r = 75%, respectively.

The value of $q_{\text{unreached}}$ and q_{base} can be obtained by the conventional method of pile end bearing capacity. **Fig. 2-9** shows the variation of α as a function of d/B (the distance to the bottom layer).

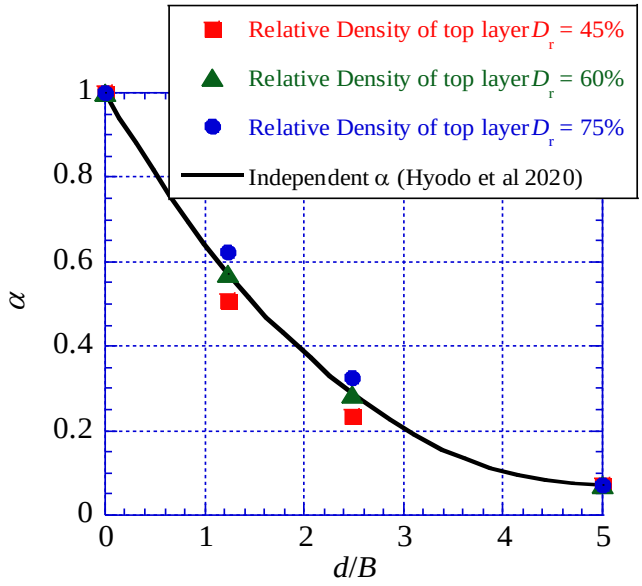

Fig. 2-9 Value of α in the method of Hyodo et al. (2020)

2.6 The Conventional Formulas for Horizontal and Vertical Bearing Capacity for the Bearing Capacity of Spiral Pile

The equation of the conventional vertical (push-in and pull-out) bearing capacity is presented in **Eq.**

(2.25) and the conventional horizontal resistance of pile can be obtained by Chang's equation **Eq. (2.26).**

$$R_u = q_p A_p + \tau_c L_c \phi \tag{2-25}$$

$$y_t = \frac{(1+\beta h)^3 + 1/2}{3EI\beta^3} H + \frac{(1+\beta h)^2}{2EI\beta^2} M \tag{2-26}$$

Where, Ru: the vertical ultimate bearing capacity (kN), q_p: the ultimate bearing capacity of the ground at the pile tip (kN/m^2), A_p: the area of the pile tip (m^2), τ_c: the peripheral frictional force (kN/m^2), L_c: the thickness of the layer for which peripheral frictional force is considered (m), ϕ: the length of the pile circumference (m), y_t: the horizontal displacement of the pile head (m), β: characteristic value of the foundation (m^{-1}), h: the pile protrusion length (m), EI: the flexural rigidity of the pile (kN-m^2), H: the horizontal load (kN), M: the pile head moment (kN-m), q_u: the uniaxial compression strength (kN/m^2), N: N value converted by Swedish sounding test.

2.7 The Background of The Numerical Methods Used in the Thesis

2.7.1 Constitutive Equations for Rigid Plastic Finite Element Method

The rigid-plastic finite element method (RPFEM) was developed for geotechnical engineering by Tamura et al. (1984 and 1987). In this method, the limit load is calculated without any assumption of a potential failure mode. The method is effective in calculating the ultimate bearing capacity of shallow foundations and deep foundations where the soil conditions are varied, such as a multi-layered ground.

In this study, the in-house RPFEM code developed and upgraded by Hoshina et al. (2011) and Du et al. (2016), is used for estimation of the end bearing capacity of a single Incompletely End-Supported Pile. The rigid plastic constitutive equation for the Drucker-Prager yield function was employed first. Then, the non-linear shear strength property against confining pressure, introduced by Du et al. (2016) in RPFEM, was considered. The Drucker-Prager yield function is expressed with **Eq. (2-27)** and for considering the non-linear shear strength property against confining pressure, **Eq. (2-28)** referred to as the High Order yield function was used. Both yield functions are used in plane strain conditions considering the associated flow rule. Since the plane strain condition is used, the simulated end bearing capacity is that of a continuous wall, however, by employing shape factors, it can be converted to the end bearing capacity of a pile.

$$f(\sigma) = \alpha_{DP} I_1 + \sqrt{J_2} - \kappa = 0 \quad \cdots\cdots (2\text{-}27)$$

$$f(\sigma) = aI_1 + (J_2)^n - b = 0 \quad \cdots\cdots (2\text{-}28)$$

where, $\boldsymbol{I}_1 = \mathrm{tr}(\sigma_{ij})$ is the first invariant, $\boldsymbol{J}_2 = \frac{1}{2} s_{ij} s_{ij}$, α_{DP}, κ, a and b are soil parameters. α_{DP} and κ are expressed for plane strain condition as follows:

$$\alpha_{DP} = \frac{\tan\phi}{\sqrt{9+12\tan^2\phi}}, \kappa = \frac{3c}{\sqrt{9+12\tan^2\phi}} \quad \cdots\cdots (2\text{-}29)$$

where c is cohesion, ϕ is shear resistance angle.

The parameters n, a and b in the High Order yield function **Eq. (2-28)** are coefficients representing the non-linear shear strength property against confining pressure for the soil; n is standing for the strength non-linearity; a and b are relating to the shear resistance angle ϕ and the cohesion c, respectively. As a remark, when n in the High Order yield function is 0.5 the two Equations, **Eq. (2-27)** and **Eq. (2-28)** are the same. When n is higher than 0.5, the plot of $\sqrt{J_2}$ against I_1 gives a linear line with **Eq. (2-27)**, but a curved line with **Eq. (2-28) (see Fig. 2-10)**.

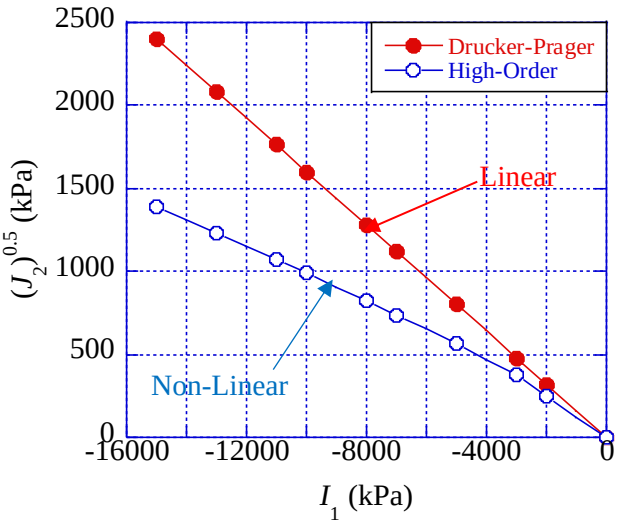

Fig. 2-10 Difference between the yield function of Drucker-Prager the and High-Order model

For the Drucker-Prager yield function, the volumetric strain rate for the Rigid Plastic constitutive equation is expressed as follows:

$$\dot{\varepsilon}_v = \mathrm{tr}(\dot{\boldsymbol{\varepsilon}}) = \mathrm{tr}\left(\lambda \frac{\partial f(\boldsymbol{\sigma})}{\partial \boldsymbol{\sigma}}\right) = \mathrm{tr}\left(\lambda\left(\alpha \boldsymbol{I} + \frac{\boldsymbol{s}}{2\sqrt{J_2}}\right)\right) = \frac{3\alpha}{\sqrt{3\alpha^2 + \frac{1}{2}}}\dot{e} \quad \cdots\cdots (2\text{-}30)$$

where λ is the plastic multiplier and $\dot{e}$ is the norm of the strain rate. $\boldsymbol{I}$ and $\boldsymbol{s}$ express the unit and the deviator stress tensors, respectively. Strain rate $\dot{\boldsymbol{\varepsilon}}$, which is a purely plastic component, should satisfy the volumetric constraint condition which is derived by **Eq. (2-31)**, as follows:

$$h(\dot{\boldsymbol{\varepsilon}}) = \dot{\varepsilon}_v - \frac{3\alpha}{\sqrt{3\alpha^2+\frac{1}{2}}}\dot{e} = \dot{\varepsilon}_v - \eta\dot{e} = 0 \cdots\cdots (2\text{-}31)$$

Any strain rate which is compatible with the Drucker–Prager yield criterion must satisfy the kinematical constraint conditions of **Eq. (2-31)**. η is a coefficient determined by **Eq. (2-31)** which is one of the dilation characteristics. The rigid plastic constitutive equation is expressed by the Lagrangian method after Tamura et al. (1987), as follows:

$$\boldsymbol{\sigma} = \frac{\kappa}{\sqrt{3\alpha^2+\frac{1}{2}}}\frac{\dot{\boldsymbol{\varepsilon}}}{\dot{e}} + \beta\left(\boldsymbol{I} - \eta\frac{\dot{\boldsymbol{\varepsilon}}}{\dot{e}}\right) \cdots\cdots (2\text{-}32)$$

The first term expresses the stress component, uniquely determined for the yield function. The second term expresses the indeterminate stress component along with the yield function. The indeterminate stress parameter β remains unknown until the boundary value problem with **Eq. (2-31)** is solved. In this study, a penalty method is used to make the computation faster and more stable following Hoshina et al. (2011), as follows:

$$\boldsymbol{\sigma} = \frac{\kappa}{\sqrt{3\alpha^2+\frac{1}{2}}}\frac{\dot{\boldsymbol{\varepsilon}}}{\dot{e}} + P(\dot{\varepsilon}_v - \eta\dot{e})\left(\boldsymbol{I} - \eta\frac{\dot{\boldsymbol{\varepsilon}}}{\dot{e}}\right) \cdots\cdots (2\text{-}33)$$

where P is a penalty constant.

For the High Order yield function, based on the associated flow rule, the strain rate is obtained as follows:

$$\dot{\boldsymbol{\varepsilon}} = \lambda\frac{\partial f(\boldsymbol{\sigma})}{\partial\boldsymbol{\sigma}} = \lambda\frac{\partial}{\partial\boldsymbol{\sigma}}(aI_1 + (J_2)^n - b) = \lambda\,(a\boldsymbol{I} + n(J_2)^{n-1}\,\boldsymbol{s}) \cdots\cdots (2\text{-}34)$$

In the above equation, λ is the plastic multiplier. The volumetric strain rate is expressed as:

$$\dot{\varepsilon}_v = \mathrm{tr}(\dot{\varepsilon}) = \mathrm{tr}\big(\lambda\,(a\boldsymbol{I} + n(J_2)^{n-1}\,\boldsymbol{s})\big) = 3a\lambda = \frac{3a}{\sqrt{3a^2+2n^2\,(b-aI_1)^{2-1/n}}}\dot{e} \cdots\cdots (2\text{-}35)$$

First stress invariant I_1 is identified from **Eq. (2-35)** as the following equation:

$$\boldsymbol{I}_1 = \frac{b}{a} - \frac{1}{a}\left\{\frac{1}{2n^2}\left[\left(3a\frac{\dot{e}}{\dot{\varepsilon}_v}\right)^2 - 3a^2\right]\right\}^{\frac{n}{2n-1}} \cdots\cdots (2\text{-}36)$$

The non-linear rigid plastic constitutive equation for the High Order yield function is finally obtained as follows:

$$\sigma = \frac{3a}{n}\left\{\frac{1}{2n^2}\left[\left(3a\frac{\dot{e}}{\dot{\varepsilon}_v}\right)^2 - 3a^2\right]\right\}^{\frac{1-n}{2n-1}}\frac{\dot{\varepsilon}}{\dot{\varepsilon}_v} + \left(\frac{b}{3a} - \frac{1}{3a}\left[\frac{1}{2n^2}\left(3a\frac{\dot{e}}{\dot{\varepsilon}_v}\right)^2 - 3a^2\right]^{\frac{n}{2n-1}} - \frac{a}{n}\left[\frac{1}{2n^2}\left(3a\frac{\dot{e}}{\dot{\varepsilon}_v}\right)^2 - 3a^2\right]^{\frac{1-n}{2n-1}}\right)\boldsymbol{I} \quad \cdots\cdots (2\text{-}37)$$

In this equation, the stress is uniquely determined for the plastic strain rate and is different from **Eq. (2-23)** for the Drucker‐Prager yield function.

The advantage of the rigid plastic constitutive equation is that only a few soil parameters such as unit weight, cohesion and shear resistance angle are necessary. In the simulation, the foundation is modeled by the rigid plastic constitutive equation as rigid material to focus on the plastic behavior of the soils around the foundation subjected to loading. So, the elastic modulus and Poisson's ratio are not necessary in the RPFEM simulation method. The High order yield function considers the reduction of the shear resistance angle due to high confining pressure, therefore, it avoids the overestimation of volumetric strain in ϕ and c-ϕ soils and it gives more reasonable end-bearing capacity values of piles in those soils.

2.7.2 Limitations of the Rigid Plastic Finite Element Method

The RPFEM has a lot of advantages among which we can enumerate: (1) Limit load is calculated without any assumption of a potential failure mode; (2) Only a few soil parameters are needed, which are the cohesion (c), the internal friction angle (ϕ) and the unit weight (γ); (3) It is effective in calculating the ultimate bearing capacity of foundations with varying soil conditions, such as a multi-layered ground and (4) It focus on the ultimate (limit) state, which cannot be performed by Elastic-Plastic FEM. However, the method has also some limitations which we are trying to highlight in this section as follows:

(1) At the present stage of the code, both (Drucker-Prager and High Order) yield functions are used in plane strain conditions only. So RPFEM cannot solve problems that necessitate axisymmetric analysis yet.

(2) It is found that when the non-associated flow rule is considered in RPFEM, the simulation time is considerably long, and the result obtain as well is not reasonable. In the Drucker-Prager yield function, when the associate flow rule is used, the dilation angle may contribute to overestimating the volumetric strain, however, this problem can be handled by the High Order yield function.

(3) The method is specially established for rigid foundations, hence for foundations that may developpe elastic behaviour, RPFEM is not suitable.

2.7.3 The Elastoplastic FEM

In this thesis, the 3D elastoplastic finite element analysis code "DBLEAVES" developed by Ye et al. (2007) will be used to analyze the bearing capacity of spiral piles subjected to combined loads. In this reproduction analysis, a spiral pile with a complicated shape will be simplified into a model using the skeleton-beam type hybrid element proposed by Zhang et al. (2000) and verified for usefulness by Danno and Kimura (2009) as shown in **Fig. 2-11**.

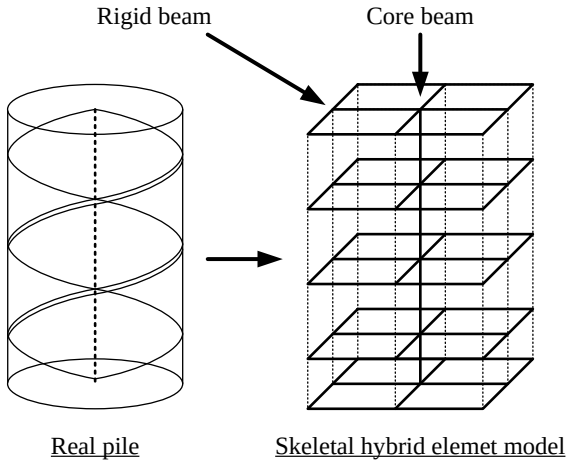

Fig. 2-11. Skelton-beam type hybrid element

2.8 Concluding Remarks

The review of the most common methods for estimating the bearing capacity of the three complex foundation types investigated in this thesis indicates that a model which balances accuracy and practicality is still missing for each foundation type investigated.

2.8.1 Remarks on the Literature of Bearing Capacity of Strip Footing on Two-Layered C-ϕ soils

As it is seen from the review, only a few studies are available with regard to the shallow foundations on two-layers c-ϕ soils. And the available theories were developed from experimental tests and analytical solutions and have limitations that restrict their use to idealized conditions. For example, the equation of Purushothamaraj et al. (1974) is applicable for any combination of key properties of a homogeneous two-layered soil system. However, the equation is too complex and has many changing parameters, which makes its application in practicable engineering less convenient. The equation of Satyanarayana and Garg (1980) is easy in application and can be used for almost any soil, however, the bearing capacity factors are obtained with an average shear resistance angle and a limited thickness of the bottom layer (H_2), which is not reflect the reality. Azam and Wang (1991) used three soils (silty clay, kaolin, and clayey sand) with very specific strength parameters in their study. The specific strength parameters of those soil have an influence on their method. Therefore, their method may lead to some discrepancies when extended to soils with different strength parameters. The equation of Bowles (1996) is also very simple and easy for application. The equation is assuming that the critical thickness of the top soil layer is equivalent to the depth of the central wedge of the failure pattern. The critical thickness of the top layer is defined here as the thickness above which the bottom layer has no influence. However, this assumption may underestimate the actual critical thickness due to punching shear failure. And underestimating the critical thickness will underestimate the contribution of the soft bottom layer, which leads to overestimating the bearing capacity.

2.8.2 Remarks on the Theoretical Formulas Applicable to End Bearing Capacity of IESP

As mentioned in the review, only the formula of Hyodo et al. (2020) exist in the literature for the end-bearing capacity of IESP. However, Hyodo et al. (2020) is applicable for sand only. Therefore, there is no concrete solution for the end bearing capacity of IESP for all different types of soils. However, some formulas of strip footing can be adapted to the end bearing capacity of IESP. **Table 2-2** shows the summary of some methods and the associated advantages and disadvantages with respect to the estimation of the end bearing capacity of IESP.

Table 2-2 Application conditions and limitations of the existing methods

Formula	Disadvantages with respect to the estimation of the end bearing capacity of IESP	Advantages with respect to the estimation of the end bearing capacity of IESP
Eq. 2-20: Terzaghi (1943), Vesic (1967) and Meyerhof (1976)	• Cannot directly estimate the end bearing capacity of IESP alone.	• Can be used to calculate q_{base} and q_{nobase} of Hyodo et al. (2020) • Can be used to calculate q_b and q_t of Azam and Wang (1991) • N_c and N_q of **Eq. 2-20** can be used in Satyanarayana and Garg (1980)
Eq. 2-24: Hyodo et al. (2020)	• Applicable for sand only. • Does not consider the strength ratio of the two soil layers.	• Gives a reasonable end-bearing capacity of IESP in sand.
Eq. 2-16: Satyanarayana and Garg (1980) and **Eq. 2-18** Bowles (1996)	• Using average values of strength parameters (not realistic).	• Can be used for any type of soil and gives reasonable results.
Eq. 2-17: Azam and Wang (1991)	• Does not consider the strength ratio of the two soil layers.	• Can be used for any type of soil and gives reasonable results.

2.8.3 Remarks on the Conventional Formulas for Horizontal and Vertical Bearing Capacity for the Bearing Capacity of Spiral Pile

When the conventional design method in Japan, which uses 1% of the pile diameter (lower limit: 15 mm) as the allowable displacement, is applied to the small-diameter piles, there is a possibility of resulting in overdesign. This is because the elastic ground reaction force method, which is generally used in the pile foundation design, overestimates the horizontal displacement of the small-diameter piles.

In addition, the large resistance to the vertical load of spiral piles is due to the effect of its integration with the surrounding ground generated during the rotational press-fitting. However, in many cases, the design takes the safe side without considering this integration effect from the rotational press-fitting. Therefore, it would be more rational to evaluate the bearing capacity characteristics of small-diameter spiral piles considering the integration effect.

Also, in the conventional design, allowable values are set for vertical load direction and horizontal load direction, and individual evaluations are performed separately. However, in reality, combined horizontal and vertical loads act on the structure. Therefore, the bearing capacity against the combined vertical and horizontal loads may be lower than the bearing capacity evaluated independently.

The spiral pile is also expected to be used as an anchor by taking advantage of its excellent pull-out resistance. However, since only the pull-out resistance is considered in the conventional anchor design, it is extremely important to evaluate the bearing capacity performance against the combined pull-out and horizontal loads and design the spiral pile anchors rationally for slope stabilization.

The objective of this research thesis was to develop easy-to-use, but accurate bearing capacity formulas for the three exceptional types of foundations that consider the realities encountered in practice and in a wide range of material parameters and geometries, encountered in practice. This was successfully achieved, using RPFEM, physical modeling and elastoplastic FEM.

CHAPTER 3- THESIS OUTLINE

3.1 Introduction

The purpose of this chapter is to give a general overview of the three papers in the thesis. Each paper chapter corresponds to one paper, describing the development of methods for estimating (1) the ultimate bearing capacity of shallow strip footings on two-layered *c-ϕ* soils (2) the ultimate end bearing capacity of Incompletely End Supported Pile (IESP) and (3) the bearing capacity characteristics of a small diameter spiral pile in soft ground subjected to combined loads, respectively. While the focus has been on providing rigorous solutions to design each of these foundations for practical applications, the conclusions and outcomes can be applied to any similar bearing capacity problem. The following is a summary of these chapters.

3.2 Chapter 4

In this chapter, the Bearing Capacity Factors of Two-Layered c-ϕ soils based are investigated based on the Rigid Plastic Finite Element Method.

Contrary to some previous research in literature that uses the average strength parameters of the two layers as the strength of the layered system, in this research, each soil layer is attributed its own strength parameters to reflect the reality. The results have shown that the bottom layer may lead to punching failure in the case of a softer bottom while in the case of a stiffer bottom layer it may lead to local failure. These effects of the bottom layer cannot be obtained with the average strength parameters suggested by the previous study. Three types of failure are obtained in each case, the case of a softer bottom layer and the case of a stiffer bottom layer. In this chapter, the conditions of occurrence of each type of failure are summarized in a chart.

In this research, we have proposed layer factors, L_c, L_q and L_γ to consider the effects of the layered system on the bearing capacity factors N_c, N_q and N_γ, respectively, of the top layer. Using the proposed layer factors and the traditional bearing capacity factors, we have proposed a formula to calculate the bearing capacity of two-layered *c-ϕ* soils. This method allows an accurate estimation of the contribution of the resistance provided by each soil layer.

3.3 Chapter 5

In this chapter the End Bearing Capacity of a single Incompletely, End-Supported Pile was investigated

based on the Rigid Plastic Finite Element Method. In the investigations, the non-linear strength property against confining stress was considered. Two yield functions were used, the Drucker-Prager yield function and the High Order yield function. Three types of soil were considered, c soil, ϕ soil and (c-ϕ soil).

While the Drucker-Prager yield function is effective for purely cohesive soils (c soils), for ϕ soil and c-ϕ soils only the High Order yield function is suitable. However, to use the High Order yield function some ameliorations were necessary. New parameters of the High Order yield function were established to consider the non-linear shear strength property of soil against the confining pressure in ϕ soil and c-ϕ soils.

Independently of the yield function (Drucker-Prager and High Order model), the end bearing capacity degrades when the pile moves away from the bottom layer and becomes constant from the distance of three times the pile diameter. A degradation factor of the end bearing capacity of IESP was defined in this chapter. The degradation factor is independent of the yield function but is affected by the bearing capacity ratio of the two layers and the soil type.

3.4 Chapter 6

In this chapter Bearing capacity characteristics of a small diameter spiral pile in soft ground subjected to combined loads were investigated. The investigations include various loading tests on small-diameter spiral piles using physical modeling and analyses using three-dimensional elastoplastic finite elements.

For the loading tests of the physical modelling, the spiral pile is installed in the ground by using rotational press-fitting force. During the installation, an integration between the spiral pile and the surrounding ground happens. This integration effect between the rotationally press-fit spiral pile and the surrounding ground was neglected by the previous research in literature, however, in this research, we were able to consider it in a simple way. To appropriately reflect the integration effect derived between the rotationally press-fit pile and the surrounding ground, corrections were done on the elements, such as an increase in the apparent pile diameter, an increase in the strength of the ground immediately below the pile tip, and an increase in the bending rigidity of the pile.

The results obtained from the physical modeling tests were accurately reproduced by the three-dimensional elastoplastic finite element method.

By using the numerical analyses, the bearing capacity characteristics of the vertical and batter spiral piles under the combined load were investigated. It was shown that the bearing capacity under the combined load might be lower than the bearing capacity evaluated independently for the vertical and horizontal loading, depending on the loading direction. The bearing capacity envelopes for a small-diameter spiral pile under the *H-V-M* combined load were able formulated for both vertical and batter piles.

CHAPTER 4: ESTIMATION OF THE BEARING CAPACITY FACTORS OF TWO-LAYERED c-ϕ SOILS BASED ON THE RIGID PLASTIC FINITE ELEMENT METHOD

Abstract

This study investigates the bearing capacity of a strip footing on two-layered *c*-ϕ soils by considering layer factors estimated using an in-house FEM code, namely, the rigid-plastic finite element method. The influences of the following ratios on the bearing capacity factors were investigated: The ratio of the tangent of the angle of friction of the bottom layer to that of the top layer; the ratio of the cohesion of the bottom layer to that of the top layer; the ratio of the unit weight of the bottom layer to that of the top layer, and the ratios of the embedment of the footing and the thickness of the top layer to the footing width. Based on the influences of those ratios, layer factors are determined. Several types of failure mechanics were found and the conditions of occurrence of each failure type are summarized in a chart. A new approach for estimating the bearing capacity of strip footings on two-layered *c*-ϕ soils is proposed. A comparison with available methods in the literature has confirmed the reliability of the proposed method, showing the application limitation of the past research.

Keywords: Footing, Bearing Capacity, Bearing Capacity Factors, *c*-ϕ soil, Layered Ground, FEM

4.1 Introduction

The ultimate bearing capacity of shallow foundations has been the subject of intensive studies such as Prandtl 1920; Prandtl 1921; Reissner 1924. Terzaghi 1943 was the first one to introduce the concept of ultimate bearing capacity and presented a comprehensive theory for the evaluation of the bearing capacity of shallow foundations. He defined a three-term bearing capacity equation by superposition of the effects of soil cohesion, soil surcharge, and the weight of soil. For a general case of centric vertical loading of a rigid strip footing on a cohesive frictional soil surface with a uniform surcharge of q, the ultimate bearing capacity (q_{ult}) is given as:

$$q_{\text{ult}} = cN_{\text{c}} + qN_{\text{q}} + 0.5\gamma BN_{\gamma} \quad \cdots\cdots (4\text{-}1)$$

where c = cohesion; q = overburden pressure; γ = unit weight of the soil; N_{c}, N_{q} and N_{γ} = bearing capacity factors and B = footing width.

Subsequently, the bearing capacity theory went through many modifications to take into account different features such as foundation shape, load inclination, ground slope, non-symmetrical loads, and water table by many researchers. Among others, we can enumerate Meyerhof 1963, Hansen 1970, Vesic 1973. The form of equations used by Meyerhof 1963, Hansen 1970, Vesic 1973 for determining the ultimate bearing capacity of symmetrically loaded strip footings is the same as that of Terzaghi 1943, but their approaches and assumptions to solve the problem are different. The equation they have proposed can be written as:

$$q_{\text{ult}} = cN_{\text{c}}S_{\text{c}}d_{\text{c}}i_{\text{c}} + qN_{\text{q}}S_{\text{q}}d_{\text{q}}i_{\text{q}} + 0.5\gamma BN_{\gamma}S_{\gamma}d_{\gamma}i_{\gamma} \quad \cdots\cdots (4\text{-}2)$$

where S_{c}, S_{q} and S_{γ} = shape factors; d_{c}, d_{q} and d_{γ} = depth factors; i_{c}, i_{q} and i_{γ} = inclination factors; c, q, γ, N_{c}, N_{q} and N_{γ} and B are the same as defined in **Eq. 4-1**.

All these theoretical analyses dealt with so far assume that the subsoil is isotropic and homogeneous to a considerable depth. However, in nature, soil is generally non-homogeneous, and shallow foundations are, sometimes, located on a soil layer of finite thickness overlying a thick stratum of another soil.

A series of researchers have contributed their findings towards estimating the bearing capacity of footings on natural or artificially stratified soil media. Many researchers focused on the bearing capacity of footing on dense sand over clay, such as Meyerhof 1974, Kenny and Andrews 1979, Hanna and

Meyerhof 1980, Griffiths 1982, Das and Dallo 1984, Michalowski and Shi 1995, Burd and Frydman 1997, Okamura et al. 1998, Shiau et al. 2003, Qin and Huang 2008, Huang and Qin 2009 and Salimi et al. 2018. For layered clayey soil, Button 1953 was the first to analyse footings on layered soils of different cohesion. Many other studies were conducted for clayey layers, including those of Meyerhof and Hanna 1978, Sivareddy and Srinivasan 1967, Brown and Meyerhof 1969, Desai and Reese 1970a, 1970b, Merlfleld et al. 1999, Huang and Qin 2009, and Y. Xiao et al. 2018. The bearing capacity of the shallow foundations on layered sand strata has been investigated by many researchers, such as Meyerhof 1976, Meyerhof and Hanna 1978, Hanna 1981, 1982, Das and Munoz 1984, Farah 2004, Kumar et al 2007, Ma et al. 2010, Khatri et al. 2017, and Salimi et al. 2019. In comparison studies concerning shallow foundations in two-layered c-ϕ soils have received less attention. The ultimate bearing capacity of two-layered c-ϕ soil was studied by Purushothamaraj et al. 1974, Satyanarayana and Garg 1980, Florkiewicz 1989, Azam and Wang 1991, and Bowles 1996. However, most of these studies are empirical and used the average strength of two soil layers as the shear strength of the layered system, which leads to misestimation of the bearing capacity.

In this study, by attributing each soil layer its shear strength, the Rigid Plastic FEM analysis was used to estimate the bearing capacity of two-layered c-ϕ soils. The estimation of layer factors L_c, L_q and L_γ was focused on. Just like the shape factors, inclination factors and depth factors to take into account foundation shape, load inclination, and foundation depth respectively, this study aims to propose layer factors L_c, L_q and L_γ to take into account the effect of the bottom layer of two-layered c-ϕ soil on the bearing capacity of the top layer. Therefore, this study aims to propose a new approach to determining the bearing capacity of strip footing on two-layered c-ϕ soils. Meanwhile, the conditions of occurrence of different failure types are proposed in this study.

4.2 Constitutive Equations for Rigid Plastic Finite Element Method

The rigid-plastic finite element method (RPFEM) was developed for geotechnical engineering by Tamura et al. 1984, 1987. In this method, the limit load is calculated without any assumption of a potential failure mode. The method is effective in the calculation of the ultimate bearing capacity of shallow foundations where the soil conditions are varied, such as a multi-layered ground. The advantage of the rigid plastic constitutive equation is that only a few soil parameters, such as unit weight, cohesion,

and shear resistance angle are necessary.

In this study, the in-house RPFEM code developed and updated by Hoshina et al. 2011 and Du et al. 2016, is used for estimation of the bearing capacity of strip footings on two-layered *c*-ϕ soils. The rigid plastic constitutive equation for the Drucker-Prager yield function is employed in this code. The Drucker-Prager yield function is expressed with **Eq. 4-3** in plane-strain conditions considering the associative flow rule.

$$f(\sigma) = \alpha I_1 + \sqrt{J_2} - \kappa = 0 \quad \cdots\cdots(4\text{-}3)$$

where, $I_1 = \mathrm{tr}(\sigma_{ij})$ is the first invariant, $J_2 = \frac{1}{2} s_{ij} s_{ij}$, α and κ are soil parameters expressed for plane strain conditions as follows:

$$\alpha = \frac{\tan\phi}{\sqrt{9+12\tan^2\phi}}, \kappa = \frac{3c}{\sqrt{9+12\tan^2\phi}} \quad \cdots\cdots(4\text{-}4)$$

where c is cohesion, ϕ is shear resistance angle.

For the Drucker-Prager yield function, the volumetric strain rate for the Rigid Plastic constitutive equation is expressed as follows:

$$\dot{\varepsilon}_v = \mathrm{tr}(\dot{\boldsymbol{\varepsilon}}) = \mathrm{tr}\left(\lambda \frac{\partial f(\boldsymbol{\sigma})}{\partial \boldsymbol{\sigma}}\right) = \mathrm{tr}\left(\lambda\left(\alpha \boldsymbol{I} + \frac{\boldsymbol{s}}{2\sqrt{J_2}}\right)\right) = \frac{3\alpha}{\sqrt{3\alpha^2+\frac{1}{2}}}\dot{e} \quad \cdots\cdots(4\text{-}5)$$

where λ is the plastic multiplier and $\dot{e}$ is the norm of the strain rate. $\boldsymbol{I}$ and $\boldsymbol{s}$ express the unit and the deviator stress tensors, respectively. Strain rate $\dot{\boldsymbol{\varepsilon}}$, which is a purely plastic component, should satisfy the volumetric constraint condition which is derived by **Eq. 4-6**, as follows:

$$h(\dot{\boldsymbol{\varepsilon}}) = \dot{\varepsilon}_v - \frac{3\alpha}{\sqrt{3\alpha^2+\frac{1}{2}}}\dot{e} = \dot{\varepsilon}_v - \eta\dot{e} = 0 \quad \cdots\cdots(4\text{-}6)$$

Any strain rate which is compatible with the Drucker–Prager yield criterion must satisfy the kinematical constraint conditions of **Eq. 4-6**. The parameter η is a coefficient determined by **Eq. 4-6** which is one of the dilation characteristics. The rigid plastic constitutive equation is expressed by Lagrange multiplier method after Tamura et al. 1987, as follows:

$$\boldsymbol{\sigma} = \frac{\kappa}{\sqrt{3\alpha^2+\frac{1}{2}}}\frac{\dot{\boldsymbol{\varepsilon}}}{\dot{e}} + \beta\left(\boldsymbol{I} - \eta\frac{\dot{\boldsymbol{\varepsilon}}}{\dot{e}}\right) \quad \cdots\cdots(4\text{-}7)$$

The first term expresses the stress component, uniquely determined for the yield function. The second

term expresses the indeterminate stress component along with the yield function. The indeterminate stress parameter β remains unknown until the boundary value problem with **Eq. 4-6** is solved.

$$\boldsymbol{\sigma} = \frac{\kappa}{\sqrt{3\alpha^2+\frac{1}{2}}}\frac{\dot{\boldsymbol{\varepsilon}}}{\dot{e}} + P(\dot{\varepsilon}_v - \eta\dot{e})\left(\boldsymbol{I} - \eta\frac{\dot{\boldsymbol{\varepsilon}}}{\dot{e}}\right) \cdots\cdots (4\text{-}8)$$

where P is a penalty constant. This technique makes the computation faster and more stable (Hoshina et al. 2011).

The FEM, together with this constitutive equation, provides an equivalent equation for the upper bound theorem in plasticity; the method is called the RPFEM in this study. It is a noted property of this constitutive equation that the relationship between stress and the strain rate is specified. The norm of the strain rate is substantially indeterminate since the focus is placed on the limit state of the structure. Stress is determined for the normalized strain rate using its norm to determine the limit load coefficient for the prescribed load.

Therefore, the rigid plastic constitutive equation is simple and effective for assessing the limit state of the ground due to the advantage of not using an uncertain elastic modulus for the ground.

5.6 Finite Element Mesh and Analyses Parameters

Fig. 4-1 shows a schematic view of the problem and an illustration of the finite element mesh and the boundary conditions used. The density of the mesh elements was refined near the footing to capture the higher expected strain. The left and right sides of the domain were pinned, enabling movement in the vertical direction while restricting movement in the horizontal direction. The bottom boundary of the domain was fixed, restricting movement in both the horizontal and vertical directions. An increasing load in a downward direction was applied on the footing.

The footing is lying on two soil layers: a top soil layer with a thickness H, a cohesion c_1, a shear resistance angle ϕ_1 and a unit weight γ_1 and a bottom soil layer with a cohesion c_2, a shear resistance angle ϕ_2 and a unit weight γ_2. With a unit weight γ, the soil above the footing base was not modeled and was only represented by a surcharge γD_f, where D_f is the embedment of the footing.

The analyses parameters are as follows:

- The ratio of the thickness of the top layer H to the footing width B (H/B)
- The ratio of the tangent of the shear resistance angle of the bottom layer to that of the top layer

(r_ϕ = tan (ϕ_2)/ tan (ϕ_1)),

- The ratio of the cohesion of the bottom layer to that of the top layer ($r_c = c_2/c_1$),
- The ratio of the unit weight of the bottom layer to that of the top layer ($r_\gamma = \gamma_2/\gamma_1$) and
- The ratio of the embedment D_f to the footing width B (D_f/B)

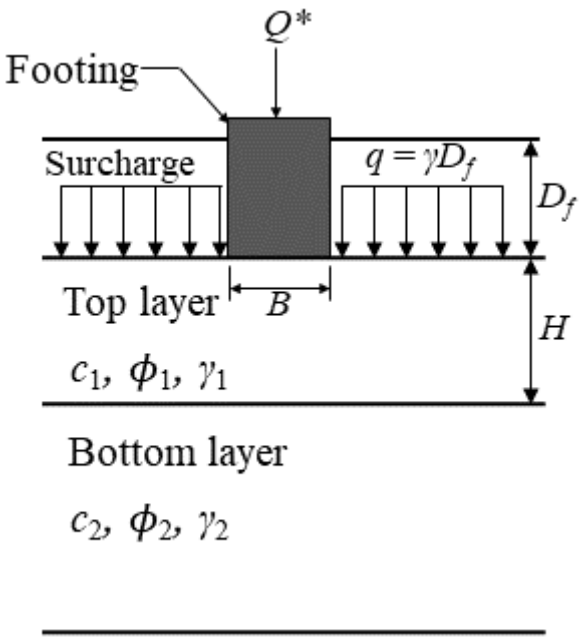

(a) Schematic view (problem definition)

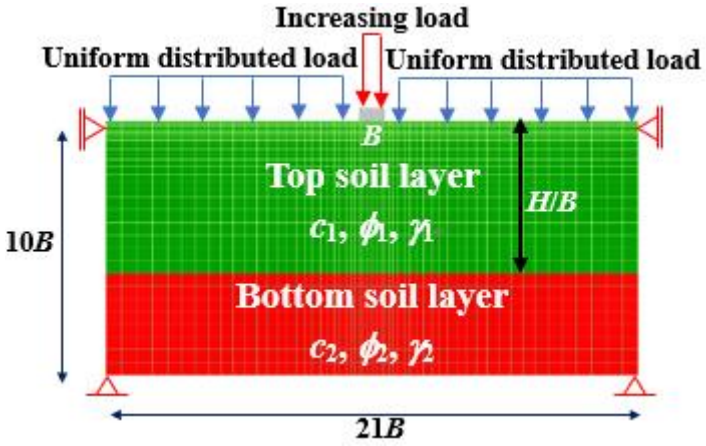

(b) FE mesh

Fig. 4-1. Schematic view and FE mesh of a strip footing on two-layered c-ϕ soils

4.4 Description of Some Existing Bearing Capacity Theories of Two-Layered *c*-ϕ Soils

Satyanarayana and Garg 1980 have proposed a simplified bearing-capacity theory for shallow foundations in *c*-ϕ soils. According to their theory, the ultimate bearing capacity of a two-layered soil is given by:

$$q_{\text{ult}} = c_{\text{av}} N_{\text{c}} + q N_{\text{q}} + 0.5\gamma_1 B N_{\gamma} \quad \cdots\cdots (4\text{-}9)$$

where

$$c_{\text{av}} = \frac{H c_1 + H_2{}^* c_2}{H + H_2{}^*}, \quad \phi_{\text{av}} = \tan^{-1}\left(\frac{H \tan\phi_1 + H_2{}^* \tan\phi_2}{H + H_2{}^*}\right), \quad H_2{}^* = (2B - H)\left(\frac{c_1 + \tan\phi_1}{c_2 + \tan\phi_2}\right)$$

N_{c}, N_{q} and N_{γ} are bearing capacity factors based on ϕ_{av}.

Azam and Wang 1991 investigated the bearing capacity of an embedded strip footing supported by two-layer *c*-ϕ soils using an elastoplastic finite-element computer program. Based on the analysis results, they developed a semiempirical equation for determining the ultimate bearing capacity. The equation proposed by Azam and Wang 1991 is:

$$q_0 = q_{\text{t}} + (q_b - q_{\text{t}})\,[1 - m(H/B)]^2 \quad \cdots\cdots (4\text{-}10)$$

q_0 = ultimate bearing capacity of strip footing over two-layer soil

q_{t} = ultimate bearing capacity of the footing supported by an infinitely thick top-layer soil, computed by the traditional bearing capacity equation using factors recommended by Vesic 1973

q_{b} = ultimate bearing capacity of the footing supported by an infinitely thick bottom-layer soil, computed by the same method as q_{t}

m = empirical parameter, which is 0.17-0.23 for two layers of clay (use of the lower value is recommended if one clay layer is highly compressible, otherwise use the average value) and 0.30 for a sand-clay layer combination and

H/B = top-layer-thickness-to-footing-width ratio, which is no more than 6 for clay-clay layers and no more than 3.5 for sand-clay layers

Bowles 1996 has also proposed a formula for the calculation of the bearing capacity of two-layered soils considering the location of the central wedge, i.e. on the top layer ($H > B/2 \tan(45 + \phi_1/2)$) and extending to the bottom layer ($H < B/2 \tan(45 + \phi_1/2)$), with $B/2 \tan(45 + \phi_1/2) = d$ the depth of the central wedge. The formula proposed by Bowles 1996 is like the one of Satyanarayana and Garg 1980

and is as follows.

$$q_{ult} = c_m N_c + q N_q + 0.5\gamma_1 B N_\gamma \quad \cdots\cdots (4\text{-}11)$$

$$d = \frac{B}{2}\tan\left(45 + \frac{\phi_1}{2}\right), \text{ if } d > H \;\; \phi_m = \left(\frac{H\phi_1 + (d-H)\phi_2}{d}\right), \quad c_m = \left(\frac{Hc_1 + (d-H)c_2}{d}\right)$$

N_c, N_q and N_γ are bearing capacity factors based on ϕ_m.

4.5 Limits of The Existing Bearing Capacity Theories of Two-Layered *c*-ϕ Soils and Merits of the Simulation Method.

The equations of Satyanarayana and Garg 1980 and Bowles 1996 both use average cohesions, average internal friction angles, empirical critical thicknesses of the top layer and do not consider the weight of the bottom layer. These assumptions do not reflect reality. Azam and Wang 1991 used three soils with specific strength parameters that influence their method. Their method may lead to some discrepancies when extended to soils possessing strength parameters different from those in their study.

The RPFEM on the other hand does not use average strength parameters of the soil layers, does not have any assumption on the critical thicknesses of the top layer and can be used for any soil parameters. The ability of RPFEM to estimate the bearing capacity of strip footing has been already confirmed in the references of Hoshina et al. 2011, Du et al. 2016, etc.

Fig. 4-2 shows the comparison between the previous study and RPFEM. The characteristics of soils used for comparison are shown in **Table 4-1.** The footing width B was 1 m, and the embedment D_f was 1B. In Bowles 1996 and Satyanarayana and Garg 1980, the bearing capacity factors were obtained using the Terzaghi method.

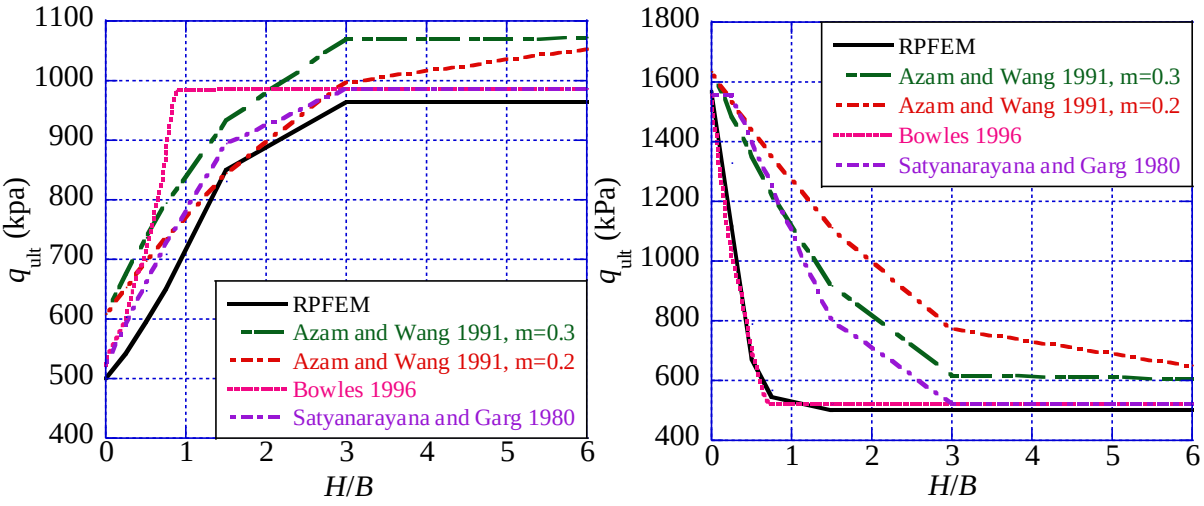

(a) Bottom layer softer than the top layer (Soil 1 under Soil 3)

(b) Bottom layer stiffer than the top layer (Soil 2 under Soil 1)

Fig. 4-2. Comparison of RPFEM with existing theories on bearing capacity of two-layered c-ϕ soils

Table 4-1. Strength parameters of soils used for comparison

	ϕ (degrees)	c (kPa)	γ (kN / m^3)
Soil 1 (Bowles 1996)	20	20	17.3
Soil 2 (Sandy loam)	35	10	15
Soil 3, Clayey sand (Azam and Wang 1991)	31	9.17	16.56

In the case of a bottom layer softer than the top layer, despite the results of RPFEM being slightly lower, there is an acceptable agreement between RPFEM, Azam and Wang 1991 (with m = 0.2) and Satyanarayana and Garg 1980. However, Bowles 1996 shows relatively higher values of bearing capacity in the range of H/B = 0.75 - 1.5. RPFEM shows constant bearing capacity from H/B = 3 (critical thickness of the top layer) higher than $d = B/2 \tan(45+\phi_1/2)$ = 0.88 assumed by Bowles 1996.

In the case of a bottom layer stiffer than the top layer, there is a good agreement between RPFEM and Bowles 1996. However, the results from Azam and Wang 1991 and Satyanarayana and Garg 1980 are much higher.

To clarify the discrepancies observed in **Fig. 4-2**, failure patterns at H/B = 0.75 are presented in **Fig. 4-3**. The black line materializes the boundary (or fictive boundary) between the top and bottom layers. The norm of the strain rate is represented by contour lines in the range of $\dot{e}_{min}$ (=0) ~ $\dot{e}_{max}$. The methods of Satyanarayana and Garg 1980 and Bowles 1996 assimilate a two-layered c-ϕ soil as a uniform soil

having strength parameters equal to the averages of the strength parameters of the layers present into the two-layered c-ϕ soil. Thus, the average strength parameters obtained from these methods are used with uniform soils in RPFEM to obtain failure patterns that may result from them.

When the bottom layer is softer than the top layer (**Fig. 4-3(a)**), RPFEM shows a punching shear failure (central wedge penetrates in the bottom layer [this study]). However, with Bowles 1996 and Satyanarayana and Garg 1980, only general shear failures are obtained. With RPFEM, a punch that breaks through the top layer acts on the bottom layer, like a footing, and the weak strength of the bottom layer contributes to a decrease in the bearing capacity. Hence, in **Fig. 4-2(a)**, RPFEM has lower bearing capacity and a critical thickness (H/B = 3) higher than $d = B/2 \tan(45+\phi_1/2) = 0.88$. The higher bearing capacities of Bowles 1996 in the range of H/B = 0.75 - 1.5 are due to the relatively high values of ϕ_m in that range. The relatively good agreement of RPFEM and Azam and Wang 1991, in **Fig. 4-2(a)**, is since the top layer used in this case (soil 3) is from Azam and Wang 1991 and therefore has specific strength parameters used by Azam and Wang 1991 to establish their formula.

In **Fig. 4-3(b)**, the shear band of Satyanarayana and Garg 1980 is wider. This is due to the high value of ϕ_{av} and justifies the high bearing capacity of Satyanarayana and Garg 1980 in **Fig. 4-2(b)**. It is also interesting that the failure of RPFEM is more localized due to the effect of the stiffer bottom layer, suggesting that with RPFEM a local shear failure may occur under certain conditions. The soils used in this case have characteristics different from those used by Azam and Wang 1991, hence the discrepancy between Azam and Wang 1991 and RPFEM. Besides, the critical distance obtained by Azam and Wang 1991 here is too high since there is no punching failure.

In conclusion, by attributing to each soil layer its strength parameters, RPFEM has shown that the bottom layer may lead to punching failure in the case of a softer bottom while in the case of a stiffer bottom layer it may lead to local failure. These effects of the bottom layer cannot be obtained with the average strength parameters suggested by the previous study. Any parameter which affects the mode of failure influences the ultimate bearing capacity as well (Hanna 1981, 1982). This shows the application limits of the previous studies and the merits of this study.

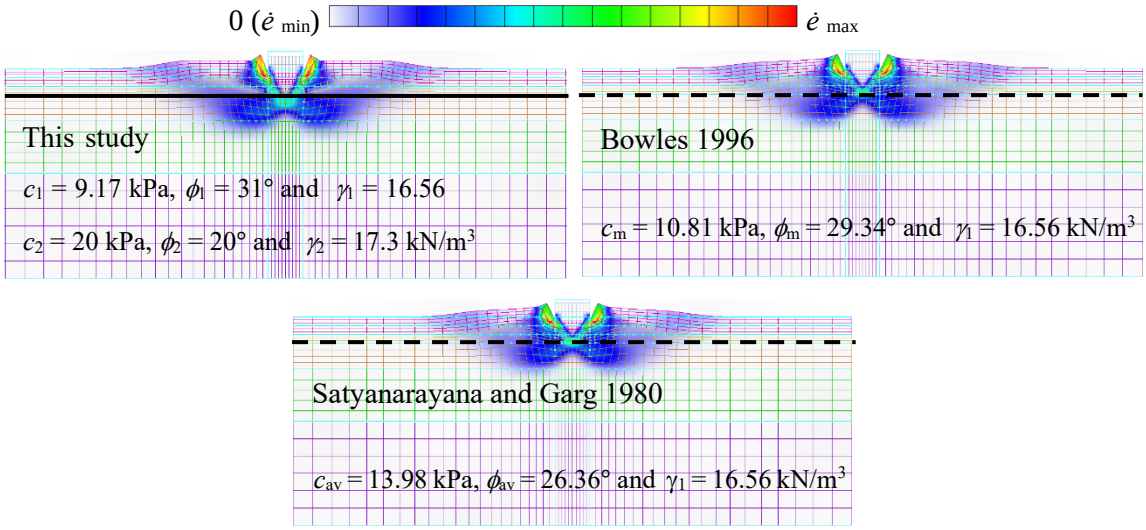

(a) Bottom layer softer than the top layer (soil 1 under soil 3)

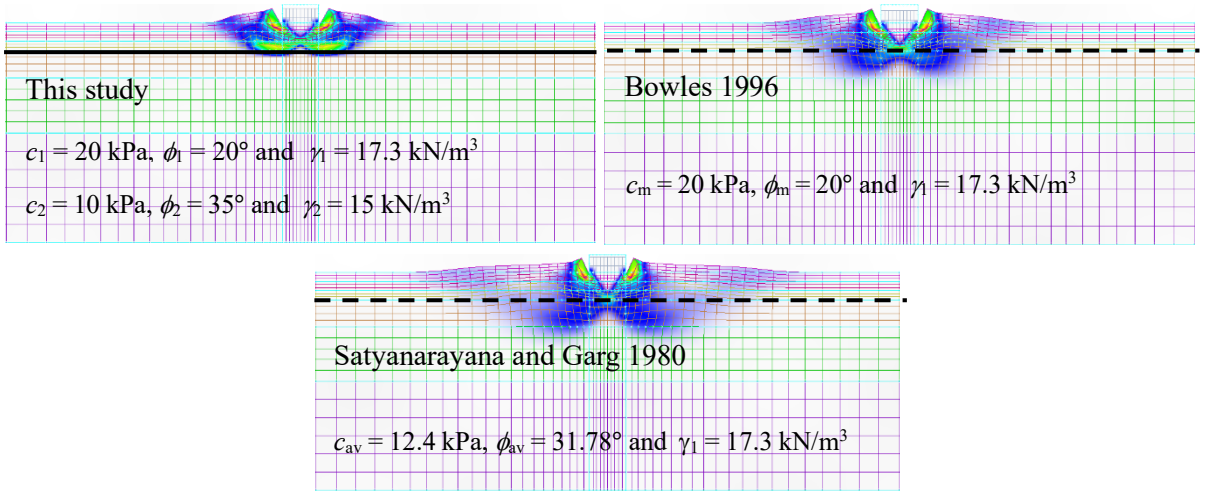

(b) Bottom layer stiffer than the top layer (soil 2 under soil 1)

Fig. 4-3. Comparison of failure patterns in the case of H/B = 0.75

4.6 Validation of the Method used in this Study

Terzaghi 1943 proposed **Eq. 4-1** and assumes that the bearing capacity factors N_c, N_q and N_γ can be obtained by superposition. Terzaghi's method of superposition is used in this study.

Fig. 4-4 shows the comparisons of the bearing capacity factors obtained from RPFEM with those from existing literature. This comparison has confirmed the ability of the simulation method to estimate the bearing capacity factors of uniform grounds.

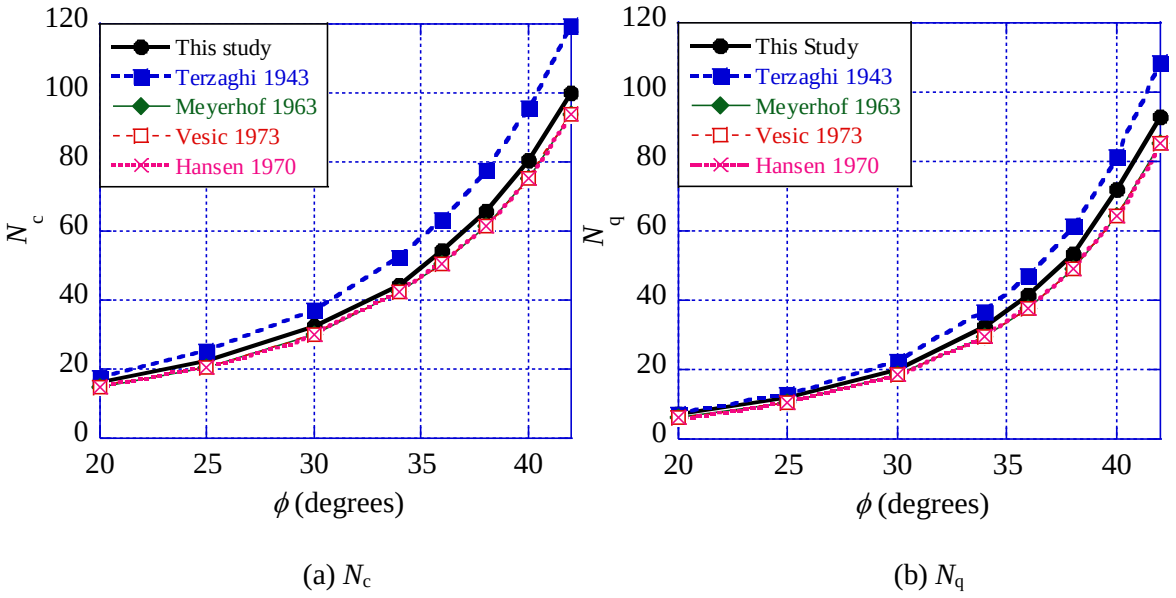

(a) N_c (b) N_q

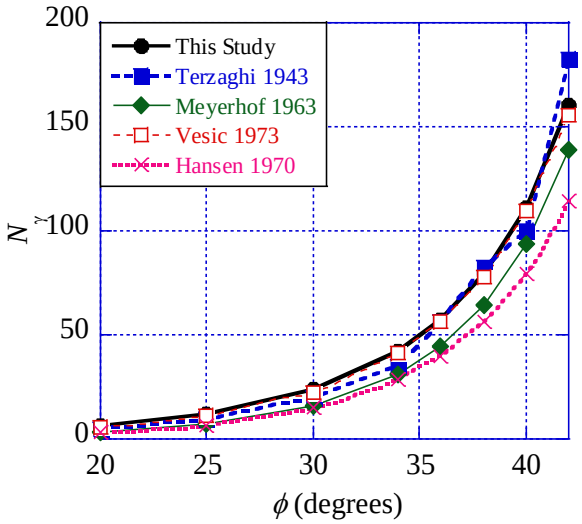

(c) N_γ

Fig. 4-4. Comparison of the bearing capacity factors of uniform grounds from different methods

For a two-layered c-ϕ soil the bearing capacity factors are referred to as N_c*, N_q* and N_γ*, in this study. Salami et al. 2019 have studied the bearing capacity of two-layered sand using Finite Element Limit Analysis, where the bottom layer is softer than the top layer. They have found a new failure pattern which they named transitional failure mechanic (transition between general failure and punching failure). Salami et al. 2019 defined the bearing capacity factor N_γ* corresponding to transitional failure. **Fig. 4-5** below compares the N_γ* of Salami et al. 2019 and those obtained with RPFEM. There is a good agreement between the two methods. However, the study of Salami et al. 2019 also has some limits: (1)

They used the ratio $\gamma_1/\gamma_2 = 1.2$ only in their study. (2) Under certain conditions, the N_γ* of Salami et al. 2019 are zero (0) when $H/B = 0$; which is not realistic since, at $H/B = 0$, N_γ* should be equal to N_γ (bearing capacity factor of a uniform ground).

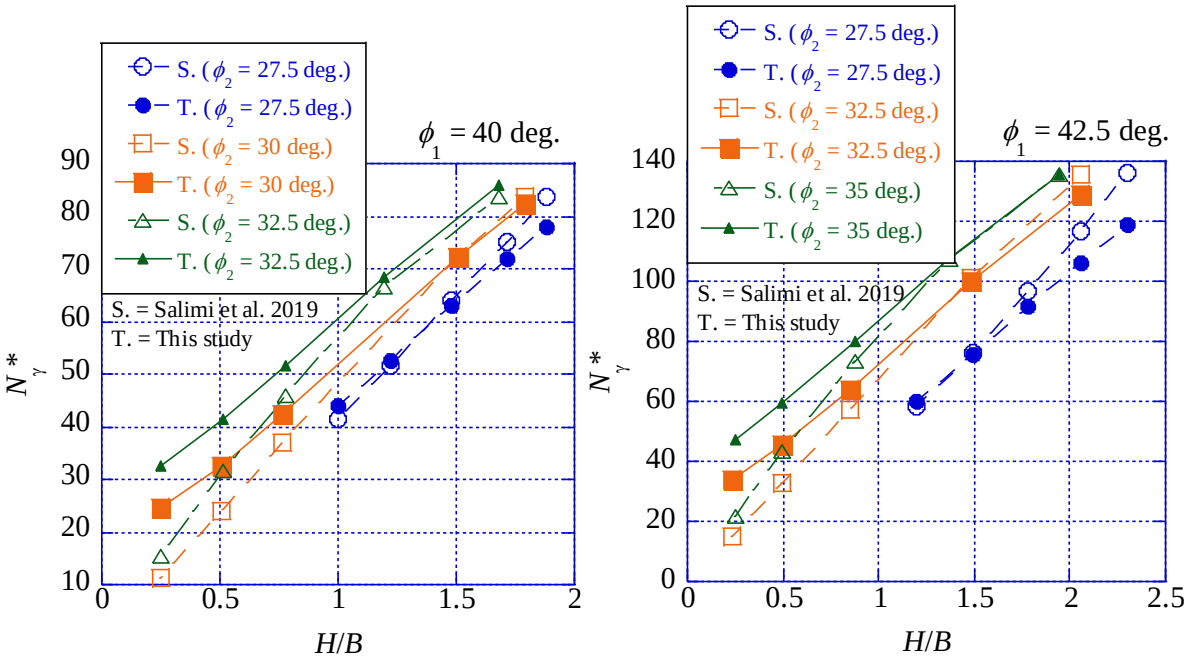

(a) $\phi_1 = 40°$ **(b)** $\phi_1 = 42.5°$

Fig. 4-5. Comparison of this study and Salami et al. 2019

4.7 Bearing Capacity Factors of Strip Footing in Two-Layered Cohesive-Friction Soils

4.7.1 Methodology of Determining the Layer Factors L_c, L_q and L_γ

The chart in **Fig. 4-6** explains the method used to determine the layer factor L_c, L_q and L_γ. **Fig. 4-6(a)** shows the bearing capacity factors N_c, N_q and N_γ of a uniform soil (one layered c-ϕ soil) and the bearing capacity factors N_c*, N_q* and N_γ* of a two-layered c-ϕ soil with a top layer having the same characteristics as the uniform soil. **Fig. 4-6(b)** explains how N_c*, N_q* and N_γ* are calculated. The layer factors are then obtained as ratios of N_i* to N_i, with i = c, q, γ (i.e. $L_c = N_c^*/ N_c$, $L_q = N_q^*/ N_q$ and $L_\gamma = N_\gamma^*/ N_\gamma$). Layer factors, therefore, reflect the influence of the bottom layer on the bearing capacity factors N_c, N_q and N_γ.

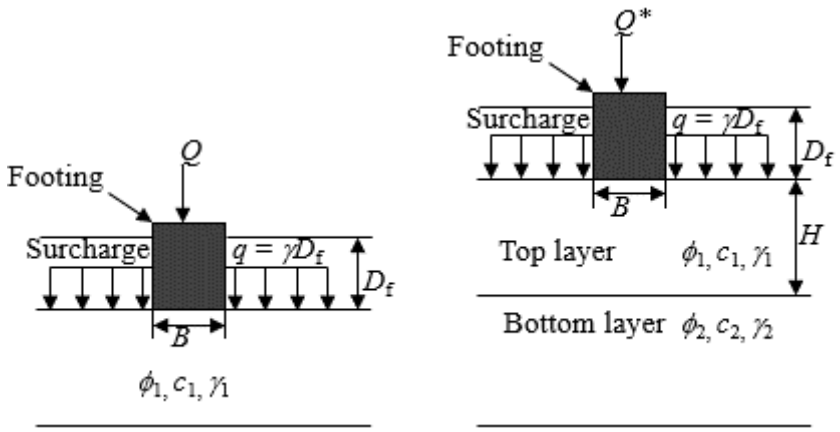

One soil layer | Two soil layers

$Q = c_1 N_c + qN_q + 0.5\,\gamma_1 B N_\gamma$ | $Q^* = c_1 N_c^* + qN_q^* + 0.5\,\gamma_1 B N_\gamma^*$

(a) Schematic view of a strip footing on one soil layer (left) and two soil layers (right)

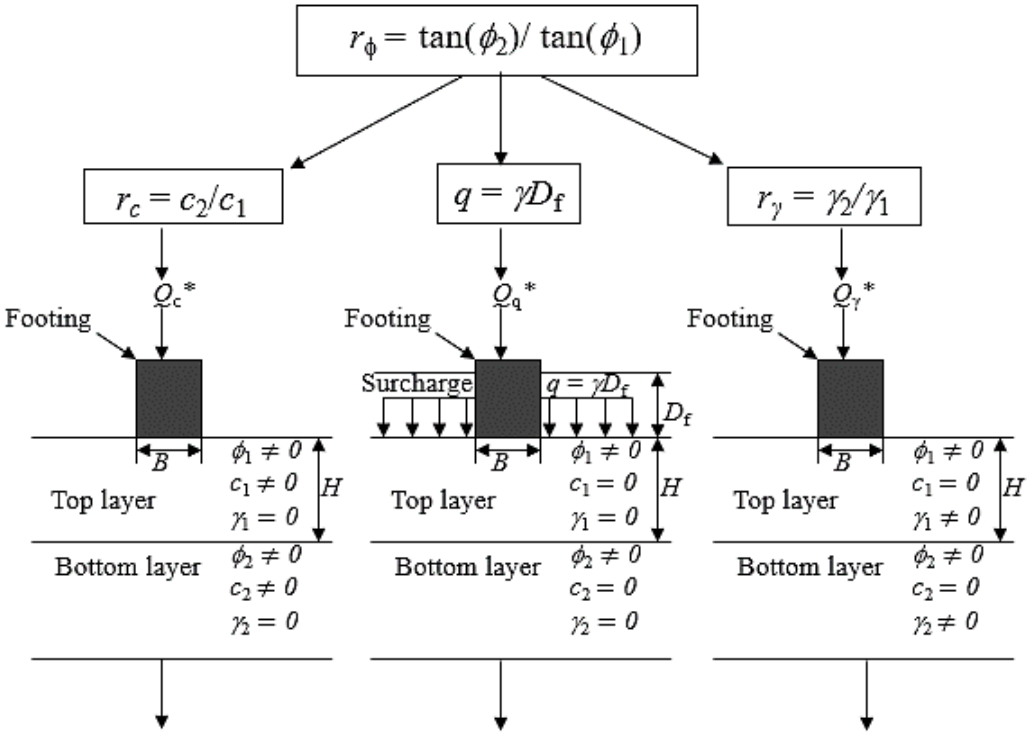

$q_c^* = c_1 N_c^*$	$q_q^* = qN_q^*$	$q_\gamma^* = 0.5\gamma_1 B N_\gamma^*$
$N_c^* = q_c^* / c_1$	$N_q^* = q_q^* / q$	$N_\gamma^* = q_\gamma^* / 0.5\gamma_1 B$
$L_c = N_c^* / N_c$	$L_q = N_q^* / N_q$	$L_\gamma = N_\gamma^* / N_\gamma$
$L_c = f\,(H/B, r_\phi, r_c)$	$L_q = f\,(H/B, r_\phi, D_f)$	$L_\gamma = f\,(H/B, r_\phi, r_\gamma)$

(b) Layer factors

Fig. 4-6. Methodology of determining the layer factors L_c, L_q and L_γ

4.7.2 Comparison of N_i* and N_i (with i = c, q, γ)

This section compares the bearing capacity factors N_i* and N_i, defined above.

The embedment $D_f = 1B$ and the ratios $r_c = r_\gamma = 1$ with $c_1 = c_2 = 25$ kPa and $\gamma = \gamma_1 = \gamma_2 = 18$ kN/m^3. The ratio r_ϕ was varied from 0.4 to 2.5. The ϕ_2 was fixed and ϕ_1 was calculated accordingly to respect the imposed range of r_ϕ. In the case of $r_\phi \leq 1$, $\phi_2 = 20°$ and in the case of $r_\phi \geq 1$, $\phi_2 = 42°$.

The comparison result is shown in **Fig. 4-7** for $H/B = 0.25$. **Fig. 4-7** clearly shows that when $r_\phi < 1$, the N_i* are lower than the N_i illustrating the decrease of the bearing capacity by the bottom layer of a two-layered c-ϕ soil. However, when $r_\phi > 1$, the N_i* are higher than the N_i meaning that the bottom layer will increase the bearing capacity in that case. The amount of decrease (when $r_\phi < 1$) or increase (when $r_\phi > 1$) of the bearing capacity by the bottom layer is symbolized by the gaps between N_i* and N_i. In the case of $r_\phi \leq 1$, the gaps between N_i* and N_i keep increasing when r_ϕ decreases. However, in the case of $r_\phi \geq 1$ the gaps between N_i* and N_i increase with increasing r_ϕ, reach maximums before decreasing. Since the layer factors are ratios of N_i* to N_i ($L_i = N_i$*/ N_i), this means: In the case of $r_\phi \leq 1$, the more r_ϕ is smaller, the more the layer factors will decrease. However, in the case of $r_\phi \geq 1$, a larger ratio r_ϕ does not give a greater value of the layer factors, the maximums layer factors are rather obtained with an optimum ratio r_ϕ.

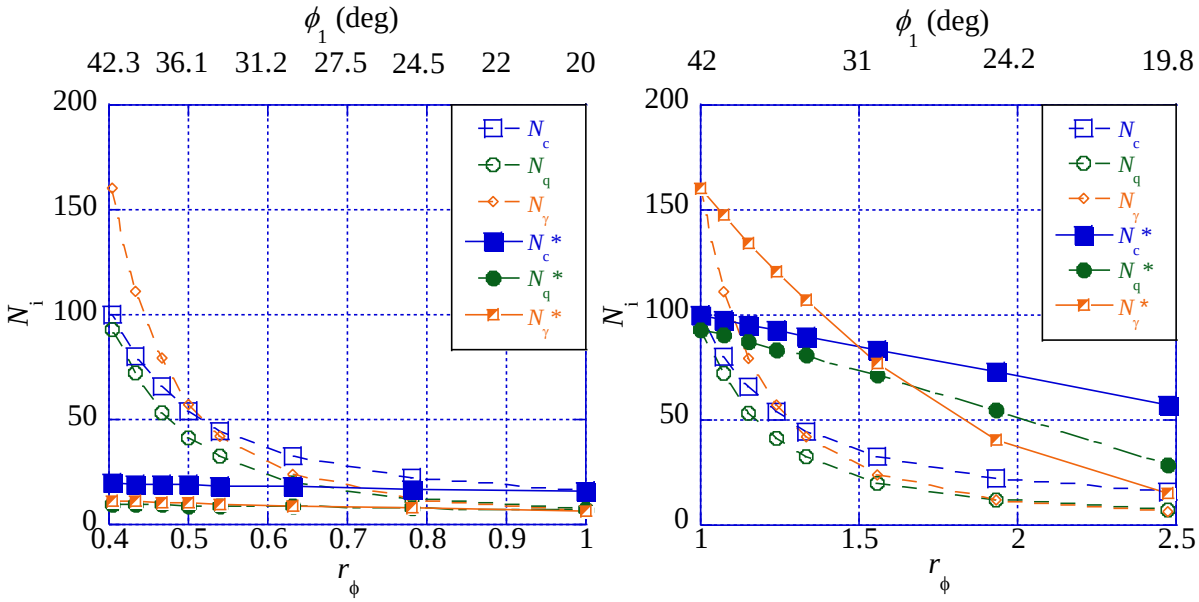

(a) $r_\phi \leq 1$ ($\phi_2 = 20°$) **(b)** $r_\phi \geq 1$ ($\phi_2 = 42°$)

Fig. 4-7. Comparison of N_i* with N_i when $H/B = 0.25$

4.7.3 Influence of Parameter ϕ_2 on the Layer Factors

Fig. 4-8 to **Fig. 4-10** show the influence of the friction angle of the second layer (ϕ_2) on the layer factors L_c, L_q, L_γ respectively, while keeping the same values of the ratio r_ϕ but changing the value of ϕ_2. For each ϕ_2, the corresponding values of ϕ_1 were calculated to respect the range r_ϕ = 0.4 to 2.5. The influence of r_ϕ is testified by $L_i < 1$ for $r_\phi \leq 1$ and $L_i > 1$ when $r_\phi \geq 1$ (where i = c, q, γ). The greater ϕ_2 is, the greater the influence of r_ϕ.

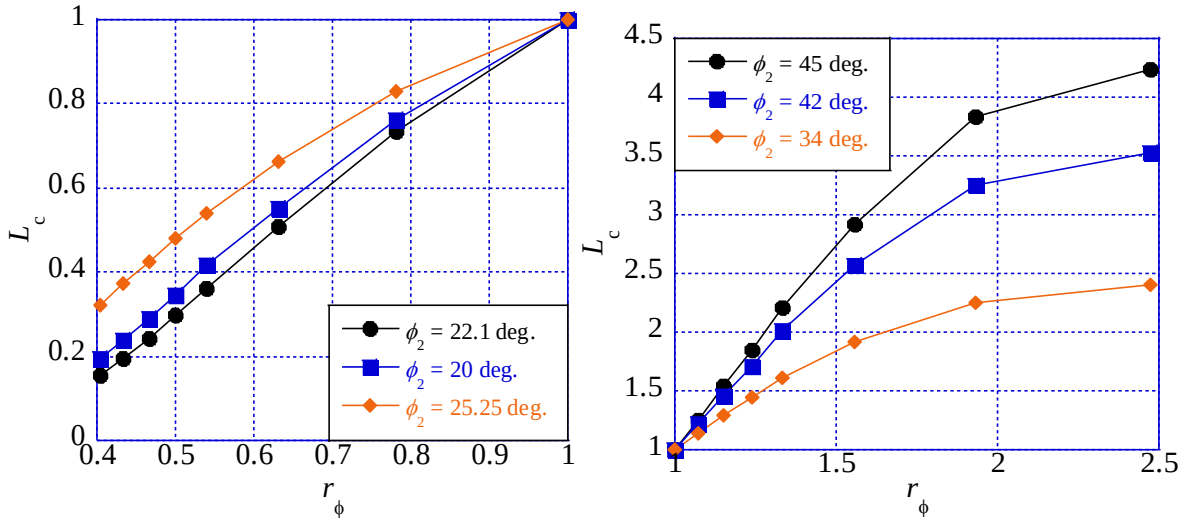

(a) Influence of ϕ_2 on L_c, $r_\phi \leq$ 1and H/B = 0.25 **(b)** Influence of ϕ_2 on L_c, $r_\phi \geq 1$ and H/B = 0.25

Fig. 4-8. Influence of ϕ_2 on L_c ($c_1 = c_2$ = 25 kPa, r_c = 1)

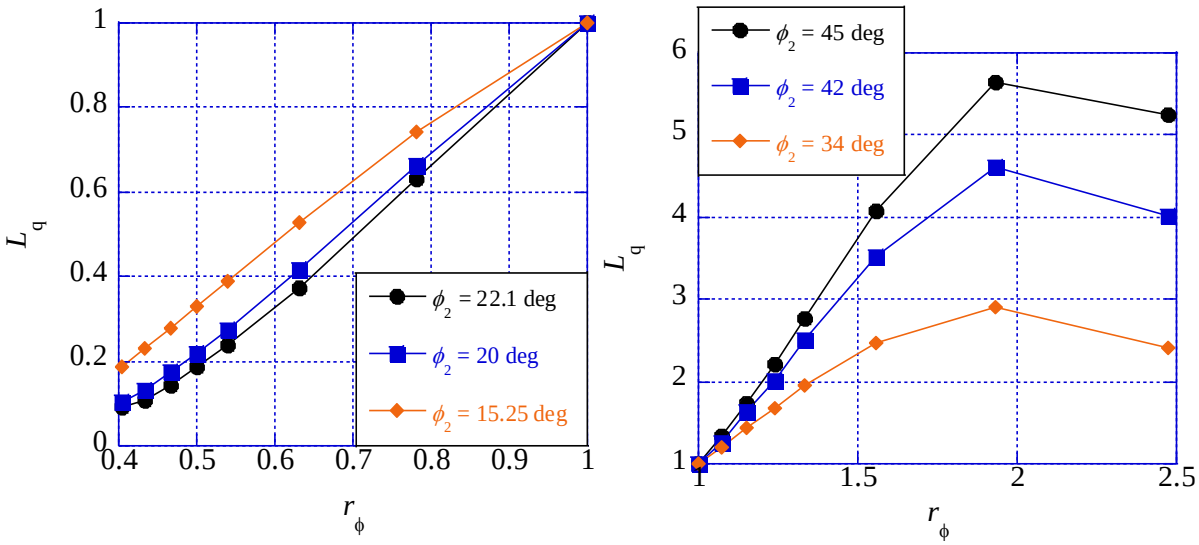

(a) Influence of ϕ_2 on L_q, $r_\phi \leq$ 1and H/B = 0.25 **(b)** Influence of ϕ_2 on L_q, $r_\phi \geq 1$ and H/B = 0.25

Fig. 4-9. Influence of ϕ_2 on L_q (γ = 18 kN/km^3, D_f = 1B)

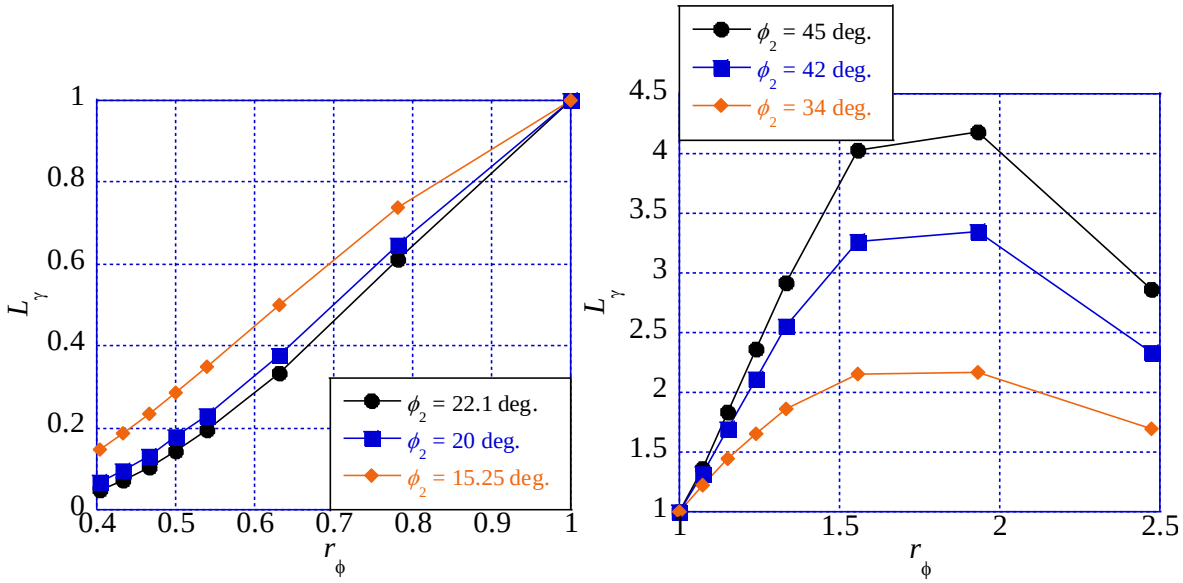

(a) Influence of ϕ_2 on L_γ, $r_\phi \leq$ 1and H/B = 0.25 **(b)** Influence of ϕ_2 on L_γ, $r_\phi \geq 1$ and H/B = 0.25

Fig. 4-10. Influence of ϕ_2 on L_γ ($\gamma_1 = \gamma_2$ = 18 kN/km^3, r_γ = 1)

In **Fig. 4-11(a)**, **Fig. 4-12(a) and Fig. 4-13(a)** the layer factors L_i obtained with ϕ_2 = 20° are plotted against those obtained with ϕ_2 = 15.5° , 22.1° , 25° and in **Fig. 4-11(b)**, **Fig. 4-12(b) and Fig. 4-13(b)** the L_i obtained with ϕ_2 = 42° are plotted against those obtained with ϕ_2 = 35° ; 40° ; 44.5°.

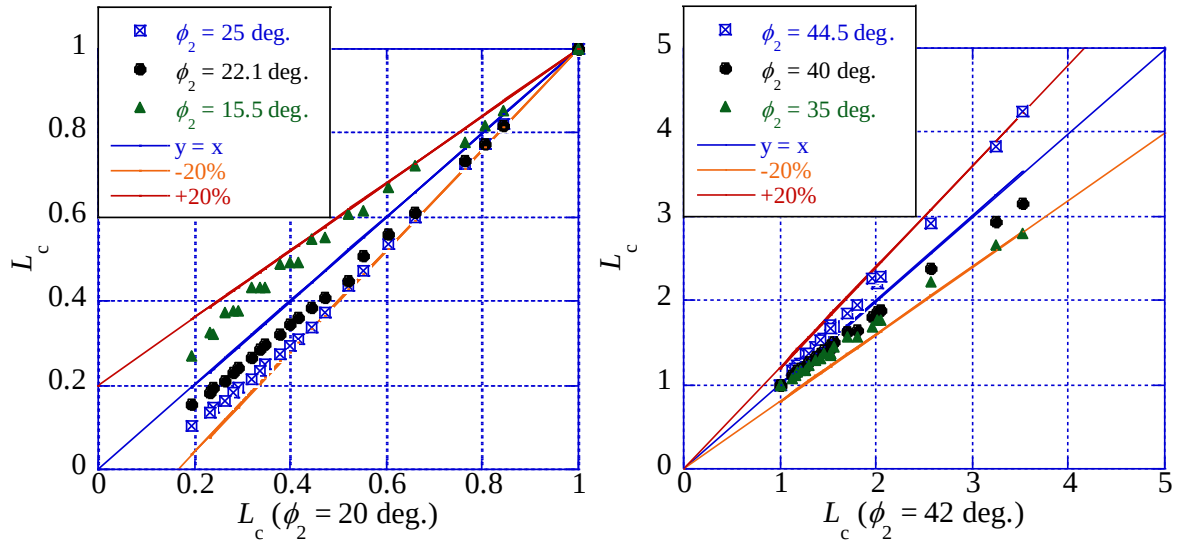

(a) L_c of ϕ_2 = 20 ° against L_c of ϕ_2 = 15.5°; 22.1°; 25° ($r_\phi \leq 1$; H/B = 0.25, 0.50 and 0.75)

(b) L_c of ϕ_2 = 42 ° against L_c of ϕ_2 = 35°; 40°; 44.5° ($r_\phi \geq 1$; H/B = 0.25, 0.50 and 0.75)

Fig. 4-11. Influence of ϕ_2 on L_c (with r_c = 1)

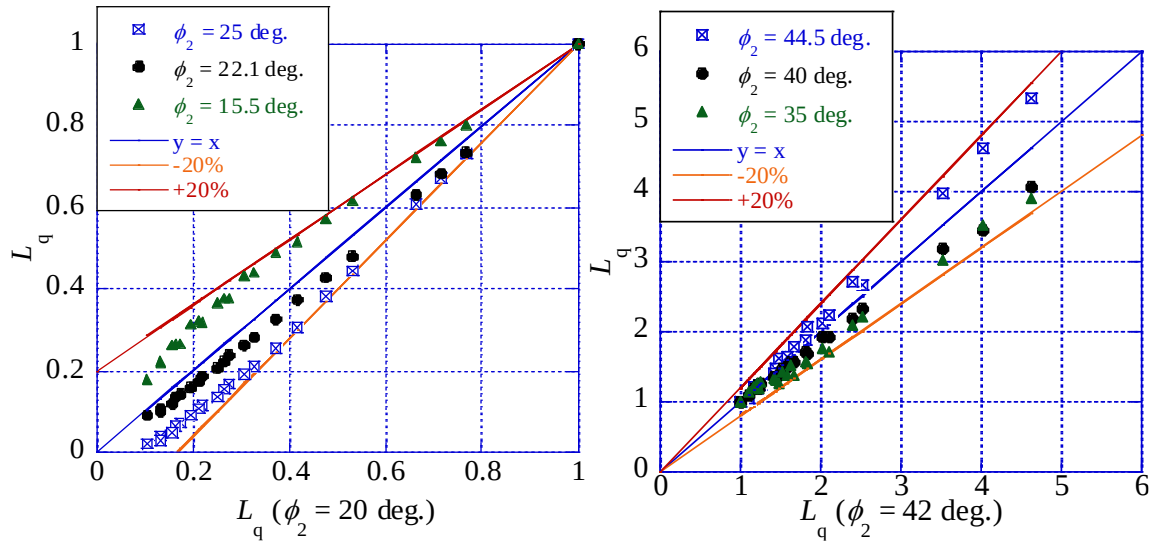

(a) L_q of ϕ_2 = 20 ° against L_q of ϕ_2 = 15.5°; 22.1°; 25° ($r_\phi \leq 1$; H/B = 0.25, 0.50 and 0.75)

(b) L_q of ϕ_2 = 42 ° against L_q of ϕ_2 = 35°; 40°; 44.5° ($r_\phi \geq 1$; H/B = 0.25, 0.50 and 0.75)

Fig. 4-12. Influence of ϕ_2 on L_q (with D_f = 1B)

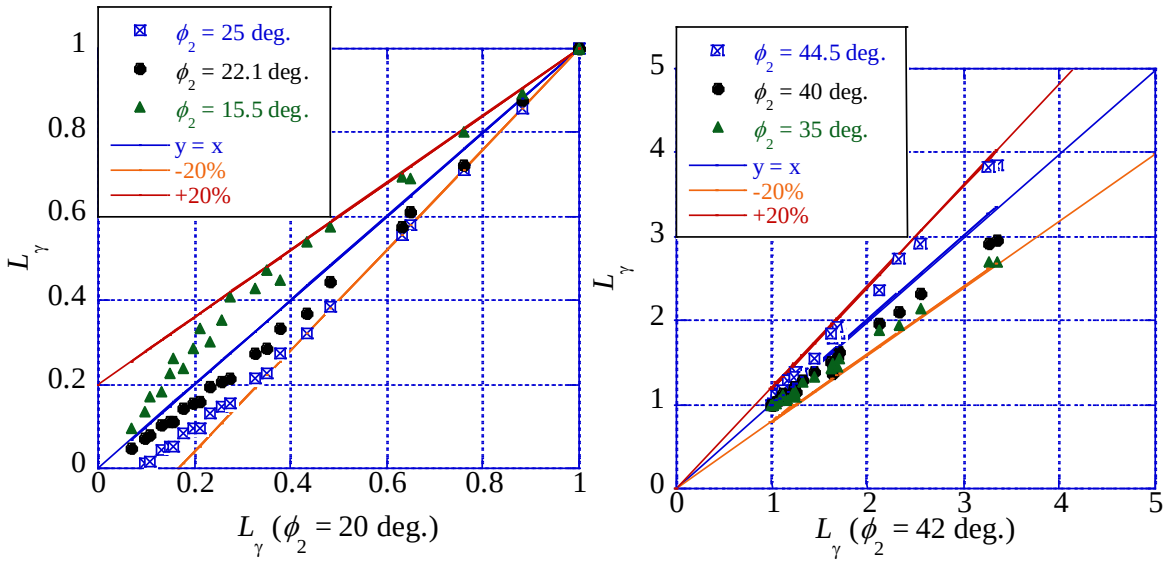

(a) L_γ of ϕ_2 = 20 ° against L_q of ϕ_2 = 15.5°; 22.1°; 25° ($r_\phi \leq 1$; H/B = 0.25, 0.50 and 0.75)

(b) L_γ of ϕ_2 = 42 ° against L_q of ϕ_2 = 35°; 40°; 44.5° ($r_\phi \geq 1$; H/B = 0.25, 0.50 and 0.75)

Fig. 4-13. Influence of ϕ_2 on L_γ (with r_γ = 1)

From those figures, the variations of L_i are within 20% when ϕ_2 is between 15.5 deg. to 25 deg. for the case of $r_\phi \leq 1$; H/B = 0.25, 0.50 and 0.75, and when ϕ_2 is between 35 deg. to 44.5 deg. for the case of $r_\phi \geq 1$; H/B = 0.25, 0.50 and 0.75. Therefore, it can be concluded that the influences of the friction

angle of the second layer (ϕ_2) on L_c, L_q and L_γ are relatively small, and the ratio r_ϕ is the most influencing. Therefore, for simplicity, in the rest of this study, $\phi_2 = 20°$ and $\phi_2 = 42°$ were chosen for the case of $r_\phi \leq 1$ and the case of $r_\phi \geq 1$, respectively.

4.7.4 Influence of *H*/*B* on the Layer Factors (Design Charts Part I)

As depicted in the diagram in **Fig. 4-6**, the thickness of the top soil layer (*H*/*B*) affects all the layer factors L_i (With $i = c, q, \gamma$). For the investigation of the influence of the normalized thickness of the top soil layer (*H*/*B*) on the layer factors, $r_c = 1$, $D_f = 1B$ and $r_\gamma = 1$ (with $c_1 = c_2 = 25$ kPa and $\gamma = \gamma_1 = \gamma_2 = 18$ kN/m^3) were used with the r_ϕ defined in **Section 4.7.2.** The layer factor obtained with the above conditions **(i.e.,** $r_c = 1$, $D_f = 1B$ and $r_\gamma = 1$) are referred to as $L_c^{r_c = 1}$, $L_q^{D_f = 1B}$ and $L_\gamma^{r_\gamma = 1}$ in this study.

The relationships between the parameters r_ϕ and *H*/*B* and the layer factors L_i are depicted in **Fig. 4-14**. The influence of r_ϕ is testified by $L_i < 1$ in the case of $r_\phi \leq 1$ and by $L_i > 1$ when $r_\phi \geq 1$. The influence of r_ϕ decreases when *H*/*B* increase. No influence of r_ϕ ($L_i = 1$) starts to be noticed from a critical thickness *H*/*B**.

In the case of $r_\phi \leq 1$, the critical thicknesses are *H/B** = 6 for L_c and *H/B** = 3 for L_γ. However, for L_q, the critical thickness is higher than *H/B* = 6. When $r_\phi \geq 1$, the critical thicknesses *H/B** are 1.5 for L_c and L_q and 0.75 for L_γ.

Eq. 4-12 below is proposed for the calculation of $L_c^{r_c = 1}$, $L_q^{D_f = 1B}$ and $L_\gamma^{r_\gamma = 1}$**.**

$$L_i = a r_\phi^{\,5} * e^{b r_\phi} \quad \text{(4-12)}$$

where i = c, q, γ. The equations of the coefficients *a, b, c, d, e* and *f* are presented in **Table 4-2**.
The mechanical and technical bases of **Eq. 4-12** are illustrated in **Fig. 4-6 (b). Fig. 4-14** can be used as design charts for estimation of the layer factor L_i.

The layer factor investigated in this section with $r_c = 1$, $D_f = 1B$ and $r_\gamma = 1$ **(i.e.,** $L_c^{r_c = 1}$, $L_q^{D_f = 1B}$ and $L_\gamma^{r_\gamma = 1}$**)** do not reflect the influence of r_c, D_f and r_γ, therefore the investigations on the influences of the parameters r_c, D_f and r_γ are necessary.

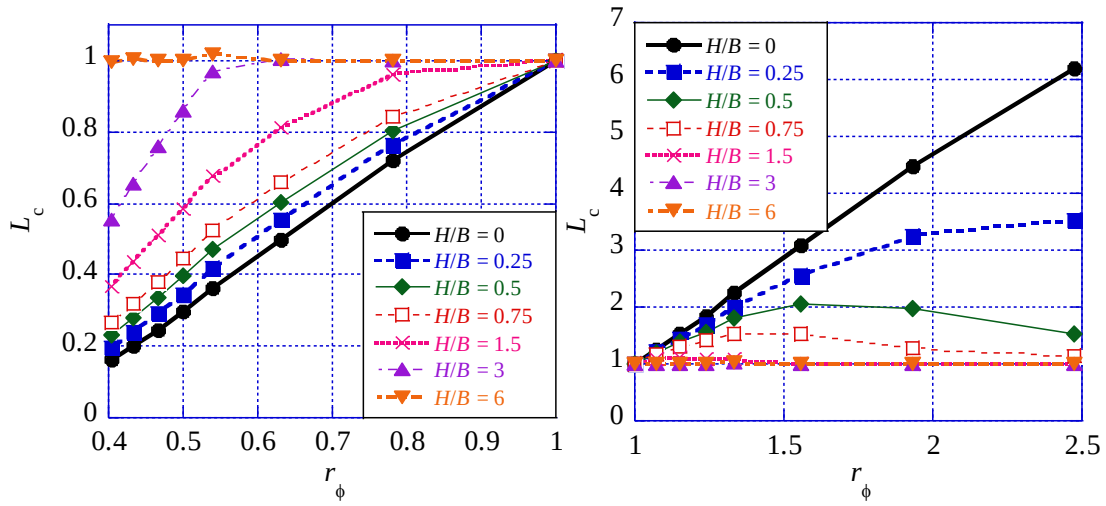

(a) Influence on N_c

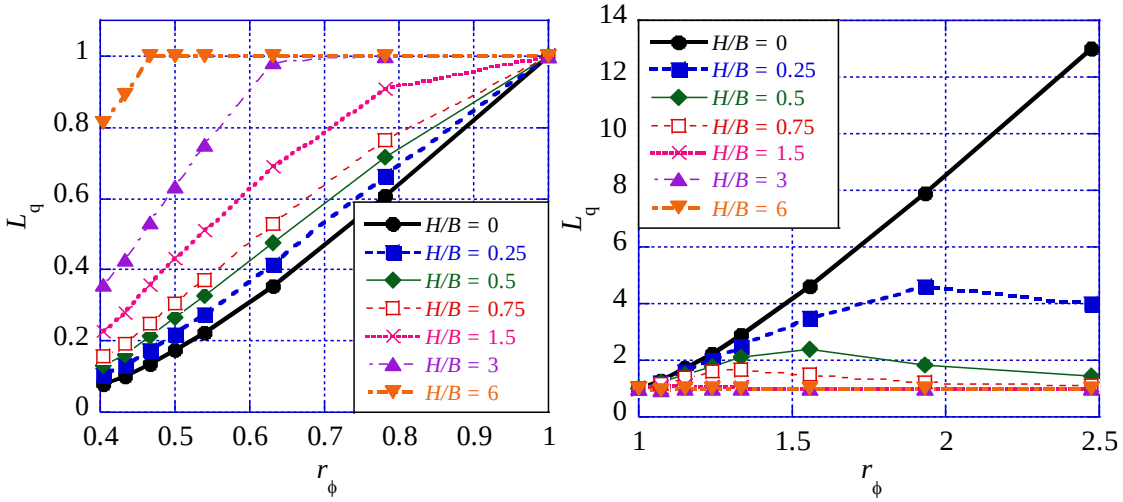

(b) Influence on N_q

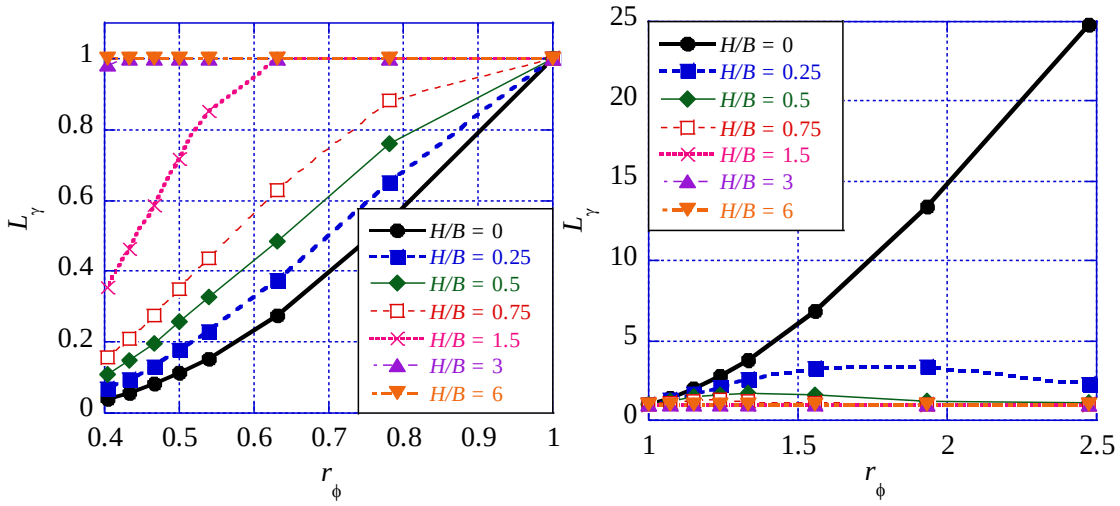

(c) Influence on N_γ

Fig. 4-14. Influence of r_ϕ and H/B on the layer factors L_i when $r_c = 1$, $D_f = 1B$ and $r_\gamma = 1$

Table 4-2. Equations of the coefficients *a*, and *b* in **Eq. 4-12**

		$r_\phi > 1$	$r_\phi < 1$
$L_c^{r_c = 1}$	*a*	$6.8844(H/B)^2 + 18.816(H/B) + 5.2077$	$37.382(H/B)^2 + 120.64(H/B) + 83.829$
	b	$-1.8311(H/B) - 1.805$	$-0.7561(H/B) - 4.6249$
$L_q^{D_f = 1B}$	*a*	$-14.801(H/B)^2 + 43.29(H/B) + 3.524$	$27.121(H/B)^2 + 48.234(H/B) + 36.29$
	b	$-2.5162(H/B) - 1.5009$	$-0.6386(H/B) - 3.8634$
$L_\gamma^{r_\gamma = 1}$	*a*	$-77.799(H/B)^2 + 86.43(H/B) + 3.4669$	$217.15(H/B)^2 - 12.096(H/B) + 18.076$
	b	$-2.8904(H/B) - 1.4771$	$-2.3144(H/B) - 2.9041$

4.7.5 Influence of r_c, D_f and r_γ on the Layer Factors (Design Charts Part II)

Below are the details on how the variation of the parameters r_c, D_f and r_γ affect the layer factors. Each parameter affects the layer L_c, L_q and L_γ respectively (See the diagram in **Fig. 4-6**). Here as well the range of r_ϕ defined in **Section 4.7.2** is used.

4.7.5.1 Influence of r_c on L_c

The relationship between L_c and the couple (r_ϕ; r_c), when $r_\phi \leq 1$, is depicted in **Fig. 4-15(a)** when $H/B = 0.25$. L_c increases with increasing r_c.

The influence of r_c can be obtained separately by dividing the curves of $r_c \neq 1$ by the curve of $r_c = 1$. The influence factor of r_c is referred to as ξ_c (i.e. $\xi_c = L_c^{r_c \neq 1} / L_c^{r_c = 1}$). **Fig. 4-15(b)** shows the ξ_c corresponding to the L_c in **Fig. 4-15(a)**. From **Fig. 4-15(b)**, it is clear that the value of the c_2 (or c_1) does not matter, only the value of the ratio r_c is important. The influence factor ξ_c increases when r_c increases and tends to converge to the unity when r_ϕ increase. The layer factor L_c can therefore be expressed as the formula in **Eq. 4-12** below. The curves of L_c and ξ_c, when $r_\phi \geq 1$, are plotted in **Fig. 4-15(c)** and **Fig. 4-15(d)**, respectively. The influence of r_c is the same as in the case of $r_\phi \leq 1$ and the same conclusions on ξ_c and the value of the c_2 (or c_1) can be drawn.

$$L_c = \xi_c L_c^{r_c = 1} \quad \text{(4-13)}$$

where ξ_c stands as the influence of r_c and $L_c^{r_c = 1}$ (L_c when $r_c = 1$) as the influence of r_ϕ.

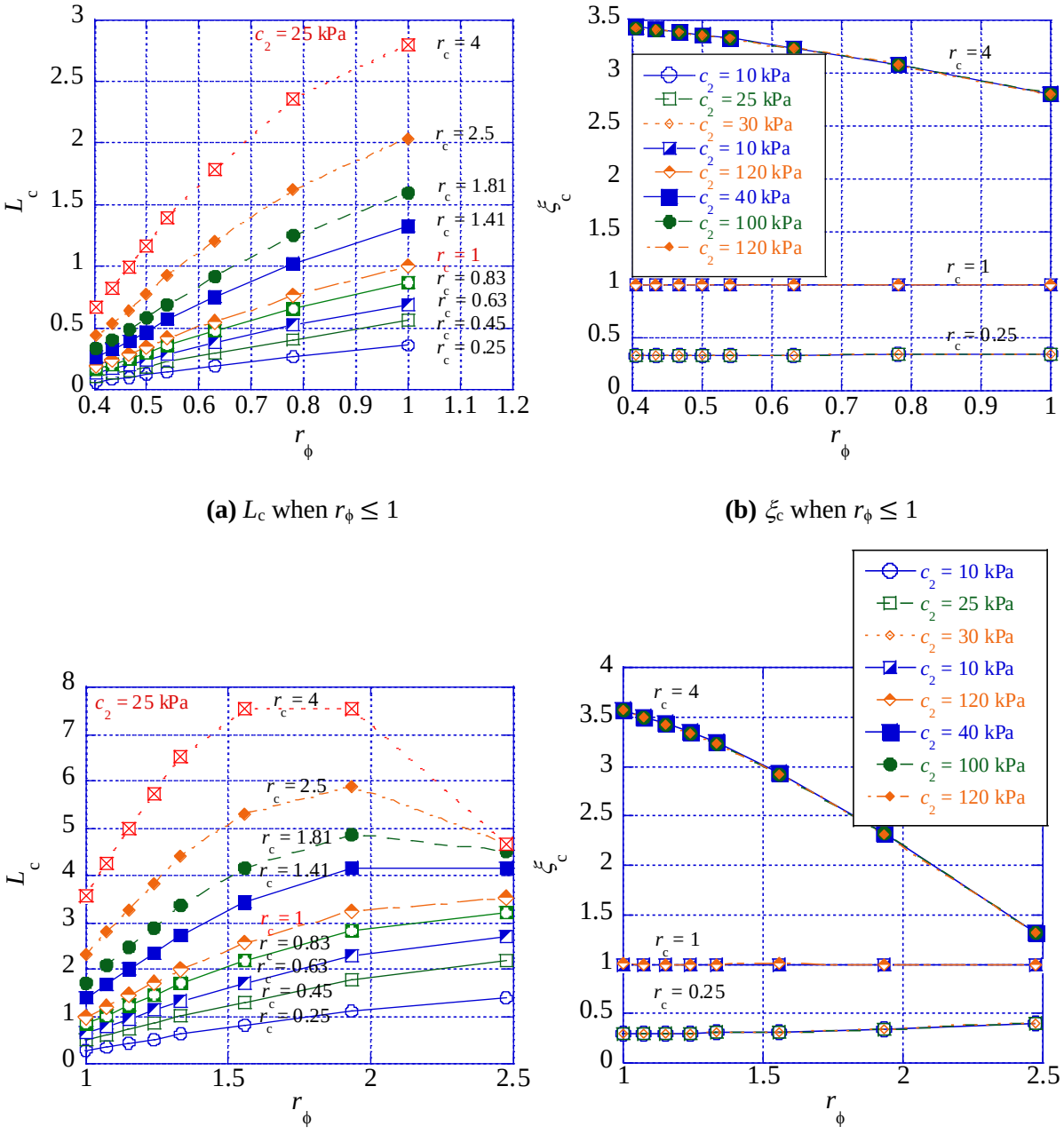

(a) L_c when $r_\phi \leq 1$ **(b)** ξ_c when $r_\phi \leq 1$

(c) L_c when $r_\phi \geq 1$ **(d)** ξ_c when $r_\phi \geq 1$

Fig. 4-15. Influence of r_ϕ and r_c on L_c when H/B = 0.25

More information about ξ_c can be obtained in **Fig. 4-16**. It shows the influence of r_ϕ and H/B on ξ_c for different values of r_c. From **Fig. 4-16(a) to Fig. 4-16(c)** are ξ_c when $r_\phi \leq 1$ and from **Fig. 4-16(d) to Fig. 4-16(f)** are ξ_c when $r_\phi \geq 1$. The same trend as in **Fig. 4-15(b) and Fig. 4-15(d)** can be observed, ξ_c converse to 1 when r_ϕ increases. However, for both $r_\phi \leq 1$ and $r_\phi \geq 1$, when $r_c > 1$ the value of ξ_c decreases with the increasing H/B while for $r_c < 1$ the inverse is observed. **Fig. 4-15** and **Fig. 4-16** can be used as design charts for the estimation of L_c.

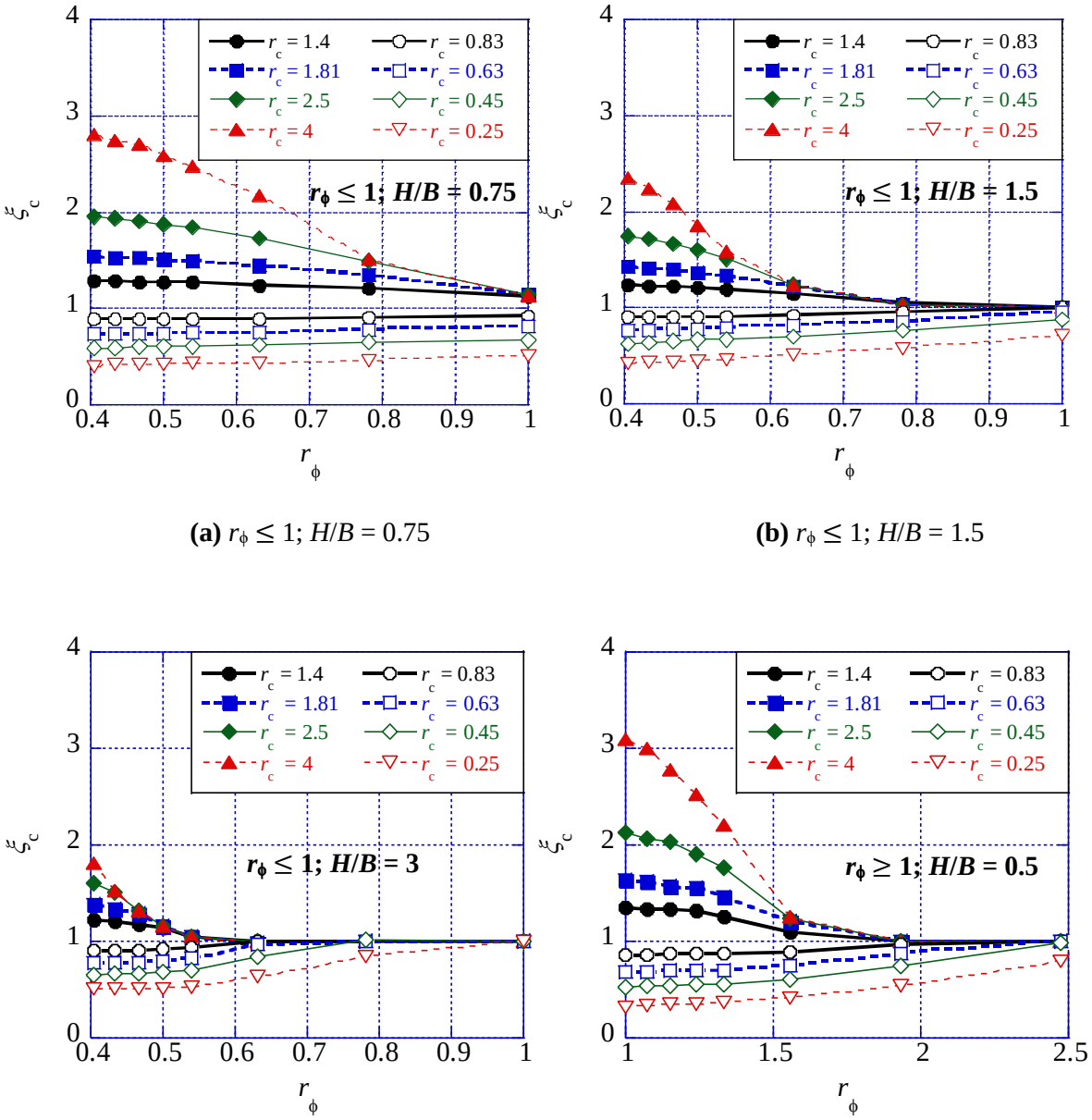

(a) $r_\phi \le 1$; $H/B = 0.75$

(b) $r_\phi \le 1$; $H/B = 1.5$

(c) $r_\phi \le 1$; $H/B = 3$

(d) $r_\phi \ge 1$; $H/B = 0.5$

Fig. 4-16. Influence of r_ϕ and H/B on ξ_c

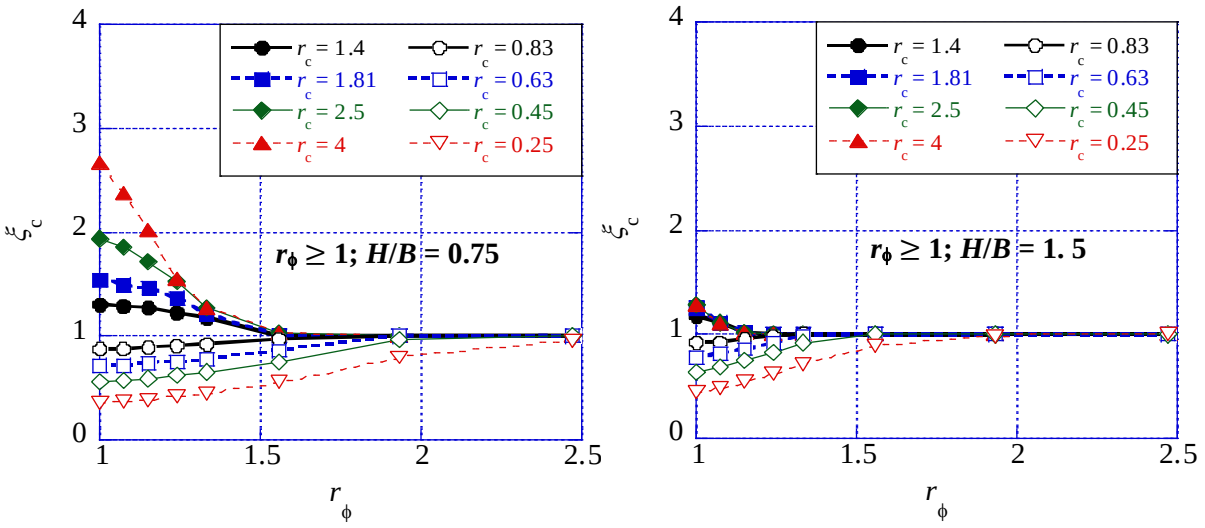

(e) $r_\phi \geq 1$; H/B = 0.75 **(f)** $r_\phi \geq 1$; H/B = 1.5

Fig. 4-16. (cont.) Influence of r_ϕ and H/B on ξ_c

4.7.5.2 Influence of D_f on L_q

The layer factor L_q, when $r_\phi \leq 1$, is presented in **Fig. 4-17(a)** as a function of r_ϕ and D_f when H/B = 0.25. For a shallow foundation, $D_f \leq$ B (Terzaghi 1943). Hence, a range of D_f = 1B to 0.25B was used. L_q inversely increases with D_f. A factor ξ_q is then defined as the ratio of the curves of $D_f \neq$ 1B to the curve of D_f = 1B (i.e. $\xi_q = L_q^{D_f \neq 1B} / L_q^{D_f = 1B}$). The relationship between ξ_q and r_ϕ and D_f is presented in **Fig. 4-17(b)** for different values of the unit weight of the surcharge soil (γ). **Fig. 4-17(b)** suggests that the influence of the value of γ on ξ_q is negligible and the factor ξ_q increases with r_ϕ but inversely increases with D_f. The layer factor L_q can be expressed with **Eq. 4-14** below.

For the case of $r_\phi \geq 1$, the curves of L_q and ξ_q are presented in **Fig. 4-17(c)** and **Fig. 4-17(d)**, respectively. L_q and ξ_q both inversely increase with D_f and the factor ξ_q increases with r_ϕ. Non-influence of the value of the unit weight of the surcharge soil (γ) is also shown in **Fig. 4-17(d)**.

$$L_q = \xi_q L_q^{D_f = 1B} \quad \text{(4-14)}$$

where ξ_q stands as the influence of D_f and $L_q^{D_f = 1B}$ (L_q when D_f = 1B) as the influence of r_ϕ.

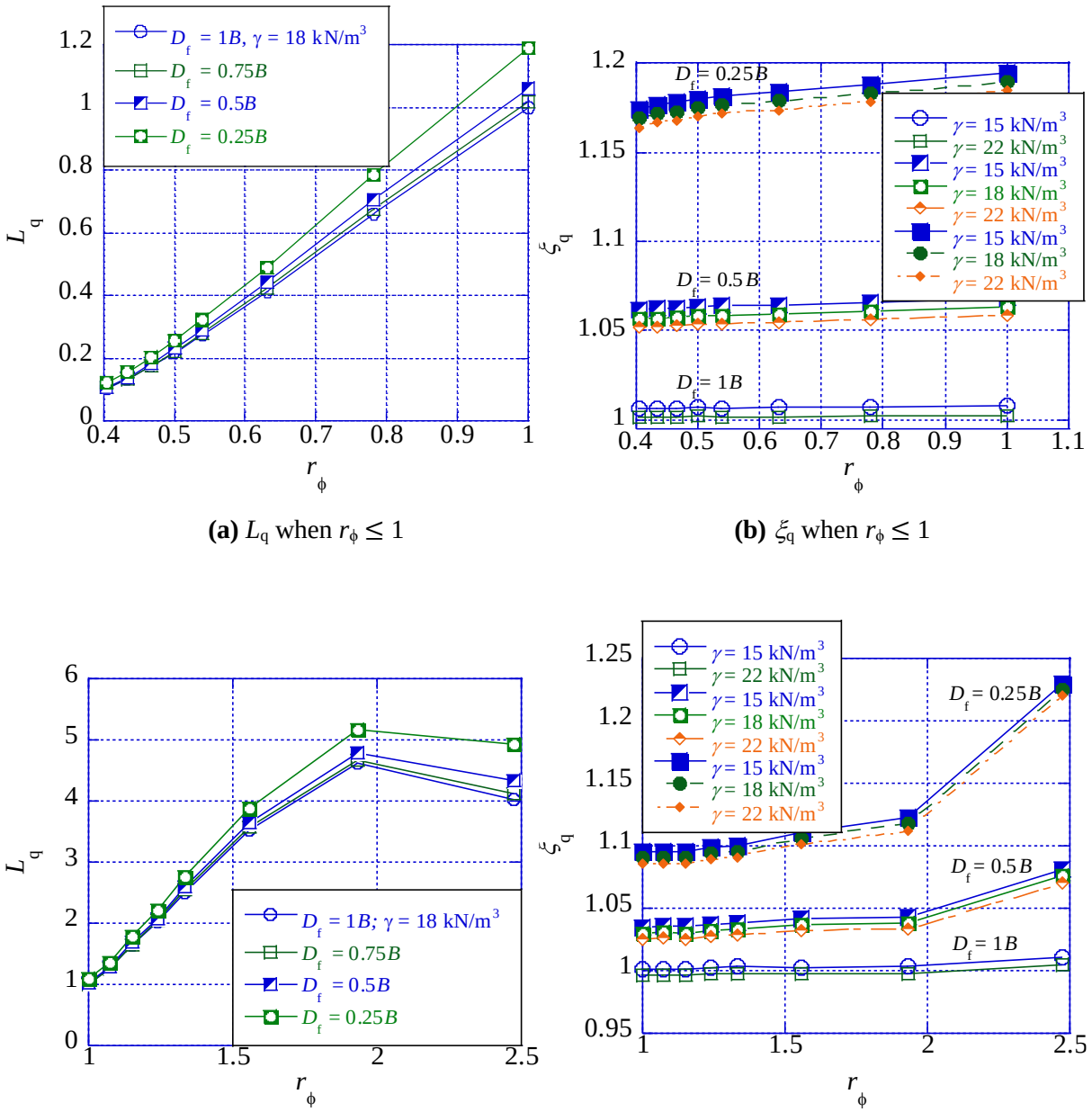

(a) L_q when $r_\phi \leq 1$ **(b)** ξ_q when $r_\phi \leq 1$

(c) L_q when $r_\phi \geq 1$ **(d)** ξ_q when $r_\phi \geq 1$

Fig. 4-17. Influence of r_ϕ and D_f on L_q when H/B = 0.25

More information about the factor ξ_q can be obtained in **Fig. 4-18**. It shows the influence of r_ϕ and H/B on ξ_q for different values of D_f. The same trend as in **Fig. 17(b) and Fig. 17(d)** is observed, ξ_q inversely increases with D_f. For $r_\phi \leq 1$, ξ_q decreases with increasing r_ϕ but increases with increasing H/B, however when $r_\phi \geq 1$, the inverse is observed. **Fig. 17** and **Fig. 4-18** can be used as design charts for the estimation of L_q.

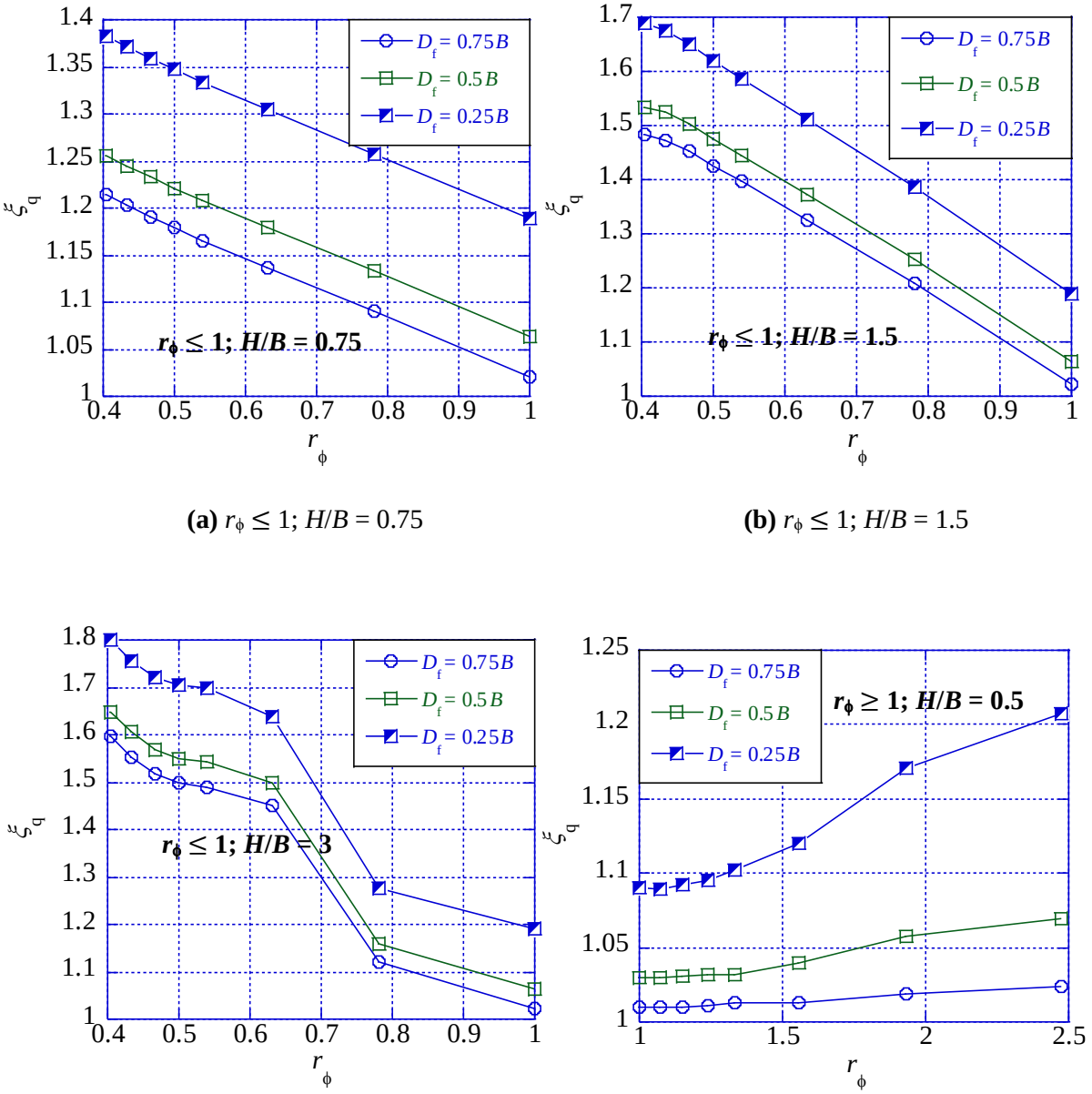

(a) $r_\phi \le 1$; $H/B = 0.75$

(b) $r_\phi \le 1$; $H/B = 1.5$

(c) $r_\phi \le 1$; $H/B = 3$

(d) $r_\phi \ge 1$; $H/B = 0.5$

Fig. 4-18. Influence of r_ϕ and H/B on ξ_q

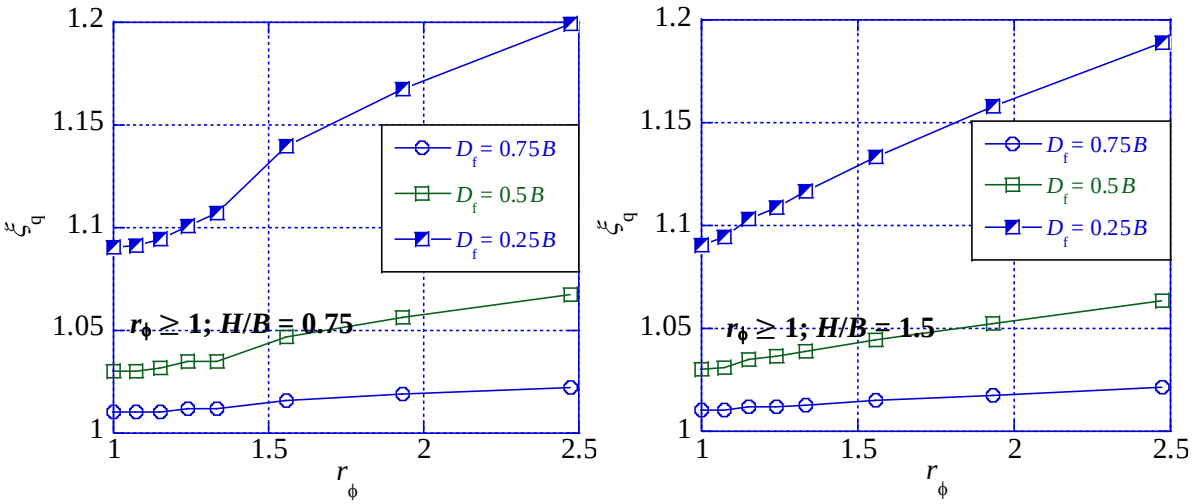

(e) $r_\phi \geq 1$; $H/B = 0.75$ **(f)** $r_\phi \geq 1$; $H/B = 1.5$

Fig. 4-18. (cont.) Influence of r_ϕ and H/B on ξ_q

4.7.5.3 Influence of r_γ on L_γ

The case of L_γ is quite similar to that of L_c. For $H/B = 0.25$, the curves of L_γ and ξ_γ are respectively presented in **Fig. 4-19(a)** and **Fig. 4-19(b)** for the case of $r_\phi \leq 1$ and **Fig. 4-19(c)** and **Fig. 4-19(d)** for the case of $r_\phi \geq 1$. Where, ξ_γ is the influence of r_γ expressed by $\xi_\gamma = L_\gamma^{r_\gamma \neq 1} / L_\gamma^{r_\gamma = 1}$.

The behaviours of L_γ and ξ_γ are similar to those of L_c and ξ_c, respectively, and here as well the influence of the value of γ_2 (or γ_1) is negligible. The layer factor L_γ can be expressed by **Eq. 4-15** below.

$$L_\gamma = \xi_\gamma L_\gamma^{r_\gamma = 1} \quad \text{(4-15)}$$

where ξ_γ stands as the influence of r_γ and $L_\gamma^{r_\gamma = 1}$ (L_γ when $r_\gamma = 1$) as the influence of r_ϕ.

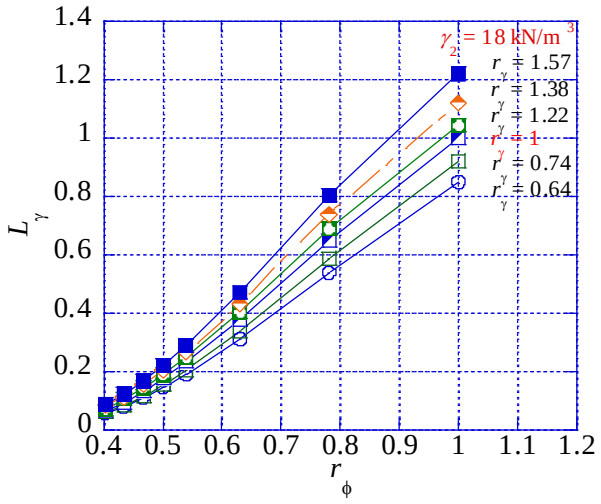

(a) L_γ when $r_\phi \leq 1$

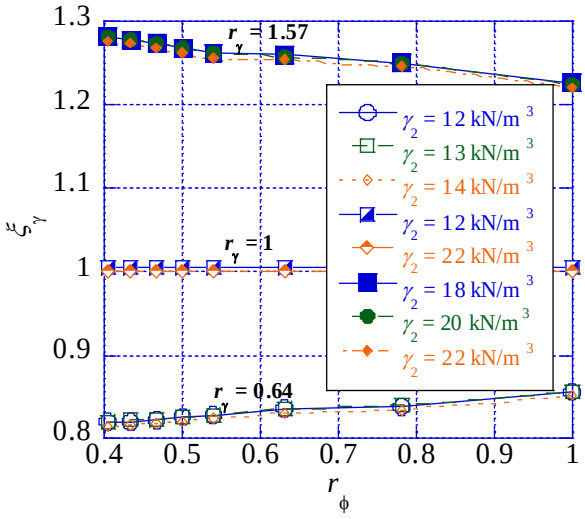

(b) ξ_γ when $r_\phi \leq 1$

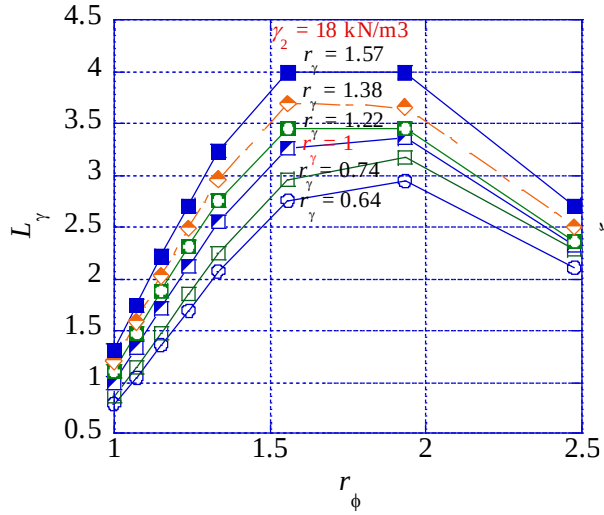

(c) L_γ when $r_\phi \geq 1$

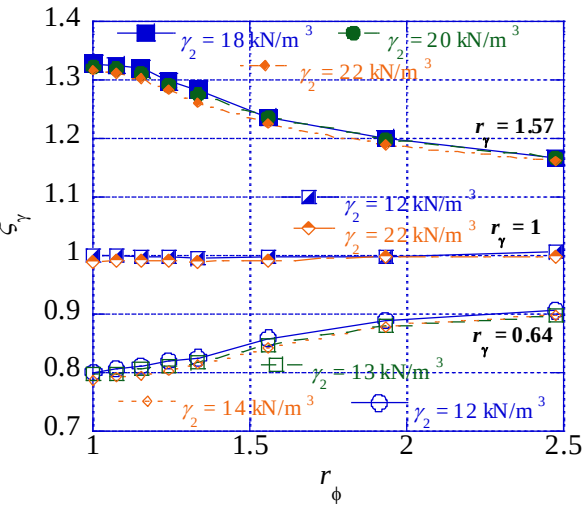

(d) ξ_γ when $r_\phi \geq 1$

Fig. 4-19. Influence of r_ϕ and r_γ on L_γ when H/B = 0.25

More information about the factor ξ_γ can be obtained in **Fig. 4-20**. It shows the influence of r_ϕ and H/B on ξ_γ for different values of r_γ. The behavior of ξ_γ is like the one of ξ_c. Here also, independently to r_ϕ, for $r_\gamma > 1$ the value of ξ_γ decreases with the increasing H/B and the inverse is observed in cases of $r_\gamma < 1$. **Fig. 19** and **Fig. 4-20** can be used as design charts for the estimation of L_γ.

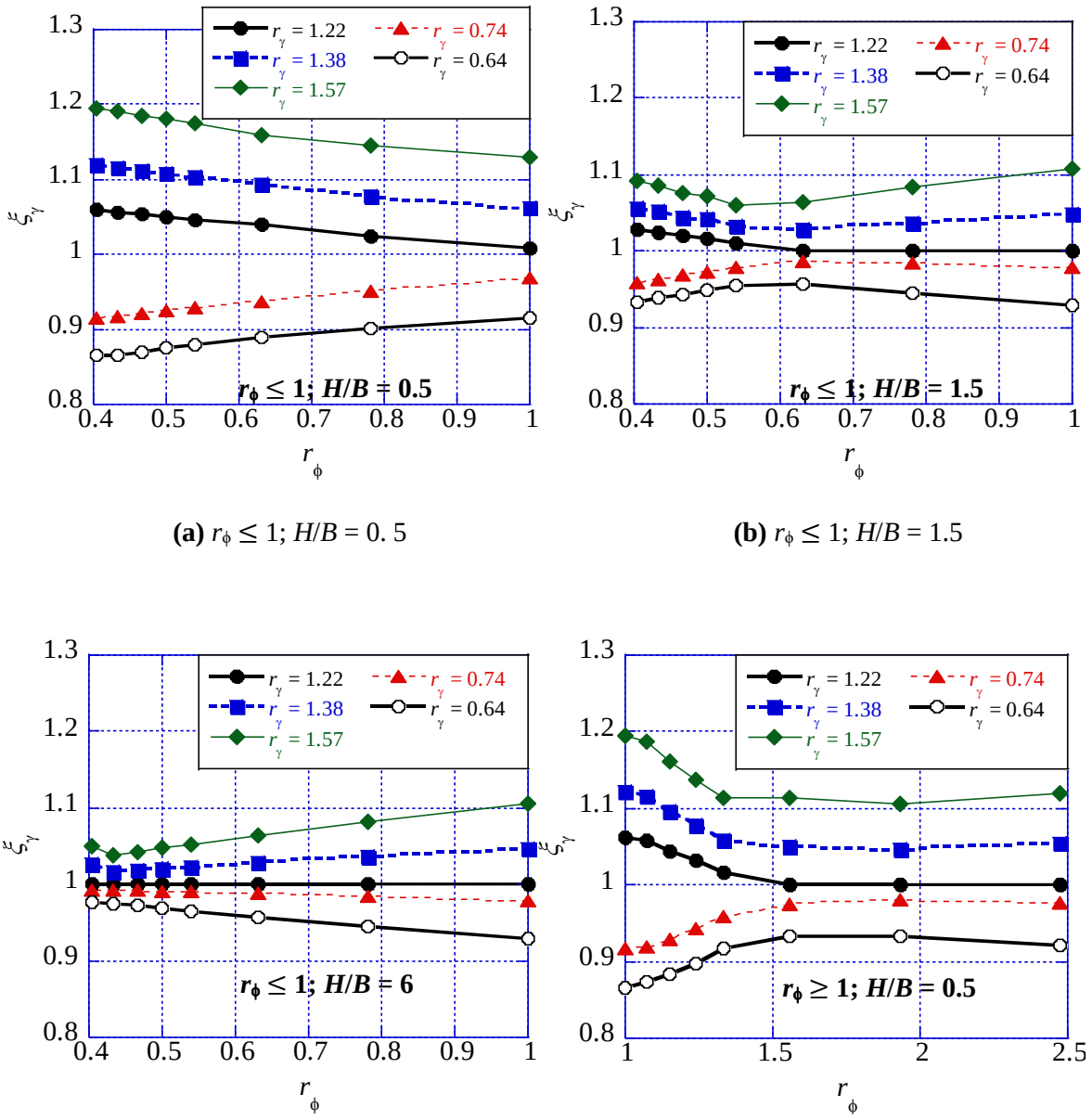

(a) $r_\phi \le 1$; $H/B = 0.5$

(b) $r_\phi \le 1$; $H/B = 1.5$

(c) $r_\phi \le 1$; $H/B = 6$

(d) $r_\phi \ge 1$; $H/B = 0.5$

Fig. 4-20. Influence of r_ϕ and H/B on ξ_γ

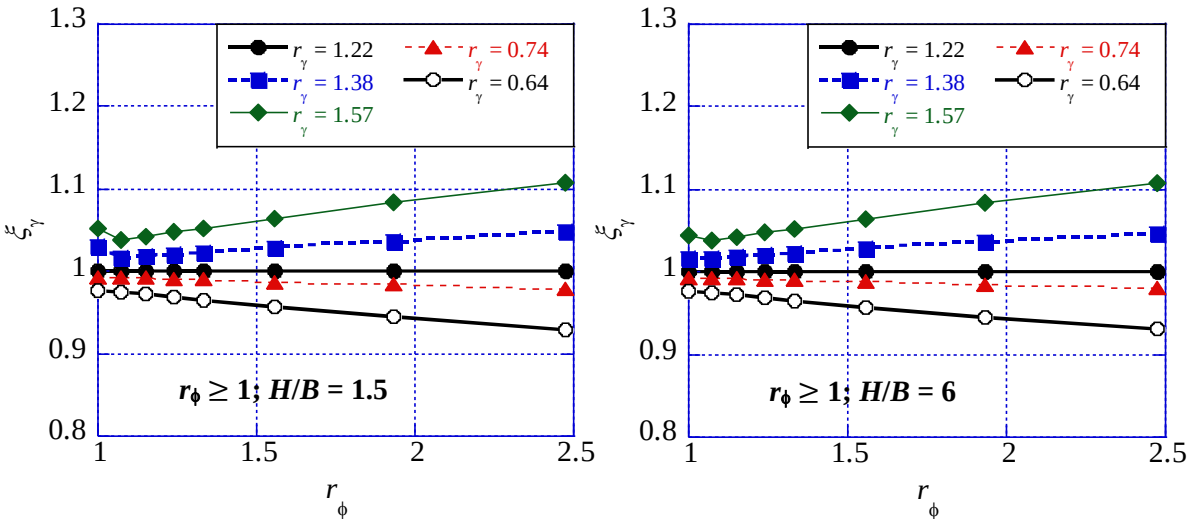

(e) $r_\phi \geq 1$; H/B = 1.5 **(f)** $r_\phi \geq 1$; H/B = 6

Fig. 4-20. (cont.) Influence of r_ϕ and H/B on ξ_γ

4.8 Bearing Capacity Formula of Two-layered *c*-ϕ Soils

Layer factors L_c, L_q and L_γ are defined in this study to consider the effect of the bottom soil layer on the bearing capacity factors N_c, N_q and N_γ of the top layer. The layer factors can be expressed as $L_c = \xi_c L_c^{r_c=1}$, $L_q = \xi_q L_q^{D_f=1B}$ and $L_\gamma = \xi_\gamma L_\gamma^{r_\gamma=1}$ (**section 4.7.5**). $L_c^{r_c=1}$, $L_q^{D_f=1B}$ and $L_\gamma^{r_\gamma=1}$ can be obtained, for many combinations of H/B and r_ϕ, using the design charts in **Fig. 4-14** or **Eq. 4-12**. The factors ξ_c, ξ_q and ξ_γ can be obtained, for many combinations of H/B and r_ϕ, from the design charts in **Fig. 4-15 to Fig. 4-20**. Therefore, by using **Eq. 4-12** (or **Fig. 4-14** as a design chart) and **Fig. 4-15 to Fig. 4-20**, the layer factors L_c, L_q and L_γ can be obtained for many combinations of H/B, r_ϕ, r_c, D_f and r_γ. The new bearing capacity formula of a strip footing on two-layered *c*-ϕ soil is then expressed by **Eq. 4-16** below. In **Eq. 4-16**, N_c, N_q and N_γ are obtained using ϕ_1 in the traditional methods.

$$q_{ult} = c_1 N_c L_c + q N_q L_q + 0.5\gamma_1 B N_\gamma L_\gamma \cdots\cdots (4\text{-}16)$$

Like **Eq. 4-12**, The mechanical and technical bases of **Eq. 4-16** are explained in **section 4-7** and illustrated with **Fig. 4-6 (b).**

4.9. Failure Patterns

The nature of bearing capacity failure in soil proposed by several authors is presented in **Fig. 4-21**. There are “Local shear failure”, “General shear failure”, “Transitional shear failure” and “Punching shear failure”.

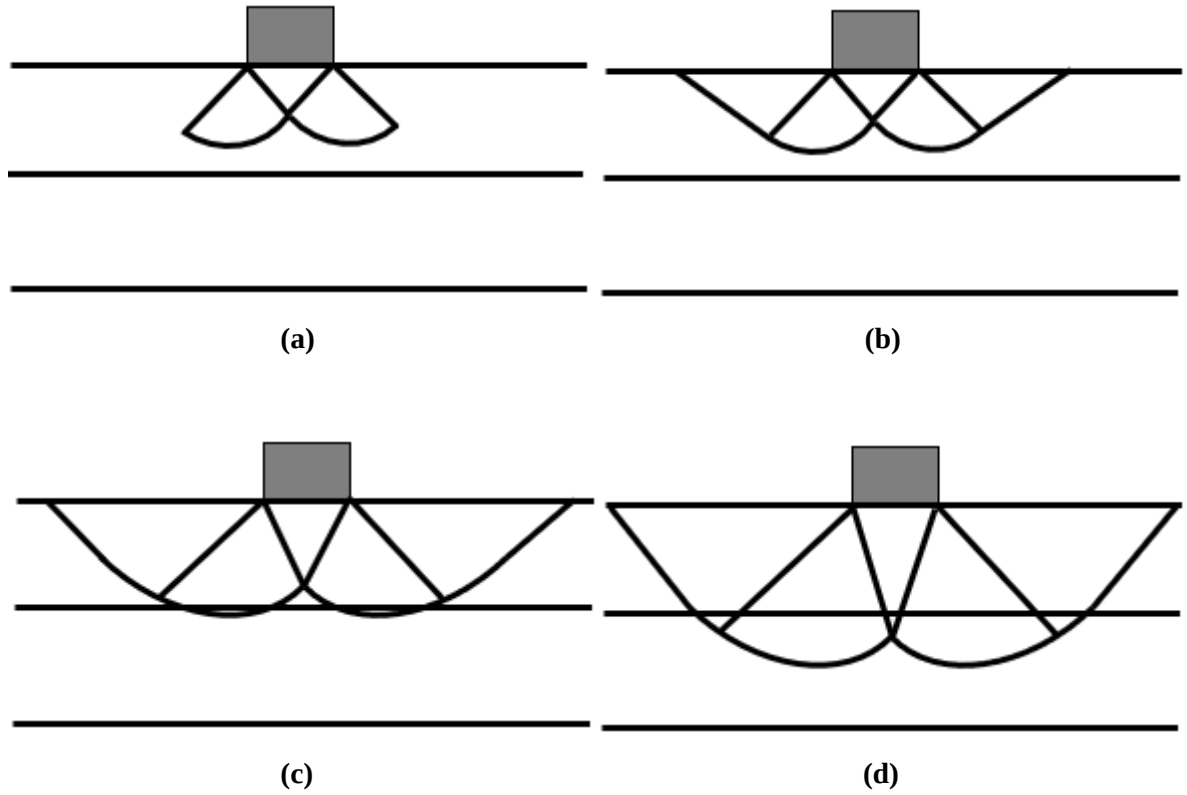

Fig. 4-21. Bearing capacity failure in soil drawn after Vesic 1973; (a) local shear failure, (b) general shear failure; drawn after Salimi et al. 2019, (c) Transitional shear failure and (d) punching shear failure

Summaries of failure patterns obtained in this study are shown in **Fig. 4-22(a)** and **Fig. 4-22(b)** for $r_\phi \leq 1$ and $r_\phi \geq 1$, respectively. The norm of the strain rate is represented by contour lines in the range of $\dot{e}_{\min}(=0) \sim \dot{e}_{\max}$. The black line is the boundary between the two soil layers.

Three types of failure modes are observed in each case of r_ϕ ($r_\phi \leq 1$ and $r_\phi \geq 1$). In the case of $r_\phi \leq 1$, a general shear failure, a transitional shear failure, and a punching shear failure are observed. In the case of $r_\phi \geq 1$, a general shear failure, a transitional shear failure, and a local shear failure are obtained.

The type of failure observed depends on the values of r_ϕ and H/B. There are specific values of r_ϕ and H/B from which the failure pattern transits from one type to another.

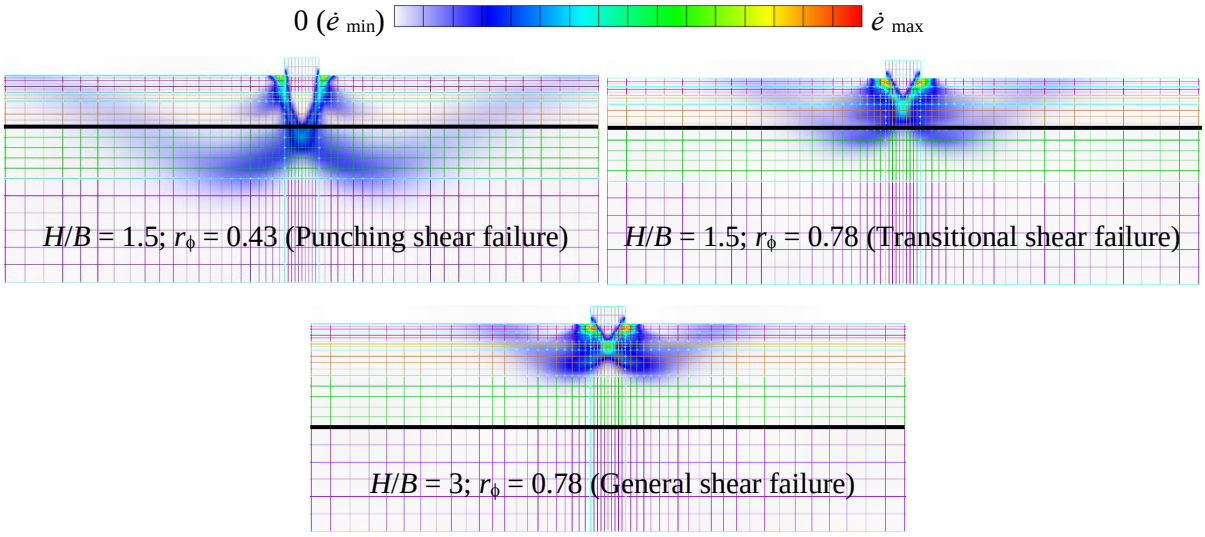

(a) For $r_\phi \leq 1$

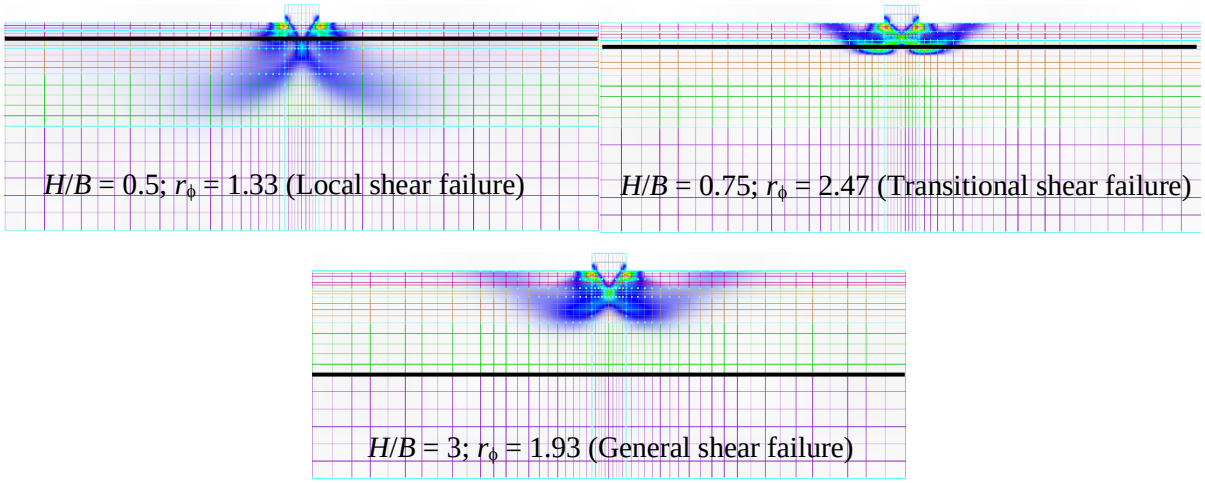

(b) For $r_\phi \geq 1$

Fig. 4-22. Failure patterns

A series of 592 cases of bearing capacity was performed to identify under which conditions each type of failure occurs. The conditions necessary for each failure type are presented in **Fig. 4-23**.

The general shear failures are obtained when the influence of the bottom layer disappears. In that case, the failure zone is confined in the top layer, resulting in $L_i = 1$ in **Fig. 4-14**. Therefore, the critical thickness of the top layer is not the depth of central wedge $B/2 \tan(45 + \phi_1/2)$ but a function of r_ϕ.

The other types of failure occur when the thickness of the top layer is smaller than the critical one.

Those failures extend into the bottom layer resulting in $L_i < 1$ when $r_\phi < 1$and $L_i > 1$ when $r_\phi > 1$, in **Fig. 4-14**. The punching shear failure occurs with high r_ϕ (closed to 1) when the thickness of the top layer is not enough to contain the central wedge under the footing. The punching shear failures under that condition are referred to as shallow transitional by Salimi et al. 2019. The local shear failure occurs for a high value of r_ϕ only when the thickness of the top layer is not enough to allow the shear planes to extend to the soil surface. The transitional shear failure is the intermediate failure between the general shear failure and the two other types of failure. It occurs when the thickness H/B is less than critical but high enough to avoid the occurrence of the punching shear failure or the local shear failure. The transitional shear failure features a geometry like that of the general shear failure but is penetrating in the bottom soil layer.

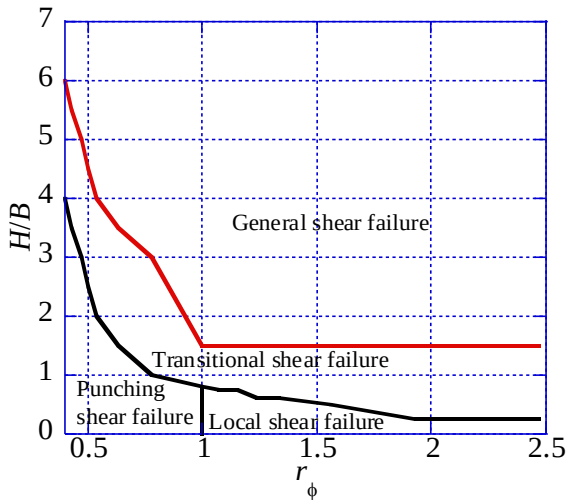

Fig. 4-23. Failure type as a function of r_ϕ and H/B

4.10. Validation of the Proposed Equation

Yao et al. (2018) studied the undrained stability of strip footing in two-layered clays by finite element limit analysis. The undrained bearing capacity factor of soft clay under stiff clay is estimated with the proposed equation and the result are compared with those from strip footing on two-layered clays without void from Yao et al. (2018). In this case, since the internal frictional angle of the clay is zero, there is no influence of r_ϕ for the proposed equation, therefore $L_c^{r_c=1}$ is equal to the unit ($L_c^{r_c=1} = 1$). The influence factors ξ_c of the ratio r_c ($r_c = c_{u2}/c_{u1}$) can be obtained from **Fig. 4-15 and Fig. 4-16** of this study, using $r_\phi = 1$. The bearing capacity factor N_c of uniform clay equal to 5.14 is considered. By

multiplying N_c with L_c = ($L_c^{r_c = 1}$ * ξc) the undrained bearing capacity factor N_c* of soft clay under stiff clay is obtained.

Fig. 4-24 (a) shows the comparison result for the case of H/B = 1. When r_c < 1 the results of **Eq. (4-16)** are slightly lower than those of Yao et al. (2018), which is on the safe side, but the difference is acceptable. For r_c > 1, Yao et al. 2018 show a constant value of N_c* which is not reasonable since for r_c > 1 the bottom clay is stiffer and should contribute to increasing N_c* (especially for H/B = 1). For r_c > 1, N_c* should be higher than 5.14 (bearing capacity factor N_c of uniform clay) as shown the results of **Eq. (4-16)**.

Based on this comparison, it can be concluded that the proposed equation can estimate the bearing capacity of strip footing on two-layered clays.

The ability of the proposed equation to estimate the bearing capacity of footing in two-layered sand is also investigated for more reliability. Das et al. (2019) studied the bearing capacity of circular footing on a weak sand layer overlying a dense sand deposit. The results of the bearing capacity factor of circular in two-layered sand from Das et al. 2019 are used to compare with those of the proposed equation. Three cases were considered: case1: [(ϕ_1 = 30 deg., γ_1 = 13.5 kN/m^3); (ϕ_2 = 40 deg., γ_2 = 17.5 kN/m^3)]; case2: [(ϕ_1 = 36 deg., γ_1 = 16 kN/m^3); (ϕ_2 = 40 deg., γ_2 = 17.5 kN/m^3)]; case3: [(ϕ_1 = 36 deg., γ_1 = 16 kN/m^3); (ϕ_2 = 44 deg., γ_2 = 19 kN/m^3)]; where ϕ_1 and ϕ_2 is the internal friction angle of the top sand and the bottom sand respectively and γ_1 and γ_2 is the unit weight of the top sand and the bottom sand respectively. From case1 to case3 the corresponding ratio r_ϕ of this study for Eq. (16) is r_ϕ = 1.67; r_ϕ = 1.15 and r_ϕ = 1.33 respectively. The corresponding ratio r_γ of this study for Eq. (16) is r_γ = 1.3; r_γ = 1.09 and r_γ = 1.19 respectively.

Das et al. (2019) defined a bearing capacity ratio (BCR), which is defined as the ratio of the bearing capacity of footing on layered sand to the bearing capacity of the footing on homogeneous sand with friction angle ϕ_2. However, in this study, the L_γ is the ratio of the bearing capacity factor of footing on layered sand to the bearing capacity factor of the footing on homogeneous sand with friction angle ϕ_1. To obtain the corresponding BCR of Das et al. (2019), the L_γ were obtained using the ratios r_ϕ and r_γ and the results were normalized with the case H/B = 0. The comparison is shown in **Fig. 4-24(b)** for each of the 3 cases. The results of **Eq. (4-16)** are slightly higher than those of Das et al. (2019). But, overall, a good agreement is obtained. This last comparison is confirming the ability of the proposed equation to estimate the bearing capacity of footing in two-layered sand for both strip footing and circular footing.

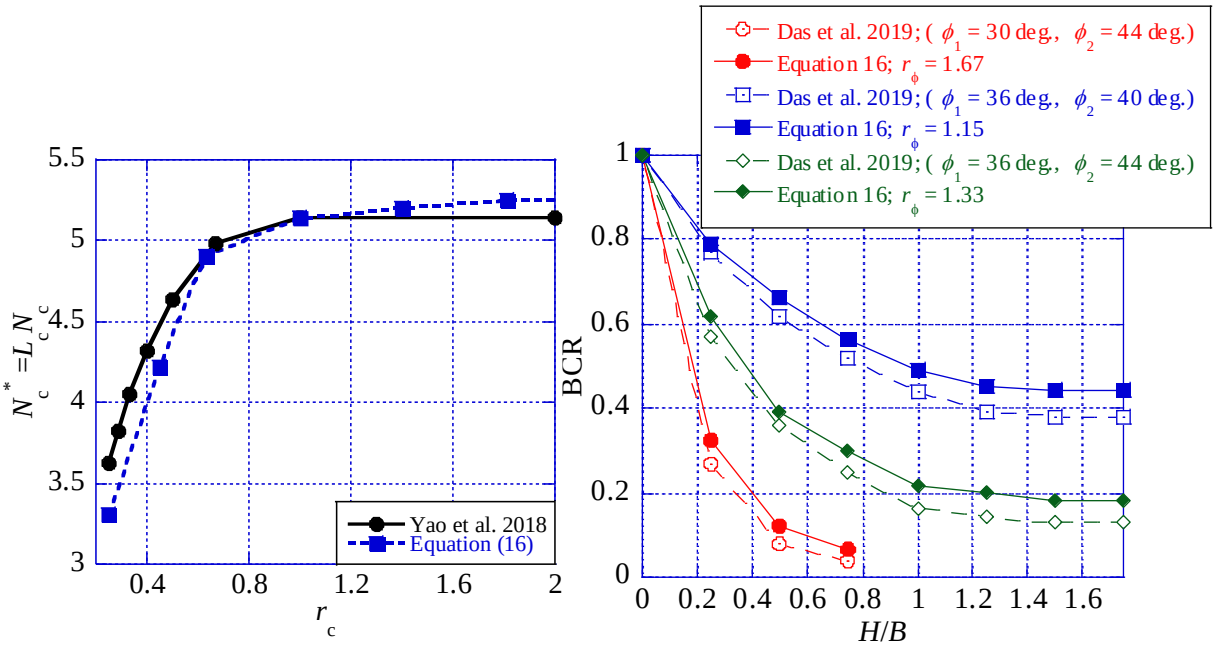

(a) Comparison with Yao et al. (2018) (b) Comparison with Das et al. (2019)

Fig. 4-24. Validation of Equation (4-16)

4.11 Conclusions

This study carried out two-dimensional RPFEM analyses in plane-strain conditions to estimate the bearing capacity of two-layered *c*-ϕ soils, using an in-house code. A constitutive equation that employs the Drucker-Prager yield function was used. The influences of the following parameters on the bearing capacity were investigated: The ratio of the tangent of the angle of friction of the bottom layer to that of the top layer; the ratio of the cohesion of the bottom layer to that of the top layer; the ratio of the unit weight of the bottom layer to that of the top layer; the embedment of the footing and the thickness of the top layer. The followings are the founding of this study:

By attributing to each soil layer its strength parameters, RPFEM has shown that the bottom layer may lead to punching failure in the case of a softer bottom while in the case of a stiffer bottom layer it may lead to local failure. These effects of the bottom layer cannot be obtained with the average strength parameters suggested by the previous study.

Three types of failure are obtained in each case; for the case of a softer bottom layer: General shear

failure, Transitional shear failure and Punching shear failure. In the case of a stiffer bottom layer: General shear failure, transitional shear failure and Local shear failure. The type of failure observed depends on the values of r_ϕ and H/B. There are specific values of r_ϕ and H/B from which the failure pattern transits from one type to another. Therefore, the critical thickness of the top layer is not the depth of central wedge $B/2 \tan (45+ \phi_1/2)$ but a function of r_ϕ. We have proposed a chart that summarizes the conditions of occurrence of different failure types encountered in the bearing capacity of two-layered c-ϕ soils.

The critical thickness (H/B^*) of the top soil layer is different for each layer factor. In the case of a softer bottom layer, the critical thicknesses are $H/B^* = 6$ for L_c and $H/B^* = 3$ for L_γ. However, for L_q, the critical thickness is higher than $H/B = 6$. For the case of a stiffer bottom layer, the critical thicknesses H/B^* are 1.5 for L_c and L_q and 0.75 for L_γ.

The value of the strength parameters of cohesion and unit weight taken individually [c_2 (or c_1), γ_2 (or γ_1)] do not have an influence on the layer factors, only the ratios (r_c and r_γ) of these parameters are important to consider as influencing factors.

Using the proposed layer factors and the traditional bearing capacity factors, we have proposed a formula to calculate the bearing capacity of two-layered c-ϕ soils.

A comparison of the proposed method with existing theories on the bearing capacity of two-layered c-ϕ soils has confirmed that the proposed method provides an accurate estimation of the bearing capacity.

We have, therefore, proposed a new simple approach for estimating the bearing capacity of strip footings in two-layered c-ϕ soils.

References

[1] Azam, G., and M.C. Wang. 1991. “Bearing capacity of strip footing supported by two-layer C-φ soils”. Transp Res Rec No. 1331, Transp Res Board: 56-66.

[2] Bowles, J.E. 1996. Foundations Analysis and Design. New York: McGraw-Hill Publishing Company.

[3] Brinch Hansen, J.A. 1970. “Revised and extended formula for bearing capacity”. Bulletin no. 28. Danish Geotechnical Institute Copenhagen: 5-11.

[4] Brown, J., G.G. Meyerhof. 1969. “Experimental study of bearing capacity in layered clays”. In Proc. Stmenth Int. Con. Soil Mech. Found. Eng., 2: 45-51.

[5] Burd, H.J., S. Frydman. 1997. “Bearing capacity of plane-strain footings on layered soils”. Can Geotech J. 34(2): 241-253.

[6] Button, S.J. 1953. “The Bearing Capacity of Footings on a Two-Layer Cohesive Subsoil”. 3rd ICSMFE. Vol. 1: 332-335.

[7] Das, P.P., V. N. Khatri, R. K. Dutta. 2019. “Bearing capacity of ring footing on weak sand layer overlying a dense sand deposit”. Geomechanics and Geoengineering. DOI: 10.1080/17486025.2019.1664775

[8] Das, B.M., K.F. Dallo. 1984. “Bearing capacity of shallow foundations on a strong sand layer underlain by soft clay”. Civ Eng Pract Des Eng. 3(5): 417-438.

[9] Das, B.M., R.F. Munoz. 1984. “Bearing capacity of eccentrically loaded continuous foundations on layered sand”. Transp Res Rec. 28-31.

[10] Desai, C.S., L. Reese. 1970a. “Ultimate capacity of circular footings on layered soils”. J Indian Nat. Soc. Soil Mech. Found. Eng. 96(1): 41-50.

[11] Desai, C.S., L. Reese. 1970b. “Analysis of circular footings on layered soils”. J Soil Mech. Found. Division, ASCE. 96(4): 1289-1310.

[12] Du, N.L., S. Ohtsuka, T. Hoshina, K. Isobe. 2016. “Discussion on size effect of footing in ultimate bearing capacity of sandy soil using rigid plastic finite element method”. Soils Found. 56(1): 93-103.

[13] Farah, C.A. 2004. “Ultimate bearing capacity of Shallow foundations on layered soils”. MSc thesis, Civil and Environmental Engineering, Concordia Univ; Quebec.

[14] Florkiewicz, A. 1989. “Upper bound to bearing capacity of layered soils”. Can Geotech J. 26(4): 730-736.

[15] Griffiths, D.V. 1982. “Computation of bearing capacity on layered soils”. In Proc., 4th int. conf., Num. meth. Geomech. 163-170.

[16] Hanna, A.M., G.G. Meyerhof. 1980. “Design charts for ultimate bearing capacity of foundations on sand overlying soft clay”. Can Geotech J. 17(2): 300-303.

[17] Hanna, A.M.. 1981. “Foundations on strong sand overlying weak sand”. J Geotech Eng Division, ASCE. 107(7): 915-927.

[18] Hanna, A.M. 1982. “Bearing capacity of foundations on a weak sand layer overlying a strong deposit”. Can Geotech J. 19(3): 392-396.

[19] Hoshina, T., S. Ohtsuka, K. Isobe. 2011. “Ultimate bearing capacity of ground by rigid plastic finite element method taking account of stress-dependent non-linear strength property”. J. Appl. Mech. 6: 191–200 (in Japanese).

[20] Huang, M., H.L. Qin. 2009. “Upper-bound multi-rigid-block solutions for bearing capacity of two-layered soils”. Comput Geotech. 36(3): 52-59.

[21] Kenny, M.J., K.Z. Andrawes. 1979. “The bearing capacity of footings on a sand layer overlying soft clay”. Geotechnique. 47(2): 339-345.

[22] Khatri, V., J. Kumar, S. Akhtar. 2017. Bearing capacity of foundations with inclusion of dense sand layer over loose sand strata. Int J Geomech. 17(10): 06017018.

[23] Kumar, A., M.L. Ohri, R.K. Bansal. 2007. “Bearing capacity tests of strip footings on reinforced layered soil”. Geotech Geol Eng. 25(2): 139-150.

[24] Ma Brouki, A., D. Benmeddour, R. Frank. 2010. “Numerical study of the bearing capacity for two interfering strip footings on sands”. Comput Geotech. 37(4): 431–439.

[25] Merlfleld, R.S., S.W. Sloan, H.S. Yu. 1999. “Rigorous plasticity solutions for the bearing capacity of two-layered clays”. Geotechnique. 49(4): 471-490.

[26] Meyerhof, G.G. 1963. “Some recent research on the bearing capacity of foundations”. Can Geotech J. 1:16–26. https://doi.org/10.1139/t63-003.

[27] Meyerhof, G.G. 1974. “Ultimate bearing capacity of footings on sand layer overlying clay”. Can Geotech J. 11(2): 223–229.

[28] Meyerhof GG. 1976. “Bearing capacity and settlement of pile foundations”. J Geotech Eng Division, ASCE. 102(3): 195–228.

[29] Meyerhof, G.G., A.M. Hanna. 1978. “Ultimate bearing capacity of foundations on layered soils under inclined load”. Can Geotech J. 15(4): 565–572.

[30] Michalowski, R.L., L. Shi. 1995. “Bearing capacity of footings over 2-layer foundation soils”. J Geotech Eng. 21(5): 421– 428.

[31] Mosadegh, A., H. Nikraz. 2015. “Bearing Capacity Evaluation of Footing on a Layered Soil using ABAQUS”. J Earth Sci Clim Change. 6:3. Doi: http://dx.doi.org/10.4172/2157-7617.1000264

[32] Okamura, M., J. Takemura, T. Kimura. 1998. “ Bearing capacity predictions on sand overlying clay based on limit equilibrium methods”. Soils Found. 38(1): 181–194.

[33] Prandtl, L. 1920. “Über die Härte plastischer Körper” [hardness of plastic bodies]. Nachr. Ges. Wiss. Goettingen. Math.-Phys. Kl. 74-85.

[34] Prandtl, L. 1921. “Uber die Eindringungsfestigkeit (Harte) plastischer Baustoffe” [the penetration resistance (hardness) of plastic building]. und die Festigkeit von Schneiden, Zeitschrift fur angewandte Mathematik und Mechanik. 1(1): 15–20.

[35] Purushothamaraj, P., B.K. Ramiah, K.N. Venkatakrishna Rao. 1974. “Bearing capacity of strip footing in two-layered cohesive-friction soils”. Can Geotech J. 11(1): 32-45.

[36] Qin, H.L., M.S. Huang. 2008. “Upper- bound method for calculating bearing capacity of strip footings on two-layer soils”. Chinese J Geotech Eng. 30(4): 611-616.

[37] Reissner, H. 1924. “Zum Erddruck problem” [earth pressure problem]. In: Biezeno, C.B., Burgers, J.M. (Eds.), In Proc. 1st Int. Con. Applied Mech, Delft, The Netherlands: 295–311.

[38] Satyanarayana, B., R.K. Garg. 1980. “Bearing capacity of footings on layered C-φ soils”. J Geotech Eng Division, ASCE. 106 Gt7: 819-824.

[39] Salimi, E.S., A.J. Abbo, G. Kouretzis. 2018. “Bearing capacity of strip footings on sand over clay”. Can Geotech J. https://doi.org/10.1139/cgj-2017-0489.

[40] Salimi, E.S., A.J. Abbo, G. Kouretzis. 2019. “Bearing capacity of strip footings on layered sands”. Comput Geotech. 114: 103101.

[41] Shiau, J.S., A.V. Lyamin, S.W. Sloan. 2003. “Bearing capacity of sand layer on clay by finite element limit analysis”. Can Geotech J. 40(5): 900–915.

[42] Sivareddy, A., R.J. Srinivasan. 1967. “Bearing capacity of footings on layered clays”. J Soil Mech Found Division, ASCE. 938M2: 83-99.

[43] Tamura, T., S. Kobayashi, T. Sumi. 1984. " Limit analysis of soil structure by rigid plastic finite element method". Soils Found. 24(1): 34-42.

[44] Tamura, T., S. Kobayashi, T. Sumi. 1987. "Rigid plastic finite element method for frictional soil". Soils and Found. 27(3): 1-12.

[45] Terzaghi, K. 1943. Theoretical soil mechanics. New York: John Wiley and Sons Inc.

[46] Vesic, A.S. 1973. "Analysis of ultimate loads of shallow foundations". J. Soil Mech. Found. Division, ASCE. 99 (1): 45-76.

[47] Yao, X., Z. Minghua, Z. and Heng. 2018. "Undrained stability of strip footing above voids in two-layered clays by finite element limit analysis". Comput Geotech. 97: 124–133.

CHAPTER 5 END BEARING CAPACITY OF A SINGLE INCOMPLETELY END-SUPPORTED PILE BASED ON THE RIGID PLASTIC FINITE ELEMENT METHOD WITH NON-LINEAR STRENGTH PROPERTY AGAINST CONFINING STRESS

Abstract

An Incompletely End Supported Pile (IESP) is a pile in a soft soil layer underlain by a hard soil layer that accidentally does not reach the bottom hard layer in practice. This study estimates the end bearing capacity of IESP by using an inhouse Rigid Plastic FEM code (RPFEM), considering shear strength non-linearity of soil against confining pressure, and soil-foundation interaction.

The effect of the distance between the pile tip and the bottom hard soil layer (*d/B*) on the end-bearing capacity of IESP was mainly investigated for three types of soil: cohesive soils, cohesionless soils and intermediate soils; while considering the-ratio (*r*) of the end bearing capacity of the pile when it reaches the bottom hard layer to that of the pile when the bottom layer has no influence.

As a result, the consideration of the shear strength non-linearity leads to an accurate estimation of the end bearing capacity-and matches previous analytical, experimental and numerical solutions. It is found that the end bearing capacity inversely decreases with the distance *d*/*B* and becomes constant around *d*/*B* = 3.

Based on the results, a formula for estimating the end bearing capacity of IESP is proposed. And comparisons with methods in existing literature have confirmed the reliability of the proposed equation.

Keywords: End Bearing Capacity, Incompletely End Supported Pile, Rigid Plastic Finite Element Method

5.1 Introduction

One of the reasons why pile foundations are used in foundation engineering is to transfer loads to a deeper and more competent soil layer when the upper soil layers are weaker. However, when the soil layers are non-horizontal, due to complex geologic formation, some pile tips may not reach the targeted stiffer bottom and end up in an upper soil layer. A schematic view of this phenomenon is shown in **Fig. 5-1** with piles in a two-layered ground. The piles that reach the stiffer bottom layer are called End Supported Piles (ESP) and those that did not reach the stiffer bottom layer are referred to as Incompletely End Supported Piles (IESP). The skin friction resistance of IESP might be the same as that of ESP, however, the end bearing capacity of IESP will be reduced by the presence of the softer soil at the pile toe. The amount of reduction of the end bearing capacity of IESP depends on the distance to the stiffer bottom layer. Hence, the main concern of this study will be the influence of the distance to the bottom layer on the end-bearing capacity of IESP. IESP happens accidentally in practice and might cause the tilting of the structure it supports. Thus, IESP can threaten the integrity of the structure it supports, it can cause the failure of the structure which can lead to fatalities and economic losses. Therefore, it is necessary to assess the end-bearing capacity of IESP appropriately to evaluate the stability and safety of the structure supported. The pile end-bearing capacity can be affected by the presence of debris at the pile tip during driven and bored piles construction procedure but note that this is not considered in this study, so this study is limited to the case without debris at the pile tip.

The end bearing capacity of a pile is analogous to the bearing capacity of a shallow foundation with a very large depth of footing (Gunaratne, 2006). There are different solutions of the end bearing capacity of piles. Theoretical methods based on geotechnical considerations such as the Prandtl's method (1921), Terzaghi's method (1943), Meyerhof's method (1963) and Vesic's method (1973) are often used to analyze the characteristics of pile end bearing capacity in a uniform ground.

Theoretical and experimental studies have been conducted to propose formulas for end bearing capacity of driven and bored and cast in place piles such as Meyerhof (1976), Vesic (1977), Janbu (1976), Coyle and Castello (1981), Eslami and Fellenius (1995 and 1997), Yasufuku and Hyde (1995), Yasufuku et al. (2001), Veiskarami et al. (2011). All these studies are not directly applicable in the case of layered soil.

Experimental studies have been conducted to investigate the end bearing capacity of pile in layered

ground. Houlsby et al. (1994) conducted an experimental study and proposed a calculation of pile end bearing capacity in layered soil. However, it does not apply to IESP. Ikeda et al. (2012) have conducted laboratory loading tests of pile in layered sand and found that the end bearing capacity decreases significantly when the pile moves away from the bottom hard layer. However, it did not propose any formula for the influence of the bottom layer on the end bearing capacity. Pholkainuwatra1et al. (2022) conducted an experimental study of pile set-up of driven piles in Bangkok clay using seven piles with their pile tips varied between 8-21 meters below ground level. The soil condition is changing with depth from soft clay with 12 meters of thickness passing by 6 meters of medium clay to 4 meters of stiff clay. However, they did not mention the effect of the layers on the bearing capacity or the formula for it.

Some researchers have used numerical analysis to investigate the end-bearing capacity of IESP. Teramoto et al. (2015) have conducted a FEM analysis to investigate the mechanical behaviors of Incompletely End-Supported Piles. They also found that the gap between the pile tip and bottom layer influences the bearing capacity but did not propose a formula. Hyodo et al. (2020) studied the end bearing capacity of IESP in sand using a three-dimensional elastoplastic FEM analysis. They proposed a ratio of the degradation of the end bearing capacity of IESP when the pile tip moves away from the bottom layer. However, their proposed formula applied to sand only.

As mentioned above, there is no concrete solution for the end bearing capacity of piles in layered grounds that considers the effect of the distance to a bottom stiffer layer for all different types of soils. Such formulas, however, exist for a shallow foundation, for example for c-ϕ soils there are the formulas of Satyanarayana and Garg (1980), Azam and Wang (1991), Bowles (1996),… which consider the distance between the footing and the bottom layer. These formulas can be used to analyze the characteristics of pile end bearing capacity in a two-layered ground, according to Gunaratne (2006).

The main objective of this study is to investigate the influence of the bottom layer on the end bearing capacity of IESP, that is, the decrease (degradation) of the end bearing capacity of IESP when the distance from the pile tip to the bottom layer increases; by using two-dimensional Rigid Plastic FEM, considering non-linear shear strength property against the confining pressure and soil-pile interaction. The effect of the ratio (r) of the end bearing capacity of the pile when it reaches the bottom hard layer (ESP) to that of the pile when the bottom layer has no influence becomes an important factor. In addition, a formula of the end bearing capacity of IESP for all types of soils (cohesive soils, cohesionless soils and intermediate soils) is proposed based on the results, while considering the influence of the end

bearing capacity ratio *r*.

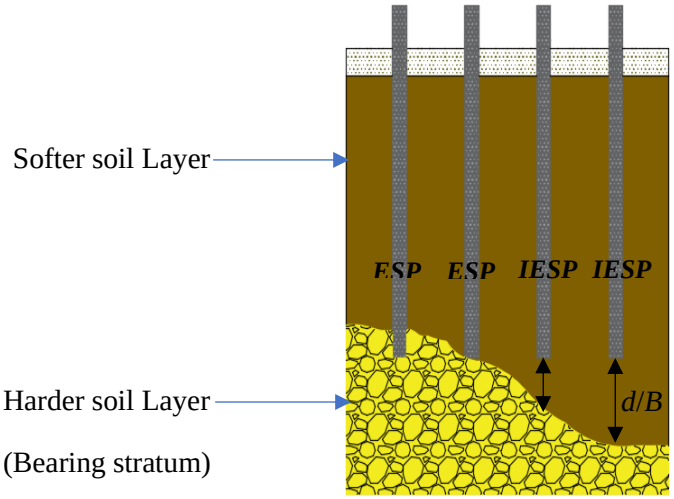

Fig. 5-1 IESP caused by a non-horizontal bearing stratum

5.2 Some Existing Formulas of Pile End Bearing Capacity

5.2.1 Theoretical Formula of Pile End Bearing Capacity

The ultimate end bearing capacity of a pile, q_{pult}, may be expressed by an equation similar to that of a footing as follow:

$$q_{\text{pult}} = cN_{\text{c}} + qN_{\text{q}} + 0.5\gamma BN_{\gamma} \quad \cdots\cdots (5\text{-}1)$$

where B = diameter or width of the pile, q = overburden pressure, c = cohesion of soil, γ= unit weight of soil and N_{c}, N_{q} and N_{γ} are bearing capacity factors for deep foundations which are different from those of shallow foundations.

Because the width B of the pile is relatively small, the third term $0.5\gamma BN_{\gamma}$ becomes insignificant in comparison with the second term qN_{q} and is dropped. Therefore **Eq. (5-1)** reduces to

$$q_{\text{pult}} = cN_{\text{c}} + qN_{\text{q}} \quad \cdots\cdots (5\text{-}2)$$

Vesic (1967) has revealed that the bearing capacity of a pile remains constant beyond a critical depth, and N_{q} depends on ϕ and D/B (where D = length of embedment, B = diameter or width of the pile).

Meyerhof (1976) proposed the critical depth ratio (D_c/B) in **Fig. 5-2** for N_{c} and N_{q}. N_{c} and N_{q} increase

with D_b/B and reach a maximum value at D_b/B equal to about 0.5 (D_c/B), where D_b is the actual thickness of the bearing stratum. In a homogeneous soil, D_b is equal to the embedded length of the pile (L); whereas, in layered soil, D_b is less than L.

Meyerhof prescribed a limiting value for q_{pult}. The expression for the limiting value, q_{pl} is:

for dense sand: $q_{pl} = 50N_q \tan\phi$ (kN/m^2) ····· (5-3)

for loose sand: $q_{pl} = 25N_q \tan\phi$ (kN/m^2) ····· (5-4)

The equation for tip resistance in sand may now be expressed as

$$q_{pult} = q'_0 N_q \leq q_{pl} \quad \cdots\cdots (5\text{-}5)$$

where q'_0 = effective overburden pressure at the tip of the pile corresponding to D_c/B and N_q = bearing capacity factor **(Fig. 5-2)**. **Eq. (5-5)** is applicable only for driven piles in sand. For bored cast-in-situ piles, the value of q_{pult} is to be reduced by one-third to one-half.

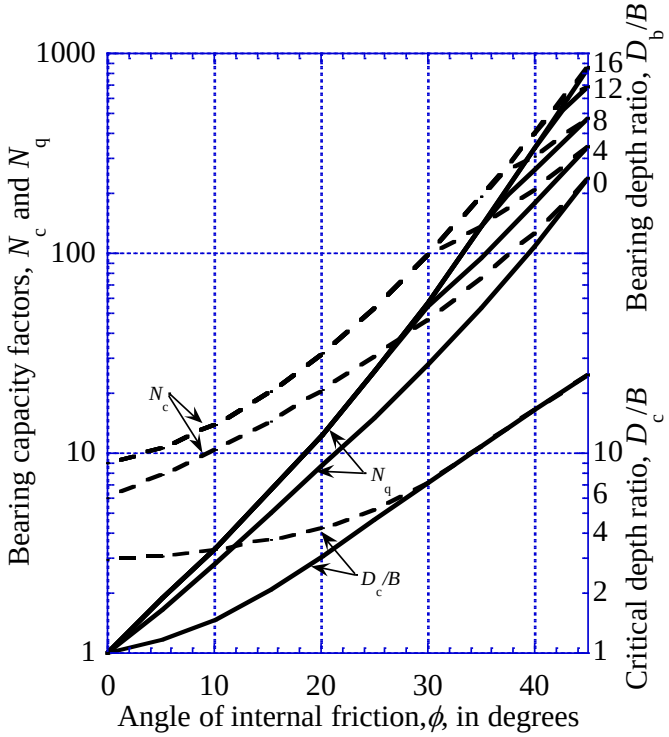

Fig. 5-2 Bearing capacity factors and critical depth ratios for driven piles. (After Meyerhof (1976))

5.2.2 Theoretical Formulas Applicable to End Bearing Capacity of IESP

Hyodo et al. (2020) studied the end bearing capacity of IESP in sand using an elastoplastic FEM and proposed **Eq. (5-6)** below to estimate the end bearing capacity.

$$q_{\mathrm{unreached}} = \alpha q_{\mathrm{base}} + (1-\alpha) q_{\mathrm{nobase}} \cdots\cdots (5\text{-}6)$$

where $q_{\mathrm{unreached}}$ is the pile end resistance of IESP, q_{base} is the pile end resistance of the completely end-supported pile, q_{nobase} is the pile end resistance of the pile with no lower hard layer and α is the degradation factor which represents the incompleteness of the pile end support. An amelioration of the formula of Hyodo et al. (2020) is proposed in this study.

On the other hand, the empirical formulas of Satyanarayana and Garg (1980) and Azam and Wang (1991) can be used to analyze the end bearing capacity of IESP in *c*-ϕ soil.

Satyanarayana and Garg (1980) conducted a study to determine the ultimate bearing capacity of footings in a two-layered *c*-ϕ soil system. They suggested empirical equations to determine: the average value of cohesion c_{av}; the average value of the angle of internal friction ϕ_{av}; and equivalent significant depth H_2 for a layered soil system. With such strength parameters, they have proposed a simplified bearing-capacity theory for shallow foundations in *c*-ϕ soils based on the Terzaghi theory as follows:

$$q_{\mathrm{ult}} = c_{\mathrm{av}} N_{\mathrm{c}} + q N_{\mathrm{q}} + 0.5 \gamma B N_{\gamma} \cdots\cdots (5\text{-}7)$$

where,

$$c_{\mathrm{av}} = \frac{H c_1 + H_2 c_2}{H + H_2}, \quad \phi_{\mathrm{av}} = \tan^{-1}\left(\frac{H \tan\phi_1 + H_2 \tan\phi_2}{H + H_2}\right), \quad H_2 = (2B - H)\left(\frac{c_1 + \tan\phi_1}{c_2 + \tan\phi_2}\right)$$

where, B = footing/pile width, H = thickness of the top layer, H_2 = thickness of the part of the bottom layer that contributes to the bearing capacity, q = overburden pressure, c_1 = cohesion of soil in the top layer, c_2 = cohesion of soil in the bottom layer, ϕ_1 = angle of friction of soil in the top layer, ϕ_2 = angle of friction of soil in the bottom layer, γ_1 = unit weight of soil in the top layer, N_{c}, N_{q} and N_{γ} are bearing capacity factors based on ϕ_{av}.

Azam and Wang (1991) investigated the bearing capacity of an embedded strip footing supported by two-layer *c*-ϕ soils using an elastoplastic finite-element computer program. Based on the analysis results, they developed a semiempirical equation for determining the ultimate bearing capacity as follows:

$$q_0 = q_t + (q_b - q_t)\,[1 - m(H/B)]^2 \quad \cdots\cdots (5\text{-}8)$$

q_0 = end bearing capacity of IESP

q_t = end bearing capacity in an infinitely thick top-layer soil

q_b = end bearing capacity on an infinitely thick bottom-layer soil

m = 0.17 - 0.23 for two layers of clay and 0.30 for a sand-clay layer combination

H/B = top-layer-thickness-to-footing-width ratio

Table 5-1 shows the summary of the different methods and the associated advantages and disadvantages with respect to the estimation of the end bearing capacity of IESP.

5.3 Constitutive Equations for Rigid Plastic Finite Element Method

The rigid-plastic finite element method (RPFEM) was developed for geotechnical engineering by Tamura et al. (1984 and 1987). In this method, the limit load is calculated without any assumption of a potential failure mode. The method is effective in calculating the ultimate bearing capacity of shallow foundations and deep foundations where the soil conditions are varied, such as a multi-layered ground.

In this study, the in-house RPFEM code developed and upgraded by Hoshina et al. (2011) and Du et al. (2016), is used for estimation of the end bearing capacity of a single Incompletely End-Supported Pile. The rigid plastic constitutive equation for the Drucker-Prager yield function was employed first.

Then, the non-linear shear strength property against confining pressure, introduced by Du et al. (2016) in RPFEM, was considered. The Drucker-Prager yield function is expressed with **Eq. (5-9)** and for considering the non-linear shear strength property against confining pressure, **Eq. (5-10)** referred to as the High Order yield function was used. Both yield functions are used in plane strain conditions considering the associated flow rule. Since the plane strain condition is used, the simulated end bearing capacity is that of a continuous wall, however, by employing shape factors, it can be converted to the end bearing capacity of a pile.

Table 5-1 Application conditions and limitations of the existing methods

Formula	Disadvantages with respect to the estimation of the end bearing capacity of IESP	Advantages with respect to the estimation of the end bearing capacity of IESP
Eq. 5-2: Terzaghi (1943), Vesic (1967) and Meyerhof (1976)	• Cannot directly estimate the end bearing capacity of IESP alone.	• Can be used to calculate q_{base} and q_{nobase} of Hyodo et al. (2020) • Can be used to calculate q_b and q_t of Azam and Wang (1991) • N_c and N_q of **Eq. 5-2** can be used in Satyanarayana and Garg (1980)
Eq. 5-5: Hyodo et al. (2020)	• Applicable for sand only. • Does not consider the strength ratio of the two soil layers.	• Gives a reasonable end-bearing capacity of IESP in sand.
Eq. 5-6: Satyanarayana and Garg (1980)	• Using average values of strength parameters (not realistic).	• Can be used for any type of soil and gives reasonable results.
Eq. 5-7: Azam and Wang (1991)	• Does not consider the strength ratio of the two soil layers.	• Can be used for any type of soil and gives reasonable results.

$$f(\sigma) = \alpha_{DP} I_1 + \sqrt{J_2} - \kappa = 0 \quad \cdots\cdots (5\text{-}9)$$

$$f(\sigma) = a I_1 + (J_2)^n - b = 0 \quad \cdots\cdots (5\text{-}10)$$

where, $\boldsymbol{I}_1 = \mathrm{tr}(\sigma_{ij})$ is the first invariant, $\boldsymbol{J}_2 = \frac{1}{2} s_{ij} s_{ij}$, α_{DP}, κ, a and b are soil parameters. α_{DP} and κ are expressed for plane strain condition as follows:

$$\alpha_{DP} = \frac{\tan\phi}{\sqrt{9+12\tan^2\phi}}, \kappa = \frac{3c}{\sqrt{9+12\tan^2\phi}} \quad \cdots\cdots (5\text{-}11)$$

where c is cohesion, ϕ is shear resistance angle.

The parameters n, a and b in the High Order yield function **Eq. (5-10)** are coefficients representing the non-linear shear strength property against confining pressure for the soil; n is standing for the strength non-linearity; a and b are relating to the shear resistance angle ϕ and the cohesion c, respectively. As a remark, when n in the High Order yield function is 0.5 the two Equations, **Eq. (5-9)** and **Eq. (5-10)** are the same. When n is higher than 0.5, the plot of $\sqrt{J_2}$ against I_1 gives a linear line with **Eq. (5-9)**, but a curved line with **Eq. (5-10)** **(see Fig. 5-3)**.

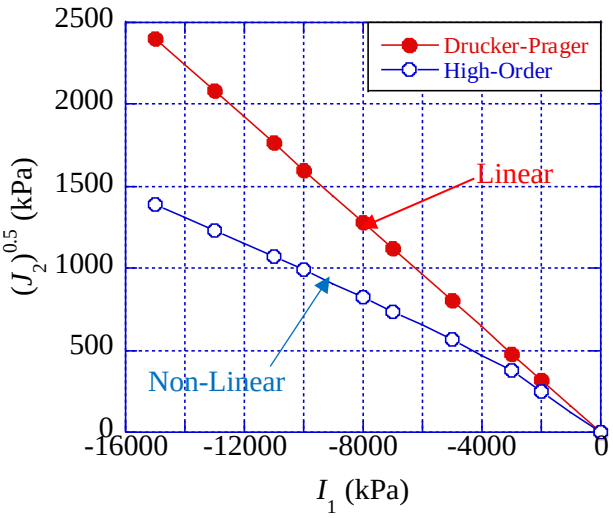

Fig. 5-3 Difference between the yield function of Drucker-Prager the and High-Order model

For the Drucker-Prager yield function, the volumetric strain rate for the Rigid Plastic constitutive equation is expressed as follows:

$$\dot{\varepsilon}_v = \mathrm{tr}(\dot{\boldsymbol{\varepsilon}}) = \mathrm{tr}\left(\lambda \frac{\partial f(\boldsymbol{\sigma})}{\partial \boldsymbol{\sigma}}\right) = \mathrm{tr}\left(\lambda\left(\alpha \boldsymbol{I} + \frac{\boldsymbol{s}}{2\sqrt{J_2}}\right)\right) = \frac{3\alpha}{\sqrt{3\alpha^2 + \frac{1}{2}}}\dot{e} \quad \cdots\cdots (5\text{-}12)$$

where λ is the plastic multiplier and $\dot{e}$ is the norm of the strain rate. $\boldsymbol{I}$ and $\boldsymbol{s}$ express the unit and the deviator stress tensors, respectively. Strain rate $\dot{\boldsymbol{\varepsilon}}$, which is a purely plastic component, should satisfy the volumetric constraint condition which is derived by **Eq. (5-13)**, as follows:

$$h(\dot{\boldsymbol{\varepsilon}}) = \dot{\varepsilon}_v - \frac{3\alpha}{\sqrt{3\alpha^2+\frac{1}{2}}}\dot{e} = \dot{\varepsilon}_v - \eta\dot{e} = 0 \quad \cdots\cdots (5\text{-}13)$$

Any strain rate which is compatible with the Drucker–Prager yield criterion must satisfy the kinematical constraint conditions of **Eq. (5-13)**. η is a coefficient determined by **Eq. (5-13)** which is one of the dilation characteristics. The rigid plastic constitutive equation is expressed by the Lagrangian method after Tamura et al. (1987), as follows:

$$\boldsymbol{\sigma} = \frac{\kappa}{\sqrt{3\alpha^2+\frac{1}{2}}}\frac{\dot{\boldsymbol{\varepsilon}}}{\dot{e}} + \beta\left(\boldsymbol{I} - \eta\frac{\dot{\boldsymbol{\varepsilon}}}{\dot{e}}\right) \quad \cdots\cdots (5\text{-}14)$$

The first term expresses the stress component, uniquely determined for the yield function. The second term expresses the indeterminate stress component along with the yield function. The indeterminate stress parameter β remains unknown until the boundary value problem with **Eq. (5-13)** is solved. In this study, a penalty method is used to make the computation faster and more stable following Hoshina et al. (2011), as follows:

$$\boldsymbol{\sigma} = \frac{\kappa}{\sqrt{3\alpha^2+\frac{1}{2}}}\frac{\dot{\boldsymbol{\varepsilon}}}{\dot{e}} + P(\dot{\varepsilon}_v - \eta\dot{e})\left(\boldsymbol{I} - \eta\frac{\dot{\boldsymbol{\varepsilon}}}{\dot{e}}\right) \quad \cdots\cdots (5\text{-}15)$$

where P is a penalty constant.

For the High Order yield function, based on the associated flow rule, the strain rate is obtained as follows:

$$\dot{\boldsymbol{\varepsilon}} = \lambda\frac{\partial f(\boldsymbol{\sigma})}{\partial\boldsymbol{\sigma}} = \lambda\frac{\partial}{\partial\boldsymbol{\sigma}}(aI_1 + (J_2)^n - b) = \lambda\,(a\boldsymbol{I} + n(J_2)^{n-1}\,\boldsymbol{s}) \quad \cdots\cdots (5\text{-}16)$$

In the above equation, λ is the plastic multiplier. The volumetric strain rate is expressed as:

$$\dot{\varepsilon}_v = \mathrm{tr}(\dot{\varepsilon}) = \mathrm{tr}\big(\lambda\,(a\boldsymbol{I} + n(J_2)^{n-1}\,\boldsymbol{s})\big) = 3a\lambda = \frac{3a}{\sqrt{3a^2+2n^2\,(b-aI_1)^{2-1/n}}}\dot{e} \quad \cdots\cdots (5\text{-}17)$$

First stress invariant I_1 is identified from **Eq. (5-17)** as the following equation:

$$\boldsymbol{I}_1 = \frac{b}{a} - \frac{1}{a}\left\{\frac{1}{2n^2}\left[\left(3a\frac{\dot{e}}{\dot{\varepsilon}_v}\right)^2 - 3a^2\right]\right\}^{\frac{n}{2n-1}} \quad \cdots\cdots (5\text{-}18)$$

The non-linear rigid plastic constitutive equation for the High Order yield function is finally obtained as follows:

$$\sigma = \frac{3a}{n}\left\{\frac{1}{2n^2}\left[\left(3a\frac{\dot{e}}{\dot{\varepsilon}_v}\right)^2 - 3a^2\right]\right\}^{\frac{1-n}{2n-1}}\frac{\dot{\varepsilon}}{\dot{\varepsilon}_v} + \left(\frac{b}{3a} - \frac{1}{3a}\left[\frac{1}{2n^2}\left(3a\frac{\dot{e}}{\dot{\varepsilon}_v}\right)^2 - 3a^2\right]^{\frac{n}{2n-1}} - \frac{a}{n}\left[\frac{1}{2n^2}\left(3a\frac{\dot{e}}{\dot{\varepsilon}_v}\right)^2 - 3a^2\right]^{\frac{1-n}{2n-1}}\right)\boldsymbol{I} \quad \text{(5-19)}$$

In this equation, the stress is uniquely determined for the plastic strain rate and is different from **Eq. (5-15)** for the Drucker-Prager yield function.

The advantage of the rigid plastic constitutive equation is that only a few soil parameters such as unit weight, cohesion and shear resistance angle are necessary. In the simulation, the pile is modeled by the rigid plastic constitutive equation as rigid material to focus on the plastic behavior of the soils around the pile subjected to vertical loading. So, the elastic modulus and Poisson's ratio are not necessary for this simulation method, and it is not intended for a specific type of pile. In addition, the High order yield function considers the reduction of the shear resistance angle due to high confining pressure, therefore, it avoids the overestimation of volumetric strain in ϕ and c-ϕ soils and it gives more reasonable end-bearing capacity values of piles in those soils.

5.4 Finite Element Mesh and Boundary Conditions

An illustration of the finite element mesh and the boundary conditions used is shown in **Fig. 5-4**. First, a hollow model and a joint elements model were used to check the interaction between end capacity and skin friction. In both models, a soft soil layer underlain by a hard soil layer was modeled. For the hollow model, a hollow was used in lieu and place of a pile. For the joint elements model, joint elements were used between the pile and the surrounding. For estimation of both end capacity and friction simultaneously, the characteristics of the joint elements were set the same as those of the surrounding ground. For estimation of the end capacity separately, the characteristics of the joints were chosen to allow a smooth condition, the same method is used by Hyodo et al. (2020). A mesh of approximately 7000 rectangular elements has been used to represent each model. The boundary conditions were set large enough to simulate an infinite soil mass. The density of the mesh elements was refined near the pile to capture the higher expected strain. The left and right sides of the domain were pinned, and the

bottom boundary of the domain was fixed. An increasing load in a downward direction was applied. The normalized distance between the hollow bottom/pile tip and the hard soil layer (d/B) was varied.

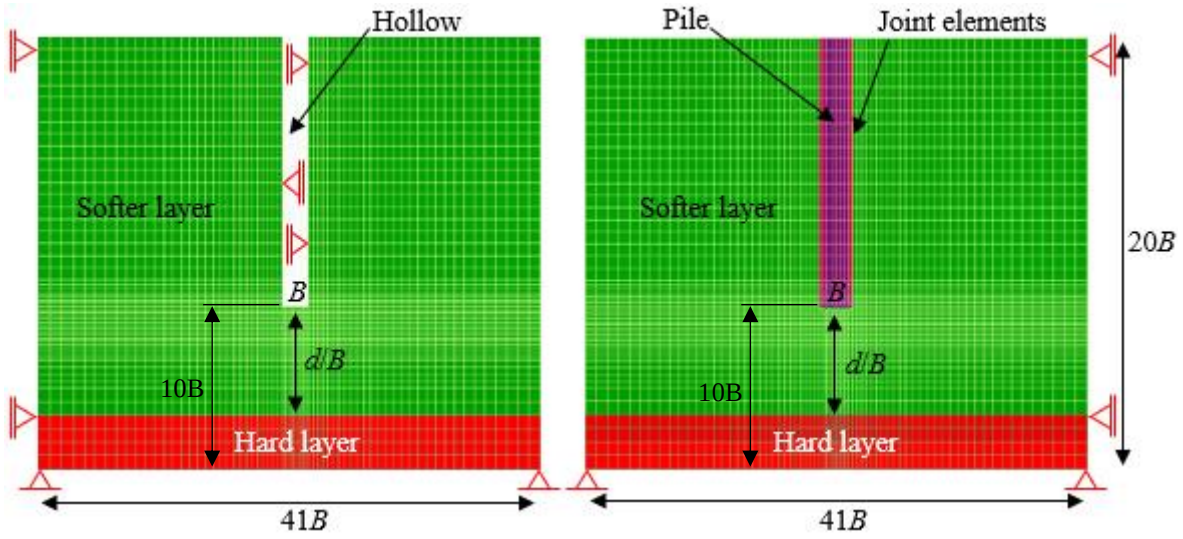

(a) Hollow type **(b)** Joint elements type

Fig. 5-4 Mesh and boundary conditions used for simulation by (a) using hollow and (b) joint elements

5.5 Validation of the Simulation Method

The simulation method is validated against the study of Pholkainuwatra1et al. (2022) who conducted an experimental study of pile set-up of driven piles in Bangkok clay (c soil). The soil conditions in their study are depicted in **Fig. 5-5**. These soil conditions are used to simulate the end bearing capacities with RPFEM using the Drucker-Prager yield function. **Fig. 5-5(c)** shows the comparison of end bearing capacities on the 32nd day after pile installation obtained by Pholkainuwatra1 et al. (2022) and the simulation results. A good agreement can be observed in **Fig. 5-5(c)**. This comparison suggests that the simulation method used in this study is reliable enough.

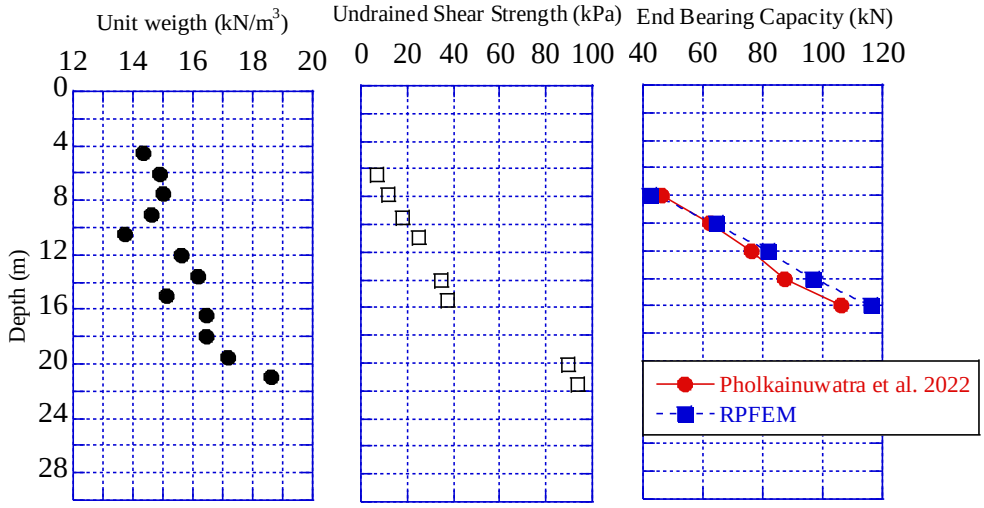

(a) Unit Weight **(b)** Undrained Shear Strenth **(c)** End Bearing Capacity

Fig. 5-5 Validation of the simulation method against Pholkainuwatra et al. (2022)

5.6 Analyses Based on the Drucker Prager Yield Function

5.6.1 Analyses Parameters For The Estimation of the Bearing Capacity of IESP

The simulation was done for a cohesive soil (*c* soil), cohesionless soil (ϕ soil) and an intermediate soil (*c*-ϕ soil**). Table 5-2** shows the soil parameters for each type of soil used in these simulation cases. These specific values are used only for illustrating the behavior of the bearing capacity. Later in this study, the bearing capacity ratio, which is a non-dimensional parameter, will be used by varying the soil parameters. The pile in this simulation has the following properties: cohesion c = 50000 kPa, shear resistance angle ϕ = 0 degrees and unit weight γ = 25 kN/m^3 to make the pile a rigid non-deformable body based on Hoshina et al. (2011) and Du et al. (2016). The pile length, as well as the embedment length, are set constant (with a slenderness of 10*B*). The unit weight of the overburden layer is also considered in the simulation. No water is considered meaning that the effective stress is equal to the total stress. The problem is under a long-term condition for ϕ soil and *c*-ϕ soil based on the peak shear strength, but *c* soil is under undrained conditions like for a short-term condition. The main parameter was the distance (*d*/*B*), the distance between the pile tip and the bottom layer (*d*) normalized by the pile width (*B*). The influence of this parameter on the total bearing capacity, the end bearing capacity and the skin friction was investigated. Note that the influence of *d*/*B* illustrates the influence of the bottom layer.

Table 5-2 Soil characteristics

Soil type	Layers	ϕ (deg.)	c (kPa)	γ (kN/m^3)
c soil	Soft layer	0	25	14
	Hard layer	0	75	17
ϕ soil	Soft layer	30	0	17.5
	Hard layer	40	0	20
c-ϕ soil	Soft layer	20	45	17
	Hard layer	35	10	19

5.6.2 Bearing Capacity of IESP

The variation of the bearing capacity of IESP as a function of the normalized distance d/B is shown in **Fig. 5-6**. Where the negative values of d/B mean that the pile is penetrating the bottom hard soil layer. Note that these negative values of d/B are used just to confirm the effect of the penetration into the bottom layer with higher strength, the main concern in this study is the parts of $d/B > 0$ that the deficiency of bearing capacity happens. The two simulation methods (Hollow and Joint) coincide for all three soil types.

For the three soil types, the skin friction contributes a lot to the total bearing capacity. The total bearing capacity and the end bearing capacity decrease with the increasing value of d/B, however, the influence of d/B on the skin friction is very small and therefore negligible. These observations mean that the bottom layer greatly influences the end bearing capacity but does not much affect the skin friction. Since the main objective of this study is to investigate the influence of the bottom layer, the end bearing capacity becomes the main concern in this study.

The decrease of the end bearing capacity expresses the degradation of the end bearing capacity when the pile moves away from the bottom layer. The end bearing capacity attains a minimum steady, equal to that of the top layer, around the distance of three times the pile diameter (critical distance $d/B^* = 3$). This value on critical distance is in good agreement with the result of Houlsby et al. (1994) who studied the end bearing capacity of pile in homogeneous uncemented sand within which a horizontal cemented carbonate sands layer was inserted as a bearing layer (See **Fig. 5-7**).

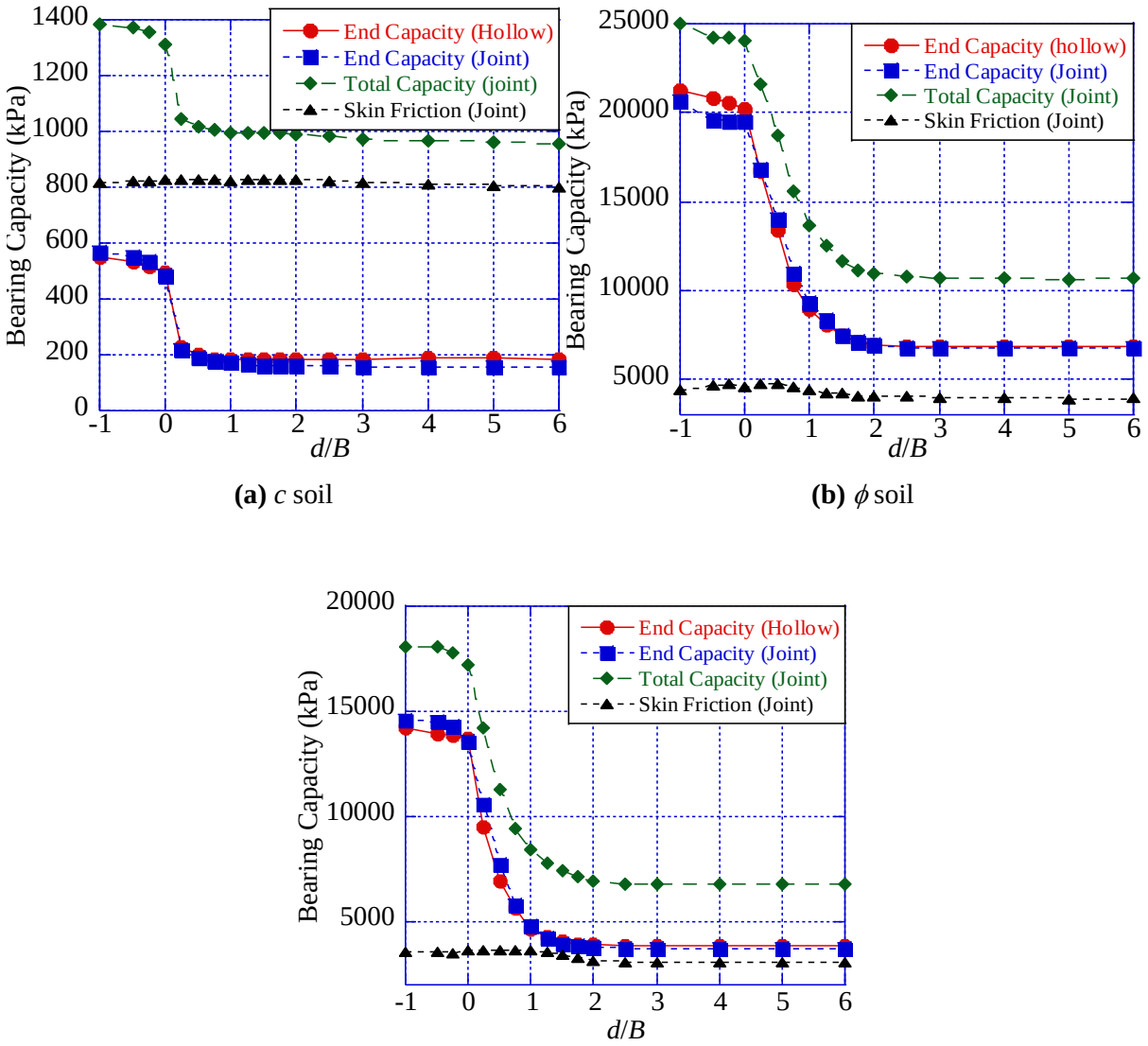

(a) *c* soil

(b) ϕ soil

(c) *c*-ϕ soil

Fig. 5-6 Influence of the distance between the pile tip and the surface of the hard layer on the end bearing capacity of IESP

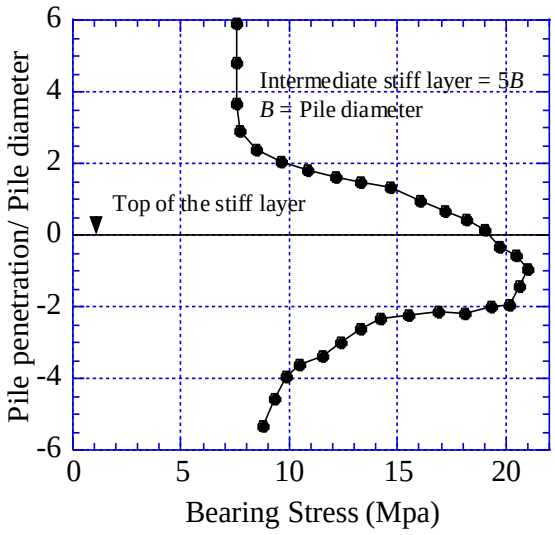

Fig. 5-7 Bearing capacity against depth obtained by Houlsby et al. (1994) for an intermediate stiff soil layer placed within a softer soil

5.6.3 The End Bearing Capacity Ratio (Analyses Parameters)

An end bearing capacity ratio r is defined as the ratio of the end bearing capacity of the case $d/B = 0$ (pile tip on the bottom layer), namely q_H, to the end bearing capacity of the pile when the bottom layer has no influence, namely q_s (**Eq. (5-20)**). q_s also represents the end bearing capacity of a uniform ground made of the top softer soil layer. By changing the soil parameters of the bottom soil layer, the following ratios r are obtained: for c soil r = 1.68 to 4.20; for ϕ soil r = 1.55 to 3.8 and for c- ϕ soil r = 1.45 to 6.35. The soil parameters used widely cover the values expected in practical engineering and are presented in **Table 5-3**. The effect of changing the ratio r on the end bearing capacity was investigated below.

$$r = \frac{q_H}{q_s} \quad \text{(5-20)}$$

Table 5-3 Soil parameters of the bottom hard layer and equivalent end bearing capacity ratios

(a) For *c* soils, with c **= 10 kPa**, ϕ **= 0 degrees** and γ **= 13.5 kN/m^3** as parameters of the top layer

End bearing capacity ratio (*r*)	ϕ **(deg.)**	c **(kPa)**	γ **(kN/m^3)**
1.68	0	40	15
2.13	0	50	16
3.19	0	75	17
3.79	0	90	17.5
4.20	0	100	18

(b) For ϕ soils, with, c **= 1 kPa**, ϕ **= 30 degrees** and γ **= 17.5 kN/m^3** as parameters of the top layer

End bearing capacity ratio (*r*)	ϕ **(deg.)**	c **(kPa)**	γ **(kN/m^3)**
1.55	34	1	18
1.95	36	1	18.5
2.42	38	1	19
3.10	40	1	20
3.80	42	1	21

(c) For c-ϕ soils, with, c **= 45 kPa**, ϕ **= 20 degrees** and γ **= 17 kN/m^3** as parameters of the top layer

End bearing capacity ratio (*r*)	ϕ **(deg.)**	c **(kPa)**	γ **(kN/m^3)**
1.45	25	30	17
2.25	30	20	17.5
2.82	32	15	18
3.75	35	10	19
6.35	40	5	20

5.6.4 Influence of the End Bearing Capacity Ratio

The behavior of the end bearing capacities for different values of the ratio *r* (**Eq. (5-20)**) was studied and the results were normalized using **Eq. (5-21)**. In **Eq. (5-21)**, $q_{(d/B^*)}$ is the end bearing capacity at the critical distance (d/B^*) and is also equal to the end bearing capacity of the pile when the bottom layer has no influence (q_s) (**Fig. 5-6**). q_0 is the end bearing capacity of the case of $d/B = 0$ which is the end bearing capacity when the pile tip is on the surface of the bottom soil layer (q_H); q_x is the end bearing capacity corresponding to a given distance $d/B = x$.

$$\xi_x = \frac{q_x - q_{(d/B*)}}{q_0 - q_{(d/B*)}} = \frac{q_x - q_s}{q_H - q_s} \quad \text{(5-21)}$$

Fig. 5-8 shows the influence of the ratio *r* on the end bearing capacity for the three soils. The end bearing capacity increases with the increase of the ratio *r*, however, the influence of *r* is different depending on the soil type. A non-influence of *r* is observed when $d/B > 0.5$ for *c* soil, $d/B > 1.5$ for ϕ soil and $d/B > 1.25$ for *c*-ϕ soil. From these results, it is found that the degradation of the end bearing capacity is influenced by the ratio *r*. For small values of *r*, the degradation is smooth, however, for high values of *r*, the degradation is sudden. The sudden degradation in the cases of high values of *r* is due to the sudden change of the end bearing capacity from very high ($d/B \leq 0$) to relatively very small (when $d/B > 0$). The normalized end-bearing capacities are depicted in **Fig. 5-9** for the three soils. The normalized end bearing capacities represent the degradation factors of the end bearing capacity when the pile goes away from the hard bottom layer. The degradation factor ξ_x inversely increases with the ratio *r*, a non-influence is observed around $d/B = 3$. The degradation factor ξ_x is also influenced by the soil type as the slopes of ξ_x testify in **Fig. 5--9**. The slopes of *c* soil are the steepest, followed by those of *c*-ϕ soil and the slopes of ϕ soil are less steeped.

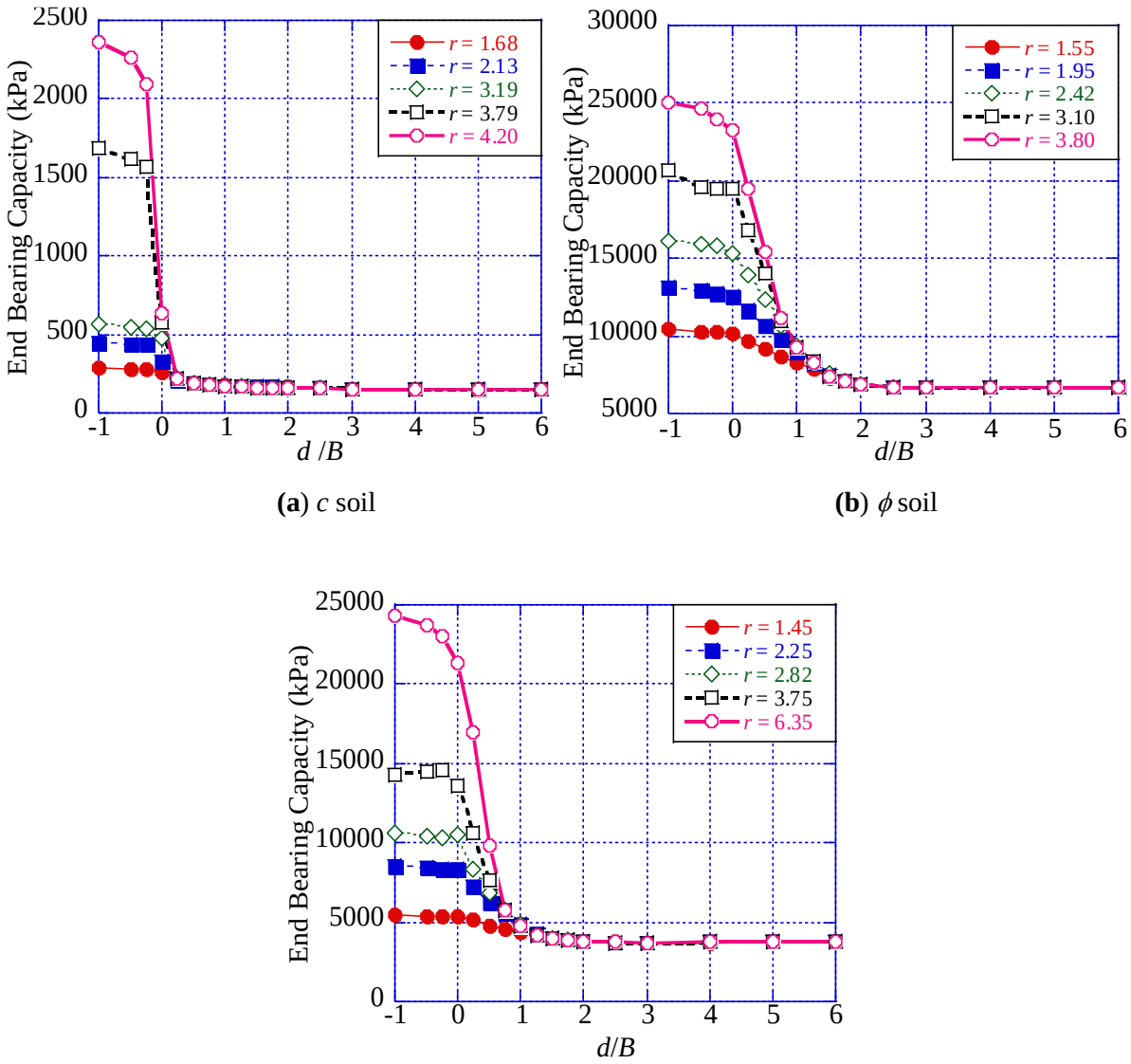

(a) *c* soil

(b) ϕ soil

(c) *c*-ϕ soil

Fig. 5-8 Influence of the ratio ***r*** on the end bearing capacity of IESP

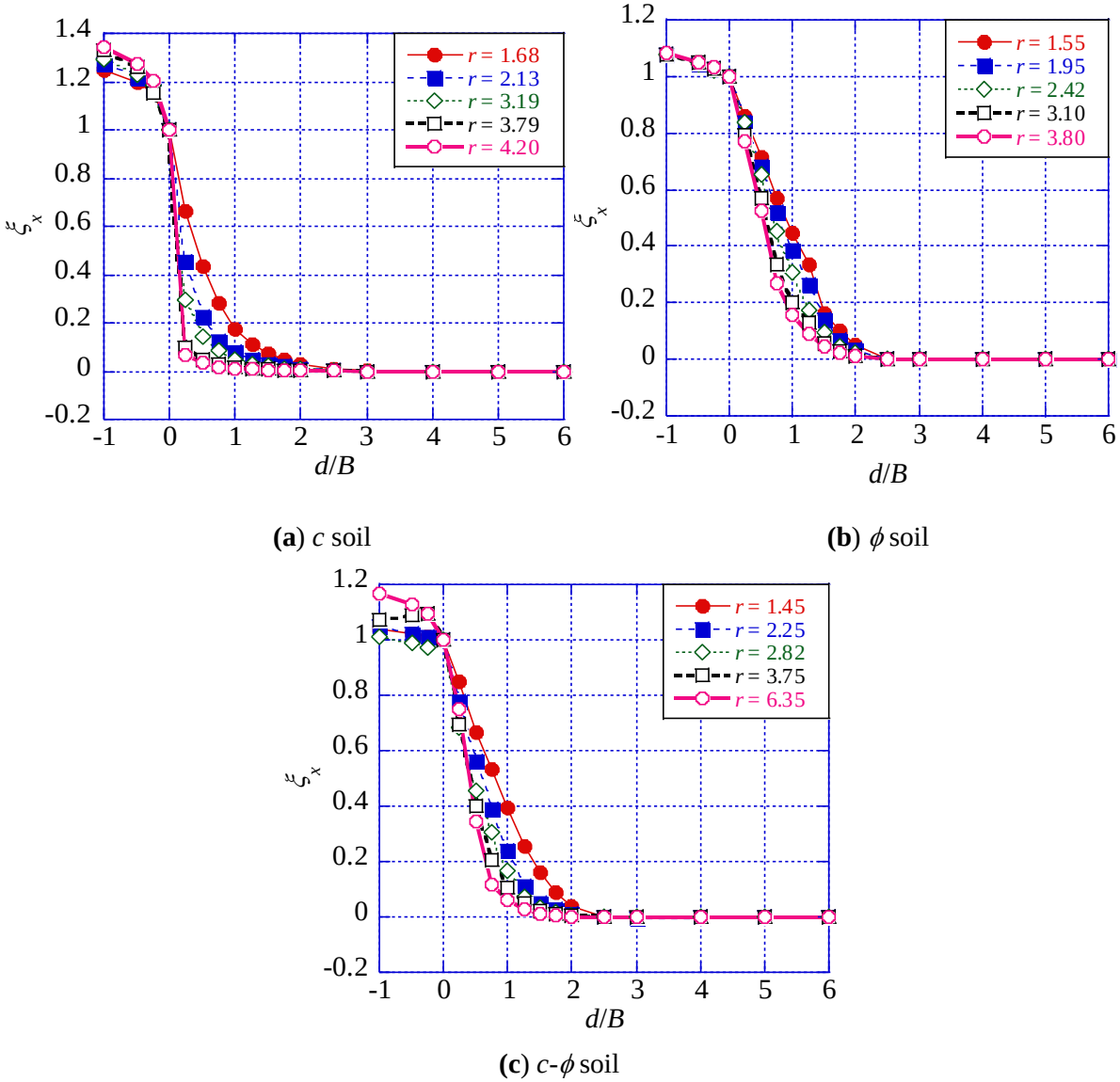

(a) *c* soil **(b)** ϕ soil

(c) *c*-ϕ soil

Fig. 5-9 Normalization of the end bearing capacities with different end bearing capacity ratios

5.6.5 Failure Patterns

Several failure mechanisms proposed by different researchers are shown in **Fig. 5-10**.

The strain rate distribution styles based on the Drucker-Prager yield function using the joint elements numerical model are shown in **Fig. 5-11**, **Fig. 5-12** and **Fig. 5-13** for the three types of soils in **Table 5-2**. The norm of the strain rate is represented by contour lines in the range of $\dot{e}_{max} \sim \dot{e}_{min}$ (= 0). The boundary conditions are sufficient since the strain rate did not reach the limits of the domain. The failure pattern is different for each type of soil. This difference might explain the difference in the value of *d/B*

from which the ratio r has no influence for each soil type in **Fig. 5-8** and the difference in the slopes of ξ_x in **Fig. 5-9**. When the distance $d/B < d/B^* = 3$, the yield zones at the collapse stage extend into the bottom layer, and the higher strength of the bottom layer contributes thus toward a greater end bearing capacity. However, for $d/B > d/B^*$, the yielding is confined into the top layer, as a result, the lower strength of the top layer reduces the end bearing capacity.

The shear bands obtained with c soil are similar to case (a) and case (b) in **Fig. 5-10**. However, in the case of ϕ soil and c -ϕ soil, all the shear bands are not ideally like those in **Fig. 5-10**. A widespread of the shear bands are observed in the case of ϕ soil and c -ϕ soil. This phenomenon can be attributed to the fact that with the Drucker-Prager yield function, the influence of the confining pressure on the shear resistance angle is not considered, therefore the volumetric strain is overestimated. On the other hand, since the shear resistance angle of the c soil is zero (0), this does not affect the c soil, hence the similarity of the shear bands of c soil with the case (a) and case (b) in **Fig. 5-10**.

The shear bands observed in ϕ soil and c -ϕ soil suggest that the Drucker-Prager yield function is overestimating the end bearing capacity for ϕ soils and c -ϕ soils. Since the High order yield function considers the influence of the confining pressure on the shear resistance angle, it might give more reasonable end-bearing capacity values of IESP, hence the need for analyses using the High order yield function.

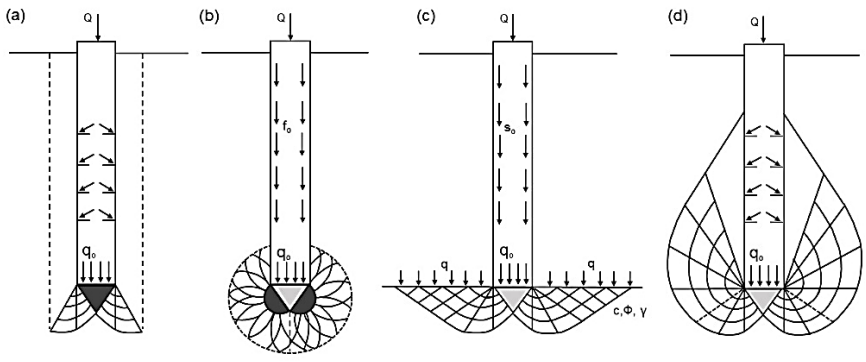

Fig. 5-10 Different failure patterns around the pile tip assumed by different researchers (Veiskarami et al (2011)): (a) Berezantzev and Yaroshenko (1962), Vesic (1963); (b) Bishop et al. (1945), Skempton et al. (1953); (c)Prandtl (1920), Reissner (1924), Caquot (1934), Bulsman (1935), Terzaghi (1943); (d) De Beer (1945), Jáky (1948), Meyerhof (1951)

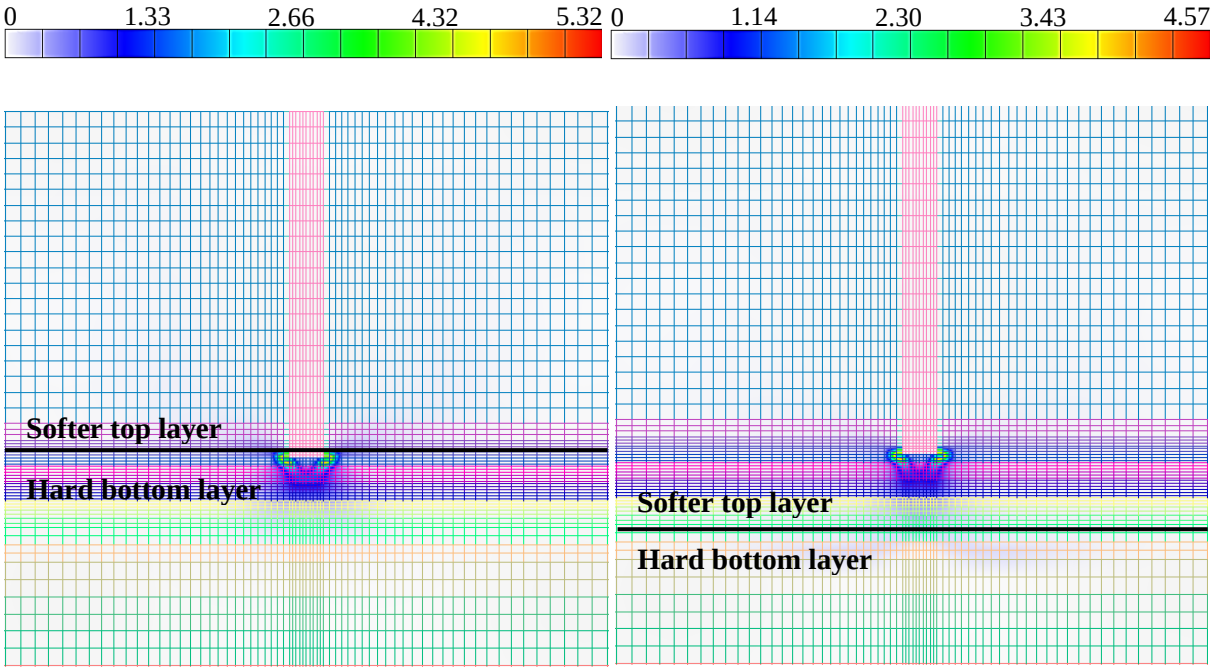

(a) $d/B = 1$ **(b)** $d/B = 3$

Fig. 5-11 Strain rate distribution from *c* soil using Drucker Prager

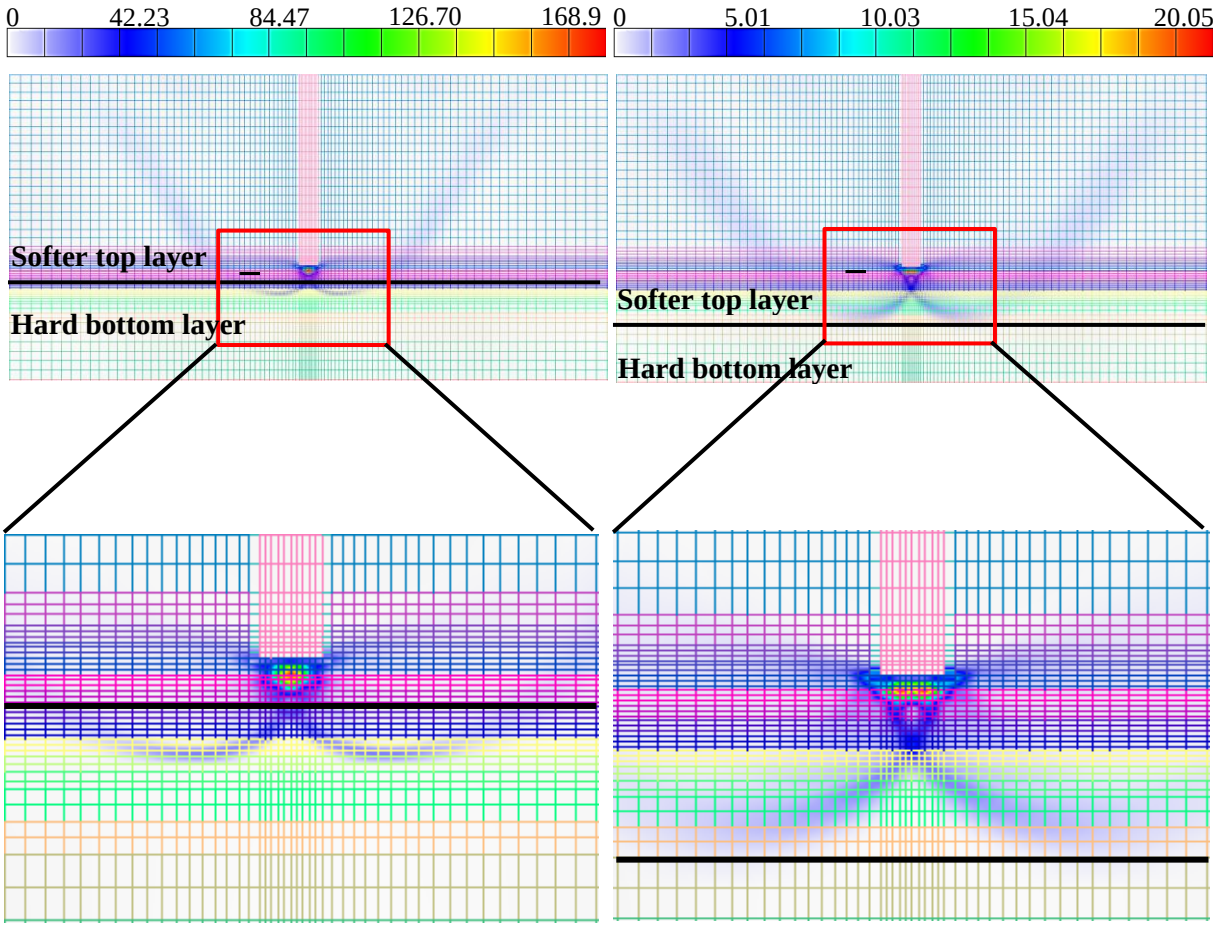

(a) $d/B = 1$ **(b)** $d/B = 3$

Fig. 5-12 Strain rate distribution from ϕ soil using Drucker Prager

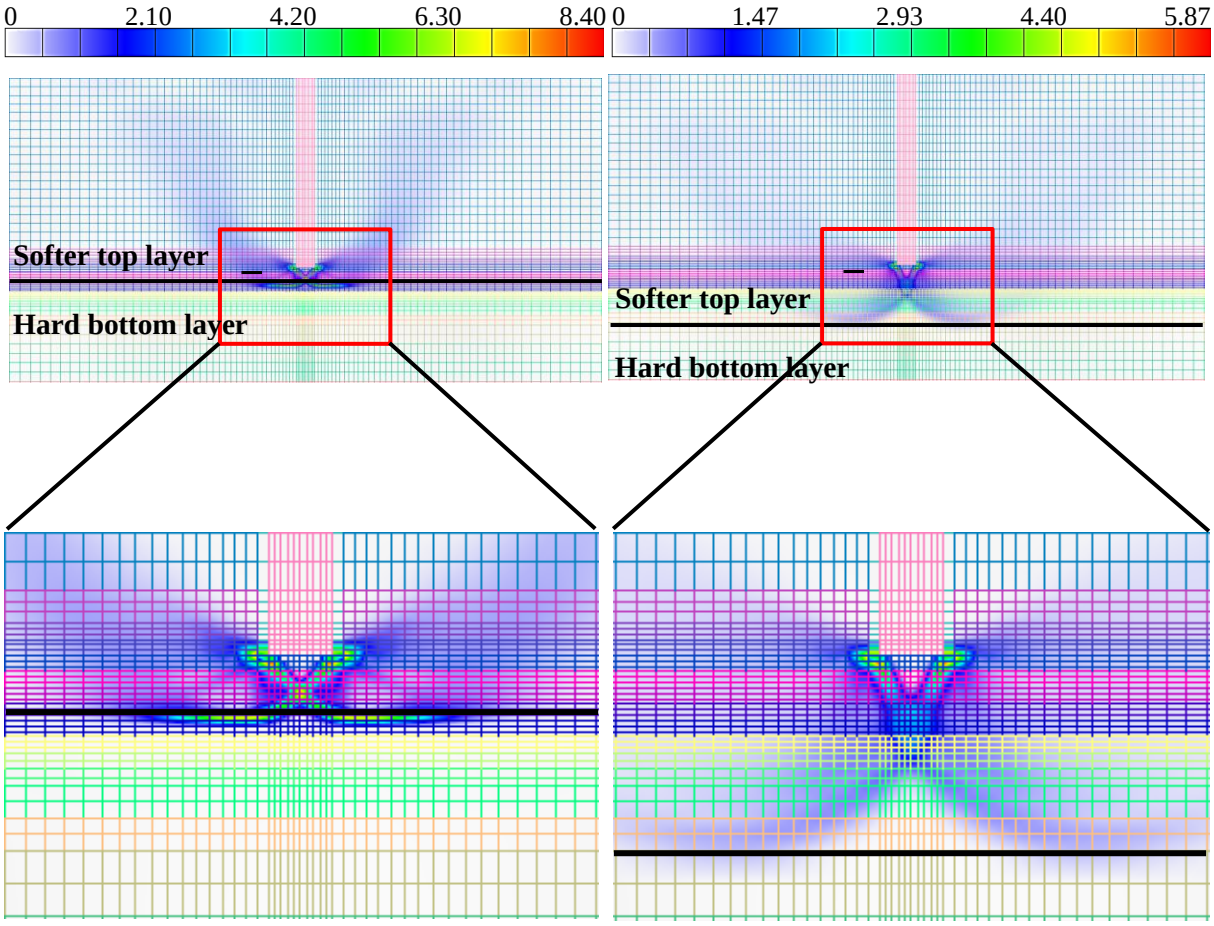

(a) $d/B = 1$ **(b)** $d/B = 3$

Fig. 5-13 Strain rate distribution from c-ϕ soil using Drucker Prager

5.7 Analyses Based on the High Order Yield Function

5.7.1 Influence of the Confining Pressure on the Shear Resistance Angle

Du et al. (2016) improved RPFEM by using the High Order yield function to introduce the non-linear shear strength property against confining pressure as so to consider the influence of particle breakage. The High Order yield function, therefore, remedies the problems related to high confining pressure, particle breakage, and overestimation of end bearing capacity of piles in soils with a shear resistance angle.

The shear resistance angle of soil decreases with increasing confining pressure, as shown in **Figs. 5-14** and **5-15**. Hettler and Gudehus (1988) have proposed **Eq. (5-22)** as a formula to express the decrease

of the shear resistance angle ϕ with an initial angle ϕ*:

$$\phi = \arcsin \frac{\sin \phi^*}{\left(\frac{\sigma_2}{\sigma_{20}}\right)^{\zeta} + \sin \phi^* \left[1 - \left(\frac{\sigma_2}{\sigma_{20}}\right)^{\zeta}\right]} \quad \text{(5-22)}$$

where σ_2 is lateral stress, ζ is estimated from triaxial tests, ϕ* is the shear resistance angle for the reference lateral stress. ζ is close to 0.1 and remains unchanged for various sands and densities.

Eq. (5-22) is used in this study to consider the decrease of the shear resistance angle due to the high confining pressure, however, instead of σ_{20} and σ_2, I_{10} and I_1 were considered to represent the confining pressure as shown in **Fig. 5-15**. Although this equation cannot be directly applied to the boundary value problems, because it was proposed based on the triaxial tests, the reduction in the shear resistance angle can be modeled for any given reference confining stress I_1. Based on **Eq. (5-22)** the obtained decrease of the shear resistance angle was then taken as a reference to determine the coefficients *a*, *b* and *n* in the high order yield function (**Eq. (5-10)**).

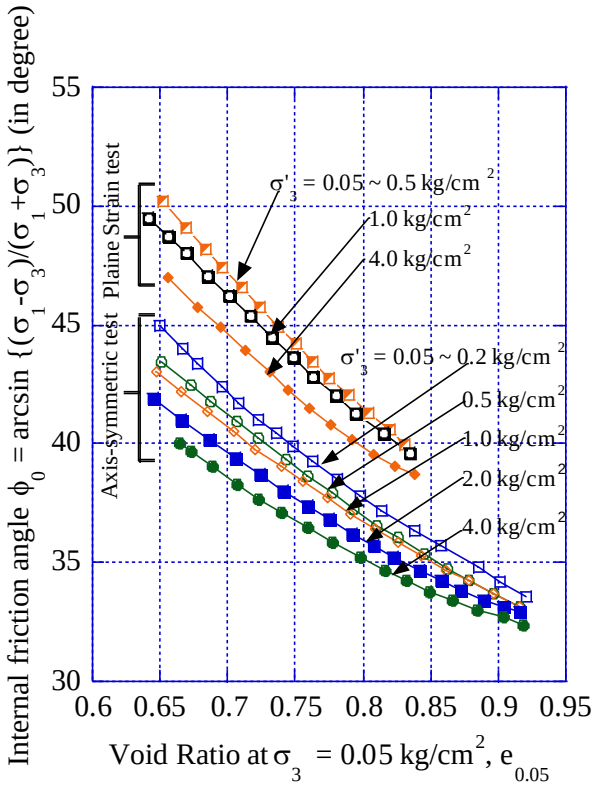

Fig. 5-14 Effect of the confining pressure on the shear strength through the experiments on Toyoura sand (Tatsuoka et al., 1986)

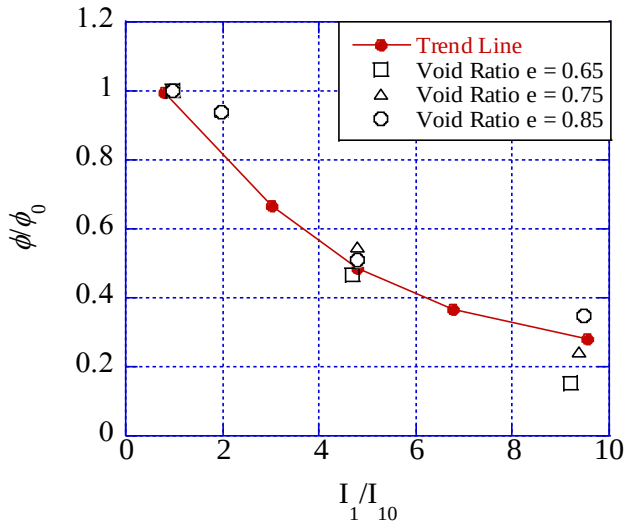

Fig. 5-15 Relationship between ϕ/ϕ_0 and I_1/I_{10} (Du et al. (2016))

Figs. 5-16 and **5-17** show the estimation results of the coefficients for the following soils: the top layer and the bottom layer of the ϕ soil and c-ϕ soil. It can be confirmed from them that the reference curve based on Helter-Gudehous (1988) can be reproduced accurately. The coefficients for the soils used in the simulation are listed in **Table 5-4**.

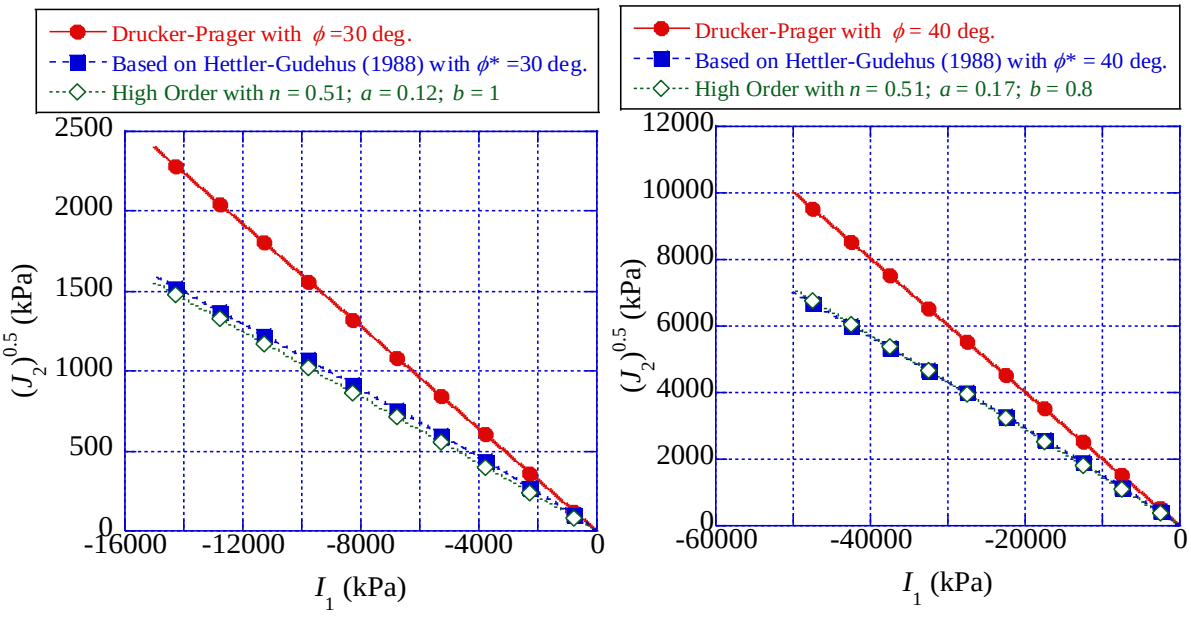

(a) ϕ* = 30 deg. (top layer)

(b) ϕ* = 40 deg. (bottom layer)

Fig. 5-16 Estimation of parameters a, b and n for ϕ soil

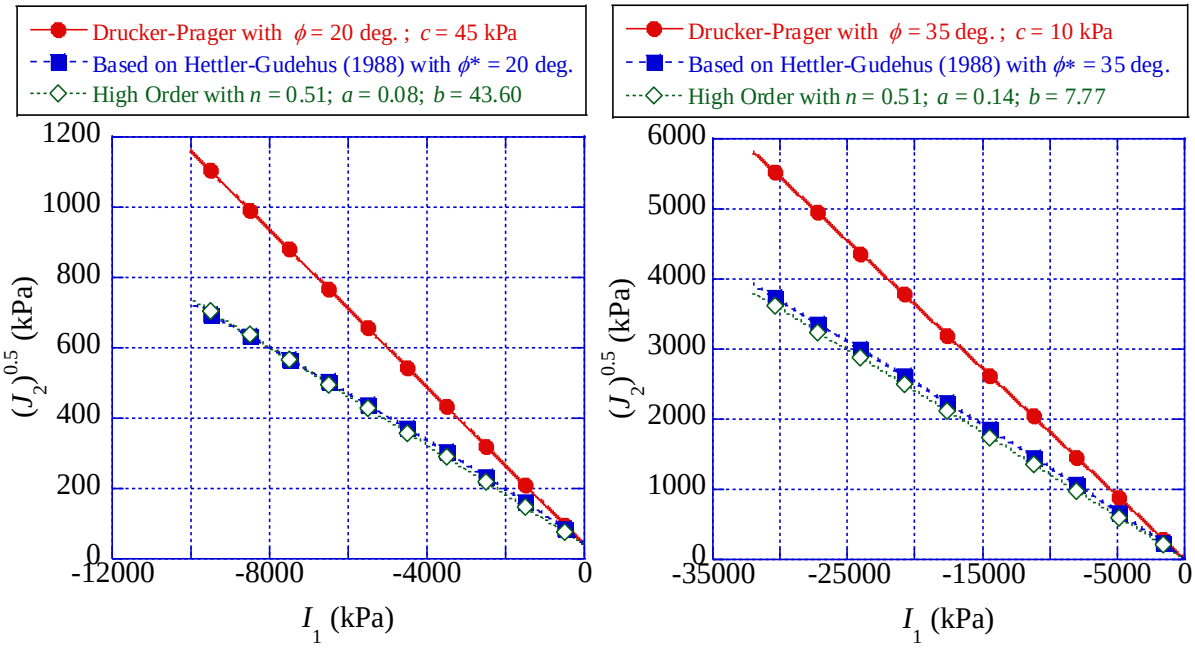

(a) ϕ^* = 20 deg., c = 45 kPa (top layer) **(b)** ϕ^* = 35 deg., c = 10 kPa (bottom layer)

Fig. 5-17 Estimation of parameters a, b and n for c-ϕ soil

Table 5-4 Coefficients for the soils used in the simulation

Soil Type	Layer	ϕ (deg.)	c (kPa)	n	a	b
ϕ Soil	**Top Layer**	30	1	0.51	0.12	1.00
	Bottom layer	40	1	0.51	0.17	0.80
c-ϕ Soil	**Top Layer**	20	45	0.51	0.08	43.60
	Bottom layer	35	10	0.51	0.14	7.77

5.7.2 Comparison of End Bearing Capacities of IESP from the two Yield Functions

By using the nonlinear shear strength parameters (n, a and b) shown in **Table 5-4**, the end bearing capacity of IESP was simulated with the High order yield function.

The variation of the end bearing capacity of IESP as a function of the distance d/B is shown in **Fig. 5-18**. Independently on the yield function used and the type of soil, the end bearing capacity decreases with the increase of d/B. It attains a minimum steady value at a critical distance d/B^* = 3.

The results from the Drucker-Prager yield function are greater than those from the High Order yield function. The difference between the results from the two yield functions is greater when the pile approaches the hard layer (range of $d/B < 3$). This can be explained by the influence of the hard layer in that range of d/B, the non-linear shear strength property against confining pressure is explicitly

observed.

Fig. 4-19 compares the degradation factors ξ_x of Drucker-Prager and High-Order yield functions. For all the cases, roughly one curve is obtained for each soil type, independently of the yield functions. This means that the values of the degradation factor ξ_x do not depend on the yield function used.

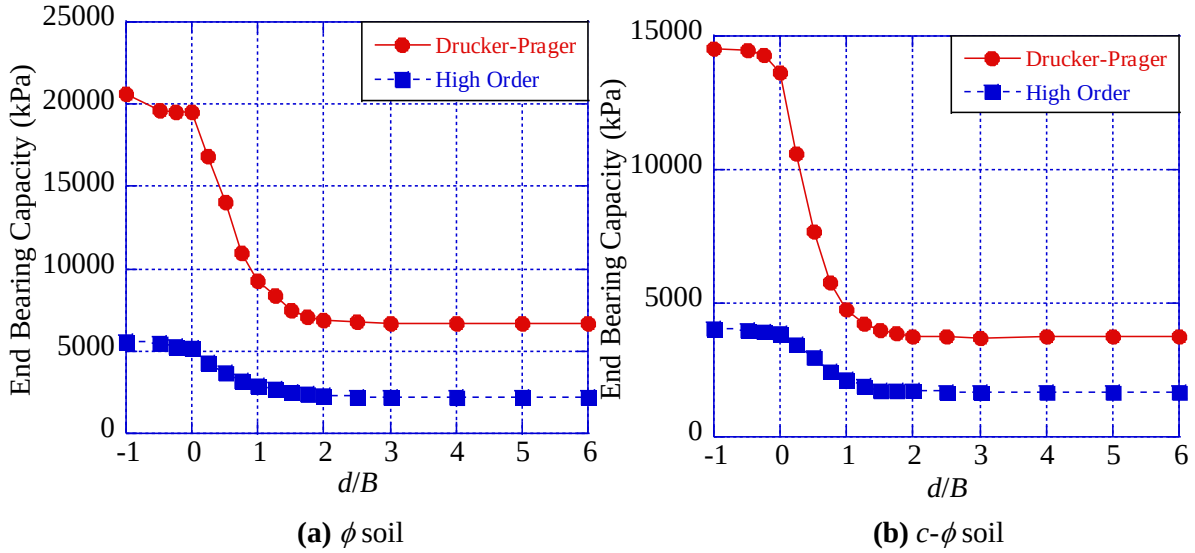

(a) ϕ soil **(b)** c-ϕ soil

Fig. 4-18 Comparison of the end bearing capacities from D.P. and H.O. yield functions

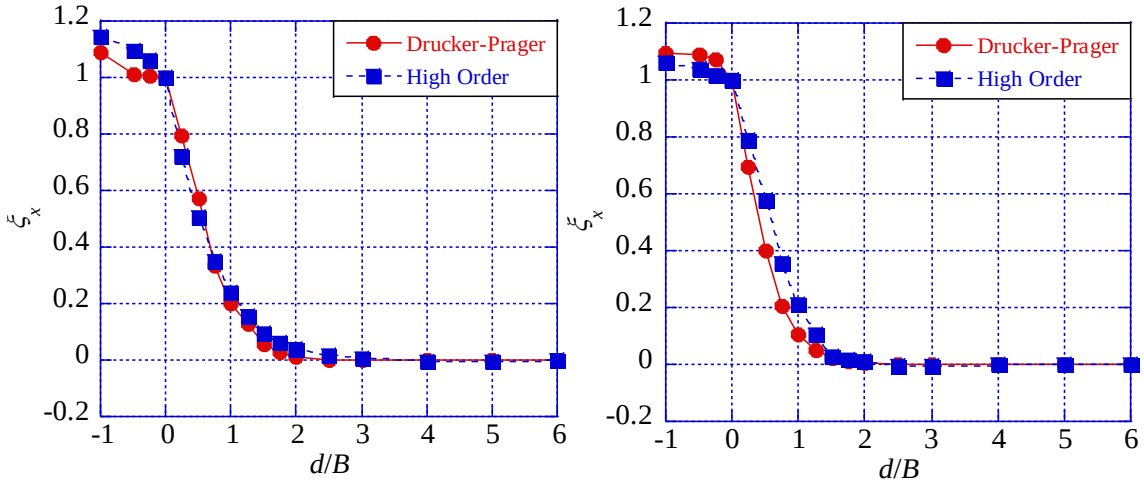

(a) ϕ soil **(b)** c-ϕ soil

Fig. 5-19 Normalized end bearing capacities from D.P. and H.O. yield functions

5.7.3 Failure Patterns

The strain rate distribution style obtained with the High Order yield function is shown in **Fig. 5-20** and **Fig. 5-21** for ϕ soil and c-ϕ soil respectively. The norm of the strain rate is presented by contour lines in the range of $\dot{e}_{max} \sim \dot{e}_{min}$ (=0). As in the case of Drucker-Prager yield (**Fig. 5-12** and **Fig. 5-13**), for both soil types, when the distance $d/B < 3$, the yield zones at the collapse stage extend into the bottom layer. However, if $d/B \geq 3$, the yielding is confined to the top layer. And the shear bands obtained with the High Order yield function are all similar to the case (a) and (c) in **Fig. 5-10**. The shear bands obtained with the High Order yield function are ideal ones and are much better than those obtained with the Drucker-Prager yield function (**Figs. 5-12** and **5-13**).

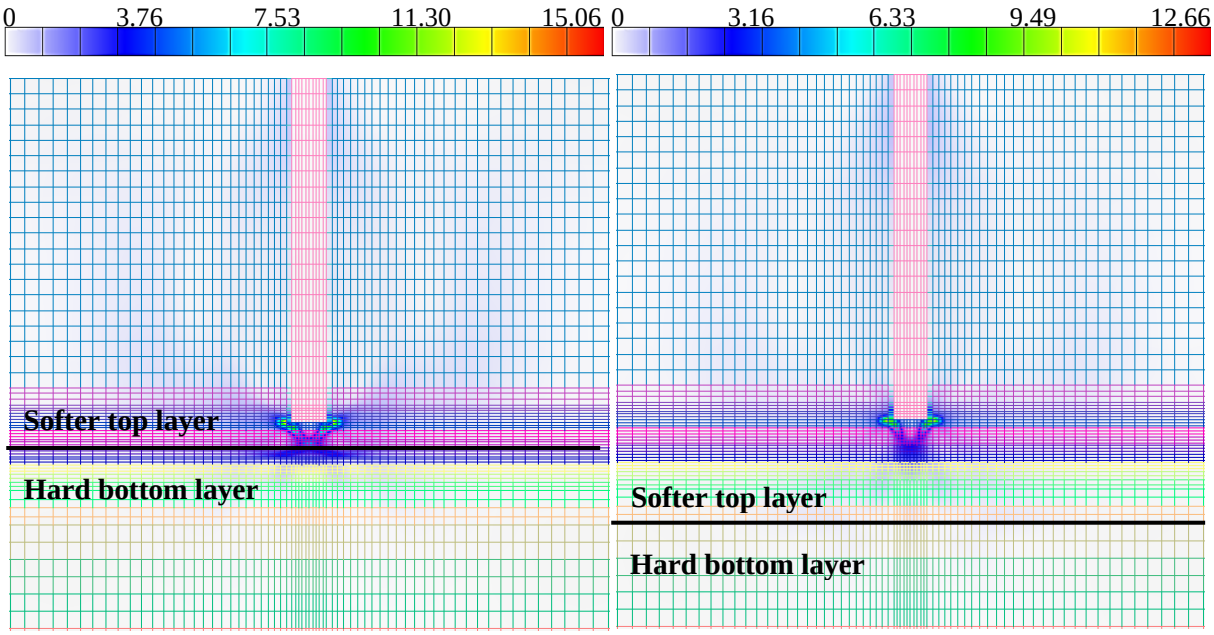

(a) $d/B = 1$ **(b)** $d/B = 3$

Fig. 5-20 Strain rate distribution from ϕ soil using the High-Order model yield function

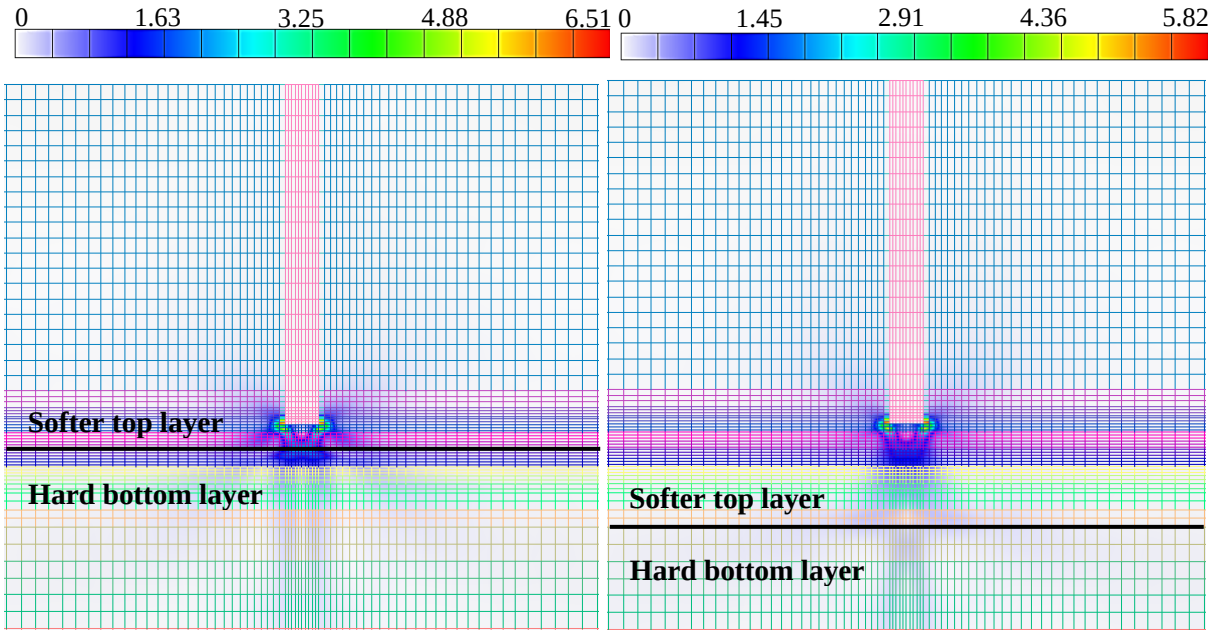

(a) $d/B = 1$ **(b)** $d/B = 3$

Fig. 5-21 Strain rate distribution from c-ϕ soil using the High-Order model yield function

5.7.4 Justification of the Differences Between the Results Obtained with the two Simulations Methods

Figs. 5-22 and **5-23** show the stress state (the relationship between the I_1 and $\sqrt{J_2}$) of all elements obtained by RPFEM for ϕ soil and c-ϕ soil, respectively.

For each soil layer of both soil types, the simulation with Drucker-Prager (D.P.) gives higher values of I_1 and $\sqrt{J_2}$. The lower values of I_1 and $\sqrt{J_2}$ of the simulations with H.O. justify localization of strain rate generation due to the reduction of shear resistance angle and dilation angle as shown in the failure patterns (**Fig. 5-20** and **Fig.** 5-**21**), resulting in the lower end bearing capacity in the simulations with H.O.

According to the simulation results, the difference between D.P. and H.O. is more significant in ϕ soil than in c-ϕ soil. It suggests that the influence of confining pressure on the shear resistance angle is more significant in ϕ soil, less significant in c-ϕ soil and absent in c soil (since $\phi = 0$ deg. in c soil).

Comparing the simulation results of the case $d/B = 1$ and the case $d/B = 3$, the more the pile is near

to the bottom layer, the higher the stress induced by the load in the ground at the failure stage (I_1) is. The stress at the failure stage is higher in the top layer than in the bottom layer and this difference is more significant for greater values of d/B. This is because the stress caused by the total load is higher near the pile tip. It may be noticed that at $d/B = 3$, the stress in the bottom layer is almost insignificant. These facts explain the decrease of the end bearing capacity with the increasing d/B and the non-influence of the bottom layer when $d/B \geq 3$.

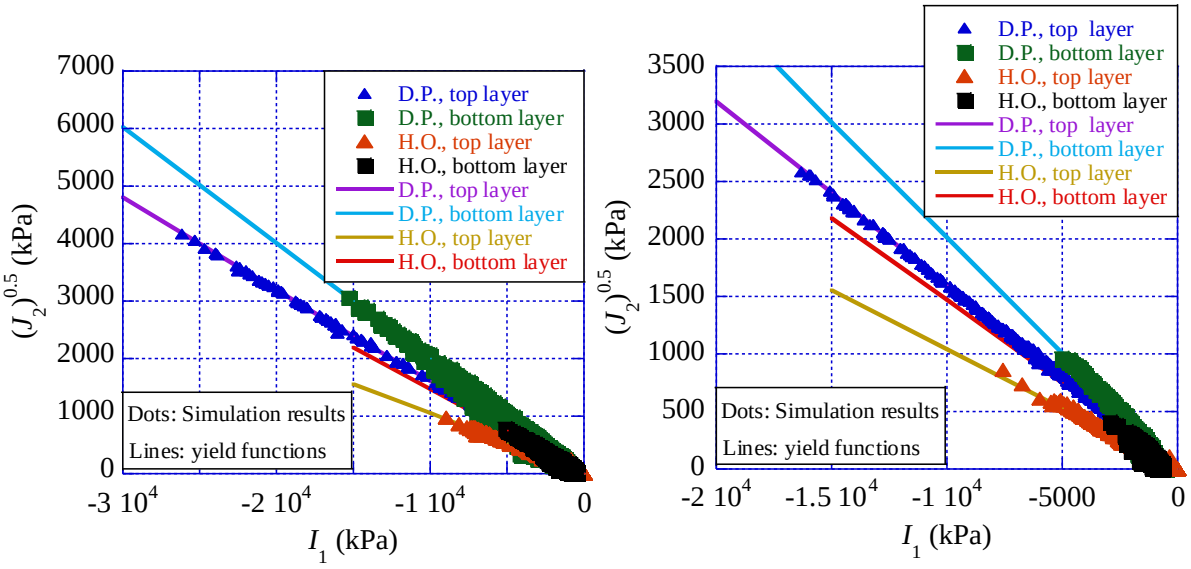

(a) $d/B = 1$ **(b)** $d/B = 3$

Fig. 5-22 Relationship between I_1 and $\sqrt{J_2}$ of ϕ soil

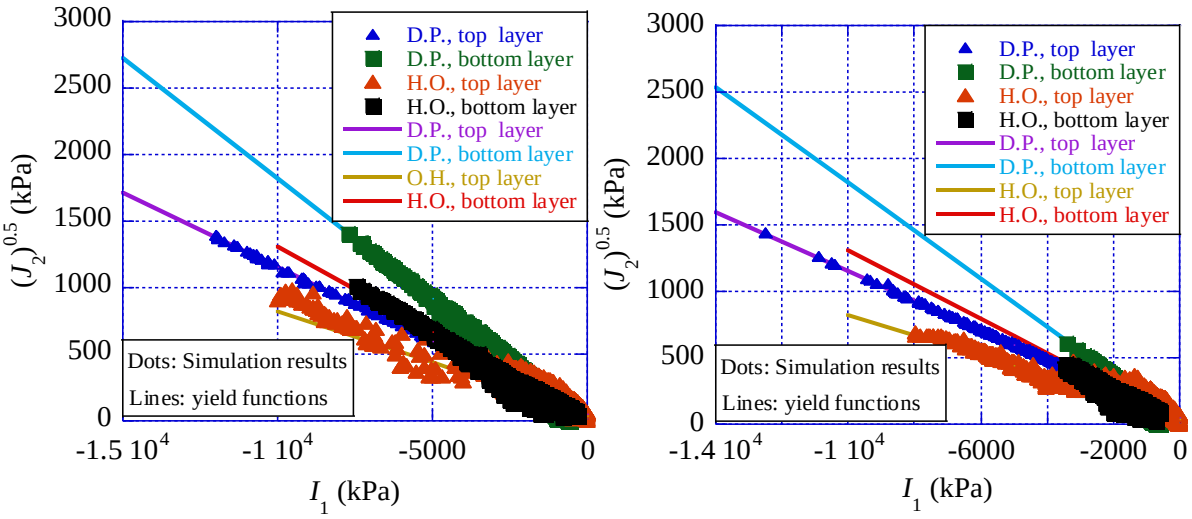

(a) $d/B = 1$ **(b)** $d/B = 3$

Fig. 5-23 Relationship between I_1 and $\sqrt{J_2}$ of c-ϕ soil

5.8 The formula for Estimation of the End Bearing Capacity of IESP

This formulation in **Eqs. (5-23)** and **(5-24)** are proposed as a formula to estimate the end bearing capacity of IESP.

$$q_x = \xi_x q_H + (1 - \xi_x) q_s = \xi_x (q_H - q_s) + q_s \quad \cdots\cdots (5\text{-}23)$$

$$\xi_x = \frac{q_x - q_s}{q_H - q_s} \quad \cdots\cdots (5\text{-}24)$$

where q_x is the end bearing capacity when $d/B = x$, q_H is the end bearing capacity when $d/B = 0$, q_s is the end bearing capacity of the pile when the bottom layer has no influence and ξ_x is the degradation factor.

q_H and q_s can easily be obtained by an analytical or numerical method. However, the values of ξ_x need to be estimated independently of q_x.

For the formula of estimating ξ_x, **Eq. (5-25)** is proposed based on the above simulation results. Where d/B is the normalized distance between the pile tip and the surface of the bottom layer and m is a coefficient that depends on soil type and the end bearing capacity ratio r.

For the different values of r of each soil type, by using **Eq. (5-24)**, ξ_x were obtained and plotted as a function of d/B. The values of m in **Eq. (5-25)** are then obtained by fitting the ξ_x of **Eq. (5-25)** to those

of **Eq. (5-24)**. Those values of *m* are plotted and are used as references to propose **Eq. (5-26)**, **Eq. (5-27)** and **Eq. (5-28)** for calculation of the value of the coefficient *m*, for *c* soil, ϕ soil and *c*-ϕ soil, respectively.

$$\xi_x = \frac{1}{1+m\cdot(d/B)} \quad \text{(5-25)}$$

$$m_c = 8.3984r - 10.528 \quad \text{(5-26)}$$

$$m_\phi = 5.66\log(r) + 0.31644 \quad \text{(5-27)}$$

$$m_{c-\phi} = 6.0712\log(r) + 0.68599 \quad \text{(5-28)}$$

The proposed formula in **Eq. (5-23)** is like the formulas of Hyodo et al. (2020) [**Eq. (5-6)]** and Azam and Wang (1991) [**Eq. (5-8)]**. **Table 5-5** shows the equivalence of the three formulas. In Hyodo et al. (2020) the degradation factor is independent of the end bearing capacity ratio *r* and applicable to sandy soil only. However, as shown in **Fig. 5-9** the degradation factor is influenced by the ratio *r* and soil type, this makes the weak point of Hyodo et al. (2020). In Azam and Wang (1991) the coefficient *m* of the degradation factor is changing according to the soil type, which is the same as in this study and makes the strong point of Azam and Wang (1991). However, *m* is independent of the bearing capacity ratio *r* which makes the weak point of Azam and Wang (1991). Therefore, it is thought that the formula proposed in this study have more advantage and applicability than the previous research.

5.9 Validation of the Proposed Formula

5.9.1 Comparison with Analytical Methods

The results from the proposed formula, are compared with those from Satyanarayana and Garg (1980) and Azam and Wang (1991) methods. The method of Meyerhof (1976) is used for the calculation of q_b and q_t in the Azam and Wang (1991) method and the Meyerhof (1976) bearing capacity factors N_c and N_q are used in Satyanarayana and Garg (1980) method. The soils in **Table 5-2** were used for the comparison.

A bored cast-in-situ pile was considered (without debris at the pile tip). At $d/B = 0$, the bearing layer is the bottom layer, in that case, the actual thickness of the bearing stratum $D_b = 0$.

The comparison is shown in **Fig. 5-24**. When q_s and q_H in the proposed equation are obtained from the RPFEM, there is a good agreement between the simulation method and the proposed equation.

For *c* soil, as shown in **Fig. 5-24(a)**, a good agreement is obtained between the Satyanarayana and Garg (1980) method, the proposed equation and RPFEM using D.P. It can be concluded that RPFEM using D.P. can estimate the end bearing capacity of IESP in *c* soil.

In the case of the ϕ soil and *c*-ϕ soil, a good agreement is obtained between all the methods except the method of RPFEM using D.P. which gives very much high values of end bearing capacity. From **Fig. 5-24(b)** and **Fig. 5-24(c),** it is clear that the D.P. yield function overestimates the end bearing capacity of IESP in the case of ϕ soil and *c*-ϕ soil. The High Order yield function gives an accurate estimation of the end bearing capacity of IESP in the case of ϕ soil and *c*-ϕ soil.

Table 5-5 Equivalence between formulas

Descriptions	Azam and Wang (1991)	Hyodo et al. (2020)	This study ((Eq. (22))
Formula	$q_0 = q_t + (q_b - q_t)\,[1 - m(H/B)]^2$	$q_{unreached} = \alpha q_{base} + (1-\alpha) q_{nobase}$	$q_x = \xi_x q_H + (1-\xi_x) q_s = \xi_x (q_H - q_s) + q_s$
End bearing capacity of IESP	q_0	$q_{unreached}$	q_x
End bearing capacity of completely end-supported pile (ESP) (when the pile reaches the bottom layer)	q_b	q_{base}	q_H
End bearing capacity of pile with no lower hard layer (no influence of the bottom layer)	q_t	q_{nobase}	q_s
Degradation factor	$[1 - m(H/B)]^2$	α	ξ_x

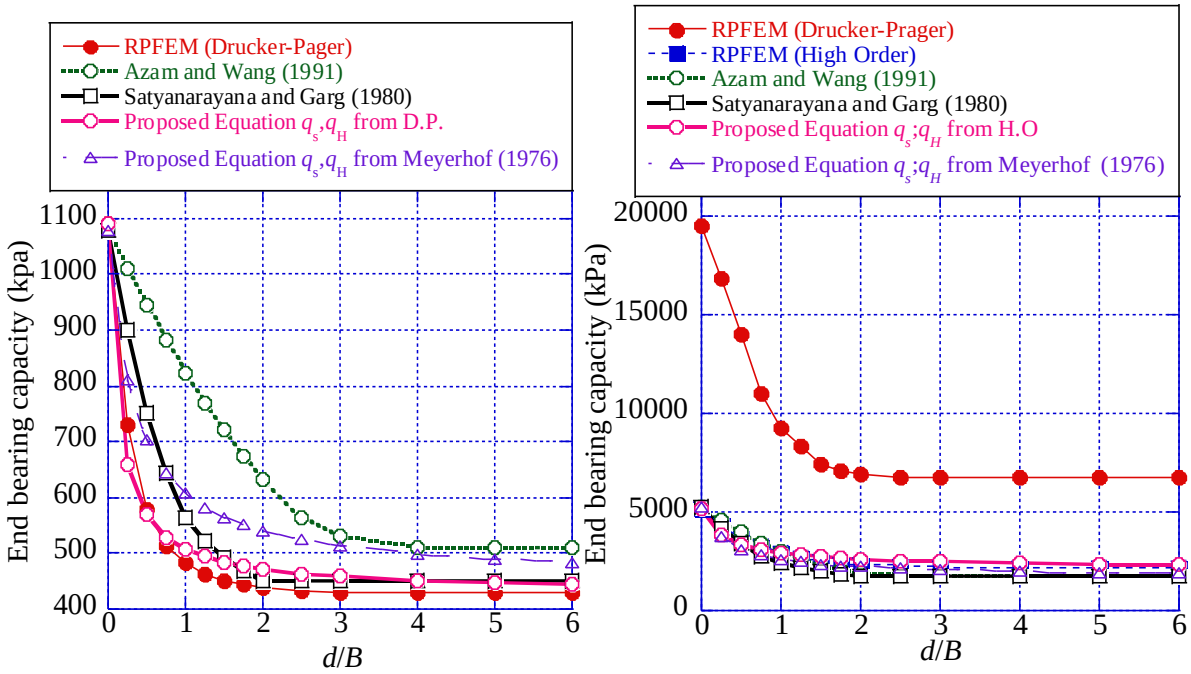

(a) *c* soils **(b)** ϕ soils

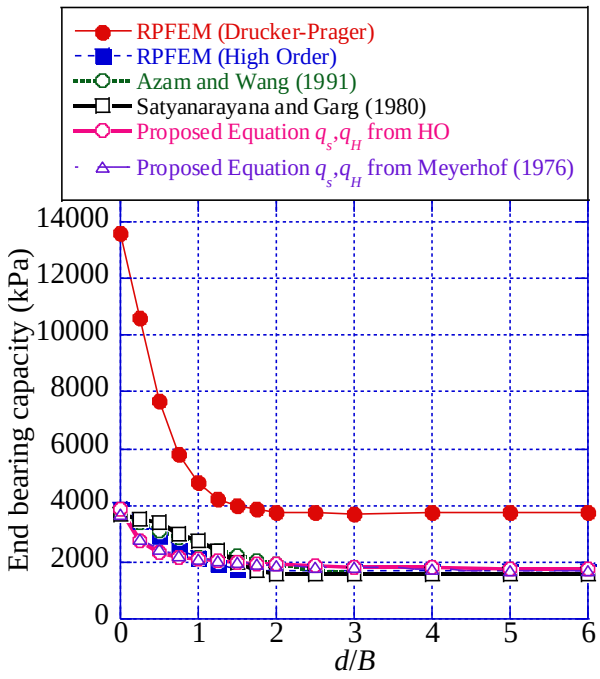

(c) *c*-ϕ soils

Fig. 5-24 Comparison with some analytical methods existing in the literature.

5.9.2 Comparison with Hyodo et al. (2020) and Ikeda et al. (2012) (Numerical and Experimental Method, Respectively)

The proposed equation is compared with Hyodo et al. (2020). In the study by Hyodo et al. (2020), the bottom layer was very dense sand with relative density D_r = 90% and the top layer was changed from loose sand to medium sand and dense sand with relative densities D_r = 45%, D_r = 60% and D_r = 75%, respectively. The corresponding end bearing capacity q_{base} (= q_H) is about 475.67 kN and q_{nobase} (= q_s) are 251.34 kN, 319.47 kN and 392.15 kN for the case of sand in the upper layer has D_r = 45%, D_r = 60% and D_r = 70% respectively, which correspond to $r = q_H/q_s$ = 1.89, 1.49 and 1.21 respectively.

By using those ratios r in **Eq. (5-25)** and **Eq. (5-27)**, it was possible to obtain the corresponding ξ_x as a function of d/B. The comparison of the obtained ξ_x with those of Hyodo et al. (2020) (α) is shown in **Fig. 5-25(a)**. There is a good agreement between the two methods.

The ξ_x were then used in **Eq. (5-23)** to obtain the corresponding q_x. **Fig. 5-25(b)** compares the ratio q_x/q_H and there is a good agreement between the two methods.

For more reliability, the laboratory loading tests with layered sand (Ikeda et al., 2012) are compared with the proposed formula. Here q_s = 30.6 kN and for d/B = 0, 0.5 and 1 the corresponding q_x are 103 kN (means q_H = 103 kN), 61.8 kN and 50 kN, respectively. Then the ratio $r = q_H/q_s$ = 3.37. The black curves in **Fig. 5-25(b)** show the comparison of q_x/q_H, there is good agreement between the experimental method and the proposed equation.

These comparisons assure the accuracy and reliability of the proposed formula against past numerical and experimental results for ϕ soils. The comparison with analytical studies can stand for validation of the proposed formula for c soils and c-ϕ soils.

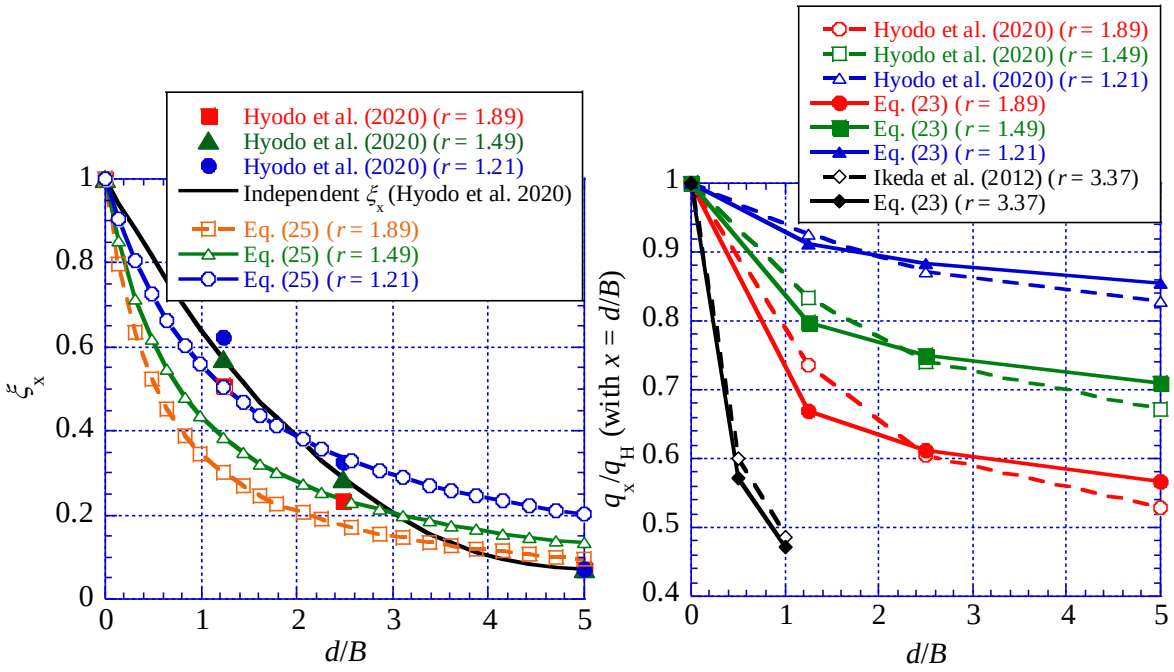

(a) Comparison of ξ_x **(b)** Comparison of the ratio q_x/q_H

Fig. 5-25 Comparison with Hyodo et al. (2020) and Ikeda et al. (2012)

5.10 Conclusions

This study carried out two-dimensional RPFEM analyses in plain strain conditions to estimate the end bearing capacity of an Incompletely End-supported single Pile (IESP). Two yield functions were used, the Drucker-Prager yield function and the High Order yield function. Three types of soil were considered, *c* soil, ϕ soil and (*c*-ϕ soil). The influences of the following parameters were investigated: the distance between the pile tip and the bottom layer normalized by the pile diameter (*d*/*B*) and the ratio *r* of the end bearing capacity of the pile on the bottom layer to that of the pile when the bottom layer has no influence. The main findings are as follows.

(1) The Drucker-Prager yield function gives reasonable results for *c* soil but is not suitable for ϕ soil and *c*-ϕ soils due to non-consideration of the influence of the confining pressure on the internal friction angle ϕ.

(2) New parameters of the High Order yield function are established to consider the non-linear shear strength property of soil against the confining pressure in ϕ soil and *c*-ϕ soils. The validity of the established High Order yield was confirmed by comparing its results with those from

existing literature. Therefore, a new yield function effective for estimating the end bearing capacity in ϕ soil and c-ϕ soil is established.

(3) Independently of the yield function (Drucker-Prager and High Order model), the end bearing capacity decreases when the pile goes far from the bottom layer and becomes constant from the distance of three times the pile diameter. The decrease of the end bearing capacity illustrates the degradation of the end bearing capacity.

(4) The degradation factor ξ_x of the end bearing capacity of IESP is independent of the yield function. However, ξ_x is affected by the bearing capacity ratio r and the soil type.

(5) An equation of the degradation factor ξ_x is established in this study as a function of the distance d/B, the end bearing capacity ratio r and the type of soil considered. By using ξ_x, a formula that gives an accurate estimation of the end bearing capacity of IESP is proposed. Its validity is confirmed by comparisons with the previous studies.

References

[1] Azam, G. and Wang, M.C., 1991. Bearing capacity of strip footing supported by two-layer C-φ soils. Washington, D. C: Transportation Research Record, Transportation Research Board No. 1331, 56-66.

[2] Bowles, J.E., 1996. Foundations Analysis and Design. McGraw-Hill Publishing Company, New York.

[3] Coyle, H.M. and Castello, R.R., 1981. New design correlations for piles in sand. Journal of Geotechnical Engineering Division, ASCE, 107(7), 965-986.

[4] Du, N.L., Ohtsuka, S., Hoshina, T. and Isobe, K., 2016. Discussion on size effect of footing in ultimate bearing capacity of sandy soil using rigid-plastic finite element method. Soils and Foundations, 56(1), 93-103.

[5] Eslami, A. and Fellenius, B.H., 1995. Toe bearing capacity of piles from cone penetration test (CPT) data. In Proceedings of the International Symposium on Cone Penetration Testing, CPT'95, Linköping, Sweden. Swedish Geotechnical Institute, October 4–5, SGI Report 3-95, Vol. 2, 453–460.

[6] Eslami, A. and Fellenius, B.H., 1997. Pile capacity by direct CPT and CPTu methods applied to 102 case histories. Canadian Geotechnical Journal, 34(6), 886–904.

[7] Gunaratne, M., 2006. The foundation engineering handbook. Taylor and Francis, London.

[8] Houlsby, G.T., Nuit, N.R.F. and Sweeney, M., 1994. End bearing capacity of piles in carbonate soil. Proceedings of the 13th International Conference on Soil Mechanics and Foundation Engineering, New Delhi, Vol. 2, 635-638.

[9] Hettler, A. and Gudehus, G., 1988. Influence of the foundation width on the ultimate bearing capacity factor. Soils and Foundations, 28(4), 81–92.

[10] Hoshina, T., Ohtsuka, S. and Isobe, K., 2011. Ultimate bearing capacity of ground by rigid-plastic finite element method taking account of stress-dependent non-linear strength property. Journal of Japan Society of Civil Engineers Ser A2 (Applied Mechanics (AM)), 68(2), 327-336 (in Japanese).

[11] Hyodo, J., Tamari, Y., Sone, A., Ozutsumi, O. and Ichii, K., 2020. A simplified method to consider the pile of insufficient length to obtain the support from bearing stratum. Journal of Asian Architecture and Building Engineering, 19(6), 626-636. DOI: 10.1080/13467581.2020.1764847

[12] Ikeda, A., Tsutiya, T. and Nagai, H., 2012. A New Formula for the Toe Resistance of a Helical Screw Pile Considering the Different Load Sharing Bearing Mechanism at the Closed-End and the Helix, AIJ Journal of Technology and Design, 18(40), 877–882.

[13] Janbu, N., 1976. Static bearing capacity of friction piles. Proceedings of the 6th European Conference on Soil Mechanics and Foundation Engineering, 1(2), 479–488.

[14] Meyerhof, G.G., 1963. Some recent research on the bearing capacity of foundations. Canadian Geotechnical Journal, 1(1), 16–26.

[15] Meyerhof, G.G., 1976. Bearing capacity and settlement of pile foundations. Journal of Geotechnical Engineering Division, ASCE 102(3), 195–228.

[16] Pholkainuwatra, P., Eua-apiwatch, S. and Yimsir, S., 2022. Experimental study of pile set-up of driven piles in Bangkok Clay. Engineering and Applied Science Research, 49(1), 96-102.

[17] Prandtl, L., 1921. Uber die Eindringungsfestigkeit (Harte) plastischer Baustoffe und die Festigkeit von Schneiden. Zeitschrift fur angewandte Mathematik und Mechanik, 1(1), 15–20.

[18] Satyanarayana, A.M. and Garg, R.K., 1980. Bearing capacity of footings on layered c-φ soils. Journal of Geotechnical Engineering Division, ASCE 106(7), 819-824.

[19] Tamura, T., Kobayashi, S. and Sumi, T., 1984. Limit analysis of soil structure by rigid-plastic finite element method. Soils and Foundations, 24(1), 34-42.

[20] Tamura, T., Kobayashi, S. and Sumi, T., 1987. Rigid plastic finite element method for frictional soil. Soils and Foundations, 27(3), 1-12.

[21] Tatsuoka, F., Sakamoto, M., Kawamura, T. and Fukushima, S., 1986. Strength and deformation characteristics of sand in plane strain compression at extremely low pressures. Soils and Foundations, 26(1), 65–84.

[22] Teramoto, S., Kimura, M. and Boonyatee, T., 2015. Parametric FEM analysis on mechanical behavior of Incompletely End-Supported Pile. Computer methods and recent advances in geomechanics-Oka; Murakami, Uzuoka and Kimoto (Eds.). London: Copyright Taylor and Francis Group, ISBN 978-1-138-00148-0.

[23] Terzaghi, K., 1943. Theoretical soil mechanics. Chapman and Hall, London.

[24] Veiskarami, M., Eslami, A. and Kumar, J., 2011. End-bearing capacity of driven piles in sand using the stress characteristics method: analysis and implementation. Canadian Geotechnical Journal, 48, 1570-1586.

[25] Vesić, A.S., 1967. Ultimate load and settlement of deep foundations in sand. Proceedings of the Symposium on Bearing Capacity and Settlement of Foundations. Durham, N.C, Duke University series, 5(6), 53–68.

[26] Vesić, A.S., 1973. Analysis of ultimate loads of shallow foundations. Journal of the Soil Mechanics and Foundations Division, 99 (1), 45-76.

[27] Vesić, A.S., 1977. Design of Pile Foundations. National Cooperative Highway Research Program, Synthesis of Practice No. 42, Transportation Research Board, Washington, DC, 68 pages.

[28] Yasufuku, N. and Hyde, A.F.L., 1995. Pile end-bearing capacity in crushable sands. Géotechnique, 45(4), 663-676.

[29] Yasufuku, N., Ochiai, H. and Ohno, S., 2001. End-Bearing Capacity of sand related to soil compressibility. Soils and foundation, 41(4), 59-71.

CHAPTER 6 BEARING CAPACITY EVALUATION OF A SMALL DIAMETER SPIRAL PILE IN SOFT GROUND SUBJECTED TO COMBINED LOADS

Abstract

In the current practice, the evaluation method of the bearing capacity for small-diameter spiral piles is a conservative method performed on the safe side since it does not consider the integration effect with the surrounding ground due to the rotational press-fitting. In addition, the evaluation method of the bearing capacity of spiral piles subjected to combined loads has not been established. In this study, a series of push-in, pull-out and horizontal loading tests on spiral piles constructed on soft and viscous ground was conducted, and a method to easily consider the integration effect of surrounding ground by rotational press-fitting is proposed. Subsequently, based on the proposed method, a small-diameter spiral pile is modelled with FEM analysis, various test results were reproduced and coefficients to consider the integration effect of the surrounding ground, in numerical analysis, are established. By the same FEM analysis method, using the established coefficients, the bearing capacity characteristics of the vertical and batter spiral pile for the combined load are obtained. Finally, based on the results, formulas for the bearing capacity envelopes in H-V-M space are proposed and the accuracies of the formulas are verified.

Keywords: spiral pile, FEM analysis, combined load, failure envelope

6.1 Introduction

The construction of photovoltaic power generation facilities has been increasing with the increasing demand for renewable energy. Many solar power generation facilities have been constructed on sites with poor ground and construction conditions. To ensure the feasibility of the solar power generation business, increasing numbers of constructions have been carried out for the facilities. The constructions include large-scale ones on relatively inexpensive land with poor conditions and those on slopes. Conventionally, the major foundation type used for photovoltaic power generation equipment is the concrete shallow foundation. However, with the abovementioned constructions on soft ground with poor conditions in mind, the development of new foundation types using small-diameter and short steel pipe piles, spiral piles, and batter piles has progressed in Japan (Araki 2013; Hirata et al. 2005; Sato et al. 2015). Generally, compressive, horizontal, and uplift loads and moments act on these piles simultaneously due to the actions of wind, earthquake, landslide, etc. Many studies reported the behaviour of other types of pile under combined loading: compressive-lateral loading (Meyerhof 1981; Meyerhof et al. 1983; Jain et al. 1987; Gotman 2000; Zhang and Small 2000; Small and Zhang 2002; Johnson 2005; Abdel-Rahman and Achmus 2006; Karthigeyan et al. 2006, 2007; Achmus and Thieken 2010; Suleiman et al. 2010; Ashour et al. 2020); lateral-uplift loading (Das et al. 1976; Ismael 1989; Darr et al. 1990; Rao and Prasad 1993; Mroueh and Shahrour 2007, 2009; Anand et al. 2012; Ayothiraman and Reddy 2014; Reddy and Ayothiraman 2015; Ashour et al. 2020). There are, however, very limited studies that reported the behaviour of spiral piles under combined loading.

The spiral pile is an advantageous pile type because it has a large resistance to vertical loads (push-in and pull-out loads). On the other hand, its disadvantage is its low flexural rigidity, its horizontal resistance is smaller than that of the steel pipe pile of the same diameter. When the conventional design method in Japan, which uses 1% of the pile diameter (lower limit: 15 mm) as the allowable displacement, is applied to the small-diameter piles, there is a possibility of resulting in overdesign. This is because the elastic ground reaction force method, which is generally used in the pile foundation design, overestimates the horizontal displacement of the small-diameter piles. In addition, the large resistance to the vertical load of spiral piles is due to the effect of its integration with the surrounding ground generated during the rotational press-fitting. However, in many cases, the design takes the safe side without considering this integration effect from the rotational press-fitting. Therefore, it is required to

properly evaluate the bearing capacity characteristics of small-diameter spiral piles and give more rational designs.

In the conventional design, allowable values are set for vertical load direction and horizontal load direction, and individual evaluations are performed separately. However, in reality, combined horizontal and vertical loads act on the structure due to the actions of wind load, landslides, etc. The bearing capacity against the combined vertical and horizontal loads may be lower than the bearing capacity evaluated independently. The spiral pile is also expected to be used as an anchor by taking advantage of its excellent pull-out resistance. However, since only the pull-out resistance is considered in the conventional anchor design, it is extremely important to evaluate the bearing capacity performance against the combined pull-out and horizontal loads and design the spiral pile anchors rationally for slope stabilization. In this way, we consider that an appropriate evaluation of the bearing capacity of small-diameter piles against the combined loads leads to the rationalization of the design of small-diameter pile foundations and anchors. In addition, in such combined loading conditions, it is common to use the H-V-M (horizontal, vertical and moments) failure surfaces/envelopes to assess the foundation's capacity to withstand these conditions.

In this study, we have conducted a series of push-in, pull-out and horizontal loading tests on spiral piles constructed on soft and viscous ground and we have proposed a method to simply consider the integration effect between the rotationally press-fit spiral pile and the surrounding ground. Next, based on the proposed method, we have modelled a small-diameter spiral pile in FEM analyses, reproduced the physical test results, and identified some additional parameters necessary for the numerical analysis. By the same analysis method, using the identified parameters, the bearing capacity characteristics of vertical and batter spiral pile under the combined load were obtained. Finally, based on the results, formulas for the bearing capacity envelopes in H-V-M space are proposed for both vertical and batter spiral piles.

6.2 Outline of the Loading Tests

Fig. 6-1 shows a schematic of the model spiral pile used in this study. It is a spiral pile manufactured by twisting a flat steel bar (SS400), and its features are as follows:

a) Construction can be done manually by applying rotational force to press-fit the piles and controlling

the amount of penetration per rotation so as to minimize the disturbance of the surrounding ground.

b) The effect of integration between the pile and the surrounding ground can be expected by rotational press-fitting, which increases the push-in and pull-out loads capacities.

c) By rotating the pile in the ground in the reverse direction, it can be easily pulled out and reused. The pile has high workability with less time-consuming installation.

As shown in **Fig. 6-1** and **Table 6-1**, the pile measures 1.3 m in length, 95 mm in external diameter, and 11 mm in plate thickness.

In the tests of this study, spiral piles were rotationally press-fitted into a cement-improved soft viscous ground (average *N* value: 3.9, uniaxial compressive strength: 58.5 kPa), and pure push-in, pure pull-out, and pure horizontal loading tests were performed following JGS (the Japanese Geotechnical Society) standards JGS 1811-2002 (Method for Static Axial Compressive Load Test of Single Piles), JGS 1813-2002 (Method for Static Axial Tensile Load Test of Single Piles) and JGS 1831-2010 (Horizontal load test of piles), respectively. Each loading test was carried out with protrusion lengths (*h*) of 50 mm, 100 mm, and 150 mm. The loads were applied using a hydraulic jack, **Fig. 6-2** shows the test device in case of pure horizontal loading.

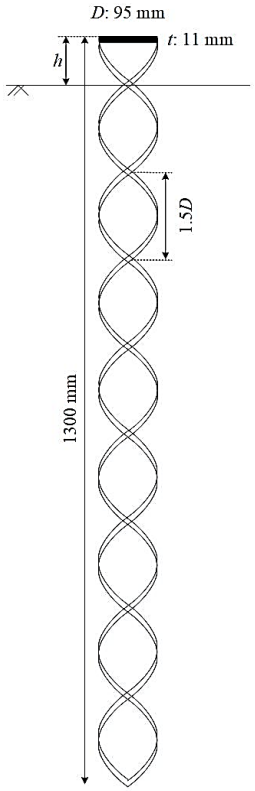

Fig. 6-1. Schematic of the spiral pile

Table 6-1. Property of the spiral pile

Material		steel SS400
Length	m	1.3
External diameter	mm	95
Plate thickness	mm	11
Young's modulus	kN/m^2	$2.05x10^8$

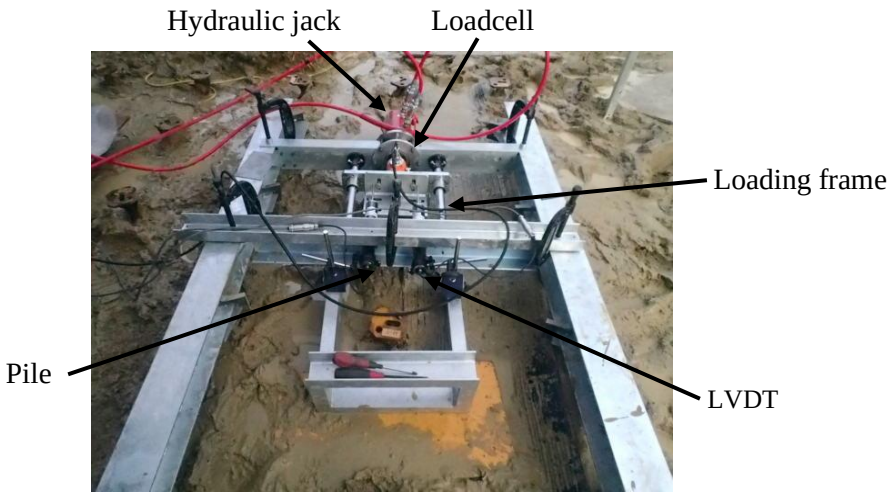

Fig. 6-2. Horizontal loading test device

6.3 Experimental Results

Fig. 6-3 shows the relationship between the load and the displacement obtained in each test. Where, the Pull-out load and the Push-in load are considered as positive load and negative load, respectively. *h*50, *h*100 and *h*150 represent the tests with loading height (*h*) of 50 mm, 100 mm, and 150 mm respectively (The loading height here is the distance from the loading point to the ground surface). Some tests were conducted twice with the same loading height (for example *h*100-1 and *h*100-2). For the vertical load, the ultimate load capacity is interpreted using the double tangent method as suggested by Shanker et al. (2007) and used by Reddy and Ayothiraman (2015). Equation of the conventional vertical (push-in and pull-out) bearing capacity is presented by **Eq. (6-1)** and the conventional horizontal resistance of pile can be obtained by Chang's equation **Eq. (6-2)**.

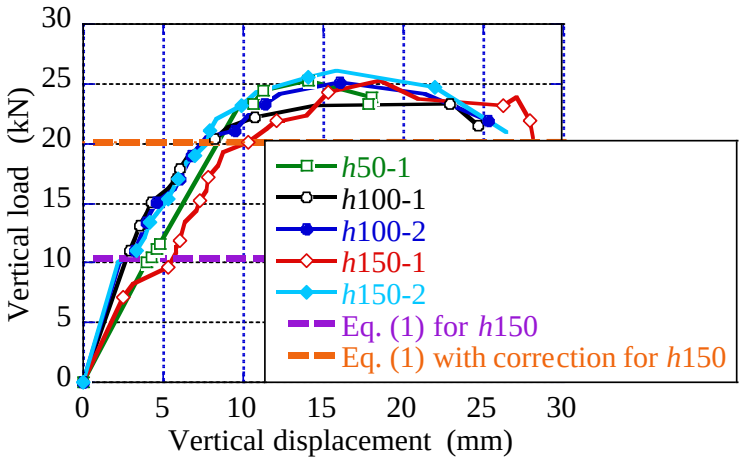

(a) Pull-out tests

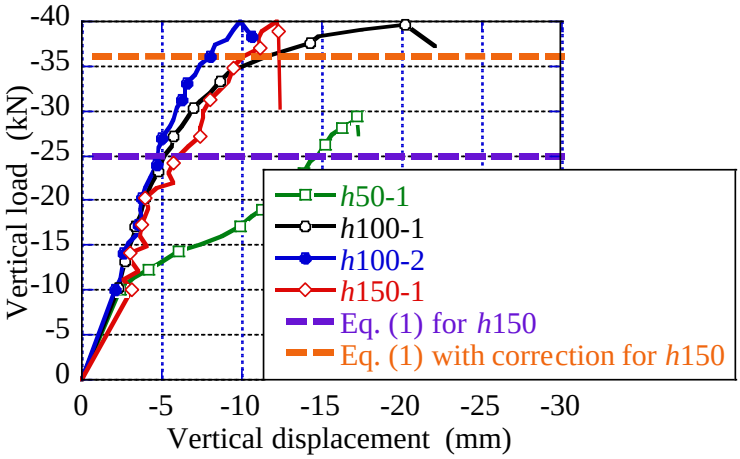

(b) Push-in tests

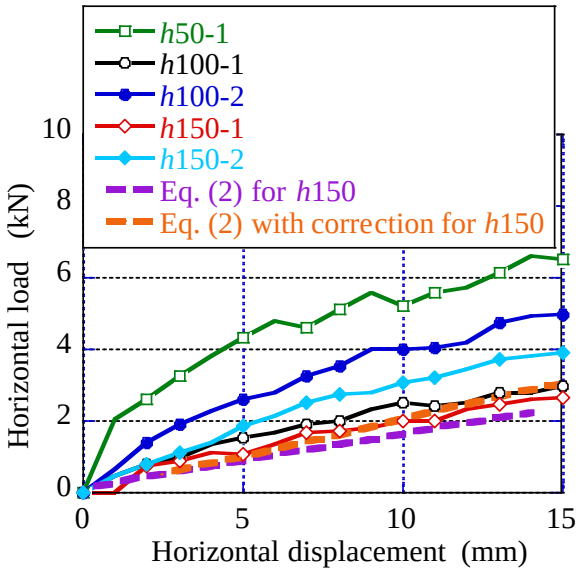

(c) Horizontal loading tests

Fig. 6-3. Loading test results

The test results in **Fig. 6-3** show that the push-in and pull-out bearing capacities calculated using the bearing capacity **Eq. (6-1)** and the horizontal resistance obtained by Chang's **Eq. (6-2)** are underestimating the actual capacity of the spiral pile. This underestimation was caused by the fact that those equations do not consider the impact of the integration of the surrounding ground generated by the rotational press-fitting, namely a direct consequence of an apparent increase in the pile diameter, the increase in the strength of the ground immediately below the pile tip, and the increase in the flexural rigidity of the pile as illustrated in **Fig. 6-4**.

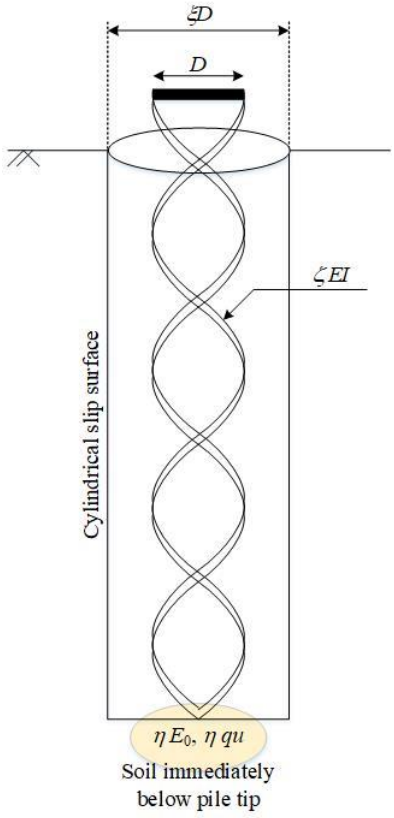

Fig. 6-4. Influence by the integration effect

In this study, the bearing capacity equation (**Eq. (6-1)**) and Chang's equation (**Eq. (6-2)**) were adapted to spiral piles by using correction coefficients ξ, η and ζ for the apparent increase in the pile diameter, the increase in the strength of the ground immediately below the pile tip, and the increase in the flexural rigidity of the pile, respectively. After the correction, the integration effect was considered without complicated procedures, using **Eq. (6-3) to (6-6)**. Since variations are observed in the experimental results, the minimum value of the correction coefficient obtained from each test was used as the representative value for the sake of safety. The obtained correction coefficients are ξ = 1.99, η = 0.73

and ζ = 1.94. These correction coefficients depend on pile size, spiral shape and characteristics of the surrounding ground, but for small diameter spiral piles in clayey soil, the application of the coefficients is generally useful, including in practical cases. Vertical bearing capacities and horizontal load – horizontal displacement relationship obtained using the corrected equations are plotted in **Fig. 6-3**. The load capacities given by these corrected equations roughly correspond to displacements equivalent to 10% of the pile diameter in the experiment.

$$R_u = q_p A_p + \tau_c L_c \phi \tag{6-1}$$

$$y_t = \frac{(1+\beta h)^3 + 1/2}{3EI\beta^3} H + \frac{(1+\beta h)^2}{2EI\beta^2} M \tag{6-2}$$

$$A_p' = \frac{\pi(\xi D)^2}{4} \tag{6-3}$$

$$q_p' = 3\eta q_u = 3\eta(15N) \tag{6-4}$$

$$\phi' = \pi \xi D \tag{6-5}$$

$$\beta' = \left(k_h' D' \Big/ 4EI' \right)^{1/4} = \left(\alpha E_0 \xi^{-3/4} \xi D \Big/ 4\zeta EI \right)^{1/4} \tag{6-6}$$

Where, R_u: the vertical ultimate bearing capacity (kN), q_p: the ultimate bearing capacity of the ground at the pile tip (kN/m^2), A_p: the area of the pile tip (m^2), τ_c: the peripheral frictional force (kN/m^2), L_c: the thickness of the layer for which peripheral frictional force is considered (m), ϕ: the length of the pile circumference (m), y_t: the horizontal displacement of the pile head (m), β: characteristic value of the foundation (m^{-1}), h: the pile protrusion length (m), EI: the flexural rigidity of the pile (kN-m^2), H: the horizontal load (kN), M: the pile head moment (kN-m), A_p': the corrected pile tip area (m^2), q_p': the corrected ultimate bearing capacity of the ground at the pile tip (kN/m^2), ϕ': the corrected pile peripheral length (m), β': the corrected characteristic value of the foundation (m^{-1}), q_u: the uniaxial compression strength (kN/m^2), N: N value converted by Swedish sounding test, k_h': the corrected coefficient of horizontal subgrade reaction force (kN/m^3), αE_0: the deformation modulus of the ground (kN/m^2).

6.4 Reproduction Analysis

In this study, the 3D elastoplastic finite element analysis code “DBLEAVES” developed by Ye et al. (2007) was used to conduct analysis corresponding to the loading tests described above and to evaluate

the bearing capacity of spiral piles subjected to combined loads. In this reproduction analysis, a spiral pile with a complicated shape was simplified into a model using the skeleton-beam type hybrid element proposed by Zhang et al. (2000) and verified for usefulness by Danno and Kimura (2009) as shown in **Fig. 6-5**. The features of this model are as follows: (1) The volume of the pile is expressed by setting parameters so that 90% of the flexural rigidity of the actual pile is distributed to the beam element of the pile core, and the remaining 10% is distributed to the solid elements that make up the pile body; thus, the interaction between the pile and the ground can be expressed accurately. (2) A bilinear elastoplastic beam element is used for the beam element of the pile core according to the Specifications for Highway Bridges, and the full plastic moment of the pile is set based on the yield stress of SS400 steel; thus, the bending failure of the pile can be expressed, and (3) By providing a rigid beam element set between the pile core and the constituent nodes, the volume effect of the pile with respect to the vertical load can be properly considered. These characteristics make it possible to express the interaction between the pile and the ground by considering the volume of the pile without losing the variety of expression and the simplicity of the deformation calculation of the pile by using the beam element. Therefore, it is possible to analyse the deformation of piles in multiple loading directions using one unified model.

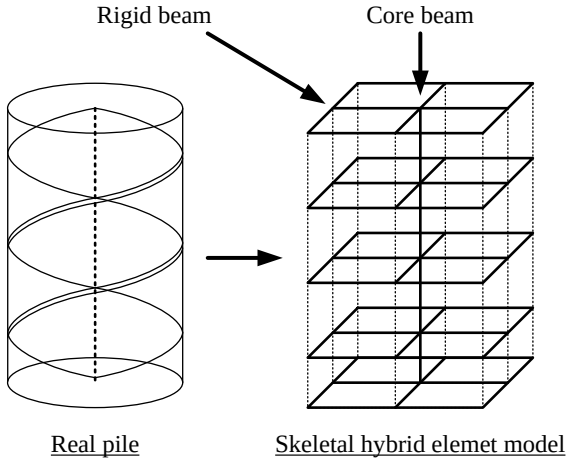

Fig. 6-5. Skelton-beam type hybrid element

The correction coefficients discussed in the above section are considered in the determination of the model dimensions and parameters in this analysis. **Table 6-2** shows the parameters used in the analysis.

Table 6-2. Hybrid element parameters

	Core beam	Solid elements around a core beam	Real pile
Section stiffness *EA* (kN)	2.12×10^5	142.0	2.12×10^5
Bending stiffness *EI* (kN-m^2)	3.73	0.42	4.15
Poisson's ratio ν	0.30	0.30	0.30
Full plastic moment M_y (kN-m)	17.91	-	17.91

The Drucker-Prager model, which is the simplest elastoplastic constitutive criterion, was used as the constitutive criterion of the ground, considering that the information on the ground is only the converted *N* value and the detailed information may be insufficient. The deformation coefficient E_s of the ground was obtained by using the converted *N* value and the following equation.

$$E_s = 700N \tag{6-7}$$

The shear strength was calculated by estimating the uniaxial compressive strength q_u from the converted *N* value using Inada's **Eq. (6-4)** (Inada, 1960) and setting the adhesive strength to 29.25 kPa and the shear resistance angle to 0 degrees. The soil parameters used in the analysis are shown in **Table 6-3**.

Table 6-3. Soil parameters

	Soil	Soil immediately below pile tip
Modulus of deformation E_0 (kPa)	2730	1993
Unit weight γ_t (kN/m^3)	16	16
Poisson's ratio ν	0.30	0.30
Adhesive stress *c* (kPa)	29.25	21.35
Shear resistance angle ϕ (deg)	0	0

According to Danno and Kimura (2009), the friction between the pile and the surrounding ground is expressed by the shear deformation of the ground elements around the pile, and the friction between the pile and the ground can be expressed without setting artificial parameters such as joint

elements. However, this study aims to analyse not only the push-in load capacity but also the pull-out load capacity, we judged that it would be difficult to accurately perform the pulling test without using joint elements. Therefore, joint elements were used at the boundary between the pile's peripheral surface and the ground. Since the integration effect of the ground around the pile due to the rotational press-fitting leads to an apparent increase in the pile diameter, it can be interpreted that a shear surface generates in the ground. Therefore, a value equal to that of the surrounding ground was used for the shear strength parameter of the joint elements. For the other parameters of the joint elements, various loading test results were taken as references to determine them. The joint element parameters are summarized in **Table 6-4**.

Table 6-4. Joint element parameters

	Joint	Remarks
Shear stiffness k_s (kN/m)	1.75×10^5	Based on loading test results
Normal stiffness k_n (kN/m)	0.14	Based on loading test results
Adhesive stress c_j (kPa)	29.25	Equal to soil
Shear resistance angle ϕ_j (deg)	0	Equal to soil
Tensile strength σ_t (kPa)	2.93	Based on loading test results
Separation judgment value	0.001	Based on loading test results

The analysis domain was set as the half-sectional domain shown in **Fig. 6-6** in consideration of the symmetry of the structure and the load used in the tests. The total number of nodes was 8,888, and the number of elements was 7,526. As for the boundary conditions, the displacement was set as free only in the vertical direction for the sides of the domain, the displacement was set as being constrained in all directions for the bottom of the domain.

Fig. 6-7 shows the comparison of the results obtained from the numerical analysis and the experimental result in **Section 6-3**. According to this comparison, the numerical analysis used can successfully reproduce the experimental result, hence the validity of the numerical method.

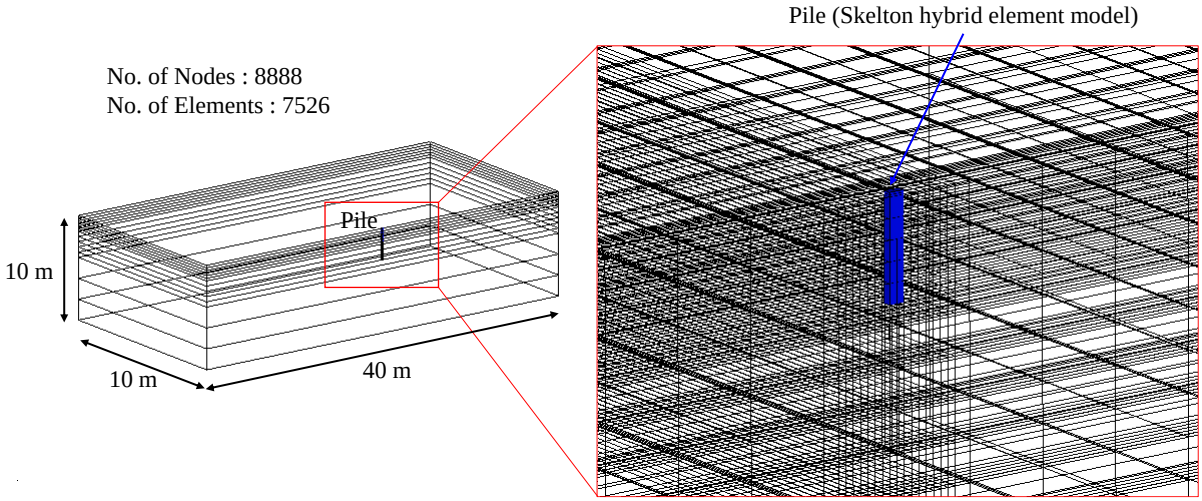

(a) A single vertical pile (α = 0°)

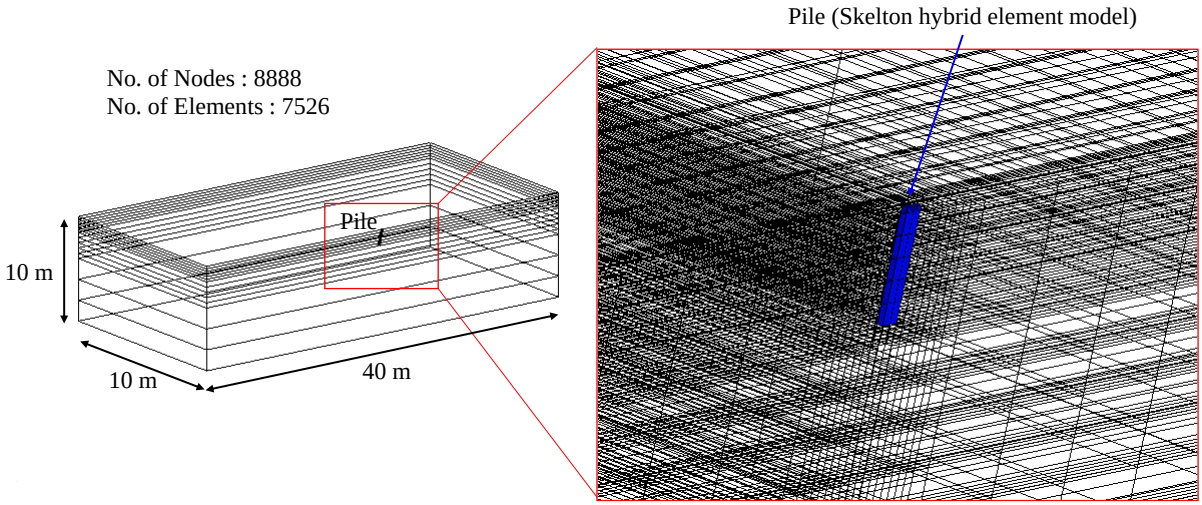

(b) A single batter spiral pile case (α = 30°)

Fig. 6-6. Analysis mesh

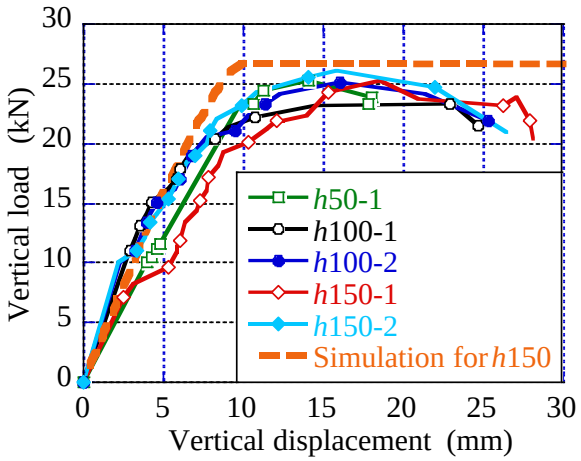

(a) Pull-out tests

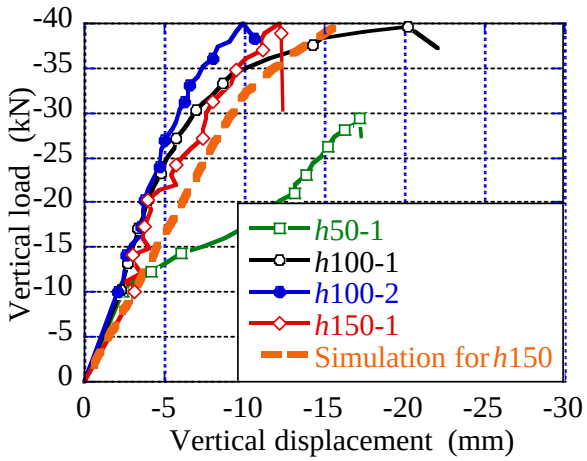

(b) Push-in tests

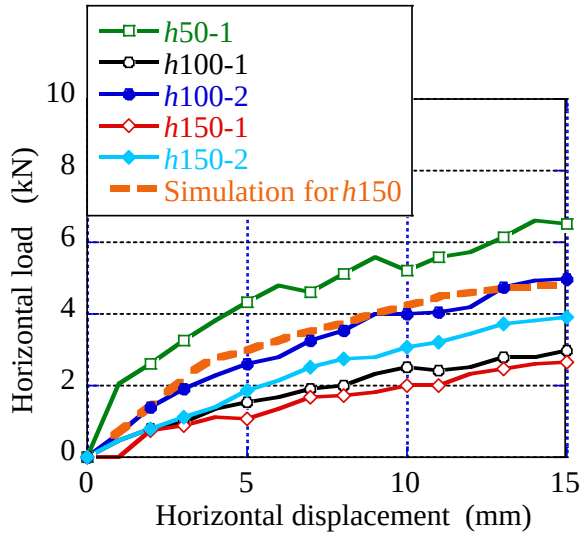

(c) Horizontal loading tests

Fig. 6-7. Numerical simulation results with loading test results

6.5 Evaluation of the Bearing Capacity Under Combined Horizontal and Vertical Loads

In this section, the evaluation of the bearing capacity of the small-diameter spiral pile under the combined horizontal and vertical loads is discussed. The evaluation was conducted by using the parameters established in **Section 6-4** and the same analysis method used in the identification of these parameters. **Fig. 6-8** shows the definition of the loading point, loading directions and loading angle. As shown in **Fig. 6-8**, the loading point was set at the ground level so that no bending moment can be generated at the pile head. In many cases of study of piles subjected to combined loads, a constant load is applied in one direction and incremental loading is applied in the other direction (Reddy and Ayothiraman 2015; Lu and Zhang 2018 and so on). However, in this study, both horizontal and vertical loads are applied simultaneously by using an inclined load. The analyses were done by changing the loading angle from -90° to 90° with 10° increments, this will allow taking account of both push-in load capacity and pull-out load capacity.

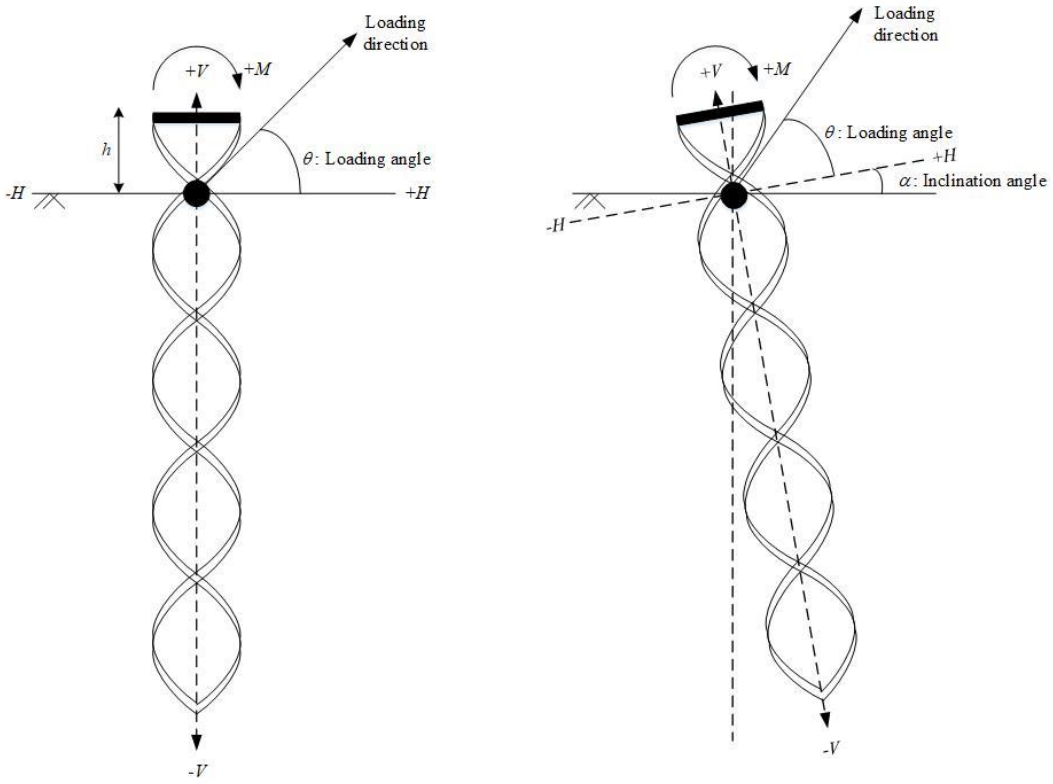

(a) Vertical pile (b) Batter pile

Fig. 6-8. Definition of the loading angle and the loading point of the combined load

Fig. 6-9(a) shows the relationship between the vertical load and the vertical displacement for all loading directions. The initial gradient of the vertical load vs. vertical displacement does not depend on the loading angle. However, the ultimate bearing capacity of pulling-out (positive loading angle) and that of pushing-in (negative loading angle) increase as the loading direction approaches the vertical direction. It can be noticed from **Fig. 6-9(a)** that the pushing-in load capacity is higher than the pulling-out capacity.

Fig. 6-9(b) shows the relationship between the horizontal load and the horizontal displacement for all loading directions. Here as well the initial gradient of the horizontal load vs. horizontal displacement curve does not depend on the loading angle, but the ultimate horizontal capacity for both positive and negative loading angles decrease as the loading direction approaches the vertical direction. The horizontal capacity for a negative loading angle is higher than that for a positive loading angle, especially when the loading direction approaches the vertical direction, this is in concordance with Ashour et al. (2020). This can be explained by the upward soil movement induced in front of the pile when the loading angle is positive, which decreases the soil strength and decreases the horizontal capacity. On the contrary, when the negative loading angle is applied, the soil in front of the pile undergoes moderate compaction or confinement which increases the soil strength and increases the horizontal capacity.

Fig. 6-9(c) shows the relationship between the loading direction and the displacement direction of the pile head. From **Fig. 6-9(c)**, it can be understood that the loading direction and the displacement direction agree with each other in the case of $\theta = \pm 90°$. However, in the other cases, the displacement angle is smaller than the loading angle, and the horizontal displacement tends to be predominant. The bending moment generated in the pile did not reach the full plastic moment, and the pile behaved within the elastic range in all the cases.

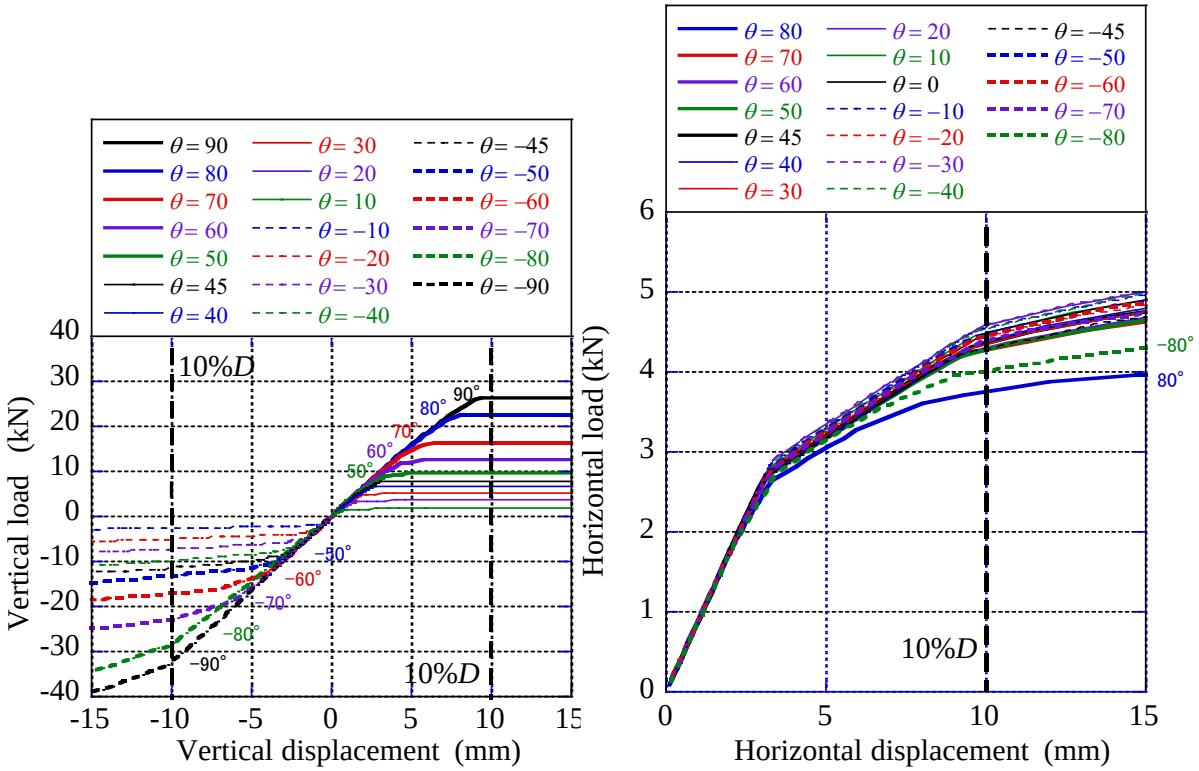

(a) Vertical load vs. vertical displacement (b) Horizontal loading vs. horizontal displacement

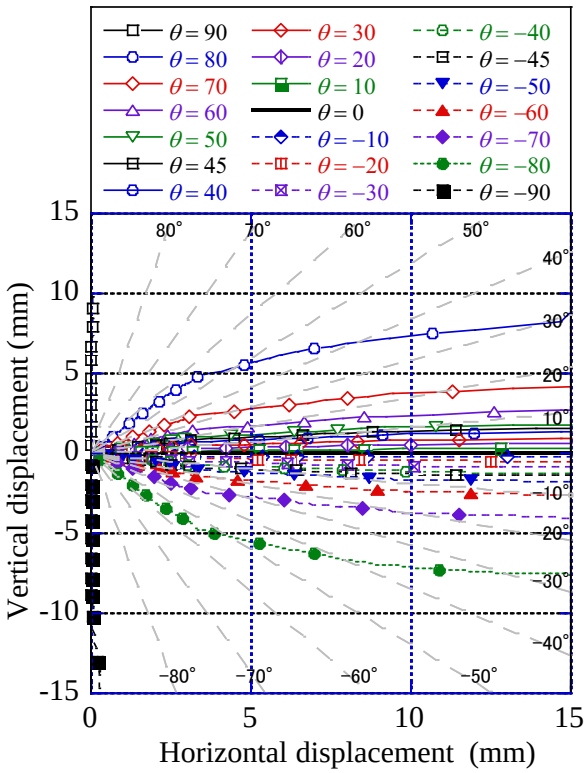

(c) Loading direction vs. displacement direction

Fig. 6-9. Numerical simulation results of the spiral pile subjected to the combined loads

Based on these results, the bearing capacity envelope for the combined horizontal and vertical loads is shown in **Fig. 6-10**. Here, the load that reaches the ultimate state the first in either the vertical or horizontal directions is defined as the bearing capacity. In other words, the bearing capacity obtained against combined loading is defined as the load that either the vertical or horizontal displacement component reaches 10%D earlier. The black broken line is showing the vertical and horizontal bearing capacity obtained against pure push-in, pull-out and lateral loading as reference. From **Fig. 6-10**, it can be observed that the ultimate load was reached first in the horizontal direction in the range from -80° to 80°. It can be noticed that the load's inclination does not much affect the horizontal response of the vertical pile, but it mainly affects its axial response, this observation is in concordance with Shahrour and Meimon (1991), Mroueh and Shahrour (2007). This envelope has a vertically long elliptical shape with the center below the origin (zero 0) because it exhibits a greater ultimate load in the push-in direction. From the above, by considering that the load that reaches the ultimate state the first in either the vertical or horizontal directions is the bearing capacity, the bearing capacity calculated individually against each pure push-in, pull-out and lateral loading was evaluated as being on the dangerous side against the combined horizontal and vertical loading. In addition, since the resistance in the vertical direction has a relatively greater margin than that in the horizontal direction, it is suggested that piles that have excellent resistance performance in the vertical direction, such as batter piles, should be investigated. The following findings were obtained from the above examinations.

(1) The resistance in the vertical direction has a relatively greater margin than the resistance in the horizontal direction.
(2) The ultimate bearing capacity obtained independently for each of the loading directions is evaluated on the dangerous side with respect to the bearing capacity under the combined loads.
(3) The pushing-in load capacity is higher than the pulling-out resistance.

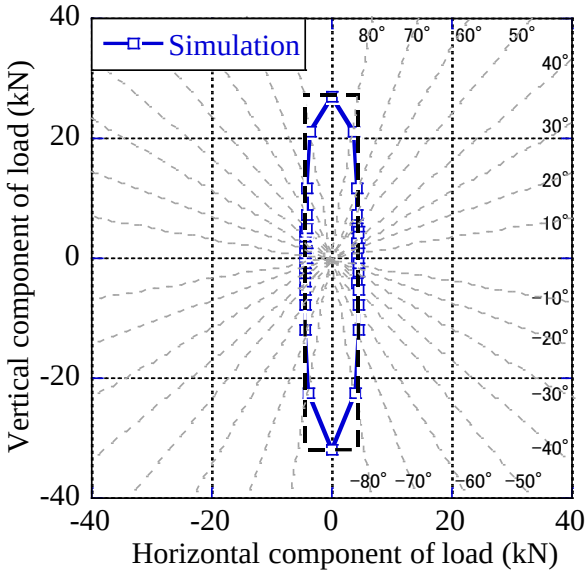

Fig. 6-10. Bearing capacity envelope of the spiral pile for the combined load (*H*-*V*)

Under the same analysis conditions, a series of analyses were performed considering the moment load (*M*) and the bearing capacity characteristics of the spiral pile for the *H*-*V*-*M* combined loads were investigated. In this analysis, the standard location of the center of mass of the superstructure of a photovoltaic power generation facility was assumed to be 1.5 m from the ground surface, and the value obtained by multiplying this by the horizontal load *H* was applied to the loading point as the moment load. In addition, as numerical experiments, analyses in which the location of the center of mass of the superstructure (equivalent to the loading height mentioned above in section 2) was changed to h = 3.0 m and h = 5.0 m were performed, and the bearing capacity characteristics for the *H*-*V*-*M* combined loads were obtained.

Fig. 6-11 shows the bearing capacity curve of the spiral pile under the combined load. As in the previous section, the bearing capacity is defined as the load that leads to the ultimate state the first in either the vertical or horizontal direction (i.e., the load when the displacement reaches 10 mm, 10% of the pile diameter). From this figure, the horizontal resistance significantly decreases when the moment load *M* is applied, and the bearing capacity envelope is scaled down in the horizontal direction compared to the case without the moment load *M* (i.e., where h = 0 m). Based on these results, we have proposed a formula for estimating the bearing capacity of the spiral pile under the *H*-*V*-*M* combined load in the next section.

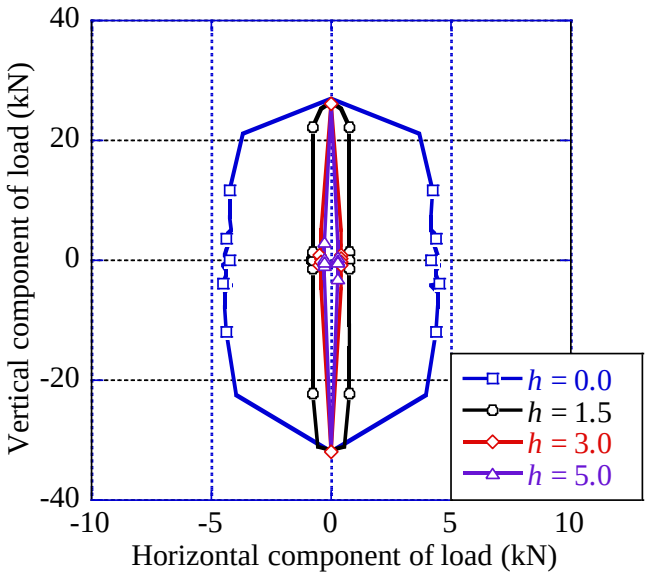

Fig. 6-11. Bearing capacity envelope for combined loads (*H*-*V*-*M*) of the vertical pile

6.6 Formula for Estimating the Bearing Capacity of Vertical Spiral Pile Under Combined Loads

From the bearing capacity characteristics of the spiral pile under the *H*-*V*-*M* combined loads discussed in the previous section, the bearing capacity envelope is expressed as a conceptual diagram in the *H*-*V*-*M* space as shown in **Fig. 6-12** and can be expressed by **Eq. (6-8)**. When this is projected onto the *H*-*V* space, it is expressed by **Eq. (6-9)**.

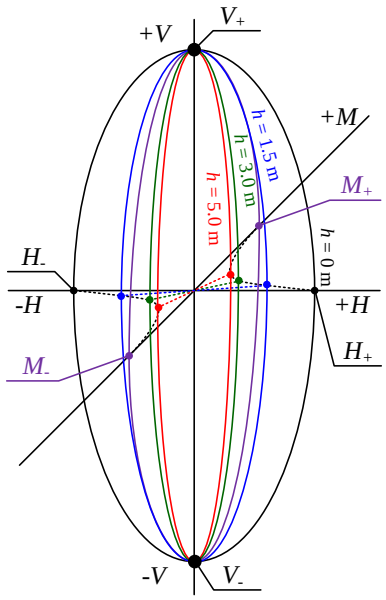

Fig. 6-12. Conceptual diagram of the bearing capacity envelope for the *H*-*V*-*M* combined load

$$\left(\frac{H}{H_{\pm}}\right)^2+\left(\frac{V}{V_{\pm}}\right)^2+\left(\frac{M}{M_{\pm}}\right)^2=1 \tag{6-8}$$

$$\left(\frac{H'}{H'_{\pm}}\right)^2+\left(\frac{V}{V_{\pm}}\right)^2=1 \tag{6-9}$$

$$H'_{\pm}=\frac{a|_{h=0}}{a+bh}H_{\pm}=\frac{3}{5(\psi\beta'\eta)^3+12(\psi\beta'h)^2+9\psi\beta'h+3}H_{\pm} \tag{6-10}$$

$$M_{\pm}=hH'_{\pm}=\begin{cases}\dfrac{3h}{5(\beta h)^3+12(\beta h)^2+9\beta h+3}H_{\pm} & \text{in case of} \quad 0\le\tan^{-1}\left(\dfrac{M}{H}\right)<\dfrac{\pi}{2}\\ M_{\pm} & \text{in case of} \quad \tan^{-1}\left(\dfrac{M}{H}\right)=0\end{cases} \tag{6-11}$$

V_+ and V- represent the pull-out (positive) and push-in (negative) bearing capacities in the direction of the pile axis, respectively, and H_+, M_+ and H_-, M_- represent the horizontal and moment load capacities with respect to the positive and negative load directions in **Fig. 6-8**. $H'_{\pm}$ is the horizontal bearing capacity when a moment load is applied; a and b are the coefficients of the first and second terms of Chang's equation (**Eq. (6-2)**), which are functions of h; and ψ is a correction coefficient to consider the influence under the ultimate state which β' in **Eq. (6-6)** does not consider sufficiently because it is determined based on Chang's equation, which is modeling elastic behavior of uniform ground along the depth. The characteristic of these estimation formulas is that if the bearing capacities in the direction of the pile axis and the direction perpendicular to the pile axis can be obtained by a loading test, the bearing capacity of the pile under the *H*-*V*-*M* combined loads can be estimated. However, further numerical simulation and loading tests are necessary because the correction coefficient also depends on pile size, spiral shape and characteristics of the surrounding ground.

In **Fig. 6-13**, we compare the numerically obtained and the estimated bearing capacities values for the combined loads when h = 0.0 m and h = 1.5 m. From this figure, it can be verified that the estimation formulas can evaluate the analyzed values with high accuracy. The coefficients of determination were calculated to verify the accuracy and are shown in **Table 6-5**. From this table, the accuracy of the estimated values is extremely high when the loading height h is low, but the estimation accuracy tends to decrease in the case of large loading height. Therefore, to improve the accuracy of the estimation formulas, it is necessary to carry out further verification using a comprehensive approach, including model and field experiments.

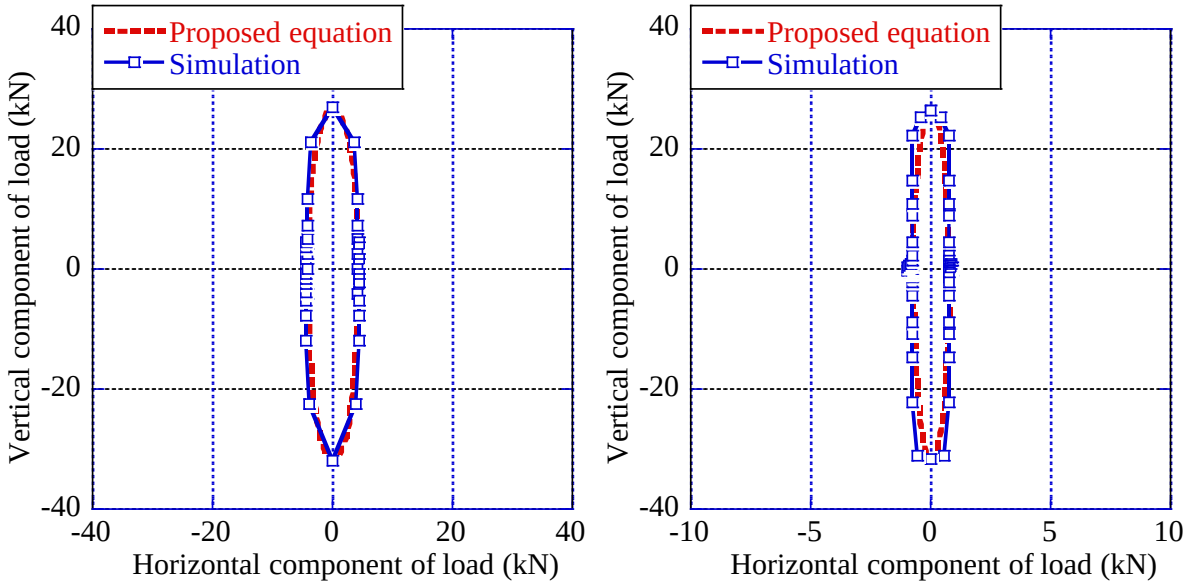

(a) at h = 0.0 m (b) at h = 1.5 m

Fig. 6-13. Comparison of the estimated and analysis values

Table 6-5. Accuracy verification of the estimated values for the vertical spiral pile subjected to the combined load (*H*-*V*-*M*)

h (m)	0	1.5	3	5
R^2	0.99	0.54	0.68	0.65

6.7 Bearing Capacity Characteristics of Batter Spiral Pile Under Combined Loads

Using the same analysis method as described in the above sections, loading analyses were performed to clarify the characteristics of the bearing capacity of the battered pile when combined loads are applied. A total of 6 series of analyses were performed by changing the inclination angle α (from the vertical direction) of the pile every 5° up to the applicable angle of 30° for lightweight piles. The loading conditions, loading point, and analysis parameters have not been changed from those of the vertical piles, but for the batter piles, the range of loading directions (angles) was from -180° to 180°. This range was set by considering that the batter piles exhibit asymmetrical bearing capacity characteristics for the loading direction. In this study by changing the loading angle from -180° to 180°, we were able to investigate the capacity of both negative and positive batter piles defined by relationships between loading direction and pile inclination direction.

Fig. 6-14 shows the bearing capacity envelopes of batter spiral piles under combined loads. As

in the previous section, the bearing capacity is defined as that of the load that leads the ultimate state the first in either the vertical or horizontal direction (i.e., the load when the displacement reaches 10 mm, 10% of the pile diameter). Comparing with **Fig. 6-10**, it can be seen that the bearing capacity envelopes of the batter spiral piles show elliptical shapes in which the pile axis direction of the batter piles is the major axis direction. This shape is in an agreement with the shape obtained by Mroueh and Shahrour (2009) who studied the response of battered piles to inclined pull-out loads. The pull-out and push-in capacities both decrease when the batter angle α increases.

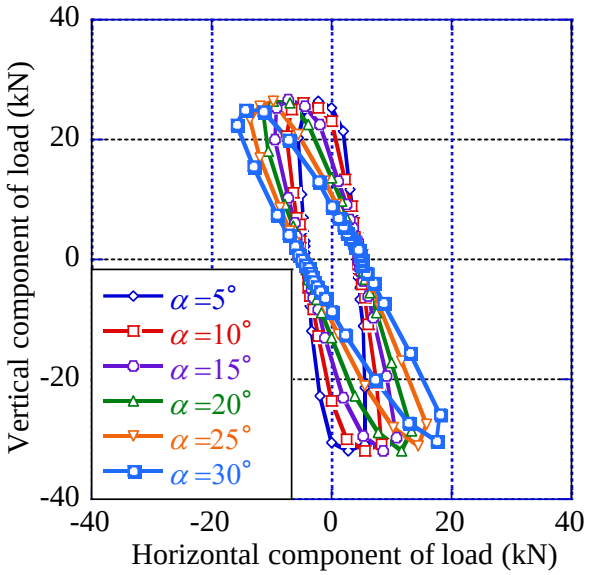

Figure 6-14. Bearing capacity envelope of the batter spiral pile for the combined load

From the characteristics of the bearing capacity of the batter spiral pile under the combined loads, the bearing capacity envelope of the small diameter spiral pile under combined loads can be formulated by the following equations.

$$\left(\frac{H^*}{H_+^*}\right)^2+\left(\frac{V^*}{V_+^*}\right)^2=1 \tag{6-12}$$

$$\left(\frac{H^*}{H_-^*}\right)^2+\left(\frac{V^*}{V_+^*}\right)^2=1 \tag{6-13}$$

$$\left(\frac{H^*}{H_-^*}\right)^2+\left(\frac{V^*}{V_-^*}\right)^2=1 \tag{6-14}$$

$$\left(\frac{H^*}{H_+^*}\right)^2+\left(\frac{V^*}{V_-^*}\right)^2=1 \tag{6-15}$$

$$\begin{pmatrix}H^*\\V^*\end{pmatrix}=\begin{bmatrix}\cos\alpha & -\sin\alpha\\ \sin\alpha & \cos\alpha\end{bmatrix}\begin{pmatrix}H\\V\end{pmatrix} \tag{6-16}$$

H^* and V^* are the horizontal load and the vertical load after the coordinate transformation by the rotation matrix using the inclination angle α of the batter pile and are expressed by **Eq. (6-16)**. V^*_+ and V^*_- represent the pull-out (positive) and push-in (negative) bearing capacities in the direction of the pile axis, respectively; H^*_+ represents the bearing capacity when the loading is applied perpendicular to the pile axis on the inclined side of the pile, and H^*_- represents when the loading is done in the reverse direction to that for H^*_+. Therefore, **Eq. (6-12)** represents the case where the loading is in the direction of the first quadrant after the coordinate transformation, and **Eq. (6-14)** represents the case where the loading is in the direction of the third quadrant. An illustration is shown in **Fig. 6-15**.

In **Fig. 6-16**, we compare the numerical and analytically estimated values of bearing capacity under the combined loads when the batter angle was 15° and 30°. In these cases, the loading height h was 0 m. From this figure, it can be verified that the evaluated values accurately represent the numerically analysed values for both of the batter angles.

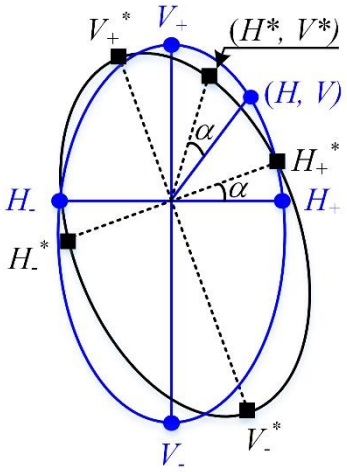

Fig. 6-15. Schematic view of the proposed **Eq. (6-12)** through **(6-16)**

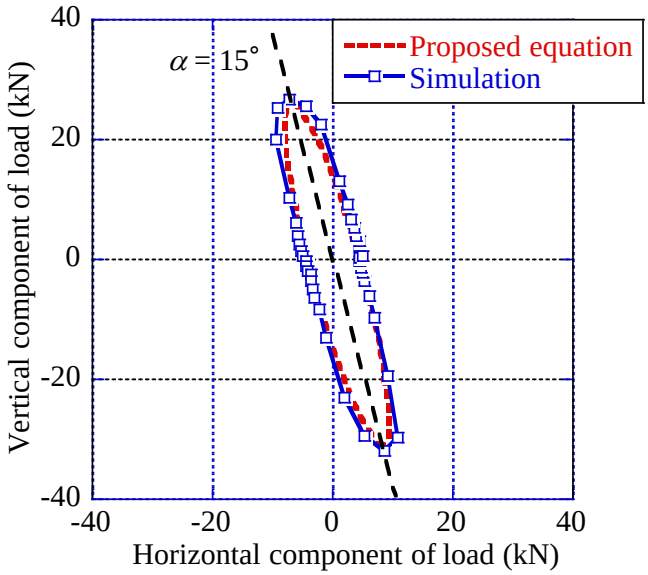

(a) for $\alpha = 15^{\circ}$

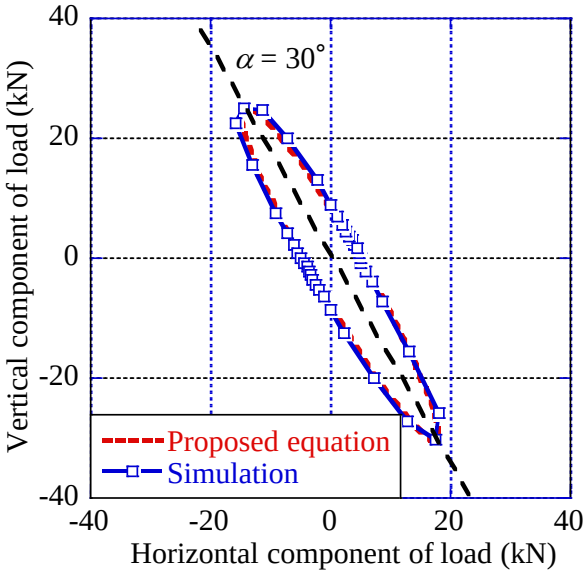

(b) for $\alpha = 30^{\circ}$

Figure 6-16. Comparison of the estimated and analysis values ($h = 0$)

The coefficients of determination were calculated to verify the accuracy and are shown in **Table 6-6**. The coefficient of determination is 0.97 or higher for each of the cases with different batter angles. This demonstrated that the proposed estimation equations are able to evaluate the bearing capacity of spiral piles under combined loads with extremely high accuracy. The above indicates that if the bearing capacity in the direction of the pile axis and that perpendicular to the pile axis can be obtained by a

loading test, the bearing capacity under the combined load can be evaluated by these estimation formulas accurately. Therefore, the high usefulness of the formulas is demonstrated.

Table 6-6. Accuracy verification of the estimated values for the batter spiral pile subjected to the combined load (*H*-*V*) when the loading height *h* was 0 m

α (deg)	0	5	10	15	20	25	30
R^2	0.99	0.97	0.99	0.99	0.99	0.99	0.98

For more reliability, the proposed equations are compared with existing literature (Mroueh and Shahrour, 2009), in which three-dimensional finite element analysis was used to investigate the response of battered piles against the combined horizontal and vertical pull-out loads while considering the nonlinear behavior of the dry medium dense sand. **Fig. 6-17** shows the comparison of the failure envelope for 3 batter angles α = 0 (vertical pile), -10 and -20 degrees. The loading height *h* was 0 m. From **Fig. 6-17** it can be seen that the proposed formulas match pretty well with the results of Mroueh and Shahrour (2009) although the failure envelopes from the proposed formulas are slightly slimmer. The slight discrepancy might be caused by the fact that the proposed formulas are established based on the simulation results for the small diameter spiral pile in clay, assuming a cylindrical shape of the slip surface around the pile. Therefore, further investigations are necessary for other types of soils.

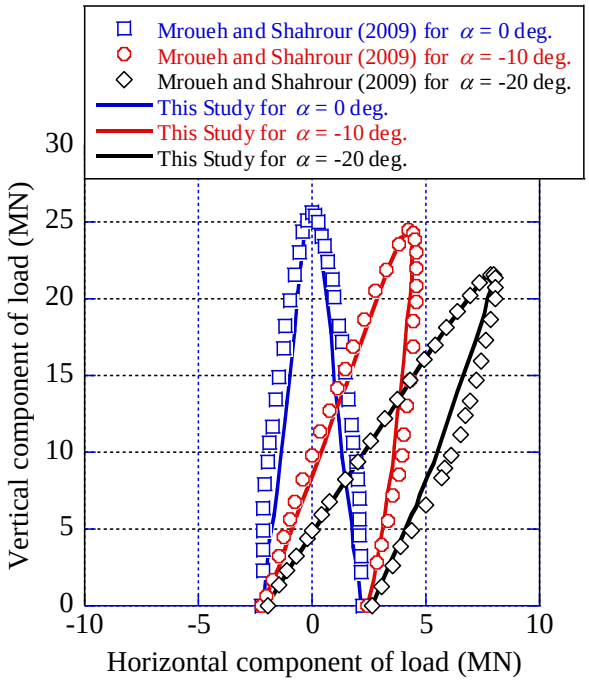

Fig. 6-17. Comparison with Mroueh and Shahrour (2009)

6.8 Summary

The findings obtained from the results of various loading tests on small-diameter spiral piles and the three-dimensional elastoplastic finite element analysis for evaluating the bearing capacity for combined loads are summarized below.

(1) The integration effect between the spiral pile and the surrounding ground derived from rotational press-fitting

The integration effect between the rotationally press-fit spiral pile and the surrounding ground was able to be considered in a simple way. To appropriately reflect the integration effect derived between the rotationally press-fit pile and the surrounding ground, corrections were done on the elements, such as an increase in the apparent pile diameter, an increase in the strength of the ground immediately below the pile tip, and an increase in the bending rigidity of the pile. As a result, we confirmed a high integration effect in both positive and negative vertical directions.

(2) Reproduction analysis results of various loading tests

The experimental results were able to be accurately expressed in each case by modeling the complex shape of the spiral pile and the integration effect on the surrounding ground from rotational press-fitting. In this modeling, the skeleton beam type hybrid element that takes into account the correction coefficients discussed in (1) was incorporated.

(3) Bearing capacity characteristics of the straight and batter spiral pile under the combined load

It was shown that the bearing capacity under the combined load might be lower than the bearing capacity evaluated independently for the vertical and horizontal loading, depending on the loading direction. In other words, there is a possibility that the ultimate bearing capacity is evaluated on the dangerous side by the conventional design method.

(4) Bearing capacity estimation formula for the combined load

We formulated the bearing capacity envelope for a small-diameter spiral pile under the *H-V-M* combined load, proposed a formula for estimating the bearing capacity of the small-diameter spiral pile, and verified the estimation accuracy of the formula. As a result, it was confirmed that the proposed estimation formula could estimate the bearing capacity curve for the *H-V-M* combined load of the spiral pile with high accuracy for each of the set inclination angles. Therefore, if the bearing capacity in the direction of the pile axis and that perpendicular to the pile axis can be obtained by a loading test, the

bearing capacity under the combined load can be evaluated by this estimation formula accurately. The accuracy of the estimated values is extremely high when the loading height *h* is low, but the estimation accuracy tends to decrease as the loading height *h* increases. Therefore, to improve the accuracy of the estimation formula, it is necessary to carry out further verification using a comprehensive approach, including model and field experiments in the future.

References

[1] Abdel-Rahman, K. and Achmus, M., 2006. Numerical modelling of the combined axial and lateral loading of vertical piles. Numerical Methods in Geotechnical Engineering, 575-581.

[2] Achmus, M. and Thieken, K., 2010. On the behavior of piles in non-cohesive soil under combined horizontal and vertical loading. Acta Geotechnica. 5, 199-210.

[3] Anand, P., Thornchaya, W., Richard, W., Witherspoon, T., W. and Nicasio, L., 2012. Inclined tensile load testing on short drilled shafts. Geotechnical Testing Journal, 35(2), 103343.

[4] Araki, K., 2013. Simple foundation method subject to small-scale structures "Pin Foundation Method". Journal of Geotechnical Engineering. 61(8), 32-33, in Japanese.

[5] Ashour, M., Alaaeldin, A. and Arab, M., G., 2020. Laterally Loaded Battered Piles in Sandy Soils. Journal of Geotechnical and Geoenvironmental Engineering. 146(1), 06019017.

[6] Ayothiraman, R. and Reddy, K., M., 2014. Model experiments on pile behaviour in loose-medium dense sand under combined uplift and lateral loads. Tunneling and Underground Construction GSP 242, 633-643.

[7] Danno, K. and Kimura, M., 2009. Evaluation of long-term displacements of pile foundation using coupled FEM and centrifuge model test. Soils and Foundations. 49(6), 941-958.

[8] Darr, K., A., Reese, L., C. and Wang, S., T., 1990. Coupling effects of uplift loading and lateral loading on capacity of piles. Offshore Technology Conference, British Maritime Technology, Teddington, 443-450.

[9] Das, B., M., Raghu, D. and Seeley, G., R., 1976. Uplift capacity of model piles under oblique loads. Journal of Geotechnical Engineering Division. 102(9), 1009-1013.

[10] Gotman, A., L., 2000. Finite-element analysis of tapered piles under combined vertical and horizontal loadings. Soil Mechanics and Foundation Engineering. 37(1), 5-12.

[11] Hirata, A., Kokaji, S. and Goto, T., 2005. Study on the Estimation of the Axial Resistance of Spiral Bar Based on Interaction with Ground. Shigen to Sozai. 121, 370-377, in Japanese.

[12] Inada, M, 1960. About the use of Swedish sounding test results. Soil mechanics and foundation engineering. 8(1), 13-18, in Japanese.

[13] Ismael, N., F., 1989. Field tests on bored piles subject to axial and oblique pull. Journal of Geotechnical Engineering. 115(11), 1588-1598.

[14] Jain, N., K., Ranjan, G. and Ramasamy, G., 1987. Effect of vertical load on flexural behaviour of piles. Geotechnical Engineering. 18(2), 185-204.

[15] Japanese geotechnical society. 2004. Method for static axial compressive load test of single Piles [JGS 1811-2002].

[16] Japanese geotechnical society. 2004. Method for Static Axial Tensile Load Test of Single Piles [JGS 1813-2002].

[17] Japanese geotechnical society. 2010. Method for lateral load test [JGS 1831-2010].

[18] Johnson, K., 2005. Load–deformation behaviour of foundations under vertical and oblique load. Ph.D. thesis. James Cook University, Australia.

[19] Karthigeyan, S., Ramakrishna, V., V., G., S., T. and Rajagopal, K., 2006. Influence of vertical load on the lateral response of piles in sand. Computers and Geotechnics. 33(2), 121–131.

[20] Karthigeyan, S., Ramakrishna, V., V., G., S., T. and Rajagopal, K., 2007. Numerical investigation of the effect of vertical load on the lateral response of piles. Journal of Geotechnical and Geoenvironmental Engineering. 133(5), 512-521.

[21] Lu, W. and Zhang, G., 2018. Influence mechanism of vertical-horizontal combined loads on the response of a single pile in sand. Soils and Foundations. 58(5), 1228-1239.

[22] Meyerhof, G., G., 1981. The bearing capacity of rigid piles and pile groups under inclined load in clay. Canadian Geotechnical Journal, 18(2), 297-300.

[23] Meyerhof, G., G., Yalcin, A., S. and Mathur, S., K., 1983. Ultimate pile capacity for eccentric inclined load. Journal of Geotechnical Engineering. 109(3), 408-423.

[24] Mroueh, H. and Shahrour, I., 2007. Response of piles to inclined uplift loads: Influence of the soil-pile interface. European Journal of Computational Mechanics. 16(3–4), 419-435.

[25] Mroueh, H. and Shahrour, I., 2009. Numerical analysis of the response of battered piles to inclined pullout loads. International Journal for Numerical and Analytical Methods in Geomechanics. 33, 1277-1288.

[26] Rao, S., N. and Prasad, Y., V., S., N., 1993. Uplift behavior of pile anchors subjected to lateral cyclic loading. Journal of Geotechnical Engineering. 119(4), 786-790.

[27] Reddy, M., K. and Ayothiraman, R., 2015. Experimental Studies on Behavior of Single Pile under Combined Uplift and Lateral Loading. Journal of Geotechnical and Geoenvironmental Engineering. 141(7), 04015030.

[28] Shahrour, I. and Meimon, Y., 1991. Analysis of the behaviour of offshore piles under inclined loads. International Conference on Deep Foundations, 277-284.

[29] Shanker, K., Basudhar, P. K. and Patra, N. R., 2007. Uplift capacity of single piles: Predictions and performance. Geotechnical and Geological Engineering. 25, 151-161.

[30] Sato, T., Harada, T., Iwasa, N., Hayashi, S. and Otani, J., 2015. Effect of shaft rotation of spiral piles under its installation on vertical bearing capacity. Japanese Geotechnical Journal. 10(2), 253-265, in Japanese.

[31] Small, J., C. and Zhang, H., H., 2002. Behavior of piled raft foundations under lateral and vertical loading. International Journal of Geomechanics. 2(1), 29-45.

[32] Suleiman, M., T., Voort, V., T. and Sritharan, S., 2010. Behavior of driven ultrahigh-perfomance concrete H-piles subjected to vertical and lateral loadings. Journal of Geotechnical and Geoenvironmental Engineering. 136(10), 1403-1413.

[33] Ye, B., Ye, G., Zhang, F. and Yashima, A., 2007. Experiment and numerical simulation of repeated liquefaction consolidation of sand. Soils and Foundations. 47(3), 547-558.

[34] Zhang, F., Kimura, M., Nakai, T. and Hoshikawa, T., 2000. Mechanical Behavior of Pile Foundations Subjected to Cyclic Lateral Loading Up to the Ultimate State. Soils and Foundations. 40(5), 1-17.

[35] Zhang, H. H. and Small, J., C., 2000. Analysis of capped pile groups subjected to horizontal and vertical load. Computers and Geotechnics. 26(1), 1-21.

CHAPTER 7 GENERAL CONCLUSIONS

7.1 General

In this research, three different kinds of foundations were studied for their bearing capacities, (1) the bearing capacity of surface strip footing on two-layered c-ϕ soils, the end bearing capacity of Incompletely End Supported Pile (IESP) and the bearing capacity characteristics of small-diameter spiral pile subjected to combined loads. The main goals of this research were to develop new bearing capacity models for each of the types of foundation cited above. Each bearing capacity model is being as realistic as possible by considering the strength parameters of each type of soil involved and considering the realities encountered in the field of construction. Therefore, the proposed bearing capacity equations are easy to use and provide consistent accuracy for a wide range of material parameters and geometries, encountered in practice. The proposed equations are developed using a detailed analysis of the results of numerical simulations (RPFEM and Elastoplastic FEM) and physical modeling. The equations are verified against published analytical, numerical and experimental test results, and it is shown that they provide accurate predictions which are sometimes better compared to current state-of-practice methods. This chapter summarises the main outcomes of the research and a discussion on future research that could build upon this work.

7.2 Main Findings

7.2.1 Findings on the Bearing Capacity of Strip Footing on Two-Layered c-ϕ Soils

(1) The Failure Mechanisms

by attributing to each soil layer its strength parameters, RPFEM has shown that the bottom layer may lead to punching failure in the case of a softer bottom while in the case of a stiffer bottom layer it may lead to local failure. These effects of the bottom layer cannot be obtained by using the average strength parameters suggested by Satyanarayana and Garg (1980), Bowles (1996) …or with the theories based on the assumption of general shear failure (Purushothamaraj et al. (1974) …). Three types of failure modes are observed in each of both cases, the case of a softer bottom layer and the case of a stiffer bottom layer. In the case of the softer bottom layer, a general shear failure, a transitional shear failure, and a punching shear failure are observed. In the case of a stiffer bottom layer, a general shear failure, a transitional shear failure, and a local shear failure are obtained. In each case, the type of failure observed function of the ratio of the tangent of the angle of friction of the bottom layer to that of the top

layer (r_ϕ) and the thickness of the top layer (H/B). This is defined by a chart in this research.

(2) The Critical Thickness of the Top Layer

The critical thickness is the thickness of the top layer above which the bottom layer has no more influence. Previous studies considered the depth of the central wedge, $B/2 \tan (45+ \phi_1/2)$, as the critical thickness of the top layer (Purushothamaraj et al. (1974), Satyanarayana and Garg (1980), Bowles (1996) …). However, in this research, it is found that the critical thickness of the top layer is not the depth of the central wedge but a function of the ratio of the tangent of the angle of friction of the bottom layer to that of the top layer (r_ϕ).

(3) The layer Factors and the Contribution of the Strength Parameters

In this research, we have proposed layer factors, L_c, L_q and L_γ to consider the effects of the layered system on the bearing capacity factors N_c, N_q and N_γ, respectively, of the top layer. The bearing capacity factors of the layered system are referred to as N_c*, N_q* and N_γ*. The layer factors are then obtained as ratios of N_i* to N_i, with i = c, q, γ (i.e. $L_c = N_c^*/ N_c$, $L_q = N_q^*/ N_q$ and $L_\gamma = N_\gamma^*/ N_\gamma$). The ratio of the tangent of the angle of friction of the bottom layer to that of the top layer (r_ϕ) and the thickness of the top layer (H/B) both affect the layer factors. Apart from these two parameters the layer factors, L_c, L_q and L_γ, are functions of the ratio of the cohesions ($r_c = c_2/c_1$), the embedment of the footing (D_f) and the ratio of unit weights ($r_\gamma = \gamma_2/\gamma_1$) respectively. It was demonstrated that the values of the strength parameters taken individually do not much matter, the ratios are the most important parameters.

(4) Layer Factors and Critical Thickness *H/B

The no influence of the bottom layer is illustrated by values of the layer factors equal to 1 ($L_i = 1$), this corresponds to the thickness of the top layer greater than the critical one. The influence of the bottom layer is illustrated by any value of layer factor different from 1 ($L_i \neq 1$), this corresponds to the thickness of the top layer less than the critical one. The critical is different for each layer factor. In the case of a softer bottom layer, the critical thicknesses are $H/B^* = 6$ for L_c and $H/B^* = 3$ for L_γ. However, for L_q, the critical thickness is higher than $H/B = 6$. In the case of a stiffer bottom layer, the critical thicknesses H/B^* are 1.5 for L_c and L_q and 0.75 for L_γ.

(5) The Proposed Equation

Using the proposed layer factors and the traditional bearing capacity factors, we have proposed a formula to calculate the bearing capacity of two-layered c-ϕ soils. In the same way as shape factors, inclination factors, depth factors, we are proposing layer factors to allow the traditional bearing capacity equations to estimate the bearing capacity of strip footing on two-layered c-ϕ soils.

7.2.2 Findings on the End Bearing Capacity of Incompletely End Supported Pile (EISP)

(1) The Yield Functions

The Drucker-Prager yield function can estimate the end bearing capacity of IESP in purely cohesive soil (c soil). However, when the soil possesses a friction angle, which means medium soils (c-ϕ soils) and cohesionless soils (ϕ soils), the Drucker-Prager yield function is not suitable. This incapacity of the Drucker-Prager yield function is due to its non-consideration of the influence of the confining pressure on the soil's internal friction angle ϕ. New parameters of the High Order yield function are established to consider the non-linear shear strength property of soil against the confining pressure in medium soils (c-ϕ soils) and cohesionless soils (ϕ soils). This allows the High Order yield function to estimate the end bearing capacity of IESP in those soil.

(2) Contribution of the Bottom soil layer, the Degradation of the End Bearing Capacity and the Critical Distance

Independently of the yield function (Drucker-Prager and High Order model), the bottom layer contributes to the increase of the end bearing capacity of IESP. The amount of contribution of the bottom layer depends on the stiffness ratio of the bottom layer to that of the top layer. However, the contribution of the bottom layer degrades when the pile tip moves away from the surface of the bottom layer. For a distance between the pile tip and the bottom layer equal to or greater than three times the pile diameter, no influence of the bottom layer is observed; in that case, the end bearing capacity of IESP is equal to that of a pile in a uniform soil made of the soil of the top soil layer. The distance of three times the pile diameter is the critical distance between the pile tip and the bottom layer.

(3) The Degradation Factor and the End Bearing Capacity Ratio

A degradation factor is defined to characterize the degradation of the end bearing capacity of IESP when its pile tip moves away from the bottom layer. The degradation factor (ξ_x) is independent of the yield function. However, ξ_x is affected by the end bearing capacity ratio (r) and the soil type. The end bearing capacity ratio is the ratio of the end bearing capacity of the pile when the tip is on the surface of the bottom layer to that of the pile when the bottom layer has no influence. This end-bearing capacity ratio represents here the stiffness ratio of the two soil layers. The value of the end bearing capacity ratio affects the decrease rate of the end bearing capacity of IESP. For small values of r, the degradation is smooth, however, for high values of r, the degradation is sudden. The sudden degradation in the cases of high values of r is due to the sudden change of the end bearing capacity from the hard layer to the softer layer. However, this effect of the end bearing capacity ratio is different for each type of soil. The c soils are more sensitive by presenting a higher decrease rate, followed by the c-ϕ soil and the of ϕ soil are less sensitive.

(4) The Proposed Equation for Estimating the End Bearing Capacity of IESP

An equation of the degradation factor ξ_x is established in this study as a function of the distance between the pile tip and the bottom layer, the end bearing capacity ratio r and the type of soil considered. The equation of the degradation factor proposed is, therefore, better than the one proposed by Hyodo et al (2020) which suggested a factor that applies to sand only and is independent of the stiffness ratio of the soil layer. By using the degradation factor, a formula that gives an accurate estimation of the end bearing capacity of IESP is proposed. The proposed Equation applies to IESP in purely cohesive soil (c soil), medium soils (c-ϕ soils) and cohesionless soils (ϕ soils).

7.2.3 Findings on the Bearing Capacity Characteristic of Small Diameter Spiral Pile

(1) The Integration Effect Between the Spiral Pile and the Surrounding Ground Derived from Rotational Press-fitting

The integration effect between the rotationally press-fit spiral pile and the surrounding ground was able to be considered in a simple way. To appropriately reflect the integration effect derived between the

rotationally press-fit pile and the surrounding ground, corrections were done on the elements, such as an increase in the apparent pile diameter, an increase in the strength of the ground immediately below the pile tip, and an increase in the bending rigidity of the pile. As a result, we confirmed a high integration effect in both positive and negative vertical directions.

(2) Reproduction Analysis Results of Various Loading Tests

The experimental results were able to be accurately expressed in each case by modeling the complex shape of the spiral pile and the integration effect on the surrounding ground from rotational press-fitting. In this modeling, the skeleton beam type hybrid element that takes into account the correction coefficients discussed in (1) was incorporated.

(3) Bearing Capacity Characteristics of the Vertical and Batter Spiral Pile Under the Combined Load

It was shown that the bearing capacity under the combined load might be lower than the bearing capacity evaluated independently for the vertical and horizontal loading, depending on the loading direction. In other words, there is a possibility that the ultimate bearing capacity is evaluated on the dangerous side by the conventional design method.

(4) Bearing Capacity Estimation Formula for the Combined Load

We formulated the bearing capacity envelope for a small-diameter spiral pile under the *H-V-M* combined load, proposed a formula for estimating the bearing capacity of the small-diameter spiral pile, and verified the estimation accuracy of the formula. As a result, it was confirmed that the proposed estimation formula could estimate the bearing capacity curve for the *H-V-M* combined load of the spiral pile with high accuracy for each of the set inclination angles. Therefore, if the bearing capacity in the direction of the pile axis and that perpendicular to the pile axis can be obtained by a loading test, the bearing capacity under the combined load can be evaluated by this estimation formula accurately.

7.3 Further Research

7.3.1 Further Research on the Bearing Capacity of Strip Footing on Two-Layered c-ϕ Soils

It is suggested to use a purely analytical demarche like the one of Purushothamaraj et al. (1974) but by considering all the types of failure patterns demonstrated in this study. Full-scale footing tests or centrifuge tests can provide more realistic failure patterns and help for a more accurate solution to the problem. The use of AI can allow the combination of cases and give more accurate layer factors.

7.3.2 Further Research on the End Bearing Capacity of Incompletely End Supported Pile (EISP)

It is suggested to investigate the problem using the ratio of strength parameters of the soil layers instead of the ratio of end bearing capacity. Here as well, full-scale pile tests or centrifuge tests can provide new insights on the problem. Consideration of more combinations of different types of soil layers like sand under clay or inversely would be welcome.

7.3.3 Further Research on the Bearing Capacity Characteristic of Small Diameter Spiral Pile

The accuracy of the proposed equation in this research is extremely high when the loading height h is low, but the estimation accuracy tends to decrease as the loading height h increases. Therefore, to improve the accuracy of the estimation formula, it is necessary to carry out further verification using a comprehensive approach, including model, field experiments and centrifuge tests in the future.

CHAPTER 8 REFERENCES

REFERENCES

[1] Abdel-Rahman, K. and Achmus, M., 2006. Numerical modelling of the combined axial and lateral loading of vertical piles. Numerical Methods in Geotechnical Engineering, 575-581.

[2] Achmus, M. and Thieken, K., 2010. On the behavior of piles in non-cohesive soil under combined horizontal and vertical loading. Acta Geotechnica. 5, 199-210.

[3] Anand, P., Thornchaya, W., Richard, W., Witherspoon, T., W. and Nicasio, L., 2012. Inclined tensile load testing on short drilled shafts. Geotechnical Testing Journal, 35(2), 103343.

[4] Araki, K., 2013. Simple foundation method subject to small-scale structures "Pin Foundation Method". Journal of Geotechnical Engineering. 61(8), 32-33, in Japanese.

[5] Ashour, M., Alaaeldin, A. and Arab, M., G., 2020. Laterally Loaded Battered Piles in Sandy Soils. Journal of Geotechnical and Geoenvironmental Engineering. 146(1), 06019017.

[6] Ayothiraman, R. and Reddy, K., M., 2014. Model experiments on pile behaviour in loose-medium dense sand under combined uplift and lateral loads. Tunneling and Underground Construction GSP 242, 633-643.

[7] Azam, G., and M.C. Wang. 1991. “Bearing capacity of strip footing supported by two-layer C-φ soils”. Transp Res Rec No. 1331, Transp Res Board: 56-66.

[8] Bowles, J.E. 1996. Foundations Analysis and Design. New York: McGraw-Hill Publishing Company.

[9] Brinch Hansen, J.A. 1970. “Revised and extended formula for bearing capacity”. Bulletin no. 28. Danish Geotechnical Institute Copenhagen: 5-11.

[10] Brown, J., G.G. Meyerhof. 1969. “Experimental study of bearing capacity in layered clays”. In Proc. Stmenth Int. Con. Soil Mech. Found. Eng., 2: 45-51.

[11] Burd, H.J., S. Frydman. 1997. “Bearing capacity of plane-strain footings on layered soils”. Can Geotech J. 34(2): 241-253.

[12] Button, S.J. 1953. “The Bearing Capacity of Footings on a Two-Layer Cohesive Subsoil”. 3rd ICSMFE. Vol. 1: 332-335.

[13] Coyle, H.M. and Castello, R.R., 1981. New design correlations for piles in sand. Journal of Geotechnical Engineering Division, ASCE, 107(7), 965-986.

[14] Danno, K. and Kimura, M., 2009. Evaluation of long-term displacements of pile foundation using coupled FEM and centrifuge model test. Soils and Foundations. 49(6), 941-958.

[15] Darr, K., A., Reese, L., C. and Wang, S., T., 1990. Coupling effects of uplift loading and lateral loading on capacity of piles. Offshore Technology Conference, British Maritime Technology, Teddington, 443-450.

[16] Das, P.P., V. N. Khatri, R. K. Dutta. 2019. "Bearing capacity of ring footing on weak sand layer overlying a dense sand deposit". Geomechanics and Geoengineering. DOI: 10.1080/17486025.2019.1664775

[17] Das, B.M., K.F. Dallo. 1984. "Bearing capacity of shallow foundations on a strong sand layer underlain by soft clay". Civ Eng Pract Des Eng. 3(5): 417-438.

[18] Das, B.M., R.F. Munoz. 1984. "Bearing capacity of eccentrically loaded continuous foundations on layered sand". Transp Res Rec. 28-31.

[19] Das, B., M., Raghu, D. and Seeley, G., R., 1976. Uplift capacity of model piles under oblique loads. Journal of Geotechnical Engineering Division. 102(9), 1009-1013.

[20] Desai, C.S., L. Reese. 1970a. "Ultimate capacity of circular footings on layered soils". J Indian Nat. Soc. Soil Mech. Found. Eng. 96(1): 41-50.

[21] Desai, C.S., L. Reese. 1970b. "Analysis of circular footings on layered soils". J Soil Mech. Found. Division, ASCE. 96(4): 1289-1310.

[22] Du, N.L., S. Ohtsuka, T. Hoshina, K. Isobe. 2016. "Discussion on size effect of footing in ultimate bearing capacity of sandy soil using rigid plastic finite element method". Soils Found. 56(1): 93-103.

[23] Eshkevari, S. S., 2018. bearing capacity of surface strip footings on layered soils. Ph.D. thesis. The University of Newcastle, Australia.

[24] Eslami, A. and Fellenius, B.H., 1995. Toe bearing capacity of piles from cone penetration test (CPT) data. In Proceedings of the International Symposium on Cone Penetration Testing, CPT'95, Linköping, Sweden. Swedish Geotechnical Institute, October 4–5, SGI Report 3-95, Vol. 2, 453–460.

[25] Eslami, A. and Fellenius, B.H., 1997. Pile capacity by direct CPT and CPTu methods applied to 102 case histories. Canadian Geotechnical Journal, 34(6), 886–904.

[26] Farah, C.A. 2004. "Ultimate bearing capacity of Shallow foundations on layered soils". MSc thesis, Civil and Environmental Engineering, Concordia Univ; Quebec.

[27] Florkiewicz, A. 1989. “Upper bound to bearing capacity of layered soils”. Can Geotech J. 26(4): 730-736.

[28] Gotman, A., L., 2000. Finite-element analysis of tapered piles under combined vertical and horizontal loadings. Soil Mechanics and Foundation Engineering. 37(1), 5-12.

[29] Griffiths, D.V. 1982. “Computation of bearing capacity on layered soils”. In Proc., 4th int. conf., Num. meth. Geomech. 163-170.

[30] Gunaratne, M., 2006. The foundation engineering handbook. Taylor and Francis, London.

[31] Hanna, A.M., G.G. Meyerhof. 1980. “Design charts for ultimate bearing capacity of foundations on sand overlying soft clay”. Can Geotech J. 17(2): 300-303.

[32] Hanna, A.M.. 1981. “Foundations on strong sand overlying weak sand”. J Geotech Eng Division, ASCE. 107(7): 915-927.

[33] Hanna, A.M. 1982. “Bearing capacity of foundations on a weak sand layer overlying a strong deposit”. Can Geotech J. 19(3): 392-396.

[34] Hettler, A. and Gudehus, G., 1988. Influence of the foundation width on the ultimate bearing capacity factor. Soils and Foundations, 28(4), 81–92.

[35] Hirata, A., Kokaji, S. and Goto, T., 2005. Study on the Estimation of the Axial Resistance of Spiral Bar Based on Interaction with Ground. Shigen to Sozai. 121, 370-377, in Japanese.

[36] Hoshina, T., S. Ohtsuka, K. Isobe. 2011. “Ultimate bearing capacity of ground by rigid plastic finite element method taking account of stress-dependent non-linear strength property”. J. Appl. Mech. 6: 191–200 (in Japanese).

[37] Houlsby, G.T., Nuit, N.R.F. and Sweeney, M., 1994. End bearing capacity of piles in carbonate soil. Proceedings of the 13th International Conference on Soil Mechanics and Foundation Engineering, New Delhi, Vol. 2, 635-638.

[38] Huang, M., H.L. Qin. 2009. “Upper-bound multi-rigid-block solutions for bearing capacity of two-layered soils”. Comput Geotech. 36(3): 52-59.

[39] Hyodo, J., Tamari, Y., Sone, A., Ozutsumi, O. and Ichii, K., 2020. A simplified method to consider the pile of insufficient length to obtain the support from bearing stratum. Journal of Asian Architecture and Building Engineering, 19(6), 626-636. DOI: 10.1080/13467581.2020.1764847

[40] Ikeda, A., Tsutiya, T. and Nagai, H., 2012. A New Formula for the Toe Resistance of a Helical Screw Pile Considering the Different Load Sharing Bearing Mechanism at the Closed End and the Helix, AIJ Journal of Technology and Design, 18(40), 877–882.

[41] Inada, M, 1960. About the use of Swedish sounding test results. Soil mechanics and foundation engineering. 8(1), 13-18, in Japanese.

[42] Ismael, N., F., 1989. Field tests on bored piles subject to axial and oblique pull. Journal of Geotechnical Engineering. 115(11), 1588-1598.

[43] Johnson, K., 2005. Load–deformation behaviour of foundations under vertical and oblique load. Ph.D. thesis. James Cook University, Australia.

[44] Jain, N., K., Ranjan, G. and Ramasamy, G., 1987. Effect of vertical load on flexural behaviour of piles. Geotechnical Engineering. 18(2), 185-204.

[45] Janbu, N., 1976. Static bearing capacity of friction piles. Proceedings of the 6th European Conference on Soil Mechanics and Foundation Engineering, 1(2), 479–488.

[46] Japanese geotechnical society. 2004. Method for static axial compressive load test of single Piles [JGS 1811-2002].

[47] Japanese geotechnical society. 2004. Method for Static Axial Tensile Load Test of Single Piles [JGS 1813-2002].

[48] Japanese geotechnical society. 2010. Method for lateral load test [JGS 1831-2010].

[49] Karthigeyan, S., Ramakrishna, V., V., G., S., T. and Rajagopal, K., 2006. Influence of vertical load on the lateral response of piles in sand. Computers and Geotechnics. 33(2), 121–131.

[50] Karthigeyan, S., Ramakrishna, V., V., G., S., T. and Rajagopal, K., 2007. Numerical investigation of the effect of vertical load on the lateral response of piles. Journal of Geotechnical and Geoenvironmental Engineering. 133(5), 512-521.

[51] Kenny, M.J., K.Z. Andrawes. 1979. “The bearing capacity of footings on a sand layer overlying soft clay”. Geotechnique. 47(2): 339-345.

[52] Khatri, V., J. Kumar, S. Akhtar. 2017. Bearing capacity of foundations with inclusion of dense sand layer over loose sand strata. Int J Geomech. 17(10): 06017018.

[53] Kumar, A., M.L. Ohri, R.K. Bansal. 2007. “Bearing capacity tests of strip footings on reinforced layered soil”. Geotech Geol Eng. 25(2): 139-150.

[54] Lu, W. and Zhang, G., 2018. Influence mechanism of vertical-horizontal combined loads on the response of a single pile in sand. Soils and Foundations. 58(5), 1228-1239.

[55] Ma Brouki, A., D. Benmeddour, R. Frank. 2010. “Numerical study of the bearing capacity for two interfering strip footings on sands”. Comput Geotech. 37(4): 431–439.

[56] Merlfleld, R.S., S.W. Sloan, H.S. Yu. 1999. “Rigorous plasticity solutions for the bearing capacity of two-layered clays”. Geotechnique. 49(4): 471-490.

[57] Meyerhof, G.G. 1963. “Some recent research on the bearing capacity of foundations”. Can Geotech J. 1:16–26. https://doi.org/10.1139/t63-003.

[58] Meyerhof, G.G. 1974. “Ultimate bearing capacity of footings on sand layer overlying clay”. Can Geotech J. 11(2): 223–229.

[59] Meyerhof GG. 1976. “Bearing capacity and settlement of pile foundations”. J Geotech Eng Division, ASCE. 102(3): 195–228.

[60] Meyerhof, G.G., A.M. Hanna. 1978. “Ultimate bearing capacity of foundations on layered soils under inclined load”. Can Geotech J. 15(4): 565–572.

[61] Meyerhof, G., G., 1981. The bearing capacity of rigid piles and pile groups under inclined load in clay. Canadian Geotechnical Journal, 18(2), 297-300.

[62] Meyerhof, G., G., Yalcin, A., S. and Mathur, S., K., 1983. Ultimate pile capacity for eccentric inclined load. Journal of Geotechnical Engineering. 109(3), 408-423.

[63] Michalowski, R.L., L. Shi. 1995. “Bearing capacity of footings over 2-layer foundation soils”. J Geotech Eng. 21(5): 421– 428.

[64] Mosadegh, A., H. Nikraz. 2015. “Bearing Capacity Evaluation of Footing on a Layered Soil using ABAQUS”. J Earth Sci Clim Change. 6:3. Doi: http://dx.doi.org/10.4172/2157-7617.1000264

[65] Mroueh, H. and Shahrour, I., 2007. Response of piles to inclined uplift loads: Influence of the soil-pile interface. European Journal of Computational Mechanics. 16(3–4), 419-435.

[66] Mroueh, H. and Shahrour, I., 2009. Numerical analysis of the response of battered piles to inclined pullout loads. International Journal for Numerical and Analytical Methods in Geomechanics. 33, 1277-1288.

[67] Okamura, M., J. Takemura, T. Kimura. 1998. “ Bearing capacity predictions on sand overlying clay based on limit equilibrium methods”. Soils Found. 38(1): 181–194.

[68] Pholkainuwatra, P., Eua-apiwatch, S. and Yimsir, S., 2022. Experimental study of pile set-up of driven piles in Bangkok Clay. Engineering and Applied Science Research, 49(1), 96-102.

[69] Prandtl, L. 1920. "Über die Härte plastischer Körper" [hardness of plastic bodies]. Nachr. Ges. Wiss. Goettingen. Math.-Phys. Kl. 74-85.

[70] Prandtl, L. 1921. "Uber die Eindringungsfestigkeit (Harte) plastischer Baustoffe" [the penetration resistance (hardness) of plastic building]. und die Festigkeit von Schneiden, Zeitschrift fur angewandte Mathematik und Mechanik. 1(1): 15–20.

[71] Purushothamaraj, P., B.K. Ramiah, K.N. Venkatakrishna Rao. 1974. "Bearing capacity of strip footing in two-layered cohesive-friction soils". Can Geotech J. 11(1): 32-45.

[72] Qin, H.L., M.S. Huang. 2008. "Upper- bound method for calculating bearing capacity of strip footings on two-layer soils". Chinese J Geotech Eng. 30(4): 611-616.

[73] Rao, S., N. and Prasad, Y., V., S., N., 1993. Uplift behavior of pile anchors subjected to lateral cyclic loading. Journal of Geotechnical Engineering. 119(4), 786-790.

[74] Reddy, M., K. and Ayothiraman, R., 2015. Experimental Studies on Behavior of Single Pile under Combined Uplift and Lateral Loading. Journal of Geotechnical and Geoenvironmental Engineering. 141(7), 04015030.

[75] Reissner, H. 1924. "Zum Erddruck problem" [earth pressure problem]. In: Biezeno, C.B., Burgers, J.M. (Eds.), In Proc. 1st Int. Con. Applied Mech, Delft, The Netherlands: 295–311.

[76] Satyanarayana, A.M., R.K. Garg. 1980. "Bearing capacity of footings on layered C-φ soils". J Geotech Eng Division, ASCE. 106 Gt7: 819-824.

[77] Salimi, E.S., A.J. Abbo, G. Kouretzis. 2018. "Bearing capacity of strip footings on sand over clay". Can Geotech J. https://doi.org/10.1139/cgj-2017-0489.

[78] Salimi, E.S., A.J. Abbo, G. Kouretzis. 2019. "Bearing capacity of strip footings on layered sands". Comput Geotech. 114: 103101.

[79] Sato, T., Harada, T., Iwasa, N., Hayashi, S. and Otani, J., 2015. Effect of shaft rotation of spiral piles under its installation on vertical bearing capacity. Japanese Geotechnical Journal. 10(2), 253-265, in Japanese.

[80] Shahrour, I. and Meimon, Y., 1991. Analysis of the behaviour of offshore piles under inclined loads. International Conference on Deep Foundations, 277-284.

[81] Shanker, K., Basudhar, P. K. and Patra, N. R., 2007. Uplift capacity of single piles: Predictions and performance. Geotechnical and Geological Engineering. 25, 151-161.

[82] Shiau, J.S., A.V. Lyamin, S.W. Sloan. 2003. “Bearing capacity of sand layer on clay by finite element limit analysis”. Can Geotech J. 40(5): 900–915.

[83] Sivareddy, A., R.J. Srinivasan. 1967. “Bearing capacity of footings on layered clays”. J Soil Mech Found Division, ASCE. 938M2: 83-99.

[84] Small, J., C. and Zhang, H., H., 2002. Behavior of piled raft foundations under lateral and vertical loading. International Journal of Geomechanics. 2(1), 29-45.

[85] Suleiman, M., T., Voort, V., T. and Sritharan, S., 2010. Behavior of driven ultrahigh-perfomance concrete H-piles subjected to vertical and lateral loadings. Journal of Geotechnical and Geoenvironmental Engineering. 136(10), 1403-1413.

[86] Tamura, T., S. Kobayashi, T. Sumi. 1984. “ Limit analysis of soil structure by rigid plastic finite element method”. Soils Found. 24(1): 34-42.

[87] Tamura, T., S. Kobayashi, T. Sumi. 1987. “Rigid plastic finite element method for frictional soil”. Soils and Found. 27(3): 1-12.

[88] Tatsuoka, F., Sakamoto, M., Kawamura, T. and Fukushima, S., 1986. Strength and deformation characteristics of sand in plane strain compression at extremely low pressures. Soils and Foundations, 26(1), 65–84.

[89] Teramoto, S., Kimura, M. and Boonyatee, T., 2015. Parametric FEM analysis on mechanical behavior of Incompletely End-Supported Pile. Computer methods and recent advances in geomechanics-Oka; Murakami, Uzuoka and Kimoto (Eds.). London: Copyright Taylor and Francis Group, ISBN 978-1-138-00148-0.

[90] Terzaghi, K. 1943. Theoretical soil mechanics. New York: John Wiley and Sons Inc.

[91] Veiskarami, M., Eslami, A. and Kumar, J., 2011. End-bearing capacity of driven piles in sand using the stress characteristics method: analysis and implementation. Canadian Geotechnical Journal, 48, 1570-1586.

[92] Vesić, A.S., 1967. Ultimate load and settlement of deep foundations in sand. Proceedings of the Symposium on Bearing Capacity and Settlement of Foundations. Durham, N.C, Duke University series, 5(6), 53–68.

[93] Vesić, A.S., 1973. Analysis of ultimate loads of shallow foundations. Journal of the Soil Mechanics and Foundations Division, 99 (1), 45-76.

[94] Vesić, A.S., 1977. Design of Pile Foundations. National Cooperative Highway Research Program, Synthesis of Practice No. 42, Transportation Research Board, Washington, DC, 68 pages.

[95] Yao, X., Z. Minghua, Z. and Heng. 2018. "Undrained stability of strip footing above voids in two-layered clays by finite element limit analysis". Comput Geotech. 97: 124–133.

[96] Yasufuku, N. and Hyde, A.F.L., 1995. Pile end-bearing capacity in crushable sands. Géotechnique, 45(4), 663-676.

[97] Yasufuku, N., Ochiai, H. and Ohno, S., 2001. End-Bearing Capacity of sand related to soil compressibility. Soils and foundation, 41(4), 59-71.

[98] Ye, B., Ye, G., Zhang, F. and Yashima, A., 2007. Experiment and numerical simulation of repeated liquefaction consolidation of sand. Soils and Foundations. 47(3), 547-558.

[99] Zhang, F., Kimura, M., Nakai, T. and Hoshikawa, T., 2000. Mechanical Behavior of Pile Foundations Subjected to Cyclic Lateral Loading Up to the Ultimate State. Soils and Foundations. 40(5), 1-17.

[100] Zhang, H. H. and Small, J., C., 2000. Analysis of capped pile groups subjected to horizontal and vertical load. Computers and Geotechnics. 26(1), 1-21.